Distribution Agreement

In presenting this thesis or dissertation as a partial fulfillment of the requirements for an advanced degree from Emory University, I hereby grant to Emory University and its agents the non-exclusive license to archive, make accessible, and display my thesis or dissertation in whole or in part in all forms of media, now or hereafter known, including display on the world wide web. I understand that I may select some access restrictions as part of the online submission of this thesis or dissertation. I retain all ownership rights to the copyright of the thesis or dissertation. I also retain the right to use in future works (such as articles or books) all or part of this thesis or dissertation.

Signature:

_____ _____

Yair Menachem Gozal Date

Identification and characterization of disease-associated proteins in frontotemporal lobar degeneration

By

Yair Menachem Gozal
Doctor of Philosophy

Graduate Division of Biological and Biomedical Science
Program in Neuroscience

_____
Allan I. Levey, M.D., Ph.D.
Advisor

_____
James J. Lah, M.D., Ph.D.
Advisor

_____ _____
Junmin Peng, Ph.D. Lary C. Walker, Ph.D.
Committee Member Committee Member

_____
Keith D. Wilkinson, Ph.D.
Committee Member

Accepted:

_____
Lisa A. Tedesco, Ph.D.
Dean of the Graduate School

_____
Date

Identification and characterization of disease-associated proteins in frontotemporal lobar degeneration.

By

Yair Menachem Gozal
B.A. Case Western Reserve University, 2002

Advisors: James J. Lah, M.D., Ph.D.
and Allan I. Levey, M.D., Ph.D.

An abstract of
A dissertation submitted to the Faculty of the Graduate School of Emory University in partial fulfillment of the requirements for the degree of Doctor of Philosophy

Program in Neuroscience
Graduate Division of Biological and Biomedical Sciences

2009

Abstract

Identification and characterization of disease-associated proteins in frontotemporal lobar degeneration.

By Yair Menachem Gozal

Frontotemporal lobar degeneration (FTLD) is the second most common cause of presenile dementia, accounting for up to 20% of cases in this age group. Characterized by circumscribed degeneration of the prefrontal and anterior temporal lobes, FTLD results in profound personality changes, altered social behavior, language disturbances, and deterioration of executive function. The most common pathological subtype of FTLD is defined by the presence of neuronal ubiquitin-immunoreactive inclusions in affected brain regions, and is thus known as FTLD-ubiquitinated (FTLD-U). The pathophysiological mechanisms underlying neurodegeneration in FTLD-U are poorly understood, and little is known about the primary aggregating proteins in this disorder. We developed and applied orthogonal quantitative proteomic strategies for the unbiased identification of disease-associated proteins in FTLD-U. Using these approaches, we proteomically profiled detergent-insoluble protein extracts prepared from frontal cortex of FTLD-U cases, unaffected controls, or neurologic controls (i.e. Alzheimer's disease; AD). Demonstrating the validity of our strategies, examination of the proteins specifically enriched in the AD samples revealed the presence of both microtubule-associated protein tau and amyloid β, two well-established AD-linked proteins, as well as several novel targets. Among the proteins altered specifically in FTLD-U, we identified TAR DNA binding protein-43 (TDP-43), a known component of ubiquitinated inclusions. Finally, we identified additional proteins enriched in detergent-resistant fractions in FTLD-U, and characterized one of them, septin 11 (SEPT11), in detail. Using

highly sensitive targeted proteomics approaches, we confirmed the enrichment of SEPT11 in FTLD-U extracts. We further showed that SEPT11 is proteolytically cleaved and, in addition to its prominent glial localization in normal brain, accumulates in thread-like pathology in affected cortex of patients. Moreover, we identified a significant association of an intronic single nucleotide polymorphism in the *SEPT11* gene with sporadic FTLD in a clinical cohort. This association was close to significance in a second cohort from Mayo Clinic, but was not replicated in a third cohort from UCLA. In sum, we have developed and validated a novel proteomics strategy that successfully identifies disease-specific proteins in neurodegeneration, and used this method to discover SEPT11 as a new protein with altered abundance, unique pathology, and potential genetic linkage to FTLD-U.

Identification and characterization of disease-associated proteins in frontotemporal lobar degeneration.

By

Yair Menachem Gozal
B.A. Case Western Reserve University, 2002

Advisors: James J. Lah, M.D., Ph.D.
and Allan I. Levey, M.D., Ph.D.

A dissertation submitted to the Faculty of the Graduate School of Emory University in partial fulfillment of the requirements for the degree of Doctor of Philosophy

Program in Neuroscience
Graduate Division of Biological and Biomedical Sciences

2009

Acknowledgements

I am grateful to the many people who have, in various ways, contributed to the completion of the work presented in this dissertation. First and foremost, I am deeply grateful to my mentors, Drs. James Lah and Allan Levey, for their guidance, optimism, criticism, and patience over the years. You have given me every opportunity to learn and succeed, and you have proven time and again that collaboration and selflessness are critical for excellence in science.

I am indebted to my thesis committee, Drs. Junmin Peng, Lary Walker, and Keith Wilkinson, for their insight, encouragement, and support. I especially thank Dr. Peng for his generous investment of time and resources in teaching me the subtleties of proteomics and mass spectrometry, the techniques which underlie much of my dissertation work. Thanks for always being available for additional mentorship, and for treating me as a member of your lab.

It has been a pleasure to work in the Center of Neurodegenerative Disease with so many extraordinary and supportive colleagues. Although there are far too many of you to name, I will always appreciate your ideas, your advice, and your friendship. I would like to specifically thank Dr. Jonathan Glass, Dr. Marla Gearing, Dr. Howard Rees, and Deborah Cooper for their extensive contributions to these studies and their assistance in the characterization of pathologic tissues. Thank you to Dr. Nick Seyfried, Dr. Eric Dammer, Duc Duong, and Dongmei Cheng for their invaluable intellectual and experimental contributions in all of my proteomic studies. Thank you also to Craig Heilman and Dr. Jason Fritz for all of your help and advice along the way.

I cannot end without thanking my family. To my parents, David and Evelyne (a.k.a. PubMom), thank you for exposing me to the wonders of laboratory science at a young age, and for providing the blueprint for the motivation, drive, and ambition necessary to succeed in academic medicine. To my sister, Lyad, and my brother, Nir, thank you for believing in me and being there for me over the years. Finally, I dedicate this dissertation to my wife, Lisa, and daughter, Emma, who have endured my late nights in the lab and supported me unconditionally throughout this process. I am thankful for your patience, your love, and your encouragement. I could never have done this without you.

Table of Contents

List of Figures

List of Tables

Chapter 1

Introduction and Background[1]

1.1 Frontotemporal lobar degeneration

Frontotemporal lobar degeneration (FTLD) is progressive neurodegenerative condition characterized by focal, often symmetric, frontal and temporal lobar atrophy (McKhann, Albert et al. 2001). As the third most common form of dementia, behind Alzheimer's Disease (AD) and Lewy Body Dementia (LBD) (Katsuse and Dickson 2005; Neary, Snowden et al. 2005), FTLD accounts for up to 5% of all cases of dementia irrespective of age (Grossman 2001; Ratnavalli, Brayne et al. 2002). In contrast to AD, which is more common in the elderly, FTLD has a predominantly presenile onset (Ratnavalli, Brayne et al. 2002; Van Deerlin, Gill et al. 2003) with an estimated 15 cases per 100,000 persons in the 45- to 64-year old age range (Bird, Knopman et al. 2003). Thus, FTLD affects individuals with extensive occupational and familial responsibilities (Grossman 2005), resulting in significant socioeconomic costs. Finally, FTLD follows a more rapid course than AD, and invariably leads to death as treatment is primarily limited to addressing associated behavioral symptoms (Roberson, Hesse et al. 2005). Therefore, it is of paramount importance to enhance our understanding of disease pathogenesis and to deliver new candidates for the development of effective therapies for this, and other, devastating neurodegenerative disorders.

[1]Portions of this chapter have been reproduced with permission from Gozal YM, Peng J, Lah JJ, and Levey AI. (2006). Proteomics of senile plaques in Alzheimer's disease. In: Montine TJ, ed. *Proteomics of Neurodegenerative Disease*. Transworld Research Network, Kerala, India. 65-81.

1.2 History and clinical description of FTLD

Arnold Pick, a German neuropsychiatrist, described the first case of what is now called frontotemporal lobar degeneration in 1892. In his landmark case report, he described the cognitive impairment, confusion, aggressiveness, and progressive language impairment of the 71-year old patient, Auguste H (Pick 1892; Spatt 2003; Kertesz 2004). Gross examination of the patient's brain at autopsy revealed asymmetric atrophy of the left temporal lobe, and the absence of any focal lesions that could have accounted for the clinical aphasia (Kertesz 2004). Interestingly, having previously worked for six months with Carl Wernicke in Berlin, Pick's particular interest in reporting the case was the unusually severe language disorder, and he emphasized that this deficit of language occurred as a result of focal and progressive degeneration (Spatt 2003; Kertesz 2005). Over the course of the next decade, Pick published a series of articles detailing six cases in which focal cortical atrophy localized in the frontal and temporal lobes was associated with circumscribed cognitive and neuropsychological deficits (Forstl 2005).

One of these patients, a 41-year-old housewife named Anna H., presented with prominent behavioral abnormalities including reduced drive, stereotypy, perseveration, aggression, and altered dietary habits (Pick 1904; Spatt 2003; Kertesz 2004). Her case is widely considered to be the first description of the behavioral syndrome of FTLD, the most prevalent clinical manifestation of this disorder (Spatt 2003; Kurz 2005).

In 1911, Alois Alzheimer provided the first detailed histopathological examination of FTLD brains (Alzheimer 1911). He reported the absence of senile plaques and tangles (Boxer, Trojanowski et al. 2005), superficial cortical spongiosis, and the presence of round intraneuronal argyrophilic inclusions bodies and achromatic neuronal

ballooning (Forstl 2005). Renamed as Pick bodies and Pick cells respectively (Altman 1923; Boxer, Trojanowski et al. 2005), these features became the pathologic hallmarks of Pick's disease **(Figure 1.1)**, a term proposed in the 1920's by several of Pick's students (Gans 1922; Onari and Spatz 1926; Kertesz 2004). As interest in the disorder matured in the following decades, however, it became clear to researchers and pathologists that the prevalence of Pick bodies on autopsy was restricted only to approximately a quarter of patients (Kertesz, Hillis et al. 2003; Kertesz 2005). This extensive mismatch between pathology and the clinical syndrome resulted in the restriction, at least in the United States, of the term, "Pick's disease," only to those FTLD cases in which pathological diagnosis revealed the presence of the cytoplasmic Pick bodies (Spatt 2003). Ironically, despite his close collaboration with Hans Chiari, Pick never examined his own cases microscopically (Spatt 2003; Forstl 2005). Thus, whether all of his original cases contained the characteristic pathological features pathognomonic of Pick's disease is unknown. In 1994, and revised in 1998, the Lund-Manchester criteria were published to provide consensus recommendations for the clinical and pathologic diagnosis of the entities incorporated under the term, FTLD (1994; Neary, Snowden et al. 1998; Kertesz, McMonagle et al. 2005).

1.3 Classification of FTLD: Clinical

Despite its identification well over a century ago, the classification of FTLD is still difficult and imprecise due to the clinical, genetic, and pathologic heterogeneity of the disorders that comprise this diagnosis. Moreover, FTLD is often misdiagnosed as AD thereby retarding the development, understanding, and characterization of this disease

A

B

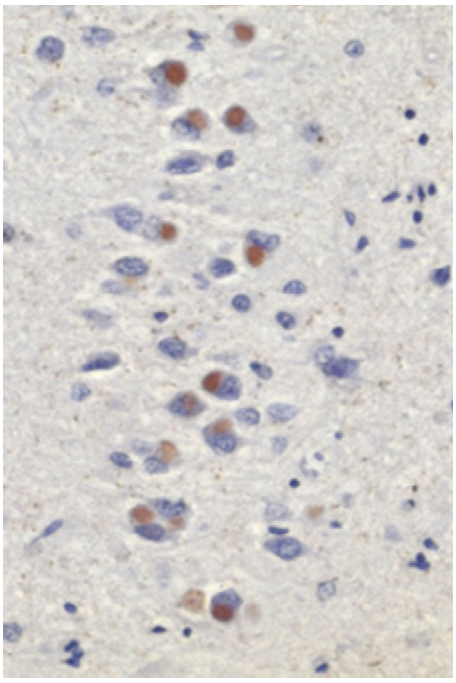

C

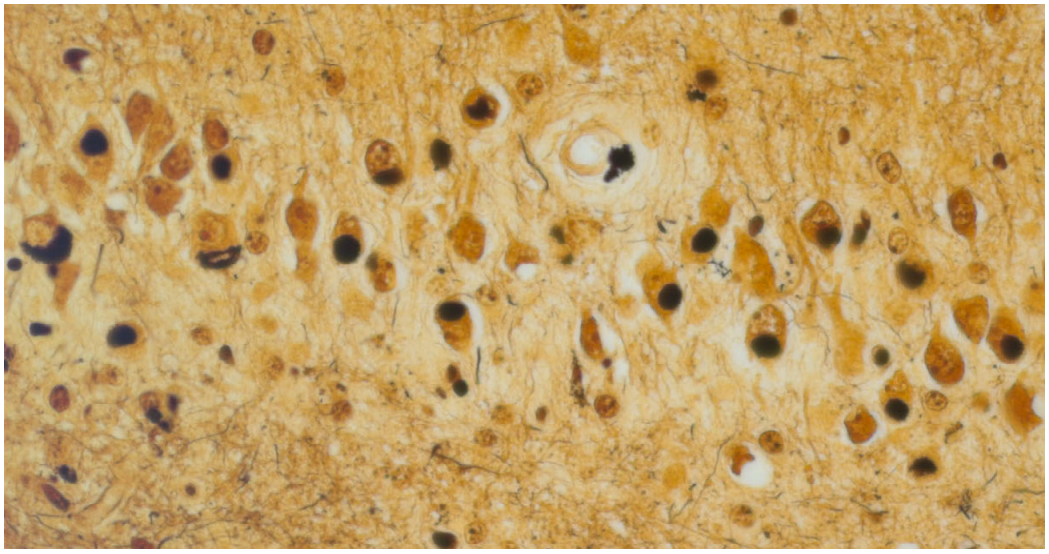

Figure 1.1 Pick's Disease. (A) Arnold Pick (from Haymaker, Webb, and Francis Schiller, The Founders of Neurology, 2nd Ed., August 1, 1970. Courtesy of Charles C Thomas Publisher, Ltd., Springfield, Illinois). Pick bodies, the hallmark feature of Pick's disease, are rounded intracellular aggregates and can be visualized by (B) tau immunohistochemistry or (C) Bielschowsky stain.

(Mendez, Selwood et al. 1993; Perry and Miller 2001). The task is further complicated by the widely diverging terminology used by different authors to describe the same condition, including “frontal dementia,” “frontal lobe dementia,” "frontal dementia of the non-Alzheimer's type," and “frontal variant of Pick’s disease” (Brun 1987; Bak and Hodges 2001). Clinically, FTLD is subdivided into three main syndromes, namely frontal variant FTD (FTD), semantic dementia (SD), and progressive nonfluent aphasia (PNFA), each of which reflects the most pronounced patient deficits at presentation (Mott, Dickson et al. 2005). In addition, clinical FTLD may occur concomitantly with the extrapyramidal signs of corticobasal degeneration (CBD), with progressive supranuclear palsy (PSP), or with motor neuron disease (Feany, Mattiace et al. 1996; Grimes, Lang et al. 1999; Neary, Snowden et al. 2000; Kertesz, Blair et al. 2007).

Behavioral abnormalities and personality changes are the distinctive features of FTD. Accounting for 40-50% of the clinical diagnoses of FTLD (Hodges 2001; Johnson, Diehl et al. 2005), FTD is characterized by insidious onset of impulsive or inappropriate behavior as a result of a lack of inhibition. This neurobehavioral decline may manifest as overactivity, restlessness, lack of social tact, swearing, and unrestrained aggression and sexuality. Conversely, it may also present as apathy, emotional blunting, and loss of drive and initiative. Stereotypic, ritualistic, compulsive, and perseverative behaviors are often observed. Finally, with disease progression, there is frequently a deterioration of dietary habits and personal hygiene. Despite these devastating changes, the patient demonstrates little insight or concern for their situation(Jackson, Lennox et al. 1996; Neary, Snowden et al. 2000; Rosen, Lengenfelder et al. 2000; McKhann, Albert et al. 2001; Sjogren and Andersen 2005).

While many of the disinhibited behaviors characteristic of FTD are also present in semantic dementia, the second clinical subtype of FTLD, language comprehension is the principal dysfunction in these patients (Boxer and Miller 2005). In this fluent progressive aphasia, which accounts for another 25-40% of FTLD diagnoses (Hodges 2001; Johnson, Diehl et al. 2005), patients present with a shrinking expressive vocabulary though they speak fluently with appropriate grammar and pronunciation (Sjogren and Andersen 2005). The problem involves understanding word meanings and reflects a fundamental loss in semantic memory (Mesulam 1982). Although patients attempt to compensate for this loss of words and their meanings by substituting stereotypic expressions and catch-all terms (Kertesz 2005), tasks such as word-to-picture naming or definitions can tease out the subtleties of this disorder (Sjogren and Andersen 2005). Interestingly, in stark contrast to AD, episodic memory in SD patients remains intact such that they are typically well-oriented and show no deficiencies in recollection (Rosen, Hartikainen et al. 2002).

The least common major clinical subtype of FTLD, PNFA, is characterized by a paucity of speech that gradually evolves into mutism (Sjogren and Andersen 2005). As the name implies, speech is nonfluent and often effortful despite preserved comprehension and semantic memory. Word retrieval, repetition, and grammar are severely impaired, while errors or transpositions of phonemes and apraxia of speech are common (Boxer and Miller 2005). Just as in SD, the progression of disease results in the eventual deterioration of communication skills and the onset of the behavioral changes of FTD (Neary, Snowden et al. 2000; Rosen, Lengenfelder et al. 2000). Therefore, it has been suggested that the clinical phenotypes of FTLD all occur within a single spectrum

and represent the anatomic distribution of the pathologic changes within the brain (Hodges 2001; Grossman 2005).

1.4 Classification of FTLD: Pathologic

As the clinical FTLD spectrum is slowly refined, a more complex, histopathology-based classification system is also being elucidated. Autopsy studies indicate that in addition to the clinical diversity of FTLD, pathological heterogeneity is also extensive (Grossman 2005). By employing contemporary histochemical and immunohistochemical staining methods, this heterogeneity has been distinguished into three distinct categories: FTLD-ubiquitinated (FTLD-U) type, dementia lacking distinctive histopathology (DLDH), and tauopathies (Woulfe, Kertesz et al. 2001). It is worth noting that these neuropathologic groups show no correlation to any specific clinical FTLD subtypes. Rather, each of the histopathologic classes may contribute to any of the clinical syndromes described previously (McKhann, Albert et al. 2001) **(Figure 1.2)**.

All three FTLD histologic categories demonstrate extensive lobar atrophy, neuronal loss, gliosis, and mild spongiosis in superficial frontal and anterior temporal cortices (Mann 1998; Rosen, Lengenfelder et al. 2000). The FTLD histologic category of FTLD-U, however, is additionally characterized by the presence of ubiquitin-positive, tau- and α-synuclein-negative intraneuronal inclusions **(Figure 1.3)**. This diagnosis, which accounts for approximately half of all cases of FTLD (Graff-Radford and Woodruff 2007; Snowden, Neary et al. 2007), is discussed extensively below. In contrast, cases of DLDH, as implied by the name, do not display any of the distinctive histologic

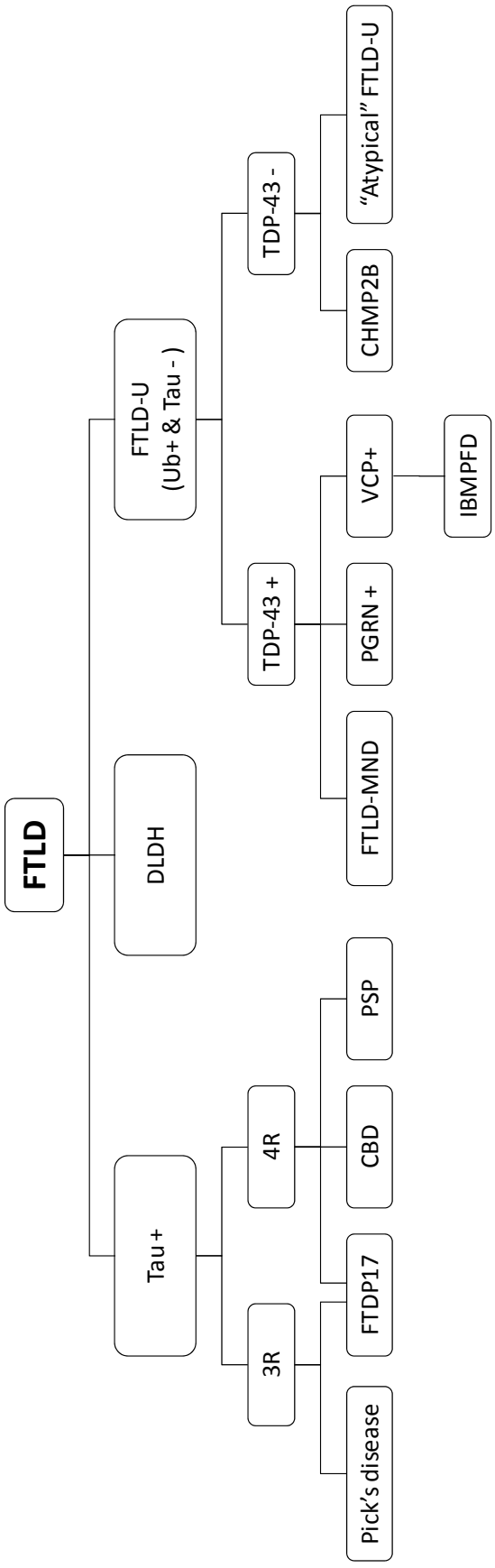
FTLD
Tau +
3R
Pick's disease
FTDP17
4R
CBD
PSP
DLDH
FTLD-MND
FTLD-U
(Ub+ & Tau -)
TDP-43 +
PGRN +
VCP+
IBMPFD
TDP-43 -
CHMP2B
"Atypical" FTLD-U

Figure 1.2 FTLD neuropathology flow chart demonstrating extensive pathologic and molecular complexity. FTLD, frontotemporal lobar degeneration; DLDH, dementia lacking distinctive histopathology; FTLD-U, frontotemporal lobar degeneration with ubiquitin-immunoreactive inclusions; 3R / 4R, tau isoforms containing 3 or 4 microtubule binding domains; TDP-43, TAR DNA binding protein-43; FTDP17, frontotemporal dementia with Parkinsonism on chromosome 17; CBD, corticobasal degeneration; PSP, progressive supranuclear palsy; FTLD-MND, frontotemporal lobar degeneration with concomitant motor neuron disease; PGRN, progranulin; VCP, valosin containing protein; CHMP2B, charged multivesicular body 2B; IBMPFD, inclusion body myopathy with Paget's disease of the bone and/or frontotemporal dementia; + presence or - absence of immunoreactivity. Adapted from (Bigio 2008).

A

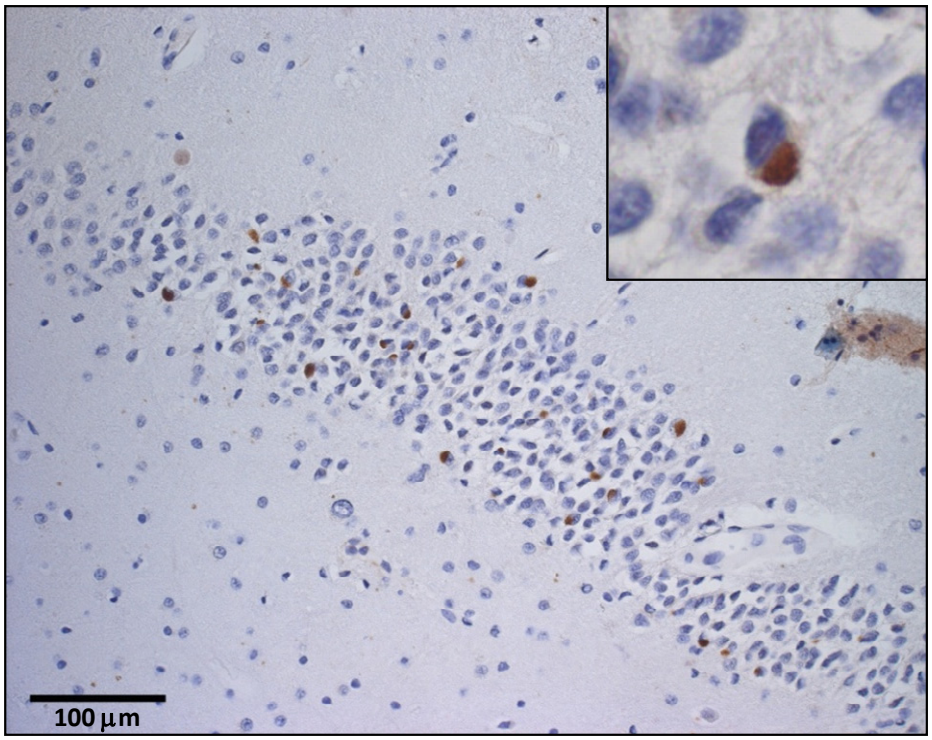

B

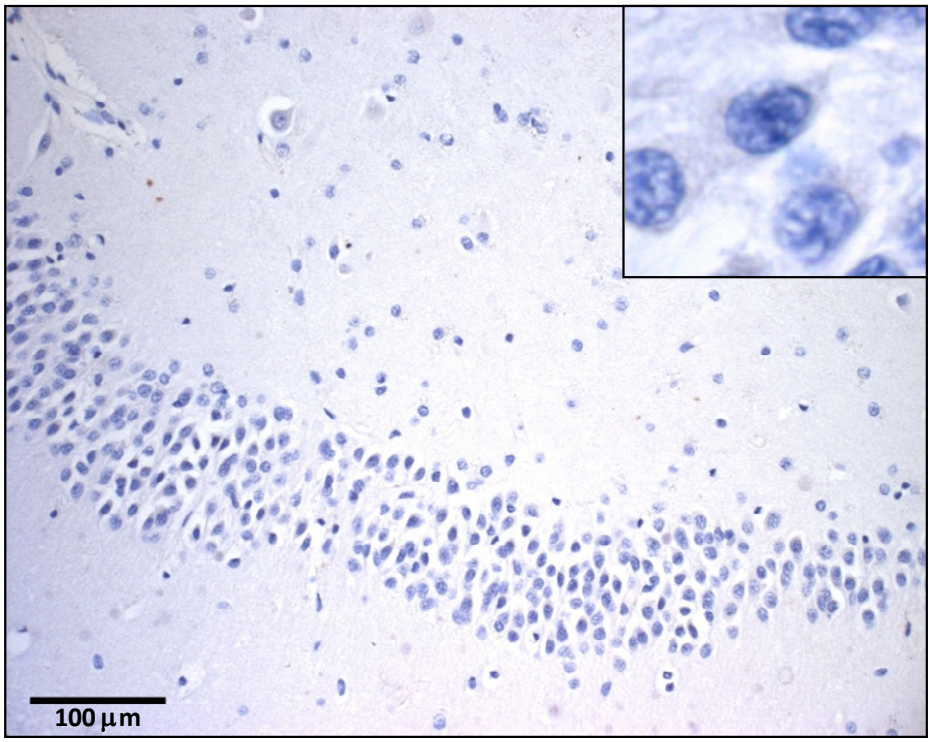

Figure 1.3 FTLD-U is characterized by ubiquitin-immunoreactive inclusions. Ubiquitin immunolabeling clearly reveals cytoplasmic inclusions in a subset of FTLD-U dentate granule cells of the hippocampus (A) but not in normal control (B).

abnormalities such as the classical Pick bodies, senile plaques, or neuronal inclusions (Knopman, Mastri et al. 1990). Instead, tau and ubiquitin immunohistochemistry is entirely unremarkable in these cases. Finally, the FTLD disorders which qualify as tauopathies demonstrate pathological features that immunochemically stain for tau, a microtubule-associated protein known to stabilize microtubules in neurons. Diseases grouped in this category account for approximately 40% of all FTLD cases (Lipton, White et al. 2004; Snowden, Neary et al. 2007) and include Pick's disease, FTD with Parkinsonism linked to Chromosome 17 (FTDP-17), and neurofibrillary tangle dementia (Mott, Dickson et al. 2005; Sergeant, Delacourte et al. 2005; Josephs, Petersen et al. 2006). In addition, tau-immunoreactive inclusions are also characteristic of FTLD cases with the motor symptoms of CBD and PSP (Hu, Parisi et al. 2007). Interestingly, these FTLD tauopathies may be further subdivided based on the number of repeats of the microtubule binding domain in the primary aggregated form of tau (Buee and Delacourte 1999). As a result of alternative splicing, tau isoforms can have either 3 repeats (3R) or 4 repeats (4R) of the domain, thereby affecting the microtubule binding affinity of each isoform (Hu, Parisi et al. 2007). In Pick's disease, neuropathology consists mainly of 3R-tau aggregated into random coiled filaments. Conversely, 4R-tau constitutes the primary aggregated form in CBD and PSP. In these disorders, the 4R-tau isoforms aggregate into twisted and straight filaments respectively. Finally, both 3R-and 4R-tau isoforms have been associated with FTDP-17, depending on the specific mutation incurred (Buee and Delacourte 1999; de Silva, Lashley et al. 2006; Hu, Parisi et al. 2007). Whether the main tau isoform in FTLD tauopathies has any bearing on the underlying pathophysiology of these disorders is currently unclear.

1.5 Motor Neuron Disease (MND) and FTLD-U

The possible association of FTLD and MND was reported as early as 1929, and this relationship was further strengthened in the following decades by an astounding number of recorded cases (Neary, Snowden et al. 2000; Bak and Hodges 2001). In these patients, the cognitive and psychiatric symptoms characteristic of FTLD occur in the presence of classical MND, commonly known as amyotrophic lateral sclerosis (ALS). The primary features of ALS are indicative of both upper and lower MND and include spasticity and hyperreflexia in the presence of wasting, weakness, and fasciculations. Interestingly, while the prevalence of dementia amongst sporadic and familial ALS patients is considered to be less than 5% and 15% respectively (Hartikainen, Helkala et al. 1993), several studies suggest that dementia rates may actually be as high as 28-48% in ALS populations (Rakowicz and Hodges 1998; Ringholz, Appel et al. 2005). Moreover, Lomen-Hoerth et al. recently demonstrated that up to 50% of ALS patients have frontal lobe dysfunction and may meet the diagnostic criteria for FTLD (Lomen-Hoerth, Murphy et al. 2003). Finally, 15% of FTLD patients develop concomitant ALS(Lomen-Hoerth, Anderson et al. 2002), an important consideration since FTLD-MND patients experience more rapid disease progression and death within three years of onset (Hodges, Davies et al. 2003).

A complementary line of evidence for the posited relationship between FTLD and ALS is suggested by the pathological findings in these diseases. In ALS, intracytoplasmic neuronal ubiquitin-immunoreactive inclusions are present in both the anterior horn cells of the spinal cord and, rarely, in pyramidal cells of the motor cortex. These inclusions are separate from the more filamentous Bunina bodies also seen in ALS, and are considered

characteristic features in ALS pathology (Leigh, Whitwell et al. 1991). In 1991, Okamoto et al. reported identical inclusions in the extramotor cortices of demented ALS patients (Okamoto, Hirai et al. 1991). These inclusions were observed within the small layer II neurons of the frontal and temporal cortices as well as in granule cells of the dentate gyrus of the hippocampus (Okamoto, Hirai et al. 1991; Okamoto, Murakami et al. 1992; Wightman, Anderson et al. 1992). To a lesser extent, inclusions were also identified in cortical layers III and V pyramidal cells and in the amygdala (Mann 1998). Moreover, the inclusions were differentiated using tau- and α-synuclein immunohistochemistry from other recognized intracytoplasmic bodies, including the Pick bodies of Pick's disease, neurofibrillary tangles of AD and neurofibrillary tangle dementia, and Lewy bodies of Parkinson's disease (PD) (Okamoto, Hirai et al. 1991). Subsequent studies demonstrated that the ubiquitin-positive inclusions previously considered unique to ALS were found not only in FTLD-MND cases, but also in cases of FTLD without motor neuron pathology (Jackson, Lennox et al. 1996). These cases were termed, FTLD-MND-type, which, when taken together with FTLD-MND cases, compose the pathological category of FTLD-U.

1.6 The Genetics of FTLD-U

The variability in the clinical and pathological presentation of FTLD is paralleled by the complexity of its genetic etiology. Nearly half of all FTLD patients present with a positive family history of dementia, with a majority of cases demonstrating an autosomal-dominant pattern of inheritance (Goldman, Farmer et al. 2005; Rollinson, Rizzu et al. 2009). In the past decade, several genes and chromosomal loci have been associated with

FTLD pathogenesis. In 1998, mutations in the gene encoding the microtubule-associated protein tau (*MAPT*) on chromosome 17q21 were identified to cause FTDP-17 (Hutton, Lendon et al. 1998; Poorkaj, Bird et al. 1998; Spillantini, Murrell et al. 1998). Since then, at least 40 different tau mutations have been identified in over 100 families with tau-based neuropathology, accounting for 10-20% of familial FTLD cases (Rademakers, Cruts et al. 2004). Notably, a number of other families have been reported with linkage on chromosome 17q21, but without *MAPT* mutations or tau aggregates (Bird, Wijsman et al. 1997; Froelich, Basun et al. 1997; Lendon, Lynch et al. 1998; Rosso, Kamphorst et al. 2001). These families were instead reported to have FTLD-U pathology, suggesting that mutations in the same chromosomal region as *MAPT* may underlie FTLD-U pathogenesis. In 2006, the discrepancy in these families was explained by the discovery of mutations in the progranulin gene (*GRN*), only 1.7 MB centromeric of *MAPT* (Baker, Mackenzie et al. 2006; Cruts, Gijselinck et al. 2006). To date, more than 50 different pathogenic *GRN* mutations have been reported in more than 80 families, making these as common as *MAPT* mutations (Gass, Cannon et al. 2006; Eriksen and Mackenzie 2007; van Swieten and Heutink 2008). However, unlike tau, mutations in *GRN* do not cause an abnormal gain-of-function in the encoded protein that might result in the accumulation of aggregated progranulin. Instead, *GRN* mutations cause a loss-of-function (haploinsufficiency) by introducing premature termination codons or missense mutations that result in rapid mRNA degradation or nonfunctional protein expression (Baker, Mackenzie et al. 2006; Eriksen and Mackenzie 2007). Therefore, although these findings establish a genetic link between progranulin and FTLD-U pathogenesis, the downstream

pathways leading to intraneuronal protein accumulation and cellular dysfunction are not known.

In addition to the more common *GRN* mutations, familial FTLD-U has also been linked to rare genetic defects in valosin-containing protein (*VCP*) on chromosome 9p21, charged multivesicular body protein 2B (*CHMP2B*) on chromosome 3p11, and additional loci on chromosome 9p21-13, 9q21-22, and 17q24 with as yet undefined mutations (Rollinson, Rizzu et al. 2009). Mutations in *VCP* cause hereditary inclusion body myopathy and Paget's disease of the bone with frontotemporal dementia (IBMPFD), a rare autosomal dominant disorder (Watts, Wymer et al. 2004; Neumann, Mackenzie et al. 2007). Many of these patients are misdiagnosed at presentation with either Alzheimer's disease or with alternative distal myopathies (van Swieten and Heutink 2008). However, neuropathology in these patients is consistent with FTLD-U, revealing ubiquitin-immunoreactive neuronal intranuclear inclusions and dystrophic neurites in neocortical regions (Forman, Mackenzie et al. 2006; Kimonis, Fulchiero et al. 2008). The mutations in *CHMP2B* were identified in a large Danish family with FTLD linked to chromosome 3, and in a few other smaller families (Skibinski, Parkinson et al. 2005). Many of the members of the Danish family developed Parkinsonism, dystonia, and pyramidal signs late in the course of their disease (van Swieten and Heutink 2008). Notably, like progranulin, neither VCP nor CHMP2B have been shown to systematically accumulate in the ubiquitin-immunoreactive neuropathology. Finally, while the mutation associated with linkage disequilibrium on chromosome 9p21-13 has not yet been definitively identified, Rollinson et al. recently proposed ubiquitin-associated protein 1 (*UBAP1*) as a likely candidate gene in this region (Rollinson, Rizzu et al. 2009). Further

characterization of the roles of mutant genes in inclusion formation and cellular toxicity is essential for advancing our understanding of FTLD-U pathogenesis, and may be critical for the development of therapeutic options for this disorder.

1.7 FTLD-U and TAR DNA binding protein-43 (TDP-43)

1.7.1 Identification of TDP-43

Neurodegenerative diseases are often defined pathologically because most, if not all, are marked by the presence of protein aggregates (Hardy and Gwinn-Hardy 1998). These aggregates, including Lewy bodies in PD and amyloid plaques in AD, appear to result from the abnormal accumulation and processing of proteins, and may ultimately lead to neuronal dysfunction and cell death (Bence, Sampat et al. 2001). Characterization of the primary protein constituents of various neurodegenerative disease lesions has resulted in significant advances in the understanding of disease processes and thus the potential development of novel therapeutic approaches. One such example was the successful discovery of the Aβ peptide, the main constituent of amyloid plaques (Masters, Multhaup et al. 1985). This discovery has resulted in the development of the amyloid cascade hypothesis, the predominant view of AD pathogenesis (Selkoe 2004), and the delineation of APP processing events.

For years, the sparse distribution and small size of the inclusions in FTLD-U precluded the use of biochemical purification and identification techniques previously employed to isolate pathological lesions seen in other neurodegenerative diseases. As such, the protein components of the inclusion bodies in FTLD-U remained undefined,

leaving FTLD-U as virtually the only neurodegenerative disorder characterized by insoluble inclusions and deposits labeled by ubiquitin only (Bigio, Johnson et al. 2004). However, in 2006, Neumann et al. identified TAR DNA binding protein-43 (TDP-43) as a major component of ubiquitinated inclusions in FTLD-U and ALS (Neumann, Sampathu et al. 2006). To resolve the long-standing enigma regarding the composition of proteinaceous aggregates in FTLD-U, the authors generated murine monoclonal antibodies by using either high M_r (>250 kDa) or low M_r (20-30 kDa) fractions from FTLD-U frontal cortex urea extracts for the immunizations (Sampathu, Neumann et al. 2006). Hybridoma supernatants (~37,000) resulting from these inoculations were screened by immunohistochemistry (IHC) until several antibodies were shown to immunolabel the ubiquitinated pathologic features characteristic of FTLD-U (Sampathu, Neumann et al. 2006). The authors then performed 2-dimensional polyacrylamide gel electrophoresis (2D-PAGE) using FTLD-U urea fractions in multiple parallel gels (Neumann, Sampathu et al. 2006). Immunoblots with the monoclonal antibodies were performed on one set of gels, and the locations of immunoreactive spots were noted. These spots were then excised from parallel gels stained with colloidal blue, analyzed by liquid chromatography coupled with mass spectrometry (LC-MS/MS), and identified as amino acid residues corresponding to TDP-43. Finally, the authors demonstrated that TDP-43 specific antibodies labeled ubiquitin-immunoreactive cytoplasmic inclusions in FTLD-U and ALS (Neumann, Sampathu et al. 2006).

1.7.2 Biology of TDP-43

TDP-43 is a highly conserved 414 amino acid nuclear protein first shown to bind and repress the transactive response (TAR) DNA sequence of human immunodeficiency virus type 1 (Ou, Wu et al. 1995). In addition to this role as a transcriptional repressor, TDP-43 has been implicated in multiple functional pathways, including promoting the stability of human low molecular weight neurofilament (hNFL) mRNA (Strong, Volkening et al. 2007), and regulating the splicing of both apolipoprotein A-II (Mercado, Ayala et al. 2005) and the human cystic fibrosis transmembrane conductance regulator (CFTR) (Buratti, Dork et al. 2001). TDP-43 has also been shown to interact with survival of motor neuron protein (SMN) in nuclear bodies known as Gemini of coiled bodies (GEMs) (Wang, Reddy et al. 2002). Interestingly, the loss of SMN protein, either by genetic mutation or deletion, results in spinal muscular atrophy, a disorder characterized by degeneration of α-motor neurons (Zhang, Xing et al. 2006). The diverse physiological functions of TDP-43 are mediated by a number of well defined structural domains. These include two RNA recognition motifs involved in RNA binding functions and a C-terminal glycine-rich motif (Wang, Wang et al. 2004). The C-terminal domain does not bind RNA but instead participates in multiple protein-protein interactions and mediates the splicing of CFTR (Buratti, Brindisi et al. 2005).

1.7.3 Molecular Signature in FTLD-U

The molecular pathways underlying TDP-43 aggregation and its pathologic significance have not yet been fully elucidated. In FTLD-U, pathologic TDP-43 redistributes from the nucleus to the cytoplasm where it aggregates, undergoes post-

translational modifications, and is enzymatically hydrolyzed into C-terminal fragments (Neumann, Sampathu et al. 2006). This phenotype can be modeled in mammalian cells by mutation of a putative TDP-43 nuclear localization signal (NLS) (Winton, Igaz et al. 2008). Although the resultant perturbation of nuclear-cytoplasmic TDP-43 trafficking results in the accumulation of cytoplasmic TDP-43 (Winton, Igaz et al. 2008), this model does not address whether TDP-43-mediated toxicity occurs as a result of a loss of function of TDP-43 in the nucleus or via a toxic gain of function independent of its normal cellular role. Recently, Johnson et al. demonstrated that TDP-43 aggregation could be recapitulated and studied in *Saccharomyces cerevisiae* (Johnson, McCaffery et al. 2008). While TDP-43 is not normally expressed in yeast, analyses in this model suggested that aggregating forms of TDP-43 are toxic, and that this toxicity is dependent on the C-terminal fragmentation of the protein. Currently, the specific protease responsible for generating truncated fragments of TDP-43, and thus imparting to the protein a toxic gain of function phenotype, is unknown. However, several groups have suggested that caspases may play a role in TDP-43 proteolytic cleavage (Zhang, Xu et al. 2007; Rohn 2009). TDP-43 has three potential caspase cleavage sites predicted to produce fragments of sizes matching those seen in disease. Moreover, both caspase-3 and caspase-7 have been shown to cleave TDP-43 in *in vitro* assays (Zhang, Xu et al. 2007). Interestingly, inhibition of caspase-mediated processing of TDP-43 using a caspase-resistant mutant protein does not prevent the deposition of insoluble TDP-43 (Dormann, Capell et al. 2009), bringing into question the functional relevance of TDP-43 caspase cleavage and the importance of C-terminal fragments in cellular toxicity.

TDP-43-immunoreactive aggregates have been identified in cell bodies and neurites of neurons and glia in affected brain regions of FTLD-U patients (Grossman, Wood et al. 2007). Based on the morphological characteristics and distribution of these aggregates, four histologic FTLD-U subtypes have been proposed. Not surprisingly, this classification of subgroups has been further complicated by the existence of two independent and competing organizational schemes with differing numbering systems (Mackenzie, Baborie et al. 2006; Sampathu, Neumann et al. 2006). In a proposed consensus scheme (Cairns, Bigio et al. 2007), histological type 1 cases are characterized by the presence of abundant dystrophic neurites in superficial cortical layers, with relatively few neuronal cytoplasmic inclusions (NCIs) and no neuronal intranuclear inclusions (NIIs). In histological type 2 cases, the primary pathological features are NCIs in the hippocampal dentate granule cells and both deep and superficial cortical layers. These cases may also have infrequent neuritic profiles and no NIIs. In contrast with the first two histological FTLD-U subtypes, type 3 cases may contain variable numbers of NIIs, typically with a "cat's eye" or "lentiform" appearance. These cases are also characterized by the presence of both NCIs and neuritic inclusions in superficial layers of the frontal and temporal cerebral cortex. FTLD-U cases with *GRN* mutations exclusively show this subtype of histology (Cairns, Bigio et al. 2007). Finally, rare histological type 4 cases, which are exclusively associated with *VCP* mutations, can be distinguished by a predominance of NIIs with few NCIs and immunoreactive neurites. Interestingly, in this subtype of FTLD-U, the pathological features are primarily restricted to the neocortical areas with relative sparing of the hippocampus (Cairns, Bigio et al. 2007). It is worth noting that these FTLD-U neuropathologic subgroups have been proposed to correlate

with specific clinical syndromes. For example, histological type 2 cases have been associated with both clinical FTD and FTLD-MND (Mackenzie, Baborie et al. 2006). However, establishing the reliability of these associations requires further investigation.

1.7.4 Genetic Variation

Although significant heterogeneity exists in the appearance and distribution of FTLD-U inclusions, these pathological features are, with rare exceptions, immunoreactive to TDP-43 (Geser, Martinez-Lage et al. 2009). Since protein aggregates in familial tauopathies contain insoluble tau deposits, there has been significant interest in examining both familial and sporadic FTLD-U cases for variation in the gene encoding TDP-43 (*TARDBP*) on chromosome 1p36. Interestingly, despite the accumulation of TDP-43 in these disorders, association studies in cohorts from Germany and the United Kingdom (Manchester cohort) did not reveal evidence of TDP-43 variation increasing risk for FTLD (Rollinson, Snowden et al. 2007; Schumacher, Friedrich et al. 2009). Moreover, sequencing of *TARDBP* coding regions in a Belgian series of sporadic FTLD patients did not identify any variants predicted to affect the encoded protein (Gijselinck, Sleegers et al. 2009). Finally, in a series of 149 French patients with FTLD-MND, sequencing revealed a single pathologic heterozygous missense mutation in exon 6 of two unrelated patients (Benajiba, Le Ber et al. 2009). A separate mutation in exon 6 was subsequently identified in a single patient with FTLD, supranuclear palsy, and choreiform movements, but without MND (Kovacs, Murrell et al. 2009). Although no additional variants have been reported in patients with a history of FTLD, there are currently more than 20 missense mutations in *TARDBP* linked to individuals with both

familial and sporadic ALS (Gitcho, Baloh et al. 2008; Kabashi, Valdmanis et al. 2008; Sreedharan, Blair et al. 2008; Van Deerlin, Leverenz et al. 2008; Yokoseki, Shiga et al. 2008). These mutations are located in the C-terminal glycine rich region of the protein, suggesting a functional role for C-terminal fragments in neurodegeneration (Benajiba, Le Ber et al. 2009; Dormann, Capell et al. 2009).

1.7.5 Disease Specificity of TDP-43

Despite the recent findings associating mutations in the *TARDBP* gene with FTLD and ALS, the specificity of pathologic TDP-43 has been questioned. Concomitant TDP-43 pathology similar to that found in FTLD-U has now been identified in up to 30% of Alzheimer's disease patients (Amador-Ortiz, Lin et al. 2007; Higashi, Iseki et al. 2007; Hu, Josephs et al. 2008; Uryu, Nakashima-Yasuda et al. 2008), 70% of cases with hippocampal sclerosis (Amador-Ortiz, Lin et al. 2007), 15% of CBD cases (Uryu, Nakashima-Yasuda et al. 2008), and as many as 30% of cases with Lewy body degeneration (Nakashima-Yasuda, Uryu et al. 2007). In addition, TDP-43 immunoreactivity has also been reported to colocalize with Pick bodies in a small proportion of Pick's disease cases (Geser, Martinez-Lage et al. 2009). As it is common for neurodegenerative diseases to exhibit overlapping pathologic profiles, these findings may simply reflect co-morbidity among these disorders (Uryu, Nakashima-Yasuda et al. 2008). However, it is also possible that TDP-43 may not be a specific marker of FTLD-U, suggesting that another, as yet unidentified, protein may be the primary component of ubiquitinated inclusions.

1.8 Proteomics in Neurodegenerative Diseases

1.8.1 Proteomics Platforms

The term "proteome" was first used by Marc Wilkins in 1996 to describe the set of all expressed proteins in a cell, tissue, or organism at a specific time (Wilkins, Sanchez et al. 1996). Cellular proteomes are entirely dynamic and may be regulated in response to various stressors by cellular alteration of protein synthesis and degradation (Greenbaum, Colangelo et al. 2003). Additionally, proteins may also be modified posttranslationally to control protein localization, abundance, and interaction, resulting in changes of protein activity and function (Banks, Dunn et al. 2000). For example, even if a protein can undergo only three post-translational modifications (e.g. phosphorylation, ubiquitination, acetylation), it may exist in eight potential protein forms if the modifications occur at a single site and are not mutually exclusive (Peng and Gygi 2001). With ~300 already recognized modification types and the high likelihood of multiple modification sites on a single protein, there can potentially be impressive diversity in protein modification states (Peng and Gygi 2001). While high throughput genomic techniques, such as cDNA microarrays and other methods based on mRNA expression, can also be applied to examine the differential gene expression in neurodegenerative diseases, the diversity of the proteome, and the added complexity from transient protein-protein interactions (Marcotte, Srivastava et al. 2003), highlights the necessity for proteomics methodologies in the study of these disorders.

Current proteomics technologies are centered on two core methods: two dimensional gel coupled with protein identification by mass spectrometry (2D gel-MS),

and LC-MS/MS **(Figure 1.4)**. In 2D gel-MS analysis, several hundreds to even thousands of protein spots are resolved by gel electrophoresis, detected, and quantified by software-assisted methods (Peng and Gygi 2001; Aebersold and Mann 2003). Protein spots displaying significant changes in abundance are excised, digested into peptides and identified by mass spectrometry in a highly automated manner. Though this method has been used successfully in many applications, including in the identification of differentially expressed proteins in neurodegenerative diseases, it is labor-intensive and very difficult to automate (Thomas 2001). The resultant potential for human error, especially when selecting 2D gels spots for sequencing, is one of several limitations of this technique. 2D-PAGE is often inadequate for complete separation of complex mixtures and, in particular, proteins of extreme *pI*, molecular weight, and hydrophobicity (Palzkill 2002). It also has narrow sensitivity and difficulties with detection of lower concentration proteins in the presence of more abundant ones (Shevchenko, Jensen et al. 1996). Finally, the 2D gel is severely affected by protein co-migration to the apparent same spots shown on the gel (Peng and Gygi 2001), confounding the identification of specific proteins.

To alleviate these limitations, alternative strategies such as LC-MS/MS have emerged and quickly become central in proteomics (Hunt, Henderson et al. 1992; Aebersold and Mann 2003). In this method, protein samples are first digested with a protease (e.g. trypsin) to generate peptides that are further fractionated by reverse phase liquid chromatography (RP LC). The peptides are then ionized and transferred into a mass spectrometer, where they are resolved based on mass-to-charge ratio (*m/z*). It should be mentioned that tandem mass spectrometry (MS/MS) itself is a high resolution

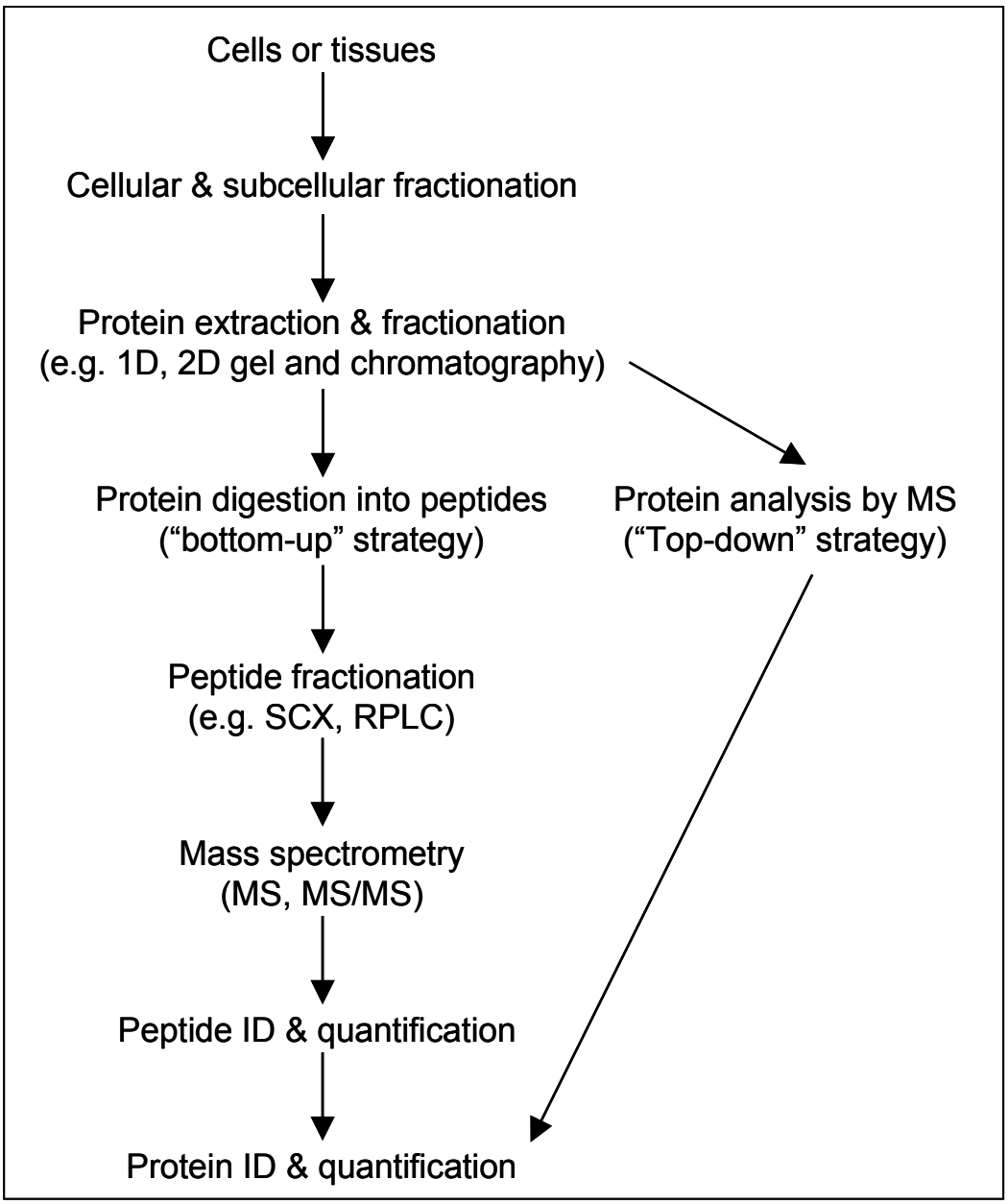

Figure 1.4 Strategies for mass spectrometry-based proteomic analysis. Proteins from biological samples are separated and analyzed as demonstrated in this schematic. For analysis via the "Top-down" approach, separation occurs at the protein level whereas for "Bottom-up" strategies, proteins are digested into peptides that are more amenable to separation and ionization. Data processing for protein identification and quantification is accomplished with advanced bioinformatics software.

separation tool, because it can physically isolate a peptide ion according to its *m/z* value (Hunt, Yates et al. 1986) despite the presence of many other co-eluting peptides. The isolated peptide is then fragmented to generate its specific MS/MS spectrum containing its sequence information (Yates, McCormack et al. 1997). Bioinformatics software can be utilized to match the experimental MS/MS spectra with theoretical (computer-produced) spectra of predicted peptides from a database to identify peptide sequences (Eng, McCormack et al. 1994). The latest mass spectrometers allow the identification of thousands of peptide/protein sequences from complex mixtures of proteins due to their fast MS/MS acquisition rates and exquisite detection sensitivity in the femtomole range (McCormack, Schieltz et al. 1997). Finally, LC-MS/MS approaches may also be used for protein/peptide quantification based on stable isotope labeling (Gygi, Rist et al. 1999) or even extracted ion current in unlabeled samples (Ong and Mann 2005). Stable isotopes can be introduced into samples by adding isotopically labeled synthetic peptides or recombinant proteins, labeling samples chemically or enzymatically *in vitro*, or incorporating the isotope metabolically *in vivo* (Ong and Mann 2005). Thus, the technique of LC-MS/MS has emerged as the method of choice for large scale proteomics (Aebersold and Mann 2003).

1.8.2 Proteomics in Alzheimer's Disease

The application of proteomic technologies in the field of neurodegeneration represents an escalating trend aimed at identifying proteins involved in the onset and progression of these disorders. Although neurodegenerative diseases such as Parkinson's disease, Huntington's disease, and ALS have been, at least superficially, studied, over the last few

years, much attention has focused on the proteomic characterization of AD, the most common cause of dementia in the elderly (Goedert and Spillantini 2006). The studies highlighted here focus not only on the large-scale unbiased profiling of amyloid plaque proteins, but also include a quantitative assessment of Aβ content. Although this is by no means a complete review of AD proteomics, these studies provide a reference for the application of proteomics technologies in the study of neurodegenerative disease.

AD has a particularly complex pathogenesis that involves multiple mechanisms including neuronal cell death, aggregated protein accumulation, oxidative damage, and chronic inflammation (Nunomura, Perry et al. 2001; Tuppo and Arias 2005). As a result, a diverse array of factors that contribute to disease initiation and propagation must be elucidated. Though genetic studies have identified several important mutations that contribute to familial AD, these methods cannot provide direct information regarding functionally active proteins. Moreover, the discovery of the genetic risks, such as that conferred by the ε4 allele of apolipoprotein E (ApoE), suggests that many of the AD-associated polymorphisms will follow complex, non-autosomal dominant patterns that may prove difficult to expose (Selkoe 1999). Therefore, considerable effort has been directed at the analysis of protein abnormalities and the breakdown of proper protein interaction in the AD brain using proteomics approaches (Butterfield and Castegna 2003). These systematic investigations have exploited the rapidly improving technologies available for proteomic profiling to further clarify and define AD disease mechanisms.

The earliest large-scale analyses of AD brains were conducted using the traditional proteomics approach of 2D gel separation, often in combination with mass spectrometry. Such studies were preferable to immunological methods that allow

structural characterization and localization, but focused only on a limited number of predetermined targets based on antibody specificity. In contrast, proteomics can cover larger and more complicated protein networks (Tsuji, Shiozaki et al. 2002) that are more representative of the complex cellular protein alterations that occur during AD. In one such early study, Mattila and Frey (Mattila and Frey 1994) resolved ~800 separate protein spots in 2D gel electrophoresis using proteins extracted from AD frontal cortical samples. Since the authors applied immobilized pH gradient (IPG) in the first dimension of electrophoresis to reduce pH gradient instability and enhance reproducibility (Corbett, Dunn et al. 1994), they were able to examine disease-related changes in protein expression by comparing the 2D maps of AD brain samples to those of unaffected controls. Though the specific proteins were not identified, four spots were markedly altered in these comparisons. One spot density was more strongly detected in AD than in control protein maps, while two spots were weaker and one was entirely absent. Conversely, a separate 2D gel analysis performed by Tsuji and colleagues (Tsuji, Shimohama et al. 1999; Tsuji and Shimohama 2001) on the temporal cortices of 15 AD patients and 15 age-matched controls demonstrated no spots that were present in controls but absent in AD. Additionally, of the 700 spots consistently identified in this study, nine spots were detected only in AD, five spots were increased in AD, and 28 spots were decreased in AD compared to normal controls. Though these results demonstrate the complexity of the inter-related AD pathological processes, they also highlight the importance of identifying the proteins exposed in these comparative studies. Without further characterization, the establishment of 2D gel databases of AD brain proteins cannot directly implicate the many pathways that contribute to disease pathogenesis.

Therefore, in a subsequent study (Tsuji, Shiozaki et al. 2002), Tsuji and colleagues applied mass spectrometry techniques to identify 35 proteins from 100 altered spots on their 2D map of AD. These spots included many proteins previously implicated in AD pathogenesis such as ApoE, α-synuclein, profilin II, β-enolase, and glutathione S-transferase P. Though these proteins accounted for only a fraction of the spots on the gel slab, the approach demonstrated the potential for the application of mass spectrometry as a rapid and sensitive method for the identification of critical proteins in neurodegenerative diseases.

Though the first step toward molecular understanding of the pathogenic mechanisms of AD focused on complete proteome analysis of AD versus non-diseased human tissues, several recent proteomics studies have concentrated on profiling specific pathologic features isolated or purified from post-mortem AD tissues. In particular, great emphasis has been placed on the identification of the proteinaceous components of senile plaques as a result of their central role within the amyloid cascade hypothesis, the proposal that the accumulation of Aβ in the brain is the primary insult driving AD pathogenesis (Hardy and Selkoe 2002). This fundamental role implies vast potential for the identification of therapeutic targets or disease biomarkers. Moreover, the specific profiling of plaques and Aβ-associated proteins may also provide a spatial context, absent in the analysis of whole brain, which may help clarify the roles of these proteins in AD neurodegeneration. The most important advantage is the significant improvement in the dynamic range of proteins covered regardless of the proteomics approach (Pieper, Gatlin et al. 2003). The purification of amyloid plaques, therefore, results in enhanced resolution

of low abundance-proteins and the identification of more proteins within each complex sample.

The enrichment of amyloid plaques and their low abundance proteins, which may mediate disease onset and progression, has been approached via several strategies. One such strategy employed traditional brute force biochemical purification techniques (Glenner and Wong 1984) and focused on the characterization of detergent-insoluble proteins from AD postmortem tissues (Woltjer, Cimino et al. 2005). More specifically, serial extractions of temporal cortex gray matter from five late-onset AD cases were performed using 1% Triton X-100 and N-lauroylsarcosine (sarkosyl). The resultant insoluble material was extracted with 70% formic acid and subsequently examined via LC-MS/MS. Though this approach does not specifically purify amyloid plaques, the analyzed samples correspond to detergent-insoluble material derived primarily from plaques and neurofibrillary tangles (Glenner and Wong 1984; Masters, Simms et al. 1985; Lee, Balin et al. 1991). The resultant samples were, therefore, enriched for aggregated plaque-related proteins. LC-MS/MS analysis identified 125 proteins derived from various functional categories including mitochondrial, cytoskeletal, and ubiquitination proteins (Woltjer, Cimino et al. 2005). Fifteen representative proteins were subsequently verified by Western blotting. These data support previous immunohistochemical and analytical findings indicating the involvement of a wide range of protein species in senile plaques (Atwood, Martins et al. 2002). More importantly, they demonstrate that, in addition to the well characterized Aβ and tau, AD aggregates include other insoluble protein species.

The use of classical biochemical purification techniques in the 1980's to enrich for neuritic plaque components produced significant advances in the understanding of the molecular pathogenesis of AD (Glenner and Wong 1984; Wong, Quaranta et al. 1985). The development of laser capture microdissection (LCM) technology over the past ten years (Emmert-Buck, Bonner et al. 1996), has given investigators a new approach to isolating these defined anatomical structures. In 2004, our group combined LCM with the highly sensitive LC-MS/MS to conduct a large scale proteomic analysis of AD amyloid plaques (Liao, Cheng et al. 2004). By staining postmortem AD tissue sections with thioflavin-S, we were able to visualize and capture ~2000 senile plaques which were compared with non-plaque regions from the same case. Analysis of the captured material via LC-MS/MS analysis identified 488 plaque proteins in two AD cases, covering as much as 80% of the proteins previously shown to localize to Aβ plaques. Since many of the proteins were also identified in non-plaque cortical regions, a relative quantitation method was employed in order to assess the changes in protein expression between plaque and non-plaque samples. This label-free quantitative method revealed 26 proteins with at least 2-fold enrichment in senile plaques. Such differential expression of proteins is indicative of the complexity of these pathological lesions. In fact, the enriched proteins corresponded to a diverse set of physiologic roles including chaperones, cytoskeletal proteins, cell adhesion proteins, inflammatory proteins, and ubiquitin-proteasomal system components. Importantly, the quantitation revealed the Aβ peptide to be 80-fold enriched in the plaques, significantly more than any other protein, despite the use of only 2% SDS to solubilize proteins (Masters, Simms et al. 1985) from the LCM caps. As the recognized major protein component of plaques (Glenner and Wong 1984), the

demonstrated enrichment of Aβ further validates the quantification techniques applied in this study, and confirms the utility of LC-MS/MS as a first-stage approach to large-scale analysis of proteins in AD plaques.

Although the relative quantitation method described above provides a novel approach to profile the differential expression of a large number of proteins, techniques based on the spiking of samples with isotopically labeled analogues to specific proteins of interest allow for more accurate and sensitive measurements of protein level. In particular, when the protein of interest can be anticipated at the time of the study, quantification of the protein in absolute molar terms can be achieved by the use of an internal standard that is a chemically-identical peptide isotopically labeled with heavier mass (Gerber, Rush et al. 2003). This approach was applied in the quantitative evaluation of both amyloid deposition and composition in the plaques of human AD brains (Rufenacht, Guntert et al. 2005). By spiking various synthetic ^{15}N-labeled Aβ peptides into senile plaque samples captured via LCM from human cortical post-mortem brain tissue, Rüfenacht and colleagues were able to analyze directly the Aβ plaque content using matrix-assisted laser desorption/ionization time-of-flight (MALDI-TOF) mass spectrometry. Quantitation was performed by comparing the mass spectral peak height of the two most dominant peaks generated from Lys-C proteolytic digestion (N-terminal fragments $A\beta_{1-16}$ and $A\beta_{17-28}$) to their respective internal standard fragment peaks. In human tissue, the amount of Aβ peptide per excised plaque was calculated to be 61±26fmol. Interestingly, we roughly estimated the amount of total protein extracted from ~2000 excised plaques to be 4 μg (Liao, Cheng et al. 2004). Given the small molecular weight of the Aβ peptide, these findings imply the presence of many other

protein constituents in senile plaques. Despite further immunohistochemical support for the complexity of plaque composition (Atwood, Martins et al. 2002), Rüfenacht and colleagues were only able to identify two proteins in addition to the Aβ peptide: cystatin A and ubiquitin. Therefore, the future absolute quantification of minor plaque components would require significant sensitivity optimization and protein separation in order to reliably detect scarce proteins present in sub-femtomole levels.

1.8.3 Proteomics in FTLD

To date, only a small number of proteomic studies in the field of FTLD are published. Among them Schweitzer et al. describes the identification of 24 differentially expressed proteins in FTDP-17 frontal cortex using 2D-gel and matrix-assisted laser desorption/ionization - time of flight (MALDI-TOF) mass spectrometry strategy (Schweitzer, Decker et al. 2006). The expression of ubiquitin C-terminal hydrolase (UCHL-1) appears to be reduced in FTDP-17, along with altered levels of multiple cytoskeletal and oxidative stress response proteins. Notably, mutations in UCHL-1, a neuronal de-ubiquitinating enzyme, have been linked to early-onset familial PD (Dawson and Dawson 2003), and downregulation of the protein has also been observed in sporadic AD and PD (Choi, Levey et al. 2004). From these results, the authors implicate ubiquitin-mediated degradation as well as the global oxidative stress response in the pathogenesis of FTDP-17 (Schweitzer, Decker et al. 2006). Finally, the remaining FTLD studies have focused on the use of proteomics to discover biomarkers in cerebrospinal fluid (CSF) from clinically-diagnosed patients (Davidsson, Sjogren et al. 2002; Hansson, Puchades et al. 2004; Ruetschi, Zetterberg et al. 2005). The authors in these studies used either 2D gel

with subsequent MALDI-TOF mass spectrometry or directly analyzed the samples using surface-enhanced laser desorption/ionization (SELDI)-TOF approaches. In the latter strategy, CSF from 16 patients was compared to that of 12 normal controls. Five ion peaks with good signal-to-noise ratio and resolution were significantly increased and five were decreased in FTLD samples, including peaks corresponding to transthyretin, cystatin C, and neurosecretory protein VGF (Ruetschi, Zetterberg et al. 2005). Although the combination of these ten biomarkers discriminated FTLD from non-demented controls with a sensitivity of 94%, a specificity of 83%, and an accuracy of 89% (Ruetschi, Zetterberg et al. 2005; Westman-Brinkmalm, Ruetschi et al. 2009), additional studies are necessary to aid in the diagnosis, and monitor the progression, of specific FTLD clinical and pathological subtypes.

1.9 Proposed Research

The goal of this dissertation is to identify important functional molecules involved in the cascade of events which ultimately leads to neurodegeneration in FTLD-U. To address this goal, we elected to examine accumulations of detergent-insoluble proteins and aggregates, as these are the pathologic hallmarks of neurodegenerative diseases. The use of quantitative proteomics approaches is essential to provide an unbiased high-throughput profile of important differentially expressed proteins in our disease samples. We hypothesized that altered proteins in FTLD-U mediate the pathogenesis and progression of this disease. Thus, their identification will enhance our understanding of FTLD-U mechanisms and may help guide the development of targeted therapies for this devastating disorder.

Aim 1: To identify disease-relevant insoluble or aggregate-associated proteins via laser capture microdissection (LCM) or biochemical fractionation. LC-MS/MS is a powerful proteomics approach that allows identification and quantification of thousands of differentially-expressed proteins by coupling chromatographic separation with a mass spectrometer capable of data-dependent acquisition of MS/MS fragmentation spectra (Peng and Gygi 2001). We applied this well-established method to examine pathological aggregate composition in FTLD-U. We analyzed proteins extracted from laser-captured hippocampal dentate granule cells, and revealed the limitations of coupling LCM and LC-MS/MS in FTLD-U samples. In addition, we demonstrated that a strategy focused on the detergent-insoluble sub-proteome can identify disease-specific proteins, and is broadly applicable for the study of neurodegenerative disorders.

Aim 2: To characterize the spatial distribution, disease specificity, and mechanistic contribution of candidate proteins in FTLD-U. Proteins found to be uniquely and/or differentially expressed in FTLD-U are considered as potential candidates for important roles in disease pathogenesis. In Aim 2, we focused on two specific proteins that were identified in Aim 1: TDP-43 and septin 11 (SEPT11). While TDP-43 has already been identified as a major component in FTLD-U (Neumann, Sampathu et al. 2006), we established a cellular model for the study of the mechanisms underlying its aggregation. Moreover, we explored potential post-translational modifications of this important disease protein. For SEPT11, we validated the changes in protein levels suggested by the proteomics analysis, and we established a pathologic association of this candidate with FTLD-U. Finally, we demonstrated that detergent-insoluble SEPT11 is proteolytically cleaved and accumulates specifically in FTLD-U, providing insights into the pathogenesis of this complex disorder.

Chapter 2.

Materials and Methods

2.1 Case Material

Post-mortem human brain tissues corresponding to diagnoses of AD, FTLD-U, PD, ALS, tauopathy, and unaffected control were obtained from the Alzheimer's Disease Research Center (ADRC) and Center for Neurodegenerative Disease (CND) Brain Bank at Emory University School of Medicine. Neuropathological assessment of AD was made according to the Consortium to Establish a Registry for Alzheimer's Disease (CERAD) criteria (Mirra, Heyman et al. 1991) as well as the National Institute on Aging (NIA)-Reagan criteria (1997). The diagnosis of FTLD-U was based on consensus criteria (McKhann, Albert et al. 2001; Trojanowski and Dickson 2001; Cairns, Bigio et al. 2007), with all cases exhibiting small, ubiquitin-positive, tau- and α-synuclein-negative neuronal cytoplasmic inclusions and immunoreactive dystrophic neurites in the hippocampal dentate gyrus or frontotemporal cortex. Additionally, TDP-43 immunoreactivity was histochemically confirmed in all FTLD-U cases. Diagnoses of PD/Lewy Body Dementia (McKeith, Dickson et al. 2005), ALS (Brownell, Oppenheimer et al. 1970; Ince, Lowe et al. 1998; Mackenzie, Bigio et al. 2007), and tauopathy (Hauw, Daniel et al. 1994; Dickson 2001; Dickson, Bergeron et al. 2002; Zhukareva, Mann et al. 2002) were also made based on established criteria. Finally, control cases had neither a clinical history nor a neuropathologic diagnosis of neurologic disease.

DNA samples were collected and stored using standard procedures. Briefly, blood samples collected by the Emory University Clinical Core were sent by courier to the Neuropathology Core laboratory for processing. Samples were centrifuged at 3000 rpm for ~15 min and labeled with a 6-digit research ID. For each patient, the following samples were collected as follows: 2mL of serum, 2mL of plasma, and a maximal amount of buffy coat. DNA was then extracted from 200µL of buffy coat with a Qiagen extraction kit (Qiagen, Valencia CA). All samples (plasma, serum, buffy coat, and DNA) were stored in secured, dedicated -80°C freezers.

2.2 Antibodies

Commercially available primary antibodies used in these studies were to the proteins septin 3 (goat polyclonal; Abcam, Cambridge MA), septin 7 (rabbit polyclonal; Santa Cruz Biotechnology, Santa Cruz CA), glial fibrillary acidic protein (mouse monoclonal; DAKO, Carpinteria CA), Tau2 (mouse monoclonal; Chemicon International, Temecula CA), ApoE (goat polyclonal; Calbiochem, Darmstadt, Germany), ankyrin B (mouse monoclonal; Santa Cruz Biotechnology), serine protease 15 (rabbit polyclonal; Atlas Antibodies, Stockholm, Sweden), YWHAH (rabbit polyclonal; Aviva Antibody Corporation, San Diego, CA), ATP6V0D1 (mouse monoclonal; Novus Biologicals, Littleton CO), TDP-43 (rabbit polyclonal; Protein Tech Group, Chicago, IL), HA (mouse monoclonal clone 16B12, Covance, Emeryville CA), SUMO-2/3 (rabbit polyclonal; Zymed Laboratories, Invitrogen, Carlsbad, CA), neuron-specific enolase (rabbit polyclonal; Chemicon International), ubiquitin (rabbit polyclonal; DAKO), and Septin 11 (goat polyclonal; N-15; Santa Cruz Biotechnology).

In addition, K48 or K63 linkage-specific ubiquitin antibodies (humanized monoclonal antibodies) were a generous gift of Dr. V. M. Dixit (Newton, Matsumoto et al. 2008). In-house septin 11 antibody (rabbit polyclonal) was raised against keyhole limpet hemocyanin (KLH)-conjugated peptide AVAVGRPSNEELRN at the extreme N-terminus of the protein. Serum from the immunized rabbit was tested by immunoblot and affinity-purified on a column using the immunizing peptide.

2.3 DNA Constructs

The full-length TDP-43 coding sequence (nucleotides 1–1245, encoding amino acids 1–414) was amplified by PCR from a TDP-43 expression plasmid (Open Biosystems, Huntsville AL; Clone ID 3038905); the forward and reverse primers were 5'-GGTA*GGATCC*ATGTCTGAATATATTCGGGTAA-3' and 5'-TTATATA*GGGCCC*CT ACATTCCCCAGCCAGA-3', respectively. Similarly, the full-length Septin 11 coding sequence (nucleotides 1-1287, encoding amino acids 1-429) was also amplified from a commercial expression plasmid (Origene, Rockville MD; Clone ID TC113610) using forward primer 5'-AGCTGCGTCTAGAATGGCCGTGGCCGTGGG-3' and reverse primer 5'-ATACGATATTTCTAGAACTGCAAAAGCAGGTGAATG-3'. The PCR products were digested and cloned into the pcDNA3.1-HA expression vector downstream of the two-HA motifs (peptide YPYDVDYA). The TDP-S6 splice variant (nucleotides 1-888 (Wang, Wang et al. 2004), encoding amino acids 1-295) was also cloned into pcDNA3.1-HA. The three N-terminal HA expression vectors were confirmed by DNA sequencing (Agencourt Bioscience Corporation, Beverly MA). The SUMO-2 construct was a kind gift from Dr. Keith Wilkinson (Emory University) as described

(Mukhopadhyay, Ayaydin et al. 2006). Mature SUMO-2, with C-terminal diglycine at amino acid positions 92-93, was subcloned into pEGFP-C3 vector (CLONETECH Laboratories Inc., Mountain View CA).

2.4 Laser Capture Microdissection (LCM)

2.4.1 Preparation of Tissue for LCM

Isolation of hippocampal dentate gyrus granule cells by LCM was performed based on previously developed protocols (Emmert-Buck, Bonner et al. 1996; Goldsworthy, Stockton et al. 1999). Ethanol-fixed, paraffin-embedded 10μm-thick hippocampal sections mounted on uncoated and uncharged glass slides were deparaffinized in xylene and rehydrated. Sections were subsequently stained for 1 minute in Histogene Staining Solution (Arcturus, Mountain View, CA), differentiated in 75% ethanol for 1 min, subjected to dehydration in graded alcohols, cleared for 5 min in fresh xylene, and air-dried for 5 min. Finally, sections were desiccated prior to LCM (Emmert-Buck, Bonner et al. 1996).

2.4.2 LCM

LCM was performed using a Pixcell II laser capture system (Arcturus). Hippocampal dentate granule cells were visualized and captured with short-duration pulses (1ms) of an infrared laser (laser spot size: 7.5μm) using a laser power setting of 80-90 milliwatts. Typically, granule cells of the dentate gyrus from 3-4 consecutive

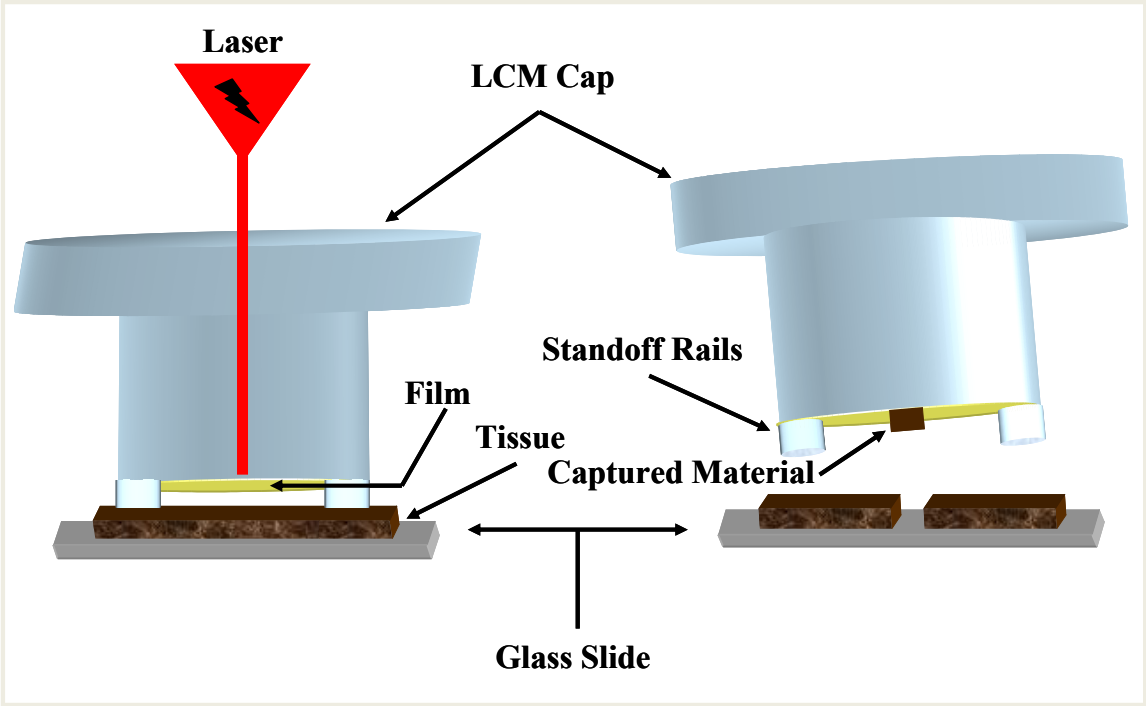

Figure 2.1 Laser capture microdissection. When a polymer-coated cap is placed on the top of fixed tissue, standoff rails prevent the direct contact of the coat with the tissue to reduce contamination. Under a microscope, a laser pulse generates enough energy to melt the coated film resulting in the gluing of the area of interest to the cap. Lifting the cap leads to the removal of targeted area of tissue.

sections were captured on a single CapSure Macro LCM cap (Arcturus) **(Figure 2.1)**, and 50-60 sections were processed from each individual.

2.4.3 Protein Extraction from LCM Caps

Prior to processing of the captured tissue, each cap was visually inspected for the capture of any contaminating material removed during the lifting of the transfer film of the cap from the slide. Granule cells from dentate gyri were clearly visualized since the morphology of captured material was unaltered during the transfer from the slide to the cap. The caps were then extracted with 20µl of lysis buffer composed of 2% sodium dodecyl sulfate (SDS), 10% glycerol, 10mM dithiothreitol (DTT), 1mM ethylenediaminetetraacetic acid (EDTA), and protease inhibitor cocktail (Roche Applied Science) in phosphate-buffered saline, pH 7.2. Following a 15 min extraction at 65^{o}C, the buffer was collected and replaced with a fresh 20µl aliquot of lysis buffer for a second incubation at 65^{o}C for 15 min. In order to minimize the volume of extracted protein samples, the lysis buffer was reused in the sequential extractions of up to 4 caps. Due to evaporation during each of the incubations at 65^{o}C, the lysis buffer volume was replenished with ddH_2O (warmed to 65^{o}C) during the transfer of buffer from one cap to the next so as to maintain appropriate lysis buffer solute concentrations for the following extraction. This procedure was repeated until all caps corresponding to a particular case were extracted, and the extracts were then pooled to produce one extracted sample for each case. Finally, to increase recovery of cysteine-containing peptides and promote the identification of thiol-containing peptides, the samples were alkylated in the dark at room temperature with 50mM iodoacetamide for 30 min after the extractions.

To normalize total proteins submitted for proteomic analysis, protein concentration was estimated from a modified silver staining (Shevchenko, Wilm et al. 1996) of 1-5% of the sample proteins resolved on a 6-12% SDS gel (0.75mm) for 4 hr (100mV for 0.75 hr; 250mV for 3.25 hrs). Proteins were quantified by densitometric analysis using Scion Image software (Scion Corporation, Frederick, MD) in comparison with standard protein markers previously quantified using known concentrations of BSA.

2.5 Sequential Biochemical Fractionation

2.5.1 Human Frontal Cortex

Sequential extractions were performed as described (Neumann, Sampathu et al. 2006) with slight modification **(Figure 2.2)**. Briefly, post-mortem frontal cortex was extracted at 5mL/g (volume/weight) with ice-cold low salt (LS) buffer (10mM Tris, pH 7.5, 5mM EDTA, 1mM DTT, 10% sucrose, 10mM b-glycerophosphate, 10mM sodium orthovanadate, 10mM tetrasodium pyrophosphate, 50mM sodium fluoride, 1x Roche complete protease inhibitor cocktail). Protein concentration of the resulting homogenate was determined by the bicinchoninic acid (BCA) method (Pierce, Rockford, IL). Cases were subsequently either extracted individually or as equally pooled samples. For label-free proteomics experiment of detergent-extracted samples, ten cases each of AD, FTLD-U, and unaffected controls were pooled by diagnosis (3mg total protein per case). Notably, the FTLD-U pool and subsequent extraction was duplicated to discern experimental variance.

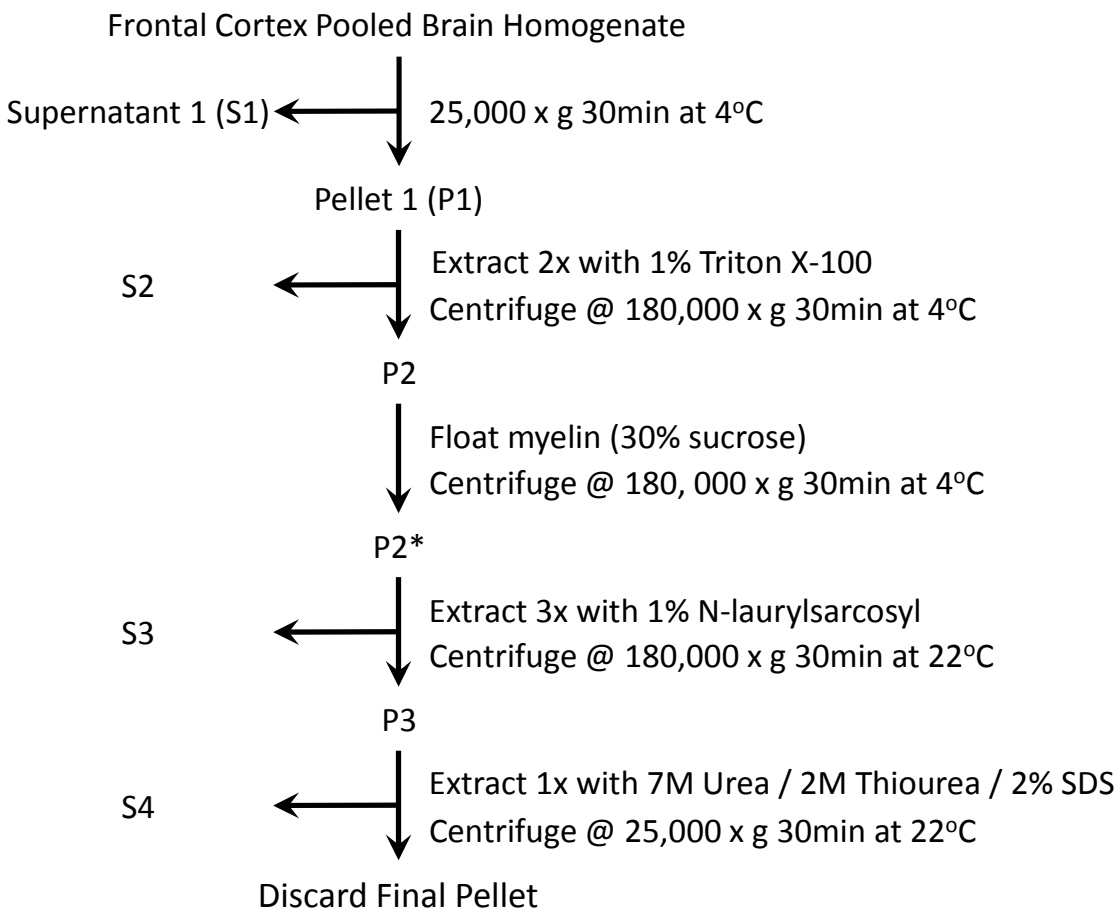

Figure 2.2 Diagram of sequential extraction protocol used to generate detergent-insoluble fractions for proteomic analysis.

Samples were centrifuged at 25,000 x g for 30 minutes at 4^{o}C and then washed with additional LS buffer. The resultant pellets were sequentially extracted with buffers of increasing stringency, including Triton X-100 (TX) buffer (LS buffer + 1% Triton X-100, 0.5M NaCl), myelin floatation (MF) buffer (LS buffer with 30% sucrose + 1 % Triton X-100, 0.5M NaCl), and sarkosyl (SK) buffer (LS buffer + 1% N-Lauroyl-sarcosine, 0.5M NaCl). Specifically, each sample was extracted with TX buffer and spun at 180,000 x g for 30 minutes at 4^{o}C to generate a Triton-insoluble fraction. Following two washes with TX buffer, this fraction was incubated with MF buffer and centrifuged at 180,000 x g as noted above. Pellets were then sonicated briefly, incubated in SK buffer for 30 minutes at room temperature, and centrifuged at 180,000 x g for 30 minutes at 22^{o}C. Two additional SK buffer washes were followed by extraction of the sarkosyl-insoluble fraction with urea buffer (30mM Tris, pH 8.5, 7M urea, 2M thiourea, 1% SDS), a brief sonication, and a final 30 minute centrifugation at 25,000 x g at 22^{o}C.

Since the BCA protein assay is incompatible with thiol reagents, final protein concentrations of urea-soluble fractions were obtained by estimating Coomassie Blue G-250 staining intensity of extracts (~2%) following electrophoresis in polyacrylamide gels using titrated BSA as a standard (10-fold range) (Xu, Duong et al. 2009). The gels were run ~5mm in order to increase the accuracy of quantification by concentrating the proteins in a narrow region. Signal intensity of proteins in stained gel was quantified by densitometry with an Odyssey Infrared Imaging System (Li-Cor Biosciences, Lincoln, NE). Generally, the protein yield in urea samples during sequential extraction was approximately 2.5% of the starting material.

2.5.2 Mammalian Cells

To examine the solubility of TDP-43 and TDP-S6, sequential extractions were performed as described previously (Neumann, Sampathu et al. 2006) with slight modification. Cells (~1 x 10^7) were washed twice, collected with ice-cold PBS buffer, and then lysed in SK buffer. Resulting lysates were spun at 180,000 x g for 30 min at 22^{o}C to generate the detergent-soluble samples. Insoluble pellets were washed three times with additional SK buffer, then extracted with urea buffer, and centrifuged at 25,000 x g for 30 min at 22^{o}C. Protein concentration was determined for sarkosyl fractions by the BCA protein assay (Pierce, Rockford IL) according to the manufacturer's instructions. For urea fractions, protein concentration was determined by estimating Coomassie Blue G-250 staining intensity of a small fraction of the urea extracts following electrophoresis in polyacrylamide gels using titrated BSA as a standard (Xu, Duong et al. 2009).

2.6 Proteomic Analysis

2.6.1 Stable Isotope Labeling With Amino Acids in Cell Culture (SILAC)

Cells were cultured in DMEM (deficient in L-Lysine and L-Arginine) supplemented with 5% dialyzed fetal calf serum (Invitrogen) as described (Ong and Mann 2006). For stable isotopic labeling, arginine and lysine were added in light (Arg0/Lys0, Sigma), medium (Arg6/Lys4), or heavy forms (Arg10/Lys8, Cambridge Isotope Laboratories, Andover MA) to a final concentration of 0.26 mM. Cells were cultured for seven passages to ensure full labeling, then transfected with pcDNA3.1-HA (mock), HA-TDP-43, and HA-TDP-S6 plasmids, respectively. After two days, the cells

were harvested, equally mixed, and lysed to prepare sarkosyl-insoluble, urea-soluble fractions as described above.

2.6.2 Analysis and Protein Identification by Mass Spectrometry

Proteins corresponding to LCM extracts, pooled urea samples, or SILAC-labeled samples were reduced with 10mM DTT and alkylated in the dark with 50mM iodoacetamide for 30 minutes. The samples were then separated on a 10% SDS gel (0.75 mm thickness) and stained with Coomassie Blue G-250 to both confirm equal sample loading and visualize proteins for subsequent processing. Each sample lane was then cut into five (urea samples) or six (LCM samples) gel bands and subjected to in-gel digestion (12.5 μg/mL trypsin) as previously reported (Shevchenko, Wilm et al. 1996). Briefly, Gel pieces were further fragmented into $1mm^3$ cubes in preparation for in-gel trypsin digestion. The fragments were first de-stained during a 10 min incubation in a buffer containing half acetonitrile and half 50mM sodium bicarbonate (NH_4HCO_3) by volume. Next, acetonitrile (100%) was applied to shrink the gel pieces by dehydration. At the end of the incubation, the acetonitrile was removed and the gel fragments were vacuum-dried. Trypsin was easily absorbed by the dry gel pieces by incubating with digestion buffer containing 12.5 ng/μl sequencing grade trypsin (Promega Corporation, Madison, WI) in 50mM NH_4HCO_3 on ice for 45 min. Additional 50mM NH_4HCO_3 (~ 10 μl) was added to each digestion reaction to keep the gel pieces wet during overnight proteolysis at 37^oC. Peptides were extracted from the gel pieces at room temperature by centrifugation for 1 min at 15,000 x g in a table-top microcentrifuge (Eppendorf Centrifuge 5417C, Eppendorf, Westbury, N.Y.) and subsequent collection of the supernatant. The extraction

was repeated 3 times per sample using an extraction buffer containing 5% formic acid and 50% acetonitrile. Supernatants of each extraction were pooled, vacuum dried, and stored at -20^{o}C until LC-MS/MS analysis.

The resulting peptides from each gel piece were dissolved in buffer A (0.4% acetic acid, 0.005% heptafluorobutyric acid, 5% AcN), loaded onto a C_{18} column (75 μm i.d., 10 cm long, ~300 nl/min flow rate) as described (Peng and Gygi 2001), and eluted over 2 hours during a 10-30% gradient of buffer B (0.4% acetic acid, 0.005% heptafluorobutyric acid, 95% AcN). The eluted peptides were detected by Orbitrap (350-1600 *m/z*, 1,000,000 AGC target, 1,000 ms maximum ion time, resolution 30,000 fwhm) followed by five (SILAC urea samples) or ten (LCM and pooled urea samples) data-dependent MS/MS scans in LTQ (3 *m/z* isolation width, 35% collision energy, 5,000 AGC target, 200 ms maximum ion time) on a hybrid mass spectrometer (Thermo Finnigan, San Jose, CA). Peaklists were generated by Xcalibur 2.0 SR2 software (Thermo Finnigan).

The acquired MS/MS spectra were searched against the human reference database (29,575 proteins) of the National Center for Biotechnology Information (January 2007 for LCM and pooled urea samples; December 2007 for SILAC urea samples) using the SEQUEST-Sorcerer algorithm version 3.11 r11 (Sage-N-Research, San Jose CA) (Eng, McCormack et al. 1994). Searching parameters included mass tolerance of precursor ions (±50 ppm) and product ions (±0.5 *m/z*), partially tryptic restriction, fixed mass shift for modification of carboxyamidomethylated Cys (+57.0215 Da), dynamic mass shifts for oxidized Met (+15.9949), Lys (+4.02511 for $^{4}H_2$ or +8.01420 for $^{13}C_6{}^{15}N_2$) and Arg (+6.02013 for $^{13}C_6$ or +10.00827 for $^{13}C_6{}^{15}N_4$), five maximal modification sites and three

maximal missed cleavages. Only *b* and *y* ions were considered during the database match. To compare medium and heavy labeled samples, searches were performed with static modifications +4.02511 on Lys and +6.02013 on Arg and dynamic modifications of +3.98909 on Lys and +3.98814 on Arg to account for mass difference between medium and heavy labeled peptides.

To evaluate false-discovery rate (FDR), all original protein sequences were reversed to generate a decoy database that was concatenated to the original database (a total of 53, 830 protein entries) (Peng, Elias et al. 2003; Elias and Gygi 2007). The FDR was estimated by the number of decoy matches (n_d) and total number of assigned matches (n_t). FDR = $2*n_d/n_t$, assuming mismatches in the original database were the same as in the decoy database. To remove false-positive matches, assigned peptides were grouped by a combination of trypticity (fully, partial and non-tryptic) and precursor ion-charge state (1+, 2+, 3+, and 4+). Each group was first filtered by mass accuracy (10 ppm for high-resolution MS), and by dynamically increasing XCorr (minimal 1.8) and ΔCn (minimal 0.05) values to reduce protein FDR to less than 0.2%. To remove redundancy during the assignment of identified peptides to proteins, all accepted proteins sharing peptides were grouped together and represented by the protein with the highest spectral count. Generally, following manual validation of the spectra (Peng, Elias et al. 2003), we accepted proteins identified by at least one unique peptide.

2.6.3 Label-free Quantification: Extracted Ion Current

Quantification of proteins in the LCM extracts and pooled urea samples was based on the comparison of paired peptides from 2 any two samples of interest (e.g.

FTLD-U / Control). Ion current intensities for identified peptides were extracted in MS survey scans of high-resolution, and a ratio of the peak intensities for the peptide precursor ion was calculated (Bondarenko, Chelius et al. 2002; Andersen, Wilkinson et al. 2003). For peptides identified in only one sample, corresponding non-sequenced ion peaks were identified for quantification in MS survey scans using the predicted *m/z*, and adjusted retention time. The resultant ratio is a measure of the relative abundance of the peptide in the two separate samples (Wang, Zhou et al. 2003). Statistical analysis to evaluate the significance of the protein changes and to correct for technical errors was performed as previously described with modifications (Li, Zhang et al. 2003; Cheng, Hoogenraad et al. 2006). Briefly, the peptide abundance ratios were logarithmically transformed ($\log_2$). The mean and associated variance of the transformed ratios was calculated for peptides quantified multiple times. Abundance ratios for all peptides of a particular protein were then averaged to determine the protein abundance ratio. A histogram of all protein abundance ratios was fitted with a normal distribution on the basis of the central limit theorem (bins of 0.25 or 0.3 = $\log_2$(ratio)). Because the majority of proteins likely display similar abundance in disease and control tissues, the abundance ratio for each protein was normalized by subtracting the fitted mean, as the mean should have been zero if sample preparation was ideal. Although most proteins in the data set correlate well with the fitted normal distribution, there are a few proteins demonstrating larger changes that distort the fit of the experimental distribution. These perturbations from the curve of the normal distribution represent proteins that are associated with disease, and presumably deviate from the normal population of unaltered proteins.

The quantified proteins were further manually examined to verify MS/MS assignment, ion peak matching, and ion intensity (signal-to-noise ratio ≥ 4). Proteins were scored in three categories, with 1 point awarded in each category: peptide quality, matching status, and extracted ion current. Proteins were scored for peptide quality if their quantitation was based only on fully tryptic peptides with no missed trypsin cleavage sites and no modifications. Only proteins whose quantitation was based on correctly matched peaks in each sample were scored for matching status. Finally, a score was awarded if the total extracted ion current for each peptide exceeded 4 times the moving average for noise level (signal to noise ratio ≥ 4).

2.6.4 Label-Free Quantification: Spectral Counts

To compare differences between the detergent-soluble and insoluble proteome for SILAC-labeled samples, we compared the identified proteins in both these samples based on spectral counts (SC). The spectral counts were first normalized to ensure that average SC per protein was the same in the two datasets (Kislinger, Cox et al. 2006). G-test was used to judge statistical significance of protein abundance difference (Xia, Liao et al. 2008). Briefly, the G-value of each protein was calculated as shown in equation (1).

$$G = 2 \times (S_{tc} \times \ln[S_{tc} \div ((S_{tc}+S_{si}) \div 2)] + S_{si} \times \ln[S_{si} \div ((S_{tc}+S_{si}) \div 2)]) \qquad (1)$$

where S_{tc} and S_{si} are the detected spectral counts of a given protein in the total cell lysate and in the sarkosyl-insoluble fraction, respectively, and "ln" is the natural logarithm. Although theoretical distribution of the G values is complex, these values approximately fit to the χ^2 distribution (one degree of freedom), allowing the calculation of related *p*-values.

2.6.5 SILAC Quantification and Bioinformatics Analysis

Quantitative pair-wise comparisons of control, TDP-S6- and TDP-43-transfected cells were carried out according to reported methods (Cheng, Hoogenraad et al. 2006; Xu, Duong et al. 2009) with slight modification. (i) Ion extraction from MS scans: The ion currents for identified peptides were extracted in MS survey scans of high-resolution (60,000), based on the isotopic ion selected for MS/MS sequencing. A number of parameters were defined, including precursor *m/z*, charge state, retention time, ion peak width, height, area, and noise level. The noise level was derived by averaging signal intensity of all ions in the MS scan after removing outliers that were at least two standard deviations away from the mean. The intensity of ions were presented by the peak height, and normalized according to the noise intensity under the assumption that the noise level of MS scans reflects, at least partially, variable ionization efficiency. The peaks used in the analysis had a minimal intensity of two signal-to-noise ratio. (ii) Ion matching among light, medium and heavy isotopes, with tolerance of 10 ppm. If a sequenced peptide could not be matched, we estimated that the maximum ion current for undetected signal was equal to the noise level, and used it to derive the peptide ratio. (iii) Data integration: The ratio of every peptide was transformed into logarithmic ($\log_2$) values that were averaged over all peptides of a particular protein to determine the protein ratio. If a protein was quantified by both matched peptide ratios and unmatched peptide ratios, only the matched data were averaged. (iv) Data normalization: According to the null hypothesis, the histogram of all protein $\log_2$ ratios was fitted to a Gaussian distribution to evaluate systematic bias (according to the mean) and experimental variation (based on standard deviation). The data were then normalized by subtracting the mean in every protein ratio.

The standard deviations (SD) in all SILAC comparisons were less than 0.4. (v) Data filtering: We selected the cutoff of $\log_2$ ratios that were outside a 95% confidence interval (~2 SD) from the mean of the Gaussian distribution. Finally, the quantified proteins were manually examined with respect to MS/MS assignment, ion peak matching and ion intensity.

2.6.6 Quantitative proteomics with culture derived isotope tags (CDIT)

HEK293 cells were cultured in DMEM (deficient in L-Lysine and L-Arginine) supplemented with 2% dialyzed fetal calf serum (Invitrogen) as described (Ong and Mann 2006). For stable isotopic labeling, heavy forms L-Arginine and L-Lysine were added (Arg10/Lys8, Cambridge Isotope Laboratories) to a final concentration of 0.13 mM. Excess proline was added at 200 mg/L to block arginine to proline conversion. Prior to SDS PAGE, 10 µg of heavy labeled HEK whole cell lysate was added to 10 µg of unlabeled urea fraction from 4 pooled FTLD-U or control cases. The mixed (light and heavy) samples were reduced with 10 mM DTT, and resolved on a 10% polyacrylamide SDS gel. After staining with Coomassie blue, each gel lane was cut into five gel bands, and bands were subjected to in-gel digestion (12.5 µg/ml trypsin). Extracted peptides were loaded onto a C_{18} column (75 µm i.d., 10 cm long, ~300 nl/min flow rate, 5 µm resin from Michrom Bioresources, Auburn, CA) and eluted during a 10-30% gradient (Buffer A: 0.4% acetic acid, 0.005% heptafluorobutyric acid, and 5% AcN; Buffer B: 0.4% acetic acid, 0.005% heptafluorobutyric acid, and 95% AcN) as described above. The eluted peptides were detected by Orbitrap (350-1500 *m/z*, 1,000,000 AGC target, 1,000 ms maximum ion time, resolution 30,000 fwhm) followed by five data-dependent

MS/MS scans in LTQ (2 *m/z* isolation width, 35% collision energy, 5,000 AGC target, 200 ms maximum ion time) on a hybrid mass spectrometer (Thermo Finnigan). Database searching and filtering was performed as described above in 2.6.2, and quantitative pair-wise comparisons between FTLD-U and control using the internal standard were carried out as described in 2.6.5.

2.6.7 Quantitative analysis of polyubiquitin chains and targeted proteins by LC/MRM

The analysis of polyubiquitin (polyUb) linkages, ubiquitin (Ub) E1 enzyme, and proteasome subunit Rpn2 was performed with metabolically heavy labeled cells as internal standards (+8.01420 for Lys and +10.00827 for Arg), using a previously reported protocol (Kirkpatrick, Hathaway et al. 2006; Xu, Duong et al. 2009). The labeled cells were spiked into transfected cells followed by protein extraction. Sarkosyl-insoluble fractions were resolved on a 1D SDS gel. The gel regions above 80 kDa, which contained the vast majority of polyUb species **(Figure 5.4)**, were used for in-gel trypsin digestion that produced a pair of light and heavy GG-linked Ub peptides corresponding to every PolyUb linkage. Digested peptides were analyzed by the same LC system as above, in which peptide ion pairs of interest were selected for fragmentation and quantified by their related product ion pairs, a process termed selective reaction monitoring (SRM) or multiple reaction monitoring (MRM).

2.6.8 Quantitative analysis of SEPT11 by targeted proteomics and LC/MRM

For targeted proteomics and peptide mapping of SEPT11, metabolically heavy-labeled HEK 293 cells (+8.01420 for Lys and +10.00827 for Arg) were transfected with tagged HA-SEPT11 constructs and harvested. The cell lysate alone (for peptide mapping) or mixed with urea extracts from 4 pooled FTLD-U cases was analyzed by LC-MS/MS as described above (2.6.2), but in a data-independent MS/MS mode to specifically identify and fragment ions corresponding to five pre-selected SEPT11 peptides **(Table 2.1)**. Quantitative MRM analysis was performed with non-transfected heavy-labeled HEK 293 cell lysate as internal standards. The labeled cells were spiked into detergent-insoluble fractions from 4 pooled FTLD-U and 4 pooled control cases. Samples were then resolved by SDS-PAGE, and the gel piece corresponding to 40-60 kDa in each sample was subjected to trypsin in-gel digestion. We then specifically quantified ion pairs for SEPT11 peptides AAAQLLQSQAQQSGAQQTK and FESDPATHNEPGVR as described in 2.6.7.

2.7 Immunohistochemistry (IHC)

2.7.1 Human Free-Floating Sections

50μm-thick brain sections were prepared with a freezing microtome (Microm, Heidelberg, Germany) with AD, FTLD-U, and control brain blocks from frontal cortex, cingulate cortex, and hippocampus. Sections were incubated in 3% hydrogen peroxide (H_2O_2) to quench endogenous peroxidase activity. Sections were subsequently incubated with normal serum followed by primary antibody overnight at 4^oC. After extensive

Table 2.1 SEPT11 peptides selected for targeted proteomics

Protein Names	Number	Peptide Sequences	[1]Labeling AA	[2]Mass Shift (Da)	[3]Precursor Ions (*m/z*)		[4]SRM Conditions		Width			[5]RT (min)
					Native (light)	IS (heavy)	Native (light)	IS (Heavy)	m/z window	Native (light)	IS (heavy)	
Septin11	1	FESDPATHNEPGVR	R14	10.01	778.36	783.4	778.8	783.8	1.6	200-1600	200-1600	31.2
Septin11	2	SYELQESNVR	R10	10.01	612.80	617.8	613.2	618.2	1.6	200-1600	200-1600	32.8
Septin11	3	AAAQLLQSQAQQSGAQQTK	K19	8.01	979.01	983.0	979.4	983.4	1.6	200-1600	200-1600	33.5
Septin11	4	DTDPDSKPFSLQETYEAK	K18	8.01	1035.98	1040.0	1036.4	1040.4	1.6	200-1600	200-1600	42.3
Septin11	5	NLSLSGHVGFDSLPDQLVNK	K20	8.01	1070.56	1074.6	1071.0	1075.0	1.6	200-1600	200-1600	67.0

[1]The selected residue for stable isotopic labeling (e.g. L8, the eighth leucine residue) [2]The mass change due to isotopic labeling [3]The *m/z* values of native and labeled peptides [4]The *m/z* range set for the isolation of both native and labeled precusor ions [5]The experimental retention time in reverse liquid chromatography.

washes with TBS, sections were incubated with biotinylated secondary antibody for 1 hour at 4^{o}C and an additional hour with avidin-biotin-peroxidase complex (Vector Elite ABC Kit, Vector Laboratories, Burlingame CA). Staining was visualized by light microscopy using 3,3'-diaminobenzidine (DAB) as a chromogen. For preabsorption studies of septin 11, primary antibodies were preincubated with 100x molar excess of the antigen overnight at 4^{o}C before incubation with the tissue.

2.7.2 Human Paraffin-Embedded Tissue

Paraffin-embedded sections of hippocampus and frontal cortex (8µm thick) were deparaffinized and microwaved in citrate buffer (0.01 M, pH 6) for 10 minutes. After cooling to room temperature for 1 hour, sections were rinsed and endogenous peroxidase activity was blocked with 3% hydrogen peroxide at 40^{o}C. Sections were then incubated with normal goat serum for 15 minutes at 40^{o}C, followed by primary antibody (diluted in 1% BSA) overnight at 4°C. The following day, sections were incubated with biotinylated goat secondary antibody for 30 minutes at 37°C, and finally with avidin-biotin peroxidase complex (Vector Laboratories) for 60 minutes at 37°C. As performed for floating sections, DAB was used as the chromogen for color development and was followed with hematoxylin counterstain.

2.7.3 Blinded Scoring of SEPT11 Immunoreactivity

Scoring of specific SEPT11 immunoreactivity was done in a blinded fashion by three independent neuropathologists. Scoring was limited to superficial cortical layers (layers 2-3) and included only thread-like structures not directly associated with glial nuclei or processes. Neuropil and astrocytic SEPT11-staining was specifically excluded

and was, therefore, not evaluated. Staining was scored as negative (0; no immunoreactivity), equivocal (1; very few threads), positive (2; threads common throughout superficial layers or showing patchy dense distribution), or very positive (3; threads densely distributed throughout superficial layers). A consensus score was determined for each of the cases examined, and typically corresponded to the median score of the three scorers. In rare cases where the three scorers differed by more than 1 point, cases were re-scored in the presence of all three scorers to achieve consensus. In analyses, samples scored as negative or equivocal were grouped together as "Low Presence of SEPT11 threads," while samples scored as positive or very positive were grouped together as "High Presence of SEPT11 threads." We considered age of onset, age at death, post-mortem interval, disease duration, tissue quality, and tissue volume as potential confounders for statistical analyses. However, none of these parameters was significantly associated with predicting the presence or absence of SEPT11 threads. Thus, statistical comparisons were conducted using Fisher's exact test.

2.8 Primary Neuronal Cultures

Primary hippocampal neuron cultures were prepared from wildtype C57BL/6 mice (Charles River Labs, Wilmington MA) at embryonic day E18. The embryos were dissected and the hippocampus isolated in dissection buffer (Hanks Balanced Salt Solution (HBSS), 10mM HEPES, 1% penicillin/streptomycin). After mild trypsinization with 0.25% trypsin and 0.01% deoxyribonuclease in dissection buffer for 15 minutes at 37^{o}C, the tissue fragments were rinsed twice with dissection buffer and twice with plating medium (buffered MEM (Gibco, Grand Island NY), 0.6% glucose (Gibco), 2 mM L-

glutamine (Mediatech Inc, Manassas VA), 10% heat-inactivated horse serum (Gibco), 1% penicillin-streptomycin). The tissue was then subjected to mechanical dissociated by repeated aspiration through a fire-polished Pasteur pipette in dissociation medium. Viable cells were determined by Trypan blue exclusion. Neurons were plated at a density of 50,000 cells/cm^2 on poly-L-lysine (Sigma, St. Louis MO) coated coverslips (Propper Manufacturing Company, Long Island City NY) and maintained in Neurobasal medium (Gibco) containing B-27 supplement (Gibco), 2 mM L-glutamine, and 1% penicillin-streptomycin at 37^oC under 5% CO_2.

2.9 Cell Culture and Immunocytochemistry (ICC)

HEK 293 cells were cultured in Dulbecco's Modified Eagle's medium (Cambrex, Walkersville MD), and supplemented with 10% fetal bovine serum (Gibco, Grand Island NY) and 1% penicillin-streptomycin (Cambrex). After plating on Matrigel-coated coverslips, cells were transfected using Fugene6 reagent (Roche, Nutley NJ) followed by immunocytochemistry two days later as previously described (Volpicelli, Lah et al. 2002). Briefly, the cells were fixed with 2% paraformaldehyde in phosphate-buffered saline (PBS), permeabilized and blocked with PBS containing 5% BSA and 0.05% Triton X-100, and incubated in primary antibodies overnight. The cells were then rinsed and incubated with either fluorophore-conjugated or biotinylated secondary antibodies (Jackson ImmunoResearch Laboratories, West Grove PA) for 60 min. Cells treated with biotinylated secondary antibodies were subsequently incubated with avidin-biotin-peroxidase complex and tyramide conjugated fluorophores per manufacturer's protocol (Perkin Elmer, Boston MA). Following additional rinses, cells were incubated with a

Hoechst reagent for nuclear localization, mounted with Vectashield (Vector Laboratories, Burlingame CA), and imaged on a Zeiss LSM 510 confocal microscope (Zeiss, Thornwood NY). Images were captured with a 1 μm optical thickness for subsequent analysis.

2.10 Western Blotting

Immunoblotting was performed according to standard procedures. Briefly, samples in Laemmli sample buffer were separated by SDS-PAGE and transferred overnight to PVDF Immobilon-P membranes (Millipore, Billercia MA). To ensure both equal loading and complete transfer of proteins from the gel, membranes were reversibly stained with Ponceau S (Diasys Europe Ltd, Workingham, England). Blots were blocked for 1 h at room temperature using 1x Blocking Buffer (USB Corporation, Cleveland OH), probed with primary antibody in TBS with 0.1% Tween 20 overnight at 4^{o}C, and incubated for 1 hour at room temperature with secondary antibodies (1:20,000) conjugated to fluorophores (Molecular Probes, Eugene OR; Rockland, Gilbertsville PA). Blots were dried, scanned, and quantified with an Odyssey Infrared Imaging System (Li-Cor Biosciences, Lincoln, NE). Data were analyzed with GraphPad Prism 4.0 software (La Jolla, CA) and statistical significance was determined by unpaired two-tailed Student's t test with $\alpha = 0.05$. For preabsorption studies of septin 11, primary antibodies were preincubated with 100x molar excess of the antigen overnight at 4^{o}C before incubation with the blot.

2.11 Biochemical Assays

To assess TDP-43 phosphorylation, total cell lysate was incubated with 0, 0.15, 0.3 or 0.6 mg/ml bovine alkaline phosphatase (Sigma Aldrich, St. Louis, MO) for 2.5 h at 37ºC, followed by Western blot analysis. For deSUMOylation, sentrin-specific endopeptidase 2 (SENP2; Boston Biochem, Cambridge MA) was incubated with 10 µg detergent-soluble or 1 µg insoluble fractions from TDP-43-transfected cells in 20-µl reactions (buffer: 50mM Tris, 100mM NaCl, 5mM DTT, pH 8.0; titrated SENP2 concentration: 0, 1 µM or 5 µM). All samples were incubated for 3 h at 37ºC, and then analyzed by Western blotting.

2.12 Genotyping and Sequencing Assays

2.12.1 SNPstream Genotyping

The SEPT11 gene (NM 018243.2) on chromosome 4q21.1 was subjected to HapMap analysis (data release 21a/phase II Jan07). Tag single nucleotide polymorphisms (SNPs) for genotyping were selected using the TagSNP Picker software (de Bakker, Yelensky et al. 2005) with the following settings: CEU population; pairwise mode; r^2 cutoff = 1.0; MAF > 0.05. In addition to the 19 tag SNPs selected for genotyping using this algorithm, we also genotyped SNP rs28541859 because of its location at a putative splice site.

For primer design, sequence information in the form of SNP rs # was entered into www.autoprimer.com. Three primers, two for PCR and one for single-base extension were designed for each SNP, and grouped into a 20-plexed panel. Using 2-10ng of genomic DNA, a 20-plex PCR was carried out in 384-well format to amplify a ~100 bp

region flanking each SNP. The PCR reaction was treated with ExoSAP reagent to remove any left-over PCR primers and dNTPs. The 20-plex extension primer pool was then added to the same PCR plate. A single-base extension reaction was performed to incorporate a differentially labeled fluorescent dNTP to the SNP position. The extension reaction was transferred to a Tag Array and spatially resolved to distinguish the 20 SNPs. All reagents were pre-formulated and included in the GenomeLab SNPware Reagent kit. The GenomeLab SNPstream Genotyping System Software Suite v2.3 (Beckman Coulter, Inc., Fullerton, CA) was used for array imaging and genotype calling. The genotype data were exported into an Excel spreadsheet for further analysis. Calculation of allelic frequency, odds ratios (OR), and associated p-values was conducted using Statistical Analysis Utility Programs available at http://www.genemapping.cn/util.htm#odds. Testing of Hardy-Weinberg equilibrium was also performed using these software tools.

2.12.2 TaqMan SNP Assay

Genotyping of SNP rs6818075 and three additional SNPs (included for validation of genotyping) captured by this tag SNP (rs2270653, rs4859731, and rs17002331) was conducted using a TaqMan Allelic Discrimination Assay (Livak 1999) on an ABI 7900HT Fast Real-Time PCR system (Applied Biosystems, Foster City, CA). SNPs were genotyped using validated TaqMan assay kits (C_29320105_10 for rs6818075; C_15958140_10 for rs2270653; C_28037158_10 for rs4859731; C_34191603_10 for rs17002331) containing 1 pair of polymerase chain reaction (PCR) primers and 1 pair of fluorescent-labeled probes (Applied Biosystems). PCR reactions were performed in 5µl reaction volumes containing 10ng of genomic DNA, 2.5µl of TaqMan Genotyping

Mastermix, and 0.125µl of primer/probe mix. The PCR program used was 10 min at 95°C, followed by 45 cycles of 15 sec at 92°C, and 1 min at 60°C. The assay endpoint was read following the PCR reactions, and allelic discrimination was accomplished using the SDS v2.1 software (Applied Biosystems).

2.12.3 Septin 11 Sequencing

All coding exons of SEPT11 were amplified by PCR using primers designed to flanking intronic sequences **(Table 2.2)**. Reactions contained a final concentration of 0.8µM for each primer and 10% Q-solution (Qiagen, Valencia, CA) and were cycled using one of three PCR protocols. The PCR reactions labeled "55," "60," or "62" were carried out at 94^{o}C for 4 min, followed by 36 cycles of 94^{o}C for 30 sec, 55^{o}C or 60^{o}C or 62^{o}C for 30 sec, and 72^{o}C for 30 sec, with a final extension at 72^{o}C for 10 min. Similarly, the PCR reaction labeled "TD 58-48" referred to a 58-48°C touchdown protocol and was carried out as follows: (1) 94^{o}C for 3 min; (2) 27 cycles of 94^{o}C for 30 sec, 58^{o}C for 30 sec, 72^{o}C for 45 sec; (3) 9 cycles of 94^{o}C for 30 sec, 48^{o}C for 30 sec, 72^{o}C for 45 sec; (4) final extension at 72^{o}C for 10 min. PCR products were purified using AMPure (Agencourt Biosciences Corporation) then sequenced in both directions using the Big Dye Terminator v3.1 Cycle Sequencing kit (Applied Biosystems, Foster City, CA) using manufacturer's protocols. Sequencing reactions were purified using CleanSEQ (Agencourt Biosciences Corporation) and analyzed on an ABI 3730 (Applied Biosystems). In all, DNA from 15 FTLD (rs6818075 genotypes: 1 homozygote, 8 heterozygotes, and 6 wild type) and 9 control (rs6818075 genotypes: 1 heterozygote and 8 wild type) cases were sequenced in this manner.

Table 2.2 *SEPT11* Sequencing Primers

Exon	Direction	Sequence	Amplicon Length (bp)	[3]PCR Program
1	F[1]	GTGGCCATGTTGCTCTAATAAAG	370	55
	R[2]	AAATTCGTGCACACACCCAC		
2	F	TGCCCTCAGCTGTGTAGAA	500	TD 58-48
	R	AGTTGCTTAACTGTGTGACAGAA		
3	F	ACAGTGACATTTCTGGTGACAG	450	TD 58-48
	R	TTTAGGCAATAGAGGACCAAG		
4	F	CTGTTCAGGGATCAGGTGATG	400	60
	R	AAAGCAGAGAACAAATTAGGGC		
5	F	AGGAGGCGTATATATTTATGGG	460	TD 58-48
	R	GGTGGCAAAGCTGGACTAC		
6	F	CATCCACCCACCAAACTGC	400	TD 58-48
	R	CACCTCCACGATTGTCACATG		
7	F	CAGTAAAGGATCTTCAGATGGTC	440	60
	R	TGTATTAATCTTCACCCACCAG		
8	F	GTCTTTCCAACCACAGCATAAC	480	60
	R	GACAGGGATGAGAATATCTGACC		
9	F	CTCCTGACCTCGTGATCCAC	500	62
	R	TCATCTTCCCTGCACTGTAGAG		
10	F	GCTTTGGCTTGTCATGTAGAG	370	TD 58-48
	R	TTCTACCACCCAACAACATTC		

[1]Sense primer [2]Antisense primer [3]See Chapter 2: Materials and Methods for detailed PCR program information

Chapter 3

Proteomic analysis of ubiquitin-positive inclusions in frontotemporal lobar degeneration: Application of laser capture technology.[2]

3.1 Introduction:

Frontotemporal lobar degeneration (FTLD) is a progressive neurologic disorder that manifests profound behavioral, personality, and language symptoms (Neary, Snowden et al. 2005; Kumar-Singh and Van Broeckhoven 2007). In the past few decades, the pathologic classification of FTLD has been primarily accomplished using biochemical and immunohistochemical approaches to differentiate the composition of proteinaceous aggregates found in the brain. Three major neuropathological subtypes have been identified in FTLD, including tauopathies, FTLD cases lacking distinctive histopathology, and FTLD-ubiquitinated (FTLD-U) type (Woulfe, Kertesz et al. 2001). Recent studies have suggested that FTLD-U is the most common of these subtypes, accounting for approximately half of all FTLD cases (Graff-Radford and Woodruff 2007; Snowden, Neary et al. 2007). The histopathologic hallmark of FTLD-U is the presence of

[2]Portions of this chapter have been reproduced with permission from Gozal YM, Cheng D, Duong DM, Lah JJ, Levey AI, and Peng J. (2006). Merger of laser capture microdissection and mass spectrometry: a window into the amyloid plaque proteome. Methods Enzymol. **412**:77-93.

ubiquitin-positive, tau- and α-synuclein-negative intraneuronal inclusions primarily in the hippocampal dentate gyrus and frontotemporal cortex (Kovari, Gold et al. 2004). Interestingly, a similar pathology is also seen in cases of FTLD-U with concomitant motor neuron disease (MND), which suggests that FTLD-U and MND share a common pathogenesis (Forman, Farmer et al. 2006).

Although pathological lesions in many neurodegenerative diseases exhibit ubiquitin immunoreactivity, FTLD-U inclusions are unique in that their primary protein constituents have proven difficult to characterize. This obstacle has been primarily technical in nature, as the small size and distribution of the inclusions precluded the application of biochemical purification and identification approaches common in the study of other pathologic lesions. In fact, it was only recently that the first non-ubiquitin component of FTLD-U inclusions was identified as the TAR-DNA-Binding Protein 43 (TDP-43) (Neumann, Sampathu et al. 2006), a nuclear RNA binding protein involved in exon skipping and transcriptional regulation (Buratti, Dork et al. 2001). As it is likely that inclusions are not composed of TDP-43 and ubiquitin alone, further molecular analysis of inclusion bodies is warranted.

The development of laser capture microdissection (LCM) technology over the past ten years (Emmert-Buck, Bonner et al. 1996) has given investigators a new method to isolate and study neurodegenerative disease aggregates. LCM is a rapid, reliable method for the isolation specific cells, or small biologically relevant areas, from complex tissues (Emmert-Buck, Bonner et al. 1996). Using a low-power laser to melt a thermoplastic film onto a tissue section, a target of interest as small as 3-5μm in diameter can be isolated (Bonner, Emmert-Buck et al. 1997). Multiple laser shots can be combined

on the same film in order to procure cell clusters or more complicated tissue structures (Simone, Bonner et al. 1998). Importantly, the remarkable precision demonstrated in the laser capture process, coupled with minimal direct handling and processing of the captured material, reduces contamination in collected samples. Finally, material isolated by LCM not only maintains its morphology for subsequent visual verification (Bonner, Emmert-Buck et al. 1997), it also maintains the quality of the captured tissues to minimize the impact on downstream analyses (Ornstein, Gillespie et al. 2000). One of the major limitations of LCM is the minimal amount of protein that can be recovered from the captured tissue. However, the limitation is largely alleviated by the extremely high sensitivity provided by proteomics platform such as nanoscale capillary liquid chromatography-tandem mass spectrometry (LC-MS/MS).

The combination of LCM and LC-MS/MS offers a unique opportunity to study neurodegenerative disorders because these diseases are characterized by the presence of selectively vulnerable populations of neurons (Morrison, Hof et al. 1998) and by distinct neuropathological lesions that can be microdissected and analyzed. In our lab, for example, we have previously applied this combined approach in the characterization of senile plaques from postmortem AD brain tissues (Liao, Cheng et al. 2004). Specifically, we demonstrated the co-isolation of 488 proteins with the plaques, including more than 80% of the previously documented plaque proteins. More significantly, quantitative comparison of plaques and non-plaque tissues revealed at least 2-fold enrichment of 26 proteins in the plaque regions, an indication of the complexity and diversity of cellular processes involved in the formation of plaques. Thus, in this study, we coupled LCM and LC-MS/MS to identify and quantitate proteins isolated from ubiquitinated inclusions in

the hippocampal dentate gyrus of FTLD-U patients. We reveal significant enrichment of 54 proteins in FTLD-U compared with unaffected controls, and evaluate the potential of this approach for profiling ubiquitin-immunoreactive inclusions and other complex aggregates in neurodegeneration.

3.2 Results

3.2.1 Identification of proteins enriched in FTLD-U dentate granule cells by LC-MS/MS

Using LCM, we selectively dissected the granule cell layer of the dentate gyrus, a site of abundant pathologic inclusions in FTLD-U, from three FTLD-U cases and three unaffected controls for proteomic analysis **(Table 3.1)**. To collect sufficient material for proteomics, the maximum number of granule cells from each dentate gyrus were captured **(Figure 3.1 A and B)** from 50-60 ethanol fixed, paraffin-embedded, postmortem hippocampal sections (10μm-thick) per case, requiring 3000-5000 laser pulses per section using a Pixcell II laser capture system (Arcturus). Protein captured from each case was subsequently extracted with SDS, separated by mass using SDS gel electrophoresis, and quantified to estimate total protein yield by silver stain **(Figure 3.1 C)**. For each case, ~5μg of total protein was collected by LCM of hippocampal sections. Following the division of the samples into three independent FTLD-U/control comparisons, the extracted proteins were separated on a second SDS gel. Each gel lane was subsequently cut into six pieces by molecular weight, and exposed to in-gel digestion with trypsin. The resultant tryptic peptides were analyzed by high-resolution LC-MS/MS, the method of

Table 3.1 Demographic information

Comparisons	Diagnosis	Age at Onset (yrs)	Age at Death (yrs)	Duration (yrs)	Gender (Male / Female)	PMI (hrs)
Comparison 1	FTLD-U	56	64	8	F	6
	Control		74	0	F	7
Comparison 2	FTLD-U	56	61	5	M	17.5
	Control		61	0	M	<12
Comparison 3	FTLD-U	62	71	9	F	18
	Control		57	0	F	17

A

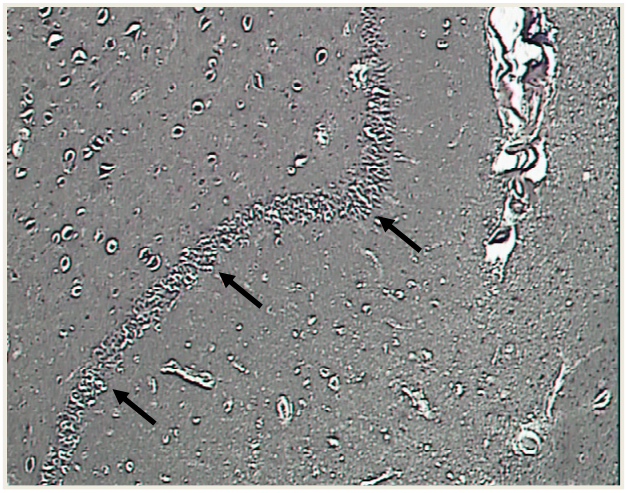

B

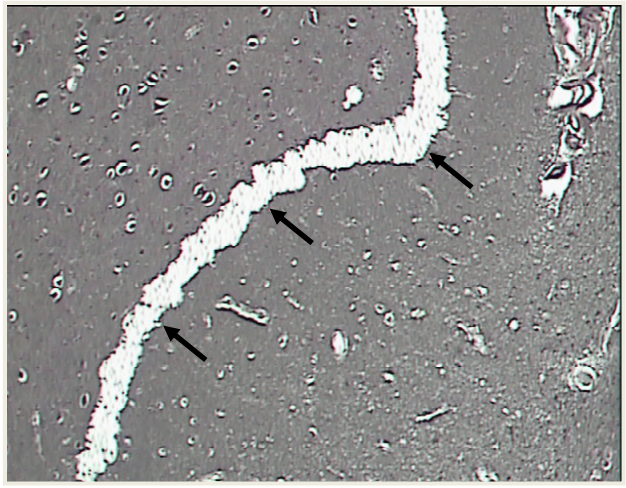

C

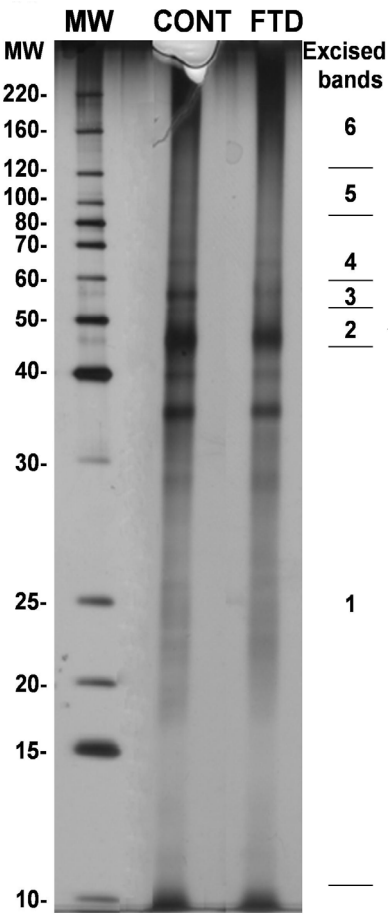
MW
CONT
FTD
MW
220-
160-
120-
100-
80-
70-
60-
50-
40-
30-
25-
20-
15-
10-
Excised bands
6
5
4
3
2
1

Figure 3.1 Dissection and preparation of LCM samples for proteomics. (A) Before and (B) after images depicting efficient removal of the hippocampal dentate gyrus via LCM. (C) Representative silver stain of extracted proteins captured from one FTLD-U case and one unaffected control. Proteins were extracted using SDS-containing lysis buffer, and a small fraction of each sample (~5%) was separated by SDS-PAGE and examined by silver staining. The remainder of each sample (~95%) was resolved on a separate SDS gel and stained with Coomassie Blue G-250. Each sample lane was then cut into 6 pieces according to the molecular weight marker as is shown on the right.

choice for large scale proteomics, on a hybrid LTQ-FT linear ion trap/7-Tesla Fourier transform ion cyclotron resonance (FT-ICR) mass spectrometer (Thermo Electron, San Jose, CA). The spectra acquired for each sample were searched against a human protein database, and further filtered by mass accuracy and matching scores. We identified 6694 peptides corresponding to 1252 proteins across the three paired case/control comparisons. Of these, 218 proteins were found in all three comparisons **(Figure 3.2)**.

3.2.2 Relative quantification of identified proteins by the label-free strategy

Quantitation of protein changes between FTLD-U and control dentate proteomes was based on the ratio of the extracted ion currents of peptides identified in each case. Abundance ratios corresponding to the relative protein abundance between the FTLD-U and control dentate proteomes were calculated for all of the peptides obtained in this experiment. To evaluate the significance of the protein changes and to correct the quantitative errors resulting from sample handling and/or ionization instability, specialized statistical methods were applied as described under "Materials and Methods" (Li, Zhang et al. 2003; Cheng, Hoogenraad et al. 2006). Briefly, abundance ratios (FTLD-U/Control) for all 1252 proteins identified in this experiment were averaged over the three comparisons, transformed into $\log_2$(ratio), and plotted as shown in **Figure 3.3**. The resultant experimental distribution was fitted to a normal distribution on the basis of the central limit theorem. Because the majority of proteins likely display similar abundance in diseased and control tissues, the $\log_2$(ratio) for each protein was normalized by subtracting the fitted mean (μ), as the mean should have been zero if sample

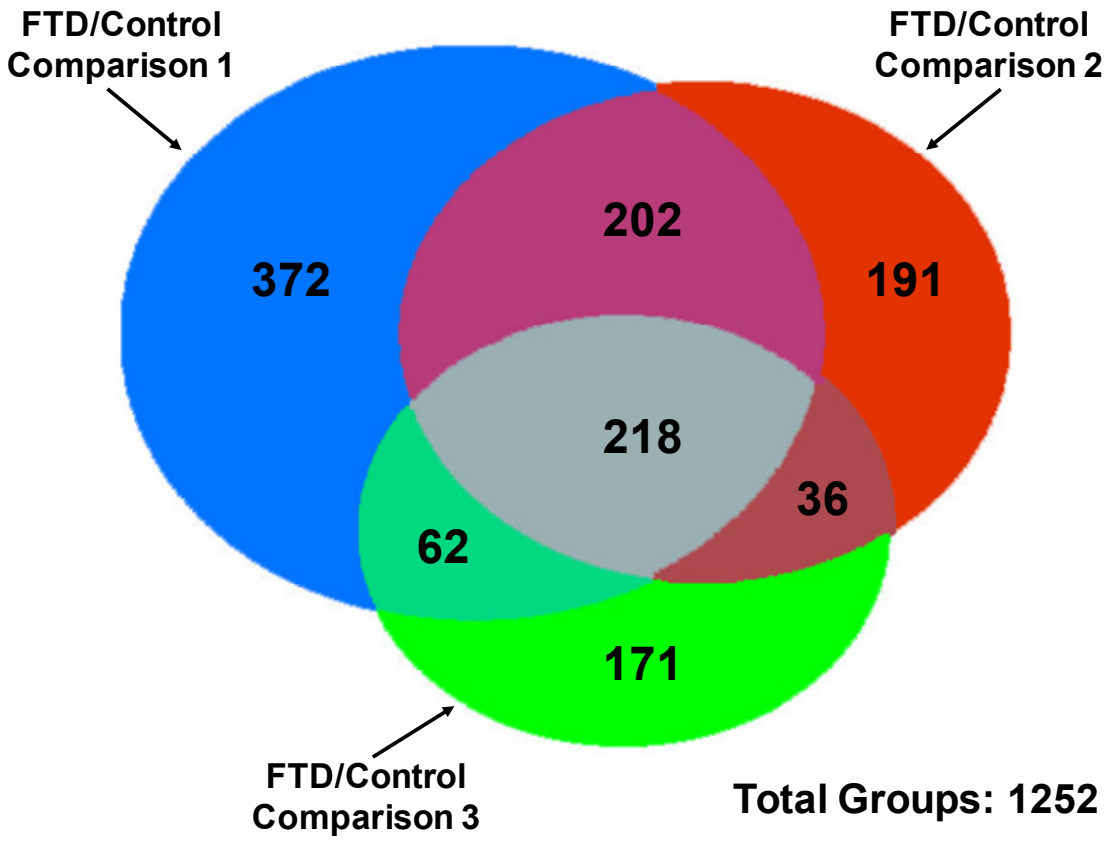

Figure 3.2 Identification of proteins in independent FTLD-U/Control comparisons. Proteins identified in each comparison are represented by colored circles. The number of overlapped proteins between comparisons is indicated in the relevant areas. A total of 1252 proteins were identified across all 3 FTLD-U/Control comparisons. Of these, 218 were independently identified in each of the three comparisons.

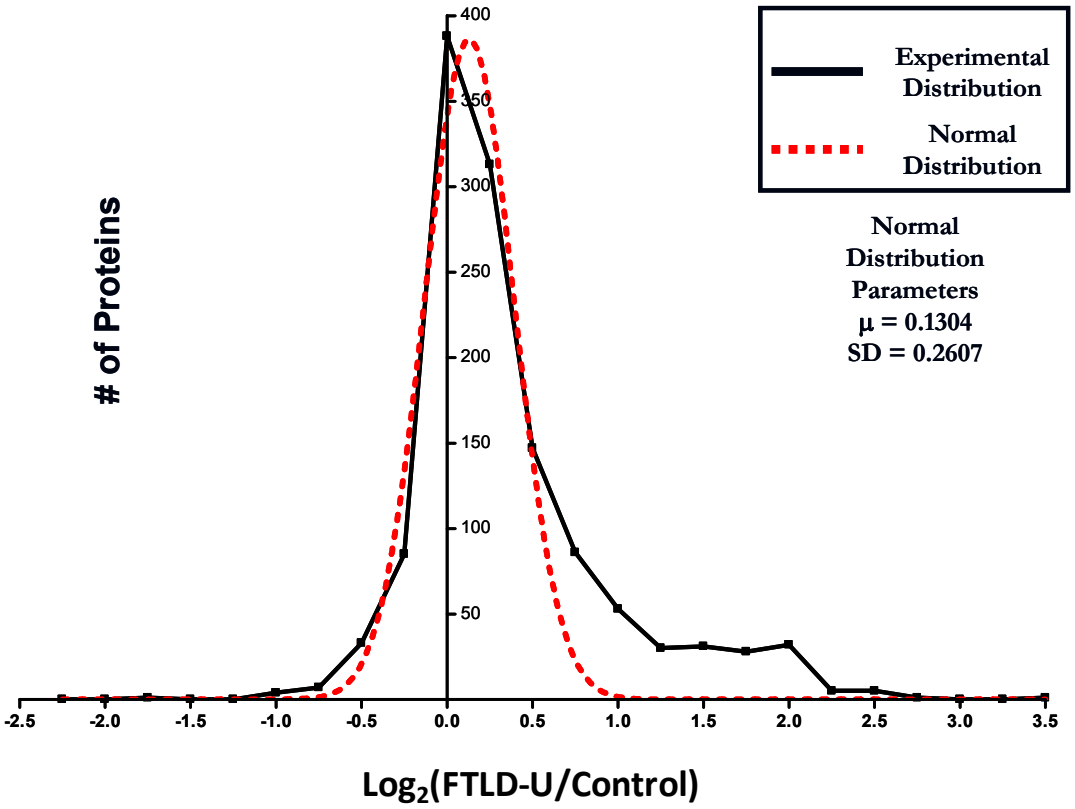

Figure 3.3 Distribution of abundance ratios reveals a subset of altered FTLD-U proteins. Logarithmic (base 2) transformation of protein ratios from FTLD-U/control comparisons was performed and plotted with each point corresponding to the number of proteins in each 0.25 unit window (black line). A normal distribution was subsequently fitted to the data (red line). Total proteins = 1252.

preparation was ideal (Cheng, Hoogenraad et al. 2006). Additionally, the fitted Gaussian distribution was used to approximate the common variance of the whole data set, a feature that was applied to establish significance thresholds for protein changes. Using these normal distribution parameters, we identified significant enrichment of 54 proteins in FTLD-U dentate granule cells compared with control. In order to increase the reliability of the dataset, we considered only the 518 proteins detected in at least 2 out of 3 FTLD-U/Control comparisons. Moreover, only proteins demonstrating consistency in the direction of the measured change (i.e. enriched in all comparisons) were included in this final list **(Table 3.2)**. Notably, TDP-43 was among the proteins meeting these filtering restrictions, and showed a moderate ~1.5 fold increase in FTLD-U.

3.2.3 Validation of selected FTLD-U enriched components

To independently verify the accuracy of the LC-MS/MS generated data, several of the most promising candidate proteins were selected based on both the availability of specific antibodies and the magnitude of enrichment in FTLD-U, and were analyzed by immunohistochemistry (IHC) and immunoblotting. The IHC technique is an ideal validation tool because it allows visual confirmation of localization of protein candidates within ubiquitin-immunoreactive inclusions using specific antibodies. Thus, IHC was performed in frontal cortex and hippocampal sections from six additional postmortem FTLD-U cases and six unaffected controls using antibodies to septin 3 **(Figure 3.4 B)**, septin 7 **(Figure 3.4 C)**, protein disulfide isomerase (data not shown), and glial fibrillary acidic protein (GFAP) (data not shown). Immunoblotting was also performed for each of

Table 3.2 Proteins enriched in FTLD-U dentate granule cells

GeneBank™ Accession Number	Protein Name	Comparison 1 Log_2 Ratio	Comparison 2 Log_2 Ratio	Comparison 3 Log_2 Ratio	Average Log_2 Ratio	Comparison 1 Total Peptides	Comparison 2 Total Peptides	Comparison 3 Total Peptides
NP_663786.1	septin 3	6.09	1.28	2.63	**3.33**	1	2	1
NP_002788.1	proteasome beta 5 subunit	0.59		4.85	**2.72**	2		1
NP_115921.1	fibronectin type III domain containing 1		0.25	4.87	**2.56**		1	1
NP_001145.1	annexin 5	0.48	0.39	5.88	**2.25**	11	4	5
NP_058431.2	v-crk sarcoma virus CT10 oncogene homolog	0.2		4.18	**2.19**	1		1
NP_000137.2	ferritin, light polypeptide	0.29	0.32	5.93	**2.18**	2	1	1
NP_000996.2	ribosomal protein S3	0.27	0.1	5.49	**1.95**	8	1	4
NP_002130.2	RNA binding motif protein, X-linked	0.87		3.03	**1.95**	3		2
NP_005653.3	voltage-dependent anion channel 3	0.18	0.03	5.54	**1.92**	6	4	2
NP_004243.1	solute carrier family 9 (sodium/hydrogen exchanger)	0.05		3.56	**1.81**	2		1
NP_444505.1	ribosomal protein P0	0.08	0.2	4.84	**1.71**	4	1	1
NP_808592.1	N-acylsphingosine amidohydrolase (acid ceramidase) 1	2.73	0.55		**1.64**	2	1	
NP_112738.1	heterogeneous nuclear ribonucleoprotein D		0.71	2.51	**1.61**		2	1
NP_524149.1	smooth muscle and non-muscle myosin alkali light chain	0.09		2.61	**1.35**	2		1
NP_000399.1	glycerol-3-phosphate dehydrogenase 2 (mitochondrial)	1.06	1.56		**1.31**	1	1	
NP_009204.1	prohibitin 2	1.06	0.17	2.58	**1.27**	9	8	5
NP_005309.1	H1 histone family, member 0	0.7		1.81	**1.26**	1		2
NP_005134.1	haptoglobin	0.78		1.73	**1.26**	3		5
NP_060921.2	centromere protein J		1.28	1.17	**1.23**		1	1
NP_003320.2	thioredoxin	0.56	0.22	2.76	**1.18**	3	1	2
NP_000524.3	proteolipid protein 1 isoform 1		0.35	2.01	**1.18**		2	2
NP_002956.1	S100 calcium-binding protein A9	1.54		0.74	**1.14**	5		1
NP_036246.1	caspase 14 precursor	1.46		0.8	**1.13**	1		2
NP_000468.1	albumin precursor	0.92	1.01	1.44	**1.12**	12	6	12
NP_005304.3	protein disulfide isomerase-associated 3	0.8	1.37	1.09	**1.09**	10	3	5
NP_000467.1	adenylate kinase 1	0.56	0.2	2.47	**1.08**	4	4	2
NP_942599.1	RAB6A, member RAS oncogene family	0.23	0.13	2.85	**1.07**	3	1	2
NP_001958.2	eukaryotic translation initiation factor 4A		0.18	1.89	**1.04**		1	3
NP_000687.2	aldehyde dehydrogenase 9A1	0.33		1.72	**1.03**	2		1
NP_002046.1	glial fibrillary acidic protein	0.94	0.53	1.53	**1.00**	35	9	27
NP_000282.1	phosphoglycerate kinase 1	0.35	1.04	1.44	**0.94**	11	5	7
NP_002435.1	moesin		0.92	0.95	**0.94**		2	2
NP_478059.1	phosphoserine aminotransferase	0.66	0.85	1.27	**0.93**	6	5	1
NP_002842.1	protein tyrosine phosphatase, receptor-type, Z polypeptide 1	0.53	1.59	0.53	**0.88**	6	2	1
NP_055581.2	secernin 1	0.6	1.11		**0.86**	1	1	
NP_002703.1	protein phosphatase 1, regulatory subunit 7	1.1	0.58		**0.84**	2	1	
NP_002783.1	proteasome alpha 7 subunit	0.02		1.66	**0.84**	3		1
NP_066270.1	ubiquitous mitochondrial creatine kinase precursor	0.51	0.19	1.8	**0.83**	5	4	4
NP_003312.3	Tu translation elongation factor, mitochondrial	0.76	0.42	1.3	**0.83**	3	1	1
NP_001814.2	brain creatine kinase	0.78	0.69	0.98	**0.82**	8	9	13
NP_002291.1	lactate dehydrogenase B	0.48	0.19	1.71	**0.79**	10	7	8
NP_078974.1	mitochondrial glutamate carrier 1	0.47	0.55	1.33	**0.78**	3	2	3
NP_443100.1	immunoglobulin superfamily, member 8	0.09	1.45		**0.77**	3	1	
NP_003841.1	succinate-CoA ligase, ADP-forming, beta subunit	1.09	0.42		**0.76**	2	1	
NP_001011553.1	Septin 7 (cell division cycle 10)	0.4	1.06	0.77	**0.74**	6	1	2
NP_000117.1	electron transfer flavoprotein, alpha polypeptide	1.18	0.28		**0.73**	4	2	
NP_066268.1	guanine nucleotide binding protein, alpha activating polypeptide O	0.09	0.3	1.79	**0.73**	8	8	6
NP_006363.3	synaptotagmin binding, cytoplasmic RNA interacting protein		1.35	0.09	**0.72**		1	2
NP_055363.1	tropomodulin 2 (neuronal)	1.26	0.15		**0.71**	4	2	
NP_061322.2	matrin 3	0.17		1.23	**0.70**	2		2
NP_004376.2	chondroitin sulfate proteoglycan 2 (versican)	0.55	0.74	0.8	**0.70**	5	2	4
NP_003356.2	ubiquinol-cytochrome c reductase core protein I	0.43	0.92		**0.68**	3	3	
NP_149124.2	2',3'-cyclic nucleotide 3' phosphodiesterase	0.48	0.83	0.61	**0.64**	8	6	10
NP_031401.1	TAR DNA binding protein	1.16	0.11		**0.64**	1	1	

A

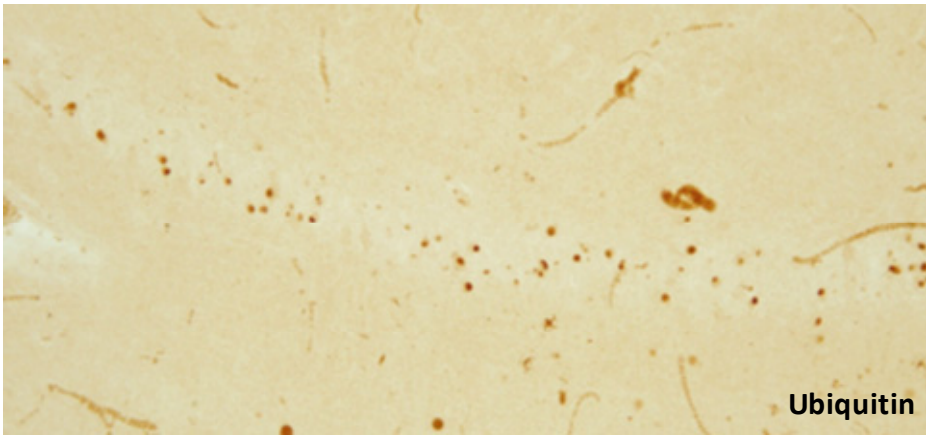

B

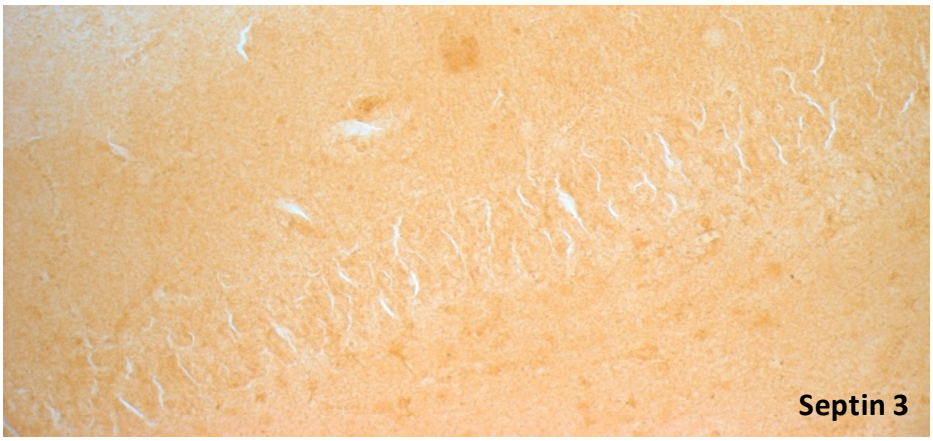

C

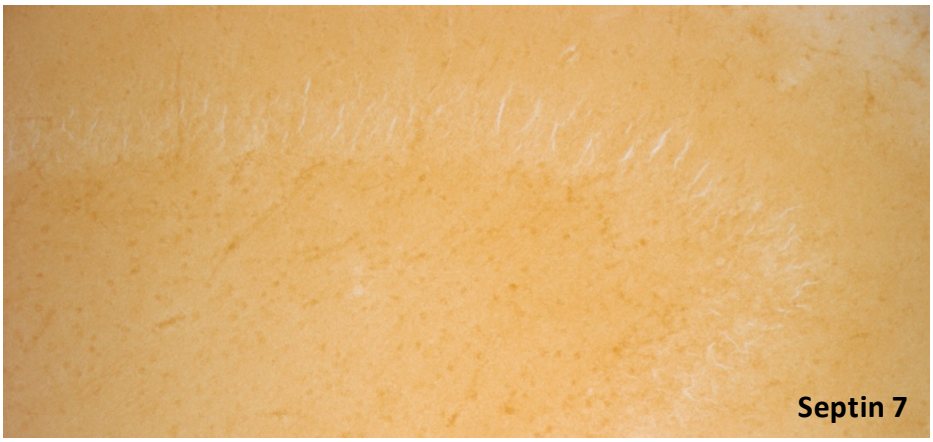

Figure 3.4 Examination of LCM proteomic candidates by immunohistochemistry. Representative staining of (A) Ubiquitin, (B) Septin 3, and (C) Septin 7 in hippocampal sections from a single FTLD-U case.

these candidates using frontal cortex homogenates prepared from the same additional cases. Notably, specific antibodies to each candidate all failed to consistently verify the changes in protein abundance suggested by the proteomics analysis. In addition, there was no difference in protein distribution between FTLD-U and control cases, nor was there overlap with ubiquitin immunoreactivity in the cases studied.

3.3 Discussion

The evaluation of ubiquitin-immunoreactive inclusions in FTLD-U has, to date, been based on conventional neuropathologic approaches aimed at differentiating these lesions from other ubiquitin-positive aggregates. As a result, immunohistochemical characterization has been limited to the subset of proteins classically associated with neurodegeneration, including β-amyloid, α-synuclein, tau, and only recently, TDP-43 (Okamoto, Hirai et al. 1991; Mackenzie, Neumann et al. 2009). However, the complete composition of inclusions and the mechanisms underlying inclusion formation are currently unclear. Here, we employed a label-free quantitative proteomics approach to characterize inclusion-enriched dentate granule cells microdissected from FTLD-U hippocampal sections. Analysis of three independent FTLD-U and control sample comparisons resulted in the identification of 1252 proteins, of which 54 were significantly altered in FTLD-U. Several of the identified proteins have been previously implicated in known pathogenic pathways in FTLD-U or ALS. These included valosin-containing protein (Gitcho, Strider et al. 2009) and clusterin (Grewal, Morgan et al. 1999), which were enriched ~1.3-fold and ~1.4-fold, respectively. More importantly,

TDP-43, a known component of ubiquitin-immunoreactive inclusions, was significantly enriched in FTLD-U samples compared with controls. While identification of these established proteins serves to validate our experimental strategy, we were unable to verify the proteomic changes in selected target proteins by immunohistochemistry and immunoblotting. Thus, the high false-discovery rate raises serious concerns regarding the design of our LCM-based protein analysis strategy.

The combination of LCM and LC-MS/MS has been successfully applied in the proteomic characterization of multiple neurodegenerative disease aggregates, including amyloid plaques (Liao, Cheng et al. 2004), neurofibrillary tangles (Wang, Woltjer et al. 2005), and Lewy bodies (Leverenz, Umar et al. 2007). However, when this approach was applied to the small, sparse FTLD-U inclusions, several deficiencies were realized. First, the combination of the size and frequency of ubiquitinated inclusions in FTLD-U rendered their direct capture impractical. Thus, instead of comparing inclusion-containing dentate granule cells to unaffected granule cells within the same case, we were instead forced to make comparisons between independent FTLD-U and control cases. These types of comparisons are typically susceptible to the effects of several confounding factors common in human studies (e.g. genetic and environmental variation, post-mortem interval, etc.) and can be only partially controlled. Moreover, the capture of healthy and inclusion-bearing cells within the same sample contributed to sample heterogeneity, and neutralized the primary advantage of LCM. Despite the certain enrichment of aggregates, our samples were still largely comprised of normal cellular proteins since the inclusions are only 1-8μm in size (Okamoto, Hirai et al. 1991) and the majority of the captured neurons were healthy. In contrast with the capture of amyloid plaques (Liao, Cheng et al.

2004), where 2000 aggregates (50-100 μm in diameter) were specifically captured from four cortical sections, each FTLD-U section contained <50 of the much smaller inclusions. Consequently, the final lysate extracted from the LCM caps consisted of only a small proportion of aggregating proteins, and may have been affected by inter-case variation in the frequency of ubiquitinated inclusions. It is worthwhile to note that although it allows for effective preservation of proteins, paraffin-embedding also may have affected the protein recovery, leading to inconsistencies in the quantity of material recovered (Bonner, Emmert-Buck et al. 1997).

A second limitation in the characterization of FTLD-U inclusions using LCM in combination with LC-MS/MS was that the amount of total protein collected for each case was insufficient for proper proteomics analysis. Despite microdissecting the entire granule cell layer of the dentate gyrus from 50-60 sections per case, we obtained only ~5μg of total protein per case. This lack of material reduced the sensitivity of LC-MS/MS analysis by preventing prior fractionation and simplification of the sample, and resulted in the reduced identification of low-abundance proteins. Moreover, the low protein concentration necessitated that the samples be used in their entirety for LC-MS/MS analysis, rendering replication impractical, and precluding the use of the LCM samples in subsequent independent validation methods.

Finally, the composition of the lysis buffer used to extract captured materials from LCM caps may also be a potential contributor to the high false-discovery rate in this experiment. LCM offers the advantage of accessibility to microdissected tissue embedded in the thermoplastic film (Bonner, Emmert-Buck et al. 1997). Thus, any aqueous buffer can be applied directly to the cap in small volumes to facilitate various downstream

molecular analyses (Craven and Banks 2001). The composition of the lysis buffer is highly dependent on the nature of the tissue and proteins to be solubilized. Therefore, ensuring proper solubility of proteins in the extraction buffer is the limiting factor for subsequent proteomic investigation. We selected to use a buffer containing 2% SDS to solubilize FTLD-U aggregates because this buffer had been sufficiently stringent for use in solubilizing laser-captured amyloid plaques (Liao, Cheng et al. 2004). However, since SDS has been reported to dissolve some aggregates poorly (Masters, Simms et al. 1985), it is possible that 7M urea or formic acid would have better suited for use on FTLD-U inclusions.

The marriage of LCM, a method that facilitates the enrichment of specific anatomical regions from complex tissues, and mass spectrometry may have a profound impact on the study of neurodegenerative diseases. Although our findings in this study are not representative of the molecular composition of ubiquitin-immunoreactive inclusions in FTLD-U, the strategy described herein can be applied in the study of other neurodegenerative diseases characterized by defined neuropathological lesions that are difficult to isolate biochemically. Moreover, the abovementioned shortcomings in this study may allow for the development of new, more broadly applicable, quantitative proteomics strategies for the characterization of aggregated proteins. We have applied such strategies in the subsequent chapters of this dissertation to identify disease-specific proteins in both AD and FTLD-U. Since the completion of this study, there have been significant improvements in both LCM and mass spectrometric technologies. For example, improved optics, throughput, and specificity of capture in LCM have allowed for more rapid collection of purer samples for analysis. Given that the isolation and

molecular profiling of the ubiquitin-positive inclusions is critical for the elucidation of important pathways in FTLD-U pathogenesis, it may be worthwhile to revisit the use of LCM in the characterization of these lesions.

Chapter 4

Proteomics analysis reveals novel components in the detergent-insoluble subproteome in Alzheimer's disease.[3]

4.1 Introduction

Alzheimer's disease (AD) is a progressive neurological disorder characterized by impairment of memory and cognitive decline (Blennow, de Leon et al. 2006). Accounting for more than 20 million cases worldwide, AD is both the most common neurodegenerative disorder and the most prevalent form of dementia (Bergamaschini, Canziani et al. 1999; Goedert and Spillantini 2006). Multiple pathways have been implicated in AD pathogenesis, including neuronal cell death, oxidative damage, chronic inflammation, and protein aggregation (Nunomura, Perry et al. 2001; Ross and Poirier 2004; Tuppo and Arias 2005). Pathologically, AD is characterized by neuronal loss, gliosis, and the accumulation of two major lesions: senile plaques composed primarily of amyloid-β peptide (Aβ) (Glenner and Wong 1984) and neurofibrillary tangles (NFTs)

[3]Portions of this chapter have been reproduced with permission from Gozal YM, Duong DM, Gearing M, Cheng D, Hanfelt J, Funderburk C, Peng J, Lah JJ, and Levey AI. (2009). Proteomics analysis reveals novel components in the detergent-insoluble subproteome in Alzheimer's disease. J Proteome Res.

composed primarily of hyperphosphorylated microtubule-associated protein, tau (Lee, Balin et al. 1991). Most lesion components, including Aβ and tau (Glenner and Wong 1984; Masters, Simms et al. 1985; Lee, Balin et al. 1991), have been identified using brute-force biochemical or immunological approaches (Atwood, Martins et al. 2002). However, these methods allow only the identification of a limited number of high-abundance targets. Due to the complex pathogenesis of AD and the dynamic nature of cellular proteins, proteomics methodologies have quickly emerged as invaluable high-throughput strategies for the unbiased identification of disease-specific proteins.

Recent efforts have been directed at the analysis of protein abnormalities in the AD brain using proteomic approaches (Butterfield and Castegna 2003). Large-scale proteomics analyses were first conducted using traditional two-dimensional (2D) gel separation, often in combination with mass spectrometry, identifying important proteins in key pathogenic pathways (Mattila and Frey 1994; Tsuji, Shimohama et al. 1999; Tsuji and Shimohama 2001; Tsuji, Shiozaki et al. 2002; Cottrell, Galvan et al. 2005). However, this approach is limited by the narrow sensitivity of 2D gel-based technique, susceptibility to human error, and bias against proteins of extreme p*I*, molecular weight, and hydrophobicity (Palzkill 2002). To alleviate these limitations, liquid chromatography coupled with tandem mass spectrometry (LC-MS/MS) has emerged as the preferred first-stage strategy for large-scale proteomics (Aebersold and Mann 2003). This approach allows the identification and quantification of thousands of differentially-expressed proteins directly from complex protein mixtures with superb sensitivity in the low femtomole range (McCormack, Schieltz et al. 1997). Moreover, both quantitative and descriptive LC-MS/MS strategies have been successfully used in the characterization of

AD related proteins. We first combined laser capture microdissection (LCM) with LC-MS/MS to identify a total of 488 proteins that co-isolate with senile plaques (Liao, Cheng et al. 2004; Gozal, Cheng et al. 2006). Further label-free quantitative comparison of plaque and non-plaque tissues based on extracted ion currents of identified peptides revealed at least two-fold enrichment of 26 proteins in the plaque regions. LC-MS/MS analysis of NFTs isolated by LCM quickly followed (Wang, Woltjer et al. 2005), demonstrating an additional 72 NFT-associated proteins identified by multiple unique peptides. Finally, a descriptive profile of detergent-insoluble proteins from temporal cortex of late onset AD post-mortem samples revealed an additional 125 proteins with reduced detergent solubility (Woltjer, Cimino et al. 2005). These data highlight the diversity of cellular processes involved in aggregate formation, and emphasize the need for thorough analysis of the complex neuropathological lesions associated with AD.

Although the rapid developments in proteomic technologies offer the opportunity to revisit pathologic aggregate composition, significant optimization of experimental design strategies and data processing is necessary to reduce false positives and improve analysis depth. A variety of factors can affect protein expression, quality, and stability in the post-mortem tissues used to study neurodegenerative disorders (Hynd, Lewohl et al. 2003). For example, the interval between death and the processing of the brain (post-mortem interval, PMI) must be matched across cases to control for protein degradation that begins immediately after death (Fountoulakis, Hardmeier et al. 2001). In addition, clinical and pathophysiological heterogeneity, age, sex, and race are important sources of biological variability (Kim, Voshol et al. 2004), and may be controlled by implementation of a pooling strategy. Although pooling may complicate subsequent

statistical comparisons, combining samples dilutes the between-subject variance (Leger and Didrichsons 1994) and helps reduce false-positive rates in proteomic experiments. Additionally, detection of disease-specific proteins can be enhanced by reducing the complexity of the analytes. Despite the exquisite sensitivity of LC-MS/MS, large-scale analyses of complex samples, such as total homogenates, often result in the identification of only the most abundant cellular proteins. Thus, it may be useful to simplify the sample by focusing on the examination of the subproteomes with highest relevance to neurodegeneration.

In this study we establish a strategy for unbiased proteomic characterization of post-mortem human neurodegenerative disease tissues. To validate our approach and further identify new protein targets, we used proteomics to profile disease-specific protein changes in detergent-insoluble extracts of pooled AD frontal cortex cases. Frontal cortex is a selectively vulnerable region in AD (Terry and Katzman 1983), and has been shown to contain abundant protein aggregates characterized by reduced solubility in multiple neurodegenerative disorders (Wang, Woltjer et al. 2005; Woltjer, Cimino et al. 2005; Mitsui, Doi et al. 2006; Neumann, Sampathu et al. 2006). Thus, we used a label-free quantitation strategy based on extracted ion currents of identified peptides to compare the detergent-insoluble subproteome with the profiles obtained from pools of both unaffected control and frontotemporal lobar degeneration (FTLD) cases. Inclusion of the FTLD cohort to filter the selection of proteins that are specific to AD rather than non-selectively altered as a result of common processes involved in neurodegeneration resulted in our identification of 11 proteins with disproportionate enrichment in AD extracts. These included several proteins already implicated in AD along with a group of

proteins not previously linked to AD. Identification of these proteins validates our proteomic strategy for the examination of human neurodegenerative disease samples, and suggests that our systematic examination of insoluble brain extracts can provide important new clues for understanding the pathways underlying the formation of AD pathological lesions.

4.2 Results

4.2.1 Protein identification in urea samples by LC-MS/MS

The proteomic profiling of AD detergent-insoluble aggregated protein fractions was initialized with sample optimization and preparation as illustrated in **Figure 4.1 A**. In our strategy, frontal cortical samples from postmortem AD, FTLD-U and control cases (n = 10 per diagnosis) were individually homogenized and examined prior to pooling by SDS-PAGE followed by silver staining (data not shown). Although there were some differences in band intensities, there was little degradation of proteins such that the pattern of major bands was similar between cases. To minimize inter-case variation, homogenates from 10 cases of each diagnosis **(Table 4.1)** were then combined into a single pool with each case contributing 3 mg total protein. The FTLD-U pooled samples were divided into two identical samples that were processed in parallel as "technical replicates" to discern experimental variances and improve capacity to accurately identify disease-specific proteins (Kendziorski, Zhang et al. 2003; Allison, Cui et al. 2006). AD, control, and both FTLD-U pools were serially extracted with triton X-100, sarkosyl, and urea buffers. Urea-soluble fractions were then separated by mass via SDS-PAGE

A

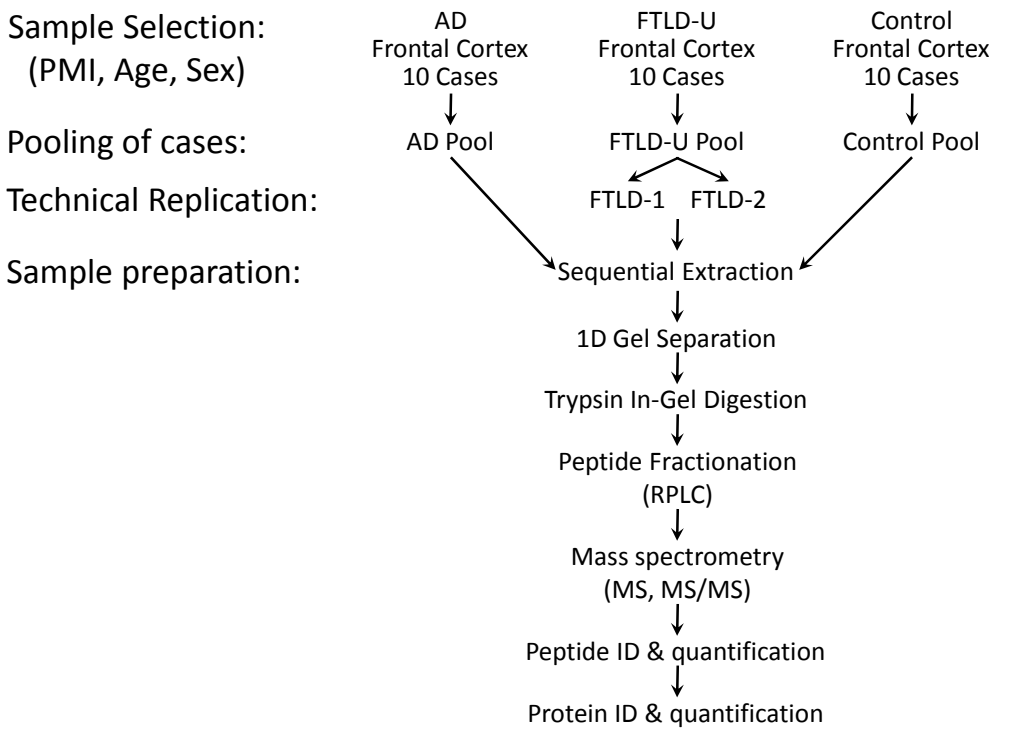
Sample Selection:
(PMI, Age, Sex)
Pooling of cases:
Technical Replication:
Sample preparation:
AD
Frontal Cortex
10 Cases
FTLD-U
Frontal Cortex
10 Cases
Control
Frontal Cortex
10 Cases
AD Pool
FTLD-U Pool
Control Pool
FTLD-1
FTLD-2
Sequential Extraction
1D Gel Separation
Trypsin In-Gel Digestion
Peptide Fractionation
(RPLC)
Mass spectrometry
(MS, MS/MS)
Peptide ID & quantification
Protein ID & quantification

B

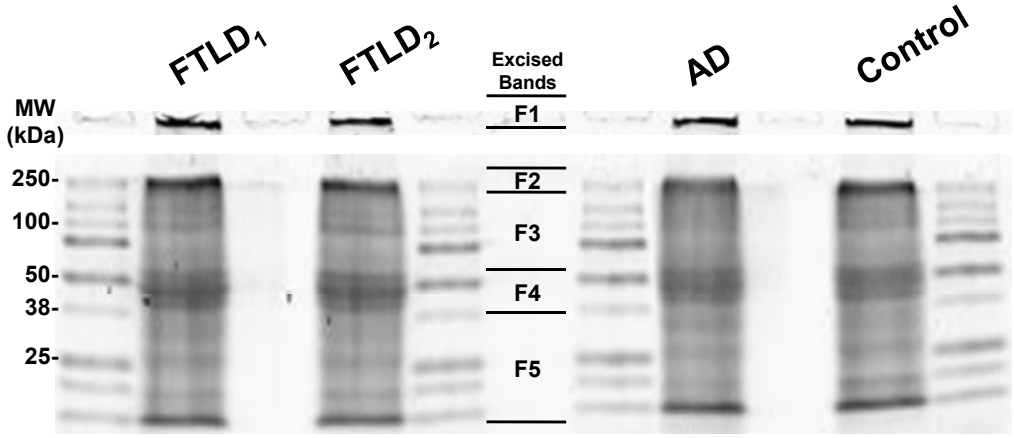
FTLD1
FTLD2
Excised Bands
AD
Control
MW (kDa)
250-
100-
50-
38-
25-
F1
F2
F3
F4
F5

Figure 4.1 Sample preparation for proteomic analysis. (A) Diagram of the strategy for sample preparation and "bottom-up" proteomics analysis in which proteins are digested into peptides for improved separation and ionization. (B) SDS-PAGE gel of the isolated urea fractions stained with Coomassie Blue G-250. The gel lanes were excised in 5 pieces as indicated (F1-F5).

Table 4.1: Demographics of patient pools used for proteomic characterization[1].

Diagnosis	n[2]	PMI (hr)[3]	Age at Death	Duration (years)[4]	Sex (#F/#M)[5]
AD	10	11.5	66.1	9.4	6/4
Normal Control	10	8.1	64.6	NA	6/4
FTLD-U	10	12.1	65.7	7.1	6/4

[1]Complete demographic data for individual cases in pool are listed in Table 6.1 [2]Number of cases in pool [3]Average post-mortem interval in hours [4]Average duration of disease from diagnosis to death in years [5]Sex: *M* male *F* female.

(Figure 4.1 B), excised in 5 bands from the gel, and trypsin-digested. To minimize variation associated with HPLC column performance and ionization efficiency, the tryptic peptide mixtures for each sample were analyzed sequentially under identical LC-MS/MS conditions on a high-resolution mass spectrometer. These spectra were searched against a human protein database, and further stringently filtered by mass accuracy and matching scores. A total of 1,045 proteins (3,216 peptides) were identified in all four samples and these were clustered into 512 protein groups based on shared peptides.

4.2.2 Relative quantification of proteins in urea samples by the label-free strategy

The comprehensive profiling of protein expression in AD detergent-insoluble preparation requires both the identification and the quantitation of proteins. To determine which of the identified proteins were preferentially enriched in AD, a quantitative protein comparison based on the extracted ion current (XIC) of identified peptides was performed. Abundance ratios corresponding to the relative protein abundance between AD and FTLD-U or control samples were calculated for all 512 proteins identified. Abundance ratios for each possible comparison (e.g. AD/Control) were converted logarithmically and plotted as a histogram **(Figure 4.2 A and B)**. Theoretically, only the abundance of disease-related proteins should be altered in each comparison, and each Gaussian distribution fits the data very well (range of $r^2 = 0.93$ to 0.98), confirming the assumption that the majority of the proteins display similar abundance in disease and control urea extracts. Additionally, the fitted normal distribution was used to approximate the common variance of the whole data set, a feature that was used to establish significance thresholds for protein changes (Cheng, Hoogenraad et al. 2006). The means

A

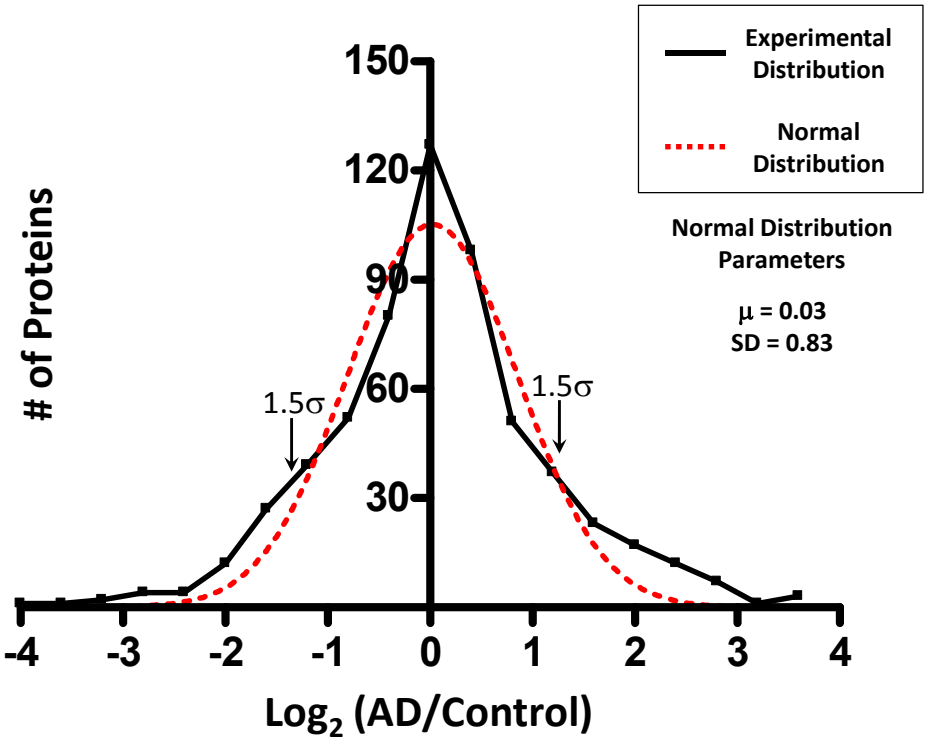
Experimental Distribution
Normal Distribution
Normal Distribution Parameters
μ = 0.03
SD = 0.83
# of Proteins
150
120
90
60
30
1.5σ
1.5σ
-4
-3
-2
-1
0
1
2
3
4
Log2 (AD/Control)

B

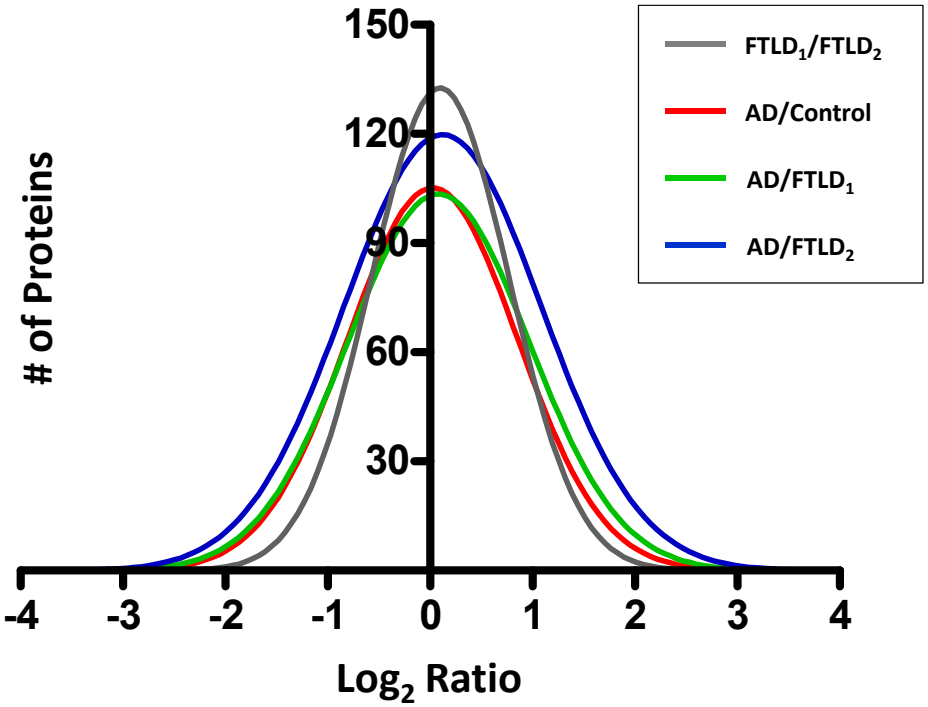
FTLD1/FTLD2
AD/Control
AD/FTLD1
AD/FTLD2
# of Proteins
150
120
90
60
30
-4
-3
-2
-1
0
1
2
3
4
Log2 Ratio

Figure 4.2 Statistical evaluation and filtering of proteomics data. (A) Abundance ratios for AD/Control comparison were transformed (logarithmic base 2) and plotted with each point corresponding to the number of proteins in 0.3 unit windows (black line). A Gaussian curve was subsequently fitted to the data (red line) and used to determine significance levels for protein change. (B) Fitted normal distributions for all possible case comparisons. Statistical means, standard deviations, and regression coefficients are presented in **Table 4.2**.

Table 4.2 Statistical data for fitted normal distributions

Comparison	Mean	[1]SD	r^2
AD/Control	0.03	0.83	0.93
AD/FTLD$_1$	0.08	0.89	0.97
AD/FTLD$_2$	0.12	0.96	0.94
AD/FTLD$_{avg}$	0.12	0.81	0.98
FTLD$_1$/FTLD$_2$	0.10	0.67	0.98

[1]Standard deviation of distributions

and standard deviations (SD) for all relevant case comparisons are shown in **Table 4.2**. As an initial filter for significantly changed proteins in AD, we required at least a 2-fold change in protein abundance for both AD/Control and AD/$FTLD_{avg}$ comparisons. Although for a single comparison the probability associated with this 2-fold threshold is approximately 20% according to the average of the SD values (0.82, **Table 4.2**), when two comparisons were simultaneously considered, the probability of false positives falls to ~4% (20% x 20%). According to the null hypothesis, this probability is equivalent to 21 false positives in a list of 512 proteins. However, using the 2-fold cutoff in our data, 81 proteins were accepted in the filtering, suggesting ~60 (equivalent to 81-21) proteins could theoretically be altered specifically in the AD sample. To remove the false positives in the 81 remaining proteins, we manually examined these proteins and filtered according to additional criteria **(Table 4.3, see Chapter 2: Materials and Methods),** resulting in a final list of 11 AD-specific proteins **(Table 4.4)**. Although this stringent manual processing increased our confidence in the quantitative measures, our criteria favor specificity over sensitivity in populating a list of less than the predicted 60 proteins.

The difference between the quantitative information obtained using the XIC method and the qualitative information obtained during peptide identification is further emphasized by the observation that, of the 11 AD-specific proteins in our final list, only the inflammatory complement C4 was identified in the AD sample alone. Since identification of a peptide relies on its fragmentation to produce a unique MS/MS spectrum, complex protein samples can easily saturate the sampling rates of the mass spectrometer (Roxas and Li 2008). Therefore, due to inherent limitations in the duty cycle of the instrument, only a fraction of ionized peptides can be selected for

Table 4.3 Additional filtering criteria for removal of false positives

Category	Score	
	1	**0**
Peptide Quality	Fully Tryptic no miscleavage no modification	All Others
Matching Status	Matched	Unmatched
Extracted Ion Current	Total [1]SN > 4	Total SN < 4

Criteria were based on quality assessment of protein quantification by manual scoring of corresponding peptides. A top scoring protein would receive 1 point in each of the above categories for a total of 3 points.

[1]Signal to noise ratio

Table 4.4: Proteins specifically altered in AD urea fractions compared with control and FTLD-U.

Protein	GeneBank™ Accession Number	Log_2 Ratio AD/Control	mean Log_2 Ratio AD/FTLD	Quantified Peptides
microtubule-associated protein tau	NP_058518.1	5.2	5.5	16
serum amyloid P component precursor	NP_001630.1	4.0	3.3	2
amyloid beta A4 protein precursor	NP_958817.1	3.5	3.6	5
complement component 4B	NP_001002029.1	3.4	3.1	5
serine protease 15	NP_004784.2	2.3	1.2	6
apolipoprotein E	NP_000032.1	2.1	2.5	5
14-3-3, eta polypeptide	NP_003396.1	1.9	1.4	3
14-3-3, zeta polypeptide	NP_663723.1	1.7	1.6	3
ankyrin B	NP_066187.2	1.3	1.4	1
dynamin 1	NP_004399.2	1.3	1.2	5
aquaporin 1	NP_000376.1	-2.0	-2.0	2

sequencing. Hence, many nonsequenced ion peaks remain in the MS survey scans, an issue known as "undersampling" in shotgun LC-MS/MS analyses. Even a comparison of the technical replicates, $FTLD_1$ and $FTLD_2$, which are identical samples, reveals only a 66% overlap in identified proteins. Certainly, those remaining proteins not identified in both $FTLD_1$ and $FTLD_2$ do not represent true differences between these replicates, but instead reflect the capacity for the instrument to be overwhelmed by particularly complex samples. In contrast, quantification using the XIC method is derived from the MS survey scan and is, thus, not entirely dependent on the acquisition of MS/MS scans. Once a peptide has been detected in one of the samples, its corresponding non-sequenced ion peak in all of the other samples can be localized for quantitation using the predicted *m/z* value and adjusted retention time (Gozal, Cheng et al. 2006). Using this strategy, we quantified peptides for all 35 proteins detected in the AD sample alone, and only complement C4 showed significant quantitative change.

4.2.3 Validation of selected AD-specific, detergent-insoluble proteins

To independently verify the accuracy of the LC-MS/MS generated data, we analyzed several of the proteins identified as altered in AD by immunoblotting and immunohistochemical methods. Among these, we selected several proteins that have been previously implicated in AD or have been associated with known pathogenic pathways. Notably, microtubule-associated protein tau and apolipoprotein E were among the most altered proteins, demonstrating enrichment in AD tissues of greater than 30-fold and 5-fold respectively by quantitative LC-MS/MS. Quantitative immunoblot analysis demonstrated significant enrichment of both tau and apolipoprotein E in urea fractions

from pooled AD postmortem frontal cortex samples **(Figure 4.3 A and B)**. As insoluble proteins typically aggregate focally in disease pathology, immunohistochemistry provides a complementary method to visualize the distribution of altered proteins and their relationship to neurodegenerative changes. AD frontal cortex showed extensive neuropathology with striking enrichment of immunoreactivity for tau **(Figure 4.4 A and B)** and ApoE **(Figure 4.4 C and D)** as has been well-established previously (Lee, Balin et al. 1991; Fryer, Simmons et al. 2005; Xu, Vitek et al. 2008). Although apolipoprotein E was primarily localized to amyloid plaques, there was also a striking association in multiple cases with neurofibrillary tangles in frontal cortex.

Having validated well-known AD-linked proteins by proteomics and immunological methods, we used similar methods to independently validate and characterize several novel proteins identified as increased in AD from our LC-MS/MS-based approach. Compared with control and FTLD-U cases, pooled urea samples from AD frontal cortex demonstrated up-regulation of ankyrin B, serine protease 15 (PRSS15), and 14-3-3η **(Figure 4.3)** in Western blot analysis. Immunohistochemical examination of both ankyrin B and 14-3-3η revealed thread-like structures with striking localization in plaque regions, confirming the enrichment suggested by the proteomic findings **(Figure 4.4)**. In addition to being a plaque component, 14-3-3η also appeared to be significantly enriched in the surrounding neuropil in AD tissues. These broad changes in 14-3-3η expression may suggest a more general role in AD pathogenesis. Despite extensive overexpression in AD urea fractions, serine protease 15 (PRSS15) was not associated with classical AD pathology, and its localization remained unaltered in both hippocampus and frontal cortex **(data not shown)**. Finally, although we attempted to validate changes

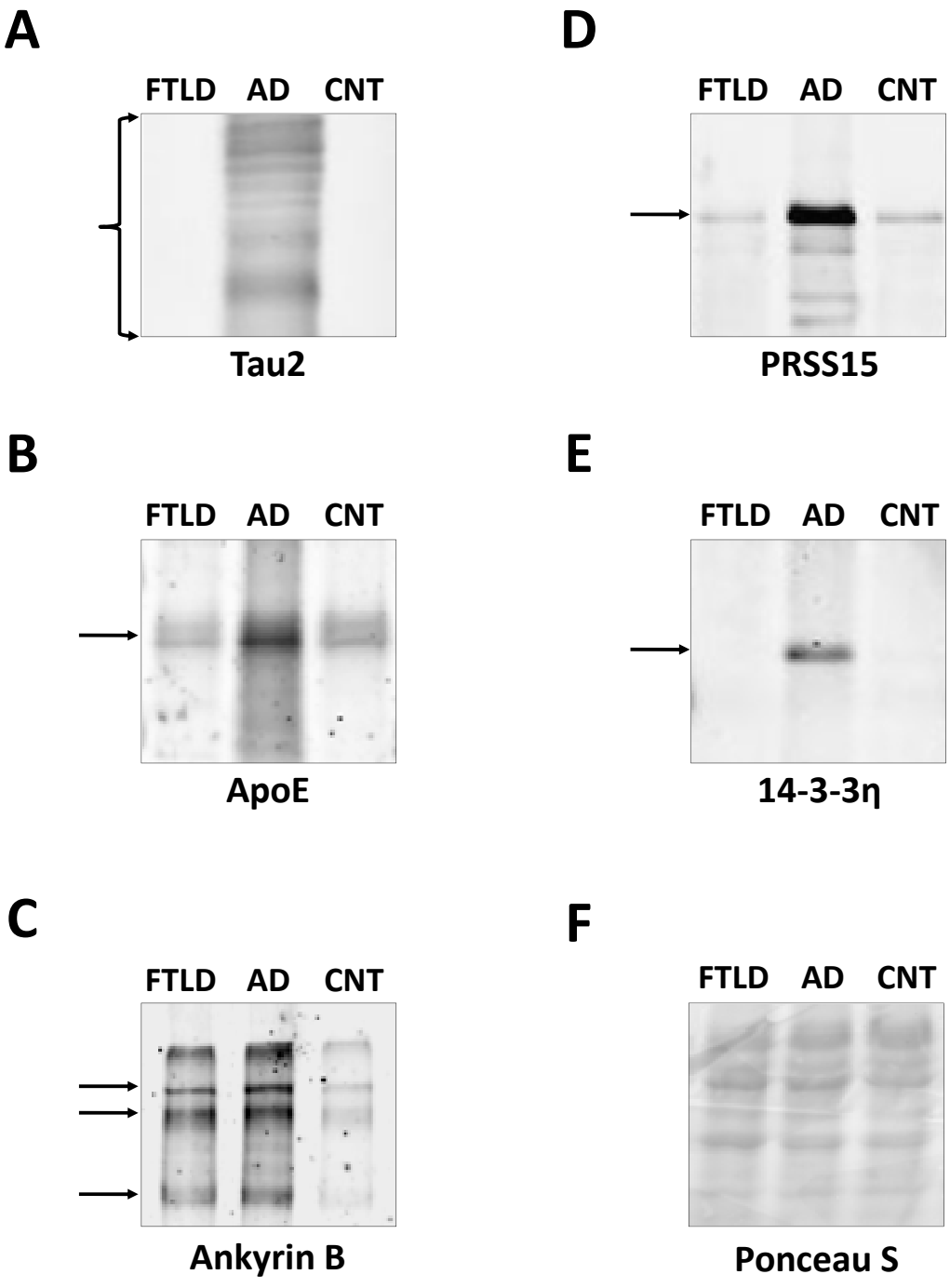
A
FTLD AD CNT
Tau2
D
FTLD AD CNT
PRSS15
B
FTLD AD CNT
ApoE
E
FTLD AD CNT
14-3-3η
C
FTLD AD CNT
Ankyrin B
F
FTLD AD CNT
Ponceau S

Figure 4.3 Confirmation of proteomic candidates by immunoblot analysis. Frontal cortex from FTLD-U, AD, and unaffected control cases were pooled by diagnosis and sequentially extracted with buffers containing triton X-100, sarkosyl, and urea. Sarkosyl insoluble (urea) samples were immunoblotted with antibodies to (A) Tau2, which recognizes both non-phosphorylated and abnormal phosphorylated tau (region shown ~30kD-60kD), (B) apolipoprotein E (36kD denoted by arrow), (C) Ankyrin B (multiple isoforms denoted by arrows at 205kD, 163kD, and 100kD), (D) Serine protease 15 (106kD denoted by arrow), and (E) 14-3-3η (28kD denoted by arrow). (F) Representative Ponceau S reversible membrane stain performed to ensure both equal loading and complete transfer of proteins from the gel.

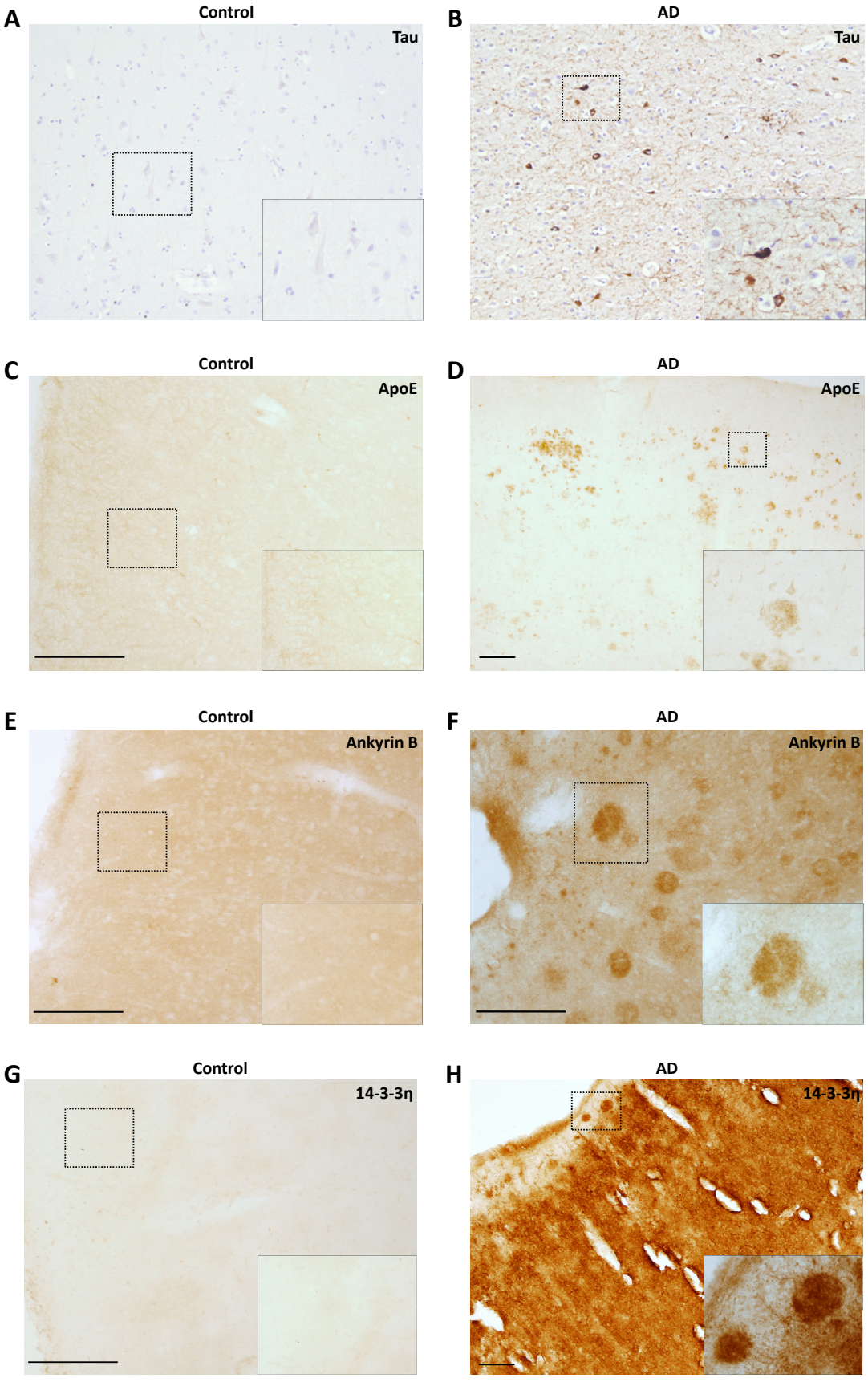
A
Control
Tau
B
AD
Tau
C
Control
ApoE
D
AD
ApoE
E
Control
Ankyrin B
F
AD
Ankyrin B
G
Control
14-3-3η
H
AD
14-3-3η

Figure 4.4 Confirmation of urea extraction proteomic candidates by immunohistochemistry (A) Tau2 immunostaining in control tissue and (B) in AD. (C) Apolipoprotein E staining in control tissue (200μm) and (D) AD (100μm). (E) Ankyrin B staining in control tissue (200μm) and (F) AD (200μm). (G) 14-3-3η staining in control tissue (200μm) and (H) AD (100μm). *(All sections from frontal cortex; Scale Bar in μm)*

in expression of dynamin 1 and aquaporin 1, the lack of specific immunoreactivity of the purchased commercially available reagents precluded confirmation of the proteomic results in these studies.

4.3 Discussion

Protein accumulation and aggregation in the brain is one of the pathologic hallmarks of neurodegenerative diseases. Interestingly, an important characteristic of these aggregates is their spontaneous conversion from functional soluble proteins to pathologic, detergent-insoluble fibrillar forms identified in diseased tissues (Pallitto and Murphy 2001; Morishima-Kawashima and Ihara 2002; Sahara, Lewis et al. 2002; Kuret, Congdon et al. 2005). The altered insoluble structure of aggregated proteins can result in both functional deficits and, more importantly, in a toxic gain of function associated with the aggregate itself or its transient intermediates (Lansbury 1999; Kim, Muresan et al. 2004). Thorough characterization of neurodegenerative disease aggregates and the aggregation process is, therefore, essential for our understanding of the molecular pathways underlying disease pathogenesis. Here, we describe an unbiased proteomics strategy for the large-scale identification of novel disease-specific proteins that may serve as biomarkers and targets for therapeutic intervention. Our study revealed a total of 512 proteins present in pathologic detergent-insoluble fractions prepared from AD frontal cortex. Using strict filtering criteria to remove proteins that were either unchanged in disease extracts compared to control or were non-specifically altered in both FTLD-U and AD, we identified 11 proteins with high specificity for AD. These included

established proteins that are classically associated with AD pathologic lesions, as well as several novel associated proteins encompassing a broad range of cellular activities. We subsequently verified five targets by immunoblotting and immunohistochemistry, highlighting the power of our proteomics approach for identifying new proteins as well as a more complete understanding of the complement of proteomic changes that are involved in neurodegeneration.

The widespread transition of proteins to detergent insolubility and the complexity of aggregate composition are well-established in neurodegeneration (Atwood, Martins et al. 2002; Liao, Cheng et al. 2004; Wang, Woltjer et al. 2005; Woltjer, Cimino et al. 2005; Neumann, Sampathu et al. 2006). As is reflected in our data, development of LC-MS/MS based proteomics has allowed for examination of complex disease samples with increasing sensitivity. Our data provide evidence for reduced detergent solubility in greater than 500 proteins in AD. Yet, when quantitatively compared with control and FTLD-U samples, only 11 proteins show significant changes that are specific to AD. Many of the unchanged proteins may be contaminants acquired during the extraction procedure or proteins that are altered generally in either neurodegeneration or during normal aging. Nevertheless, in the context of AD, the unchanged proteins contribute to the false-positive rate and suggest that due to improved sensitivity, the identification of proteins without quantitation is insufficient for establishing a specific association with disease.

Despite improved sensitivity of LC-MS/MS analyses, limitations of "undersampling" in LC-MS/MS restrict the number of peptides that can be identified in a specific sample. This technical limitation can be assessed by the inclusion of technical

replicates, or identical samples that are processed in parallel. Our comparison of the replicates $FTLD_1$ and $FTLD_2$ revealed that only two-thirds of the proteins were identified in the identical samples. Thus, since during a shotgun proteomics experiment, only a fraction of possible peptides from a complex mixture can be selected and sequenced by MS/MS (Peng and Gygi 2001), the failure to identify a peptide in a complex sample in shotgun mode does not imply the absence of that peptide in the mixture. By using the XIC method for quantitation, we quantified many peptides selected for MS/MS analysis in only one of the samples by matching their corresponding non-sequenced ion peak in all other samples. Our data, therefore, demonstrate the importance of the application of a quantitative strategy in the profiling of complex neurodegenerative disease samples.

In addition to the variability inherent in the process of mass spectrometry, identification of important disease-specific changes is complicated by the variation resulting from the use of patient samples in neuroproteomics. Theoretically, by pooling equal volumes of different patient samples with a well-characterized common pathologic phenotype, we reduce the potential for aberrations in a single sample to sway the mean (Weinkauf, Hiddemann et al. 2006). This reduction in inter-sample, or biological, variation can improve the capacity to identify the most significant and consistent changes between diseases. The potential loss of statistical power is thereby compensated by the increased confidence in the measurement of each protein concentration. However, as is typical with analysis of human tissues, each sample comparison in this study was associated with a relatively large standard deviation, including the comparison of technical replicates ($FTLD_1/FTLD_2$). Since $FTLD_1$ and $FTLD_2$ are identical pools separated prior to sequential extraction, the large variations in this comparison may be

primarily attributed to the technical error during sample preparation, SDS gel electrophoresis, in-gel digestion and the following LC-MS/MS runs. This implies that the larger standard deviations measured in the other comparisons (e.g. AD/Control) are only partially affected by true biological differences. Accordingly, our proteomic strategy could be modified to include multiple pools for each diagnosis to also allow an assessment of this biological variability.

Analysis of the detergent-insoluble proteome revealed robust differences in 11 proteins with high specificity to AD. Among these, we corroborate the extensive enrichment of key AD-associated proteins, including the microtubule-associated protein tau, Aβ, apolipoprotein E (Strittmatter and Roses 1995), serum amyloid P (Rostagno, Lashley et al. 2007), and complement component 4 (Yasojima, Schwab et al. 1999). The known association of these proteins with the pathologic features of AD, and their disproportionate enrichment in our AD detergent-insoluble extracts, substantiate the specificity of our proteomic strategy and validate the quality of our urea extract preparations. Interestingly, our strict filtering criteria removed multiple proteins known to colocalize with AD pathologic lesions, including apolipoprotein D (Navarro, Del Valle et al. 2003), αB-crystallin (Wilhelmus, Otte-Holler et al. 2006), and cathepsin-D (Nakamura, Takeda et al. 1991). While it is probable that in the effort to reduce the false-discovery rate we also eliminated certain molecules with relevance to AD pathogenesis, it is possible that some of these molecules play a more general role in neurodegeneration, and were removed by the inclusion of FTLD-U as a disease control. It is also possible that some of these molecules may be associated with AD pathology without a corresponding increase in abundance in insoluble fractions prepared from frontal cortex.

Alternatively, these molecules may non-specifically associate with AD lesions by immunohistochemistry, and may have limited involvement in the pathogenesis of the disease (Woltjer, Cimino et al. 2005). Their exclusion, coupled with the presence of proteins such as tau and Aβ among the candidates, may help validate the specificity of the remaining targets.

In addition to well-established disease proteins, we demonstrated and immunologically validated the enrichment of several novel proteins in AD detergent-insoluble fractions. Although their specific association with AD pathogenesis is not well characterized, these proteins, including ankyrin B and PRSS15, play important roles in functional pathways of particular relevance to AD pathophysiology. For example, the disruption of cytoskeletal integrity is a fundamental feature of AD and can impact microtubule stability, alter essential axonal or synaptic signaling, and influence vesicular trafficking and biogenesis (McMurray 2000). Our recently published phosphoproteomic analysis revealed that, in addition to tau, there are other abundant phosphorylated proteins the AD brain (Xia, Cheng et al. 2008). One of these proteins, ankyrin B, is a cytoskeletal component that plays a important role in synaptogenesis, stabilization of the synapse, and organization of the plasma membrane (Bennett and Healy 2008). These actions depend on the ability of ankyrin B to establish specialized protein complexes by coordinating the interactions of another skeletal protein, spectrin, with various integral membrane proteins (Bennett and Lambert 1999). In the current study, ankyrin B was preferentially enriched in AD detergent-insoluble preparations, and was localized in plaque regions by immunohistochemistry. It is possible that the aggregation of ankyrin B results in a loss of function phenotype with pervasive implications for AD pathogenesis. The absence of

ankyrin-binding activity, as is seen in ankyrin B-knockout mice (Bennett and Healy 2008), can trigger a loss of interneuron synapses that may contribute to cognitive decline in AD.

Another protein with altered abundance in AD urea fractions was PRSS15, an ATP-dependent mitochondrial matrix protein that is responsible for the degradation of oxidized proteins (Bota and Davies 2002; von Janowsky, Knapp et al. 2005). The involvement of mitochondrial dysfunction and oxidative stress in neurodegeneration is well-established (Atamna and Frey 2007). In AD, multiple studies link oxidative stress and the modulation of both Aβ levels and hyperphosphorylation of tau (Fukui and Moraes 2008). Additionally, under conditions of cellular stress, many proteins become highly susceptible to oxidative modification and must be selectively removed by proteolytic digestion (Zhang, Marcillat et al. 1990; Bota and Davies 2002). Although PRSS15 is normally present in relatively low abundance (von Janowsky, Knapp et al. 2005), in our study its expression was significantly upregulated in the pathologic insoluble preparation. Despite this upregulation, PRSS15 demonstrated no association with characteristic AD neuropathology by immunohistochemistry. We speculate that during AD, the capacity for PRSS15 to remove damaged proteins is overwhelmed, as evidenced by the accumulation of aconitase (Shin, Lee et al. 2004), a mitochondrial matrix protein that is preferentially degraded by PRSS15 (Bota and Davies 2002). The subsequent accrual and aggregation of damaged or misfolded proteins result in the exacerbation of mitochondrial dysfunction, the increased production of reactive oxygen species (ROS), and the triggering of programmed cell death.

In summary, this study illustrates the potential of proteomic applications to identify sets of disease-specific proteins linked to individual neurodegenerative diseases, as well as conserved sets of proteins involved in processes common to many neurodegenerative diseases. We were able to use a labeling-free strategy to assign quantitative information to thousands of peptides identified directly from clinical samples. As a result, we generated a highly specific profile of altered AD proteins. This profile included both well-characterized components of AD pathology and novel potential therapeutic targets with roles in various important functional pathways. Since pathologic protein aggregation is ubiquitous to all neurodegenerative diseases, the approach detailed herein may be uniformly applied to generate disease-specific profiles that may be customized to improve diagnosis or to shed light on the pathogenesis of these complex disorders.

Chapter 5

Multiplex SILAC analysis of a cellular TDP-43 proteinopathy model reveals protein inclusions associated with SUMOylation and diverse polyubiquitin chains.

5.1 Introduction

Frontotemporal lobar degeneration (FTLD) is a progressive neurodegenerative disease characterized by prominent behavioral abnormalities, personality changes, language dysfunction, and co-occurs with the development of parkinsonism and motor neuron disease in some patients (Neary, Snowden et al. 2005; Kumar-Singh and Van Broeckhoven 2007). Like other neurodegenerative diseases, FTLD is characterized by the abnormal accumulation of ubiquitinated intracellular protein aggregates (Taylor, Hardy et al. 2002; Ross and Poirier 2004). In addition to the aggregation of tau in some forms of FTLD, more than half of the cases are marked by ubiquitin-positive inclusions and are sub-classified as FTLD-U. TAR DNA-binding protein 43 (TDP-43) has been identified as a major protein component of inclusions in FTLD-U and sporadic amyotrophic lateral sclerosis (ALS) (Neumann, Sampathu et al. 2006). Pathologic TDP-43 aggregation is also observed in hereditary inclusion body myopathy and Paget's disease of the bone with frontotemporal dementia (Neumann, Mackenzie et al. 2007), as well as in some cases of

Alzheimer's and Parkinson's diseases (Amador-Ortiz, Lin et al. 2007; Nakashima-Yasuda, Uryu et al. 2007). This indicates that a common underlying mechanism may broadly define a spectrum of neurodegenerative disorders termed "TDP-43 proteinopathies" (Cairns, Neumann et al. 2007; Forman, Trojanowski et al. 2007). Here, we establish a cellular model for the study of TDP-43 aggregation, and explore the important post-translational modifications that may contribute to the accumulation of this protein in FTLD-U pathogenesis.

TDP-43 is a 414 amino-acid protein that contains two RNA recognition motifs (RRM1 and RRM2) and a glycine-rich C-terminal domain. It is highly conserved in human, mouse, fly and worm, and is expressed in all tissues including the brain (Buratti and Baralle 2001; Wang, Wang et al. 2004; Ayala, Pantano et al. 2005). First characterized to bind and repress the promoter activity of transactive response (TAR) DNA in the human immunodeficiency virus 1 (HIV-1) long terminal repeat region (Ou, Wu et al. 1995), TDP-43 was later found to regulate splicing of the apolipoprotein A2 (Mercado, Ayala et al. 2005) and the cystic fibrosis transmembrane conductance regulator (CFTR) transcripts (Buratti, Dork et al. 2001). Therefore, TDP-43 can act both as a transcriptional repressor and as a splicing regulator. Although physiological TDP-43 resides mainly in the nucleus, pathologic TDP-43 redistributes from the nucleus to the cytoplasm, where it is cleaved and forms phosphorylated and ubiquitinated inclusions (Neumann, Sampathu et al. 2006; Mackenzie, Bigio et al. 2007; Mackenzie and Rademakers 2007; Neumann, Kwong et al. 2007). However, the degree to which TDP-43 is posttranslationally modified and whether other modifications initiate nuclear translocation or aggregation events remain unknown.

The primary transcripts of TDP-43 in mouse and human undergo multiple alternative splicing events in which ten splice variants (S1-S10) have been documented (Wang, Wang et al. 2004). With the exception of full-length TDP-43, all alternatively spliced isoforms are expressed as truncated proteins that lack the glycine-rich domain. Isoforms that lack this region are no longer capable of enhancing the skipping of exon 9 of the *CFTR* gene via interactions with heterogeneous nuclear ribonucleoprotein A/B (hnRNP) (Wang, Wang et al. 2004; Buratti, Brindisi et al. 2005). To date, the vast majority of the sporadic and familial *TARDBP* gene variants found in ALS and FTLD cases (Gitcho, Baloh et al. 2008; Kabashi, Valdmanis et al. 2008; Sreedharan, Blair et al. 2008; Van Deerlin, Leverenz et al. 2008; Yokoseki, Shiga et al. 2008) are reported to have missense mutations resulting in single amino acid substitutions located in the C-terminal region. This establishes an intriguing relationship between ALS disease etiology and the function of the glycine-rich C-terminus of TDP-43. Whether TDP-43 splice variants that lack the C-terminus contribute to translocation and aggregation requires further investigation.

In this study, we overexpressed human TDP-43 and TDP-S6, a splice variant lacking the glycine rich C-terminus, in Human Embryonic Kidney-293 (HEK 293) cells and mouse hippocampal neurons. When compared to TDP-43, TDP-S6 showed nuclear to cytoplasmic translocation and extensive aggregation. Biochemical analysis revealed that TDP-S6 was almost completely sarkosyl-insoluble. Moreover, both insoluble TDP-43 and TDP-S6 displayed varying levels of post-translational modifications that included ubiquitination and/or ubiquitin-like modifications, phosphorylation and proteolytic cleavage. To assess protein differences amongst the detergent-insoluble extracts from

mock, TDP-43- and TDP-S6-transfected cells, a multiplex stable isotope labeling with amino acids in culture (SILAC) strategy was used in combination with liquid chromatography coupled with tandem mass spectrometry (LC-MS/MS) (Mann 2006). This quantitative proteomics approach metabolically introduces a mass difference into proteins by incorporation of heavy isotopic forms of arginine and lysine. Our results show an overall increase in the proteins involved in the ubiquitin-proteasome system (UPS) concomitant with overexpression of TDP-43 or TDP-S6. In addition, we identified and characterized a novel association between the small ubiquitin-like modifier-2/3 (SUMO-2/3) and TDP-43. Together our data indicate that overexpression of a truncated TDP-43 splice variant recapitulates many of the features associated with disease pathology and, that SUMOylation may have an important role in nuclear TDP-43 functions.

5.2 Results

5.2.1 Expression, localization and biochemical properties of recombinant TDP-43 and TDP-S6

We cloned and overexpressed HA-tagged (at N-terminus) human TDP-43 and TDP-S6 in HEK 293 cells **(Figure 5.1)**. Human TDP-S6 is generated via an additional splicing event within exon 6 and encodes a 295 amino acid protein in which the first 277 amino acids are identical to those of TDP-43 **(Figure 5.1A)**. Although mouse TDP-S6 has been shown to have altered nuclear structure in mammalian cells

A

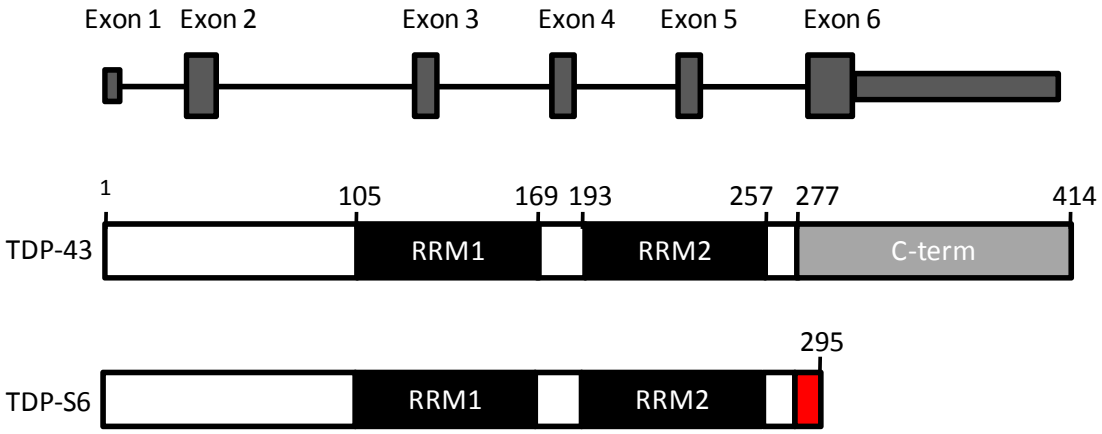
Exon 1
Exon 2
Exon 3
Exon 4
Exon 5
Exon 6
1
105
169
193
257
277
414
TDP-43
RRM1
RRM2
C-term
295
TDP-S6
RRM1
RRM2

B

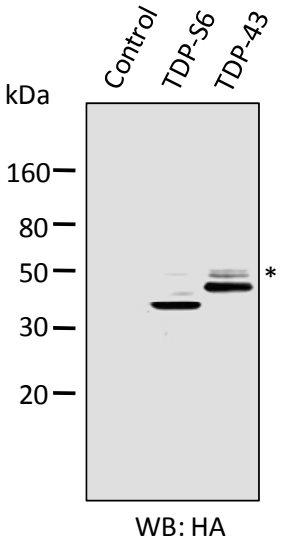
Control
TDP-S6
TDP-43
kDa
160
80
50
30
20
*
WB: HA

C

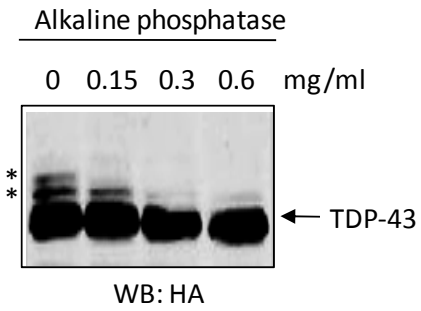
Alkaline phosphatase
0
0.15
0.3
0.6
mg/ml
**
TDP-43
WB: HA

Figure 5.1 Expression of TDP-43 and the shorter alternative splicing isoform, TDP-S6, in HEK 293 cells. (A) TDP-43 consists of six exons that encode a protein of 414 amino acids. RRM1 spans exon 3 and 4, RRM2 spans exon 5 and 6, and the glycine-rich C-terminal domain lies within exon 6. TDP-S6 is generated by an additional splicing event resulting in a reading frame shift after amino acid 277. Thus, TDP-S6 contains 18 unique amino acids (278-295) on its C-terminus (red) corresponding to residual intron RNA included during the alternative splicing event. (B) Western blotting analysis of transfected control (mock plasmid), HA-tagged TDP-43, or TDP-S6. (C) Loss of TDP-43 phosphorylation during phosphatase treatment. The HA-TDP-43 transfected total cell lysate was incubated for 2.5 hr with the addition of increasing concentration of alkaline phosphatase, followed by western analysis. Phosphorylated TDP-43 isoforms are indicated by the asterisks.

(Wang, Reddy et al. 2002), the human TDP-S6 transcript, identified in HEK 293 cells (Wang, Wang et al. 2004), has not yet been characterized. Western blotting of total cell lysate prepared from the transfected cells indicated that both recombinant proteins were expressed and recognized by the HA antibody. TDP-43 also displayed two higher molecular weight (MW) species at approximately 50 kDa **(Fig. 5.1 B and C; indicated by asterisk)**. Aftertreatment with an increasing amount of alkaline phosphatase, the upper band disappeared and the middle band became significantly weaker, whereas the intensity of unmodified TDP-43 remained stable. This supports the conclusion that TDP-43 is preferentially phosphorylated on at least two different residues of the C-terminus **(Fig. 5.1C)**, consistent with the current identification of two phosphorylation sites near the C-terminus of TDP-43 in diseased tissues (Hasegawa, Arai et al. 2008; Inukai, Nonaka et al. 2008).

Subcellular localization of full-length TDP-43 and TDP-S6 was assessed by immunofluorescence confocal microscopy. Overexpressed TDP-43 in HEK 293 cells was localized primarily in the nucleus **(Figure 5.2A, upper panel)**, consistent with the nuclear localization of endogenous TDP-43 in untransfected cells **(Figure 5.2A, upper panel, at the left bottom corner)**. In contrast, TDP-S6 formed aggregates that were mainly localized to the cytoplasm with some inclusions in the nucleus **(Figure 5.2A, middle and bottom panels)**. Observed puncta were of variable size, ranging from fine granular deposits to large, aggresome-like inclusions (Johnston, Ward et al. 1998; Bence, Sampat et al. 2001; Mi, Gan et al. 2009). To assess whether the TDP-S6 phenotype observed in HEK 293 cells could be recapitulated in neurons, we transfected primary mouse hippocampal neurons with TDP-43 or TDP-S6 constructs **(Figure 5.2B)**.

Consistent with the results in HEK 293 cells, TDP-43 in neurons was nuclear, whereas the majority of TDP-S6 formed granular deposits in the cytoplasm of somata and neurites **(Fig 5.2 B and C,** Enolase was stained as a neuron specific marker).

To evaluate the solubility of overexpressed TDP-43 or TDP-S6, HEK 293 cells were transfected with either construct and then mixed equally to eliminate experimental variability in subsequent processing. The mixed cells were sequentially extracted with sarkosyl-containing buffer and urea, and then analyzed by immunoblotting with an antibody specific to TDP-43. The differences in M_r between HA-TDP-43 (47 kDa), native TDP-43 (43 kDa), and HA-TDP-S6 (37 kDa) allowed analysis of all three proteins in a single lane **(Figure 5.3A)**. In addition, phosphorylated TDP-43 isoforms were also resolved. While almost all of HA-TDP-S6 was insoluble, 67% of unmodified HA-TDP-43 and virtually none of the native unmodified TDP-43 were present in the insoluble fraction **(Figure 5.3 A and B)**. Based on these findings, the biochemical insolubility of TDP-S6 is consistent with the phenotype observed by immunofluorescence **(Figure 5.2)**. Moreover, the overexpression of HA-TDP-43 (~2-4 fold) may account for the differences in solubility between the recombinant and native proteins, as has been recently reported (Johnson, Snead et al. 2009). Interestingly, the phosphorylated species of HA-TDP-43 (95%) and TDP-43 (45%) were enriched in the insoluble fraction, supporting previous findings linking the phosphorylation of TDP-43 with its aggregation and insolubility (Neumann, Sampathu et al. 2006). To ensure that overexpression of TDP-43 or TDP-S6 did not dramatically bias the global distribution of proteins to the insoluble fraction, the percent total protein in each fraction (detergent-soluble and insoluble) was calculated

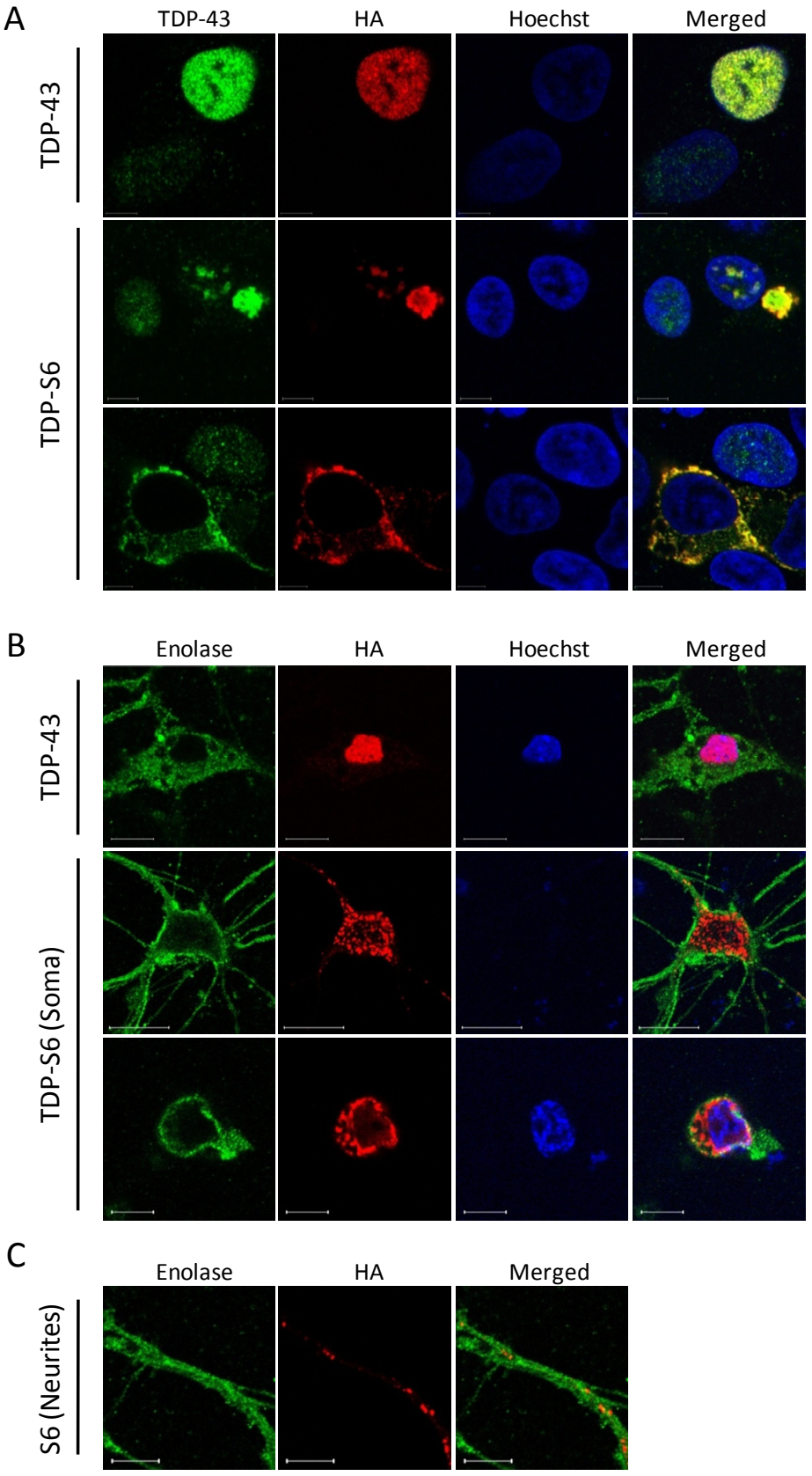
A
TDP-43
HA
Hoechst
Merged
TDP-43
TDP-S6
B
Enolase
HA
Hoechst
Merged
TDP-43
TDP-S6 (Soma)
C
Enolase
HA
Merged
S6 (Neurites)

Figure 5.2 TDP-S6 translocation and aggregation in HEK 293 cells and primary hippocampal neurons. (A) HEK 293 cells were transfected with HA-TDP-43 or HA-TDP-S6 and stained with TDP-43 antibody for both recombinant and endogenous proteins (green), HA antibody for recombinant TDP-43 exclusively (red), and Hoechst stain for the nucleus (blue). The white bars represent a distance of 10 μM. (B) Neurons were transfected and stained with a neuron-specific enolase (green), HA antibody (red) and Hoechst stain (blue). Two different sections of the same neuron, corresponding to separate focal planes, were shown in the middle and bottom panels of TDP-S6, indicating cytoplasm and nucleus, respectively. (C) TDP-S6 was also aggregated in neuronal processes, shown under higher magnification.

A

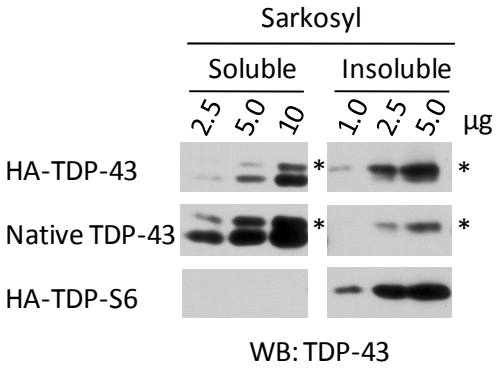

B

TDP proteins in sarkosyl-soluble and -insoluble fractions[1]

TDP expression	%Soluble	%Insoluble
Phosphorylated HA-TDP43	5%	95%
Unmodified HA-TDP43	33%	67%
Phosphorylated native TDP43	55%	45%
Unmodified native TDP43	>95%	<5%[2]
HA-TDPS6	<5%	>95%

[1]Calculated by densitometry analysis from Western blot (5 µg/well).

[2]not detected, assumed to be <5%.

C

Proteins enriched in sarkosyl-insoluble fraction

Accession#	Protein names	Spectral counts		*p* value
		Cell lysate	Urea	
Nuclear complexes				
NP_008835.5	protein kinase, DNA-activated, catalytic	5	132	7.8E-34
NP_001058.2	DNA topoisomerase II, alpha isozyme	0	49	1.7E-16
NP_001059.2	DNA topoisomerase II, beta isozyme	0	26	2.0E-09
NP_003592.2	SWI/SNF-related regulator of chromatin a5	0	21	6.9E-08
NP_006319.1	RNA binding motif protein 14	2	79	4.0E-22
NP_002130.2	RNA binding motif protein, X-linked	1	26	7.7E-08
NP_066014.1	Putative helicase, Mov10, spliceosome-associated	0	56	1.3E-18
NP_001348.2	Putative helicase, DEAH (Asp-Glu-Ala-His) box polypeptide 9	27	75	1.2E-06
NP_006436.3	U5 snRNP-specific protein	4	54	8.0E-13
NP_054733.2	U5 snRNP, 200 KD, activating signal cointegrator 1 complex	15	65	6.5E-09
NP_004238.2	U5 snRNP specific protein, 116 kD, EFTUD2	2	27	4.1E-07
NP_114032.2	heterogeneous nuclear ribonucleoprotein U isoform a	18	68	2.6E-08
NP_112604.2	heterogeneous nuclear ribonucleoprotein C isoform a	6	42	3.6E-08
NP_005959.2	heterogeneous nuclear ribonucleoprotein M isoform a	28	81	2.1E-07
NP_003760.1	splicing factor, arginine/serine-rich 9	0	16	2.5E-06
NP_002408.3	antigen identified by monoclonal antibody Ki-67	0	18	5.9E-07
NP_006176.2	nuclear mitotic apparatus protein 1 (NuMA)	6	33	5.7E-06
Caveolae				
NP_004095.4	fatty acid synthase	95	222	4.7E-13
NP_005794.1	flotillin 1	0	25	4.0E-09
NP_004466.2	flotillin 2	1	20	4.4E-06
Aggresome				
NP_003371.2	vimentin	35	204	1.3E-30
NP_001367.2	dynein, cytoplasmic, heavy polypeptide 1	11	69	7.7E-12
NP_031401.1	TAR DNA binding protein	2	25	1.5E-06
Proteasome				
NP_002788.1	proteasome beta 5 subunit	1	33	6.7E-10
NP_002790.1	proteasome beta 7 subunit proprotein	0	16	2.5E-06
NP_002784.1	proteasome beta 1 subunit	5	31	4.9E-06
NP_002779.1	proteasome alpha 3 subunit isoform 1	2	29	1.1E-07
NP_001034679.2	ubiquitin specific protease 9, X-linked isoform 3	2	30	5.9E-08
Other complexes				
NP_079199.2	nucleoporin 210	0	25	4.0E-09
NP_005955.1	myosin, heavy polypeptide 10, non-muscle	22	110	1.2E-15
NP_004332.2	carbamoylphosphate synthetase 2 in pyrimidine biosynthesis	4	40	5.0E-09
NP_000079.2	alpha 1 type I collagen preproprotein	0	17	1.2E-06
NP_036473.2	G protein-binding protein CRFG in ribosome biogenesis	0	17	1.2E-06

Figure 5.3 Characterization of sarkosyl-insoluble fraction by western blotting and mass spectrometry. (A) Western blot analysis of sarkosyl-soluble and insoluble HA-TDP-43, native TDP-43, and HA-TDP-S6 using an anti-TDP-43 antibody. The asterisks (*) indicate phosphorylated forms. (B) Densitometry analysis of multiple TDP-43 forms. (C) Large-scale profiling of sarkosyl-soluble and insoluble (urea) fractions by LC-MS/MS. Spectral counts of each identified protein were used as a semi-quantitative index to derive probability values.

from mock, HA-TDP-43-and HA-TDP-S6- transfected cells. Approximately 96-97% of all cellular proteins were detergent-soluble irrespective of the recombinant protein expressed, indicating that overexpression of our target proteins did not cause a gross increase in the total amount of protein within the insoluble fraction.

To further characterize proteins enriched in the sarkosyl-insoluble fraction, we identified proteins in the total cell lysate and in the sarkosyl-insoluble sample using a label-free LC-MS/MS approach. The relative abundance of proteins in the two samples was compared according to spectral counts, and the difference was statistically evaluated by *G*-test (Xia, Liao et al. 2008). Among 1,265 proteins profiled, the level of 267 proteins was significantly altered with corresponding *p* values below 0.01. Listed in **Figure 5.3C** are proteins with large changes, including components associated with the proteasome, caveolae, aggresomes, and a number of nuclear complexes. Specifically, flotillin-1 and -2 are markers for caveolae/lipid rafts that are highly enriched in cholesterol and are, therefore, more resistant to detergent extraction (Browman, Hoegg et al. 2007). Vimentin is a protein marker of aggresomes, and is often associated with proteasome proteins (Kopito 2000). Finally, particular DNA/RNA interacting proteins may be inherently detergent-insoluble due to their compact structure. Therefore, the protocol of sarkosyl-based differential extraction is capable of enriching both aggregated proteins and other detergent-insoluble complexes.

Further analysis of detergent-soluble and insoluble fractions from transfected cells revealed that high M_r TDP-43-immunoreactive species were more abundant in fractions corresponding to TDP-S6, rather than TDP-43, overexpression. This observation is consistent with ubiquitination or ubiquitin-like modifications typically associated with

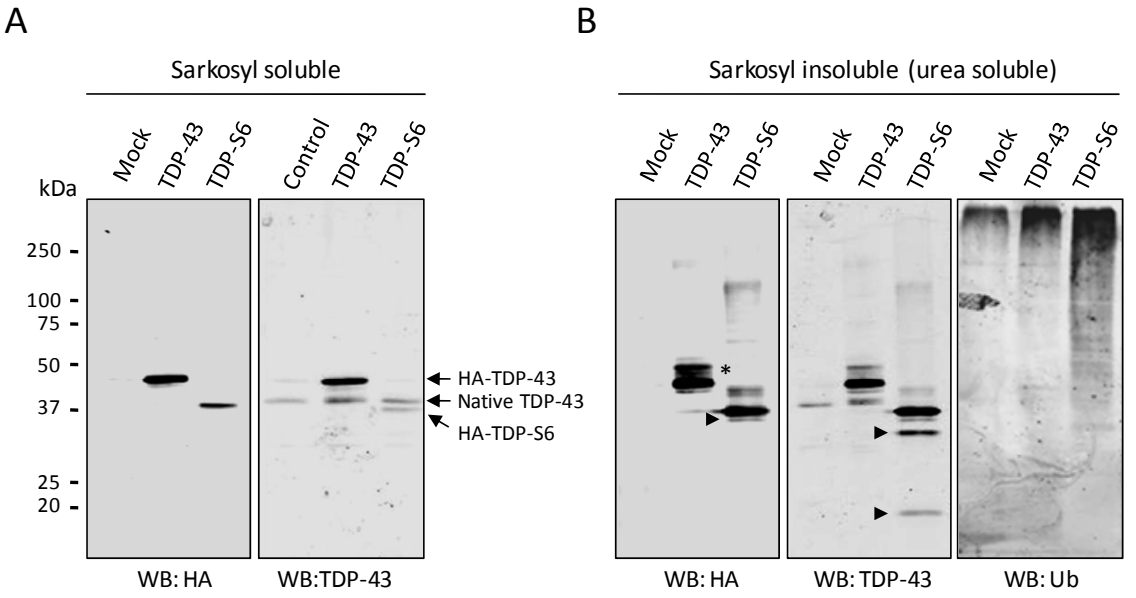

Figure 5.4 TDP-43 and TDP-S6 display posttranslational modifications reminiscent of the biochemical signature observed in neurodegeneration. HEK 293 cells were transfected with mock, HA-TDP-43, or HA-TDP-S6, and extracted by a sarkosyl-containing buffer (A). The remaining pellet was then solubilized with urea buffer (B). The sequentially solubilized proteins were analyzed by western blotting. In detergent-insoluble fractions, modified TDP-43 phosphorylated species (marked by asterisks), proteolytic fragments (marked by arrow heads), and ubiquitinated proteins were observed.

protein insolubility **(Figure 5.4)**. To this end, immunoblotting of sarkosyl-insoluble fractions with a ubiquitin-specific antibody demonstrated an increase in protein ubiquitination with TDP-43, and more dramatically with TDP-S6 overexpression **(Figure 5.4)**. TDP-S6 also displayed two short TDP-43-immunoreactive species (~30 and ~20 kDa) that were not detected by an antibody to HA. This indicates that these bands are C-terminal fragments lacking the N-terminal HA-tag. In addition, a third fragment (~37 kDa) was identified in TDP-S6 urea fractions by both TDP-43 and HA antibodies. Although TDP-S6 lacks the extreme C-terminus, the proteolytic fragmentation observed here is in agreement with reported C-terminal TDP-43 fragmentation in FTLD-U cases (Neumann, Kwong et al. 2007). The full-length TDP-43 was also cleaved, but at a much lower level (observed on overexposed images, data not shown). These results show that an increase in phosphorylation, ubiquitination, and proteolysis are correlated with the insolubility of the TDP proteins. Taken together, the microscopic and biochemical data for TDP-S6 in cell culture is highly consistent with that of pathologic TDP-43 observed in disease tissue (Neumann, Sampathu et al. 2006; Cairns, Neumann et al. 2007; Mackenzie and Rademakers 2007; Neumann, Kwong et al. 2007).

5.2.2 Quantitative analysis of the insoluble TDP-43 and TDP-S6 proteome using multiplex SILAC

Both recombinant TDP-43 and TDP-S6 are highly enriched in detergent-insoluble extracts. Therefore, we used a multiplex SILAC approach to evaluate proteins that co-enrich in the detergent-insoluble proteome of cells over-expressing TDP-43 or TDP-S6 (Olsen, Blagoev et al. 2006) **(Figure 5.5A)**. Human HEK 293 cells were fully labeled

A

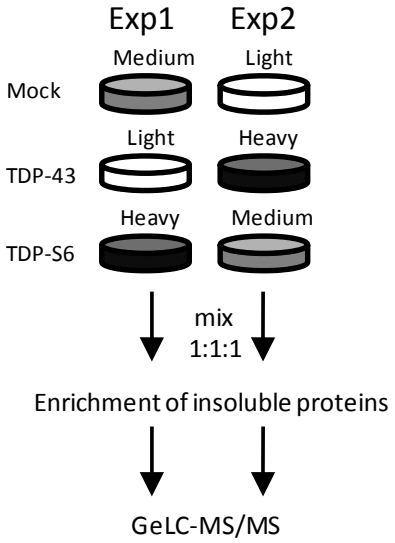

B

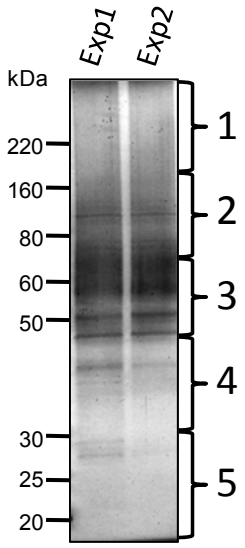

C

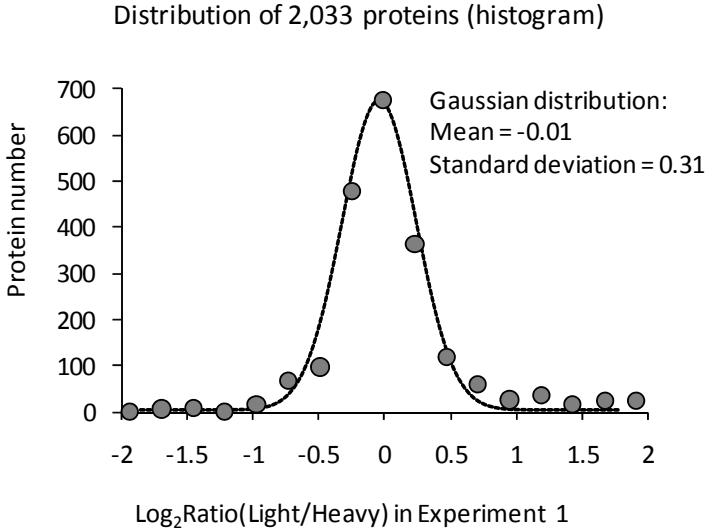

D

Experimental variations in SILAC experiments

Experiment	log_2Ratio		SD
Exp1	L/M	TDP-43/Ctl	0.26
	L/H	TDP-43/S6	0.31
	M/H	Ctl/S6	0.27
Exp2	L/M	Ctl/S6	0.23
	L/H	Ctl/TDP-43	0.30
	M/H	S6/TDP-43	0.28
Average SD of the six datasets			0.28 ± 0.03

Figure 5.5 Quantitative proteomics of sarkosyl-insoluble fraction by multiplex SILAC. (A) Diagram for biological replicates of SILAC analysis (experiment 1 and 2). The amino acid labeling order was swapped in the repeated analysis. (B) Silver-stained SDS gel of the isolated sarkosyl-insoluble fractions. The gel lanes were excised as indicated. (C) A representative fitting of a pair-wise comparison in the first experiment, shown as a histogram fitted to a Gaussian curve. (D) The experimental variations were similar in the multiple comparisons, indicated by the values of standard deviations.

with light, medium, or heavy arginine and lysine amino acids. The three labeled cell populations were transfected with either HA-TDP-43, HA-TDP-S6, or a mock plasmid. After incubation for two days, the cells were harvested, equally mixed, and subjected to sequential protein extraction. Although pooling the labeled cells reduces experimental variation during protein extraction, it is possible for biological variation to occur during cell labeling and transfection. Therefore, we performed a second independent analysis as a biological replicate with the labeled isotopes "swapped" in HEK 293 cells prior to transfection **(Figure 5.5A)**. The detergent-insoluble extracts were then resolved on an SDS gel, excised into gel bands, digested with trypsin, and analyzed by LC-MS/MS on a high-resolution Orbitrap mass spectrometer **(Figure 5.5B)**. After database searching and stringent filtering mainly by mass accuracy (≤10 ppm) and SEQUEST scores (Xcorr and ΔCn), a total of 2,670 proteins that were clustered into 1,117 groups were identified and quantified. The corresponding false-discovery rate was calculated to be less than 0.2% according to the target-decoy strategy (Peng, Elias et al. 2003; Elias and Gygi 2007).

To evaluate the quality of the quantitative data, we analyzed the results based on null hypothesis as described previously (Cheng, Hoogenraad et al. 2006). The protein ratios in all pair-wise comparisons were converted into $\log_2$ values and the resulting histogram of all values was fitted to a Gaussian distribution **(Figure 5.5C)**. The majority of proteins fit the curve, indicating that they did not change under the conditions analyzed. While the fitted mean (-0.01) suggested little systematic bias introduced by sample handling (e.g. slightly different amount of starting cells), the standard deviation (0.31) provided a good measure of the magnitude of experimental variations in the analysis. In all six pair-wise comparisons of light, medium and heavy labeling in the two

experiments, the value of standard deviation was stable (0.28 ± 0.03, **Figure 5.5D**), indicating that the variations in our SILAC analyses were consistent. Proteins were considered changed if their values fell outside more than two standard deviations (0.6, ~95% confidence interval), and showed consistency in experiment 1 and 2. A large number of proteins were removed when comparing results from experiment 1 and 2, suggesting that the biological replicate is essential to reduce false positives in the SILAC assay. The filtered proteins were further validated by manual examination of ion currents in raw files, resulting in the acceptance of six proteins with altered expression **(Table 5.1)**.

5.2.3 Validation and subcellular colocalization of SUMO-2/3 and ubiquitin

The list of proteins with altered levels in the sarkosyl-insoluble fraction included overexpressed TDP proteins (TDP-43 or TDP-S6), ubiquitin (Ub), and the small Ub like modifier SUMO-2/3. In gel band 1 (>180 kDa, **Figure 5.5B)**, the MS results (**Figure 5.6 A and B)** indicated that TDP-S6-expressing cells had more TDP in the insoluble proteome compared to TDP-43-expressing cells, consistent with the high M_r immunoreactivity in western blotting **(Figure 5.4B)**. As expected, native TDP-43 from mock transfected cells was not observed at this high M_r range. SILAC also confirmed our western blot results for Ub **(Figure 5.4B)**, which increased concomitantly with TDP levels within this M_r range. Interestingly, SUMO-2/3 was identified as a novel component enriched in TDP-43 and TDP-S6 insoluble proteome, suggesting the presence of both poly-ubiquitination and SUMOylation with protein aggregation. Subsequent immunoblotting validated the elevated levels of SUMO-2/3 in the insoluble proteome,

Table 5.1 The list of proteins altered in cells overexpressing TDP-43 or TDP-S6

#Accession	Protein Names	log_2(TDP-43/Control)	log_2(S6/Control)	log_2(S6/TDP-43)
Proteins affected by TDP-43 and TDP-S6 expression				
NP_031401.1	TDP-43 or TDP-S6	[1]2.8 ± 0.5	3.7 ± 0.5	1.3 ± 0.6
NP_002945.1	Ubiqutin	0.6 ± 0.2	2.3 ± 0.2	1.7 ± 0.1
NP_008868.3	SUMO 2/3	0.9	2.4 ± 0.1	1.2 ± 0.5
NP_005726.1	Actin-related protein 1 (ARP1)	1.2 ± 0.7	2.8	[2]NC
Proteins affected by TDP-S6 expression				
NP_006169.2	N-ethylmaleimide-sensitive factc	NC	-1	-1.2 ± 0.7
NP_056384.2	Dynamin 3	NC	-2.5	-1.2 ± 0.8

[1]The log ratios were shown as the mean of two biological replicates followed by standard deviation. If the proteins were quantified only in one experiment, the standard deviation was not available. [2]Not changed (the measured difference was not statistically significant).

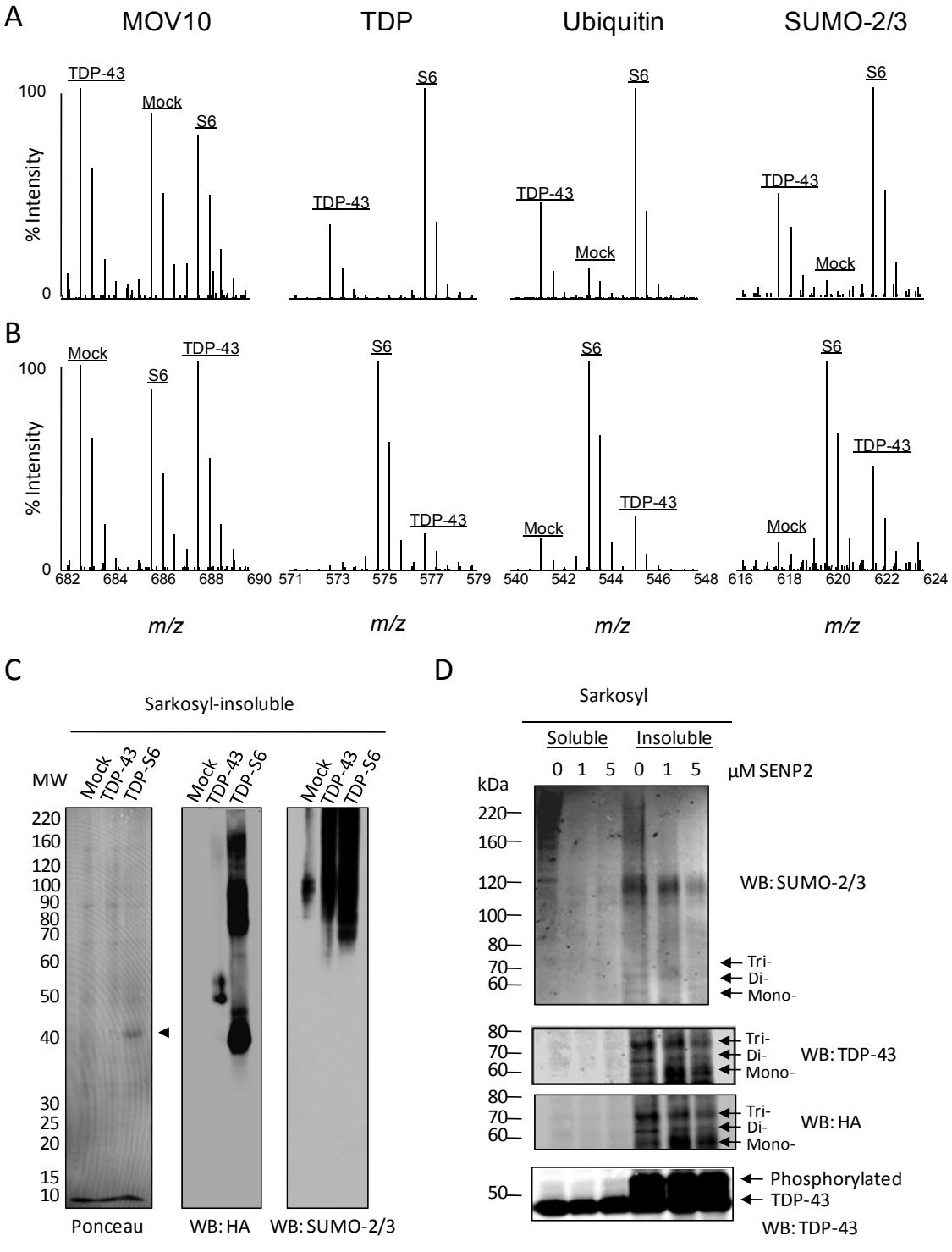
A
MOV10
TDP
Ubiquitin
SUMO-2/3
TDP-43
Mock
S6
% Intensity
100
0
B
682 684 686 688 690
571 573 575 577 579
540 542 544 546 548
616 618 620 622 624
m/z
C
Sarkosyl-insoluble
MW
Mock
TDP-43
TDP-S6
220
160
120
100
90
80
70
60
50
40
30
25
20
15
10
Ponceau
WB: HA
WB: SUMO-2/3
D
Sarkosyl
Soluble
Insoluble
0 1 5 0 1 5 µM SENP2
kDa
220
160
120
100
80
70
60
50
WB: SUMO-2/3
Tri-
Di-
Mono-
WB: TDP-43
WB: HA
Phosphorylated
TDP-43
WB: TDP-43

Figure 5.6 SILAC analysis of the TDP insoluble proteome and characterization of SUMOylation. MS spectra of detected peptide ions for MOV10 (a negative control), TDP proteins, ubiquitin (Ub), and SUMO-2/3 in GeLC-MS/MS from the top gel band (>180 kDa) in (A) Exp 1 and (B) Exp 2. (C) Western blotting of SUMO-2/3 and HA in sarkosyl-insoluble fractions from cells transfected with mock, TDP-43, and TDP-S6. (D) Both sarkosyl-soluble (10 μg) and insoluble (1 μg) fractions were incubated with SENP2, and immunoblotted with antibodies against SUMO-2/3, TDP-43, and HA. The three bands indicated by arrows correspond to TDP-43 modified by one, two, or three SUMO molecules, respectively.

and showed that this enrichment was correlated to the degree of TDP protein insolubility **(Figure 5.6C)**. This evidence suggests that insoluble TDP proteins are direct targets of SUMOylation.

To assess if TDP-43 is covalently modified by SUMO we performed a deSUMOylation assay using sentrin specific endopeptidase-2 (SENP2) (Kerscher, Felberbaum et al. 2006). An increasing amount of SENP2 was added to either detergent-soluble or insoluble samples from cells over-expressing TDP-43. Western blot with anti-SUMO-2/3 showed a decrease in high M_r SUMO-2/3 immunoreactivity with increasing enzyme concentration **(Figure 5.6D)**. In addition, three specific bands (~55, ~65, and ~75 kDa) on the blots were recognized by SUMO-2/3, TDP-43 and HA antibodies. Since unmodified HA-TDP-43 has a MW of ~45 kDa and SUMO-2/3 is ~10 kDa in size, these bands likely represent tri-, di-, and mono-SUMOylated forms of TDP-43. The tri- and di-SUMOylated HA-TDP-43 showed decreasing signals when incubated with titrated SENP2. In contrast, the mono-SUMOylated band was increased at 1μM SENP2, possibly due to processing of tri- and di-SUMOylated bands. This increase was appropriately reduced with increased SENP2 concentrations (5μM). Thus, HA-TDP-43 is directly modified by SUMO-2/3 in detergent-insoluble fractions.

To assess whether SUMO-2/3 co-localizes with TDP-43 or TDP-S6 in HEK 293 cells we performed immunofluorescence confocal microscopy **(Figure 5.7A)**. Endogenous SUMO-2/3 in untransfected cells was diffusely expressed mainly in the nucleus with some accumulation in nuclear bodies as described previously (Vertegaal, Ogg et al. 2004). In cells expressing full-length TDP-43, the majority of endogenous SUMO-2/3 was diffusely localized throughout the nucleus, although co-localization was

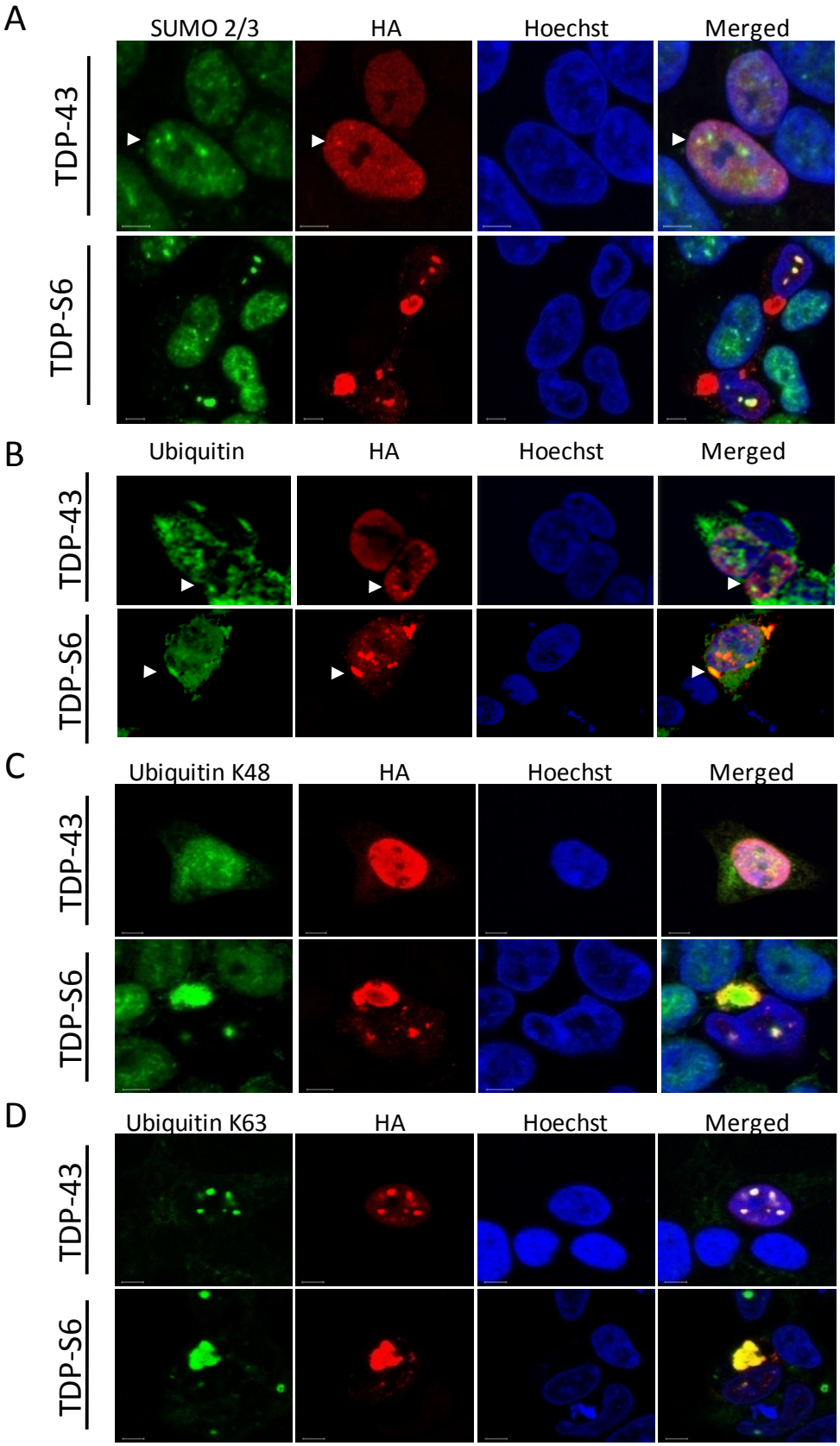
A
SUMO 2/3
HA
Hoechst
Merged
TDP-43
TDP-S6
B
Ubiquitin
HA
Hoechst
Merged
TDP-43
TDP-S6
C
Ubiquitin K48
HA
Hoechst
Merged
TDP-43
TDP-S6
D
Ubiquitin K63
HA
Hoechst
Merged
TDP-43
TDP-S6

Figure 5.7 Localization of SUMO-2/3, ubiquitin, and TDP proteins in HEK 293 cells. Cells were transfected with plasmids expressing HA-TDP-43 or HA-TDP-S6, and then co-stained with HA antibodies (red), and other antibodies (green) against (A) SUMO-2/3, (B) Ub, (C) K48 polyUb linkages, (D) and K63 polyUb linkages. The nuclei were visualized by Hoechst stain (blue). Some nuclear inclusions are indicated by arrow heads.

also observed in certain SUMO bodies when TDP-43 expression levels were higher **(Figure 5.7A, indicated by arrow heads)**. In TDP-S6-expressing cells, SUMO-2/3 was sequestered with TDP-S6 nuclear inclusions. Notably, SUMO-2/3 did not co-localize with cytoplasmic aggregates of TDP-S6. Similar results were obtained in cells co-expressing GFP-tagged SUMO-2 and TDP constructs (data not shown). These data strongly support that SUMOylation alters TDP protein solubility and localization in nuclei but not in cytoplasm.

In contrast with SUMOylation, immunofluorescence revealed that TDP-S6 cytoplasmic inclusions were almost completely co-localized with endogenous Ub **(Figure 5.7B)**. While in TDP-43 over-expressing cells Ub was visualized in both the nucleus and cytoplasm in a manner similar to Ub localization in untransfected cells, native ubiquitin was largely localized in cytoplasm in cells transfected with TDP-S6. These findings suggest that Ub is recruited specifically to cytoplasmic TDP-S6 inclusions.

Ub is attached to protein substrates in monomeric form or as polymers (polyUb) assembled through the N-terminal amino group and the side chains of all seven lysine residues (K6, K11, K27, K29, K33, K48 and K63). These diverse polyUb structures may regulate downstream signaling specificity and determine the consequence of ubiquitination (Kerscher, Felberbaum et al. 2006; Xu, Duong et al. 2009). Whereas K63 PolyUb linkage is proposed to mediate nonproteolytic events, including protein sorting and inclusion formation (Tan, Wong et al. 2008), K48 linkage and other atypical polyUb chains mediate proteasomal degradation. To elucidate the role of different PolyUb linkages in the formation of TDP protein aggregates, we examined transfected cells with

highly specific K48 or K63 linkage antibodies (Newton, Matsumoto et al. 2008), and found that both linkages were clearly present in the cytoplasmic and nuclear inclusions **(Figure 5.7 C and D)**. The results suggest that mixed polyUb chains may contribute to the formation of TDP protein aggregates.

To confirm the presence of K48 and K63 PolyUb linkages observed in TDP cytoplasmic aggregates, we analyzed the levels of all polyUb linkages in sarkosyl-insoluble proteome by targeted mass spectrometry (Kirkpatrick, Hathaway et al. 2006; Xu, Duong et al. 2009). Metabolically heavy-labeled proteins were used as internal standards for their unlabeled counterparts, allowing the quantitation of the native proteins in each sample. Using trypsin, endogenous polyUb chains and their corresponding internal standards were cleaved to generate linkage specific peptides tagged with two Gly residues (Peng, Schwartz et al. 2003). During the LC/SRM analysis, the pairs of heavy and light peptides were co-eluted and fragmented to produce pairs of product ions **(Figure 5.8 A and B)** which were used to provide sensitive measurements of the original protein abundance. The detailed LC/SRM parameters are shown in **Table 5.2**. Among all PolyUb linkages, K63 linkage increased ~3.3 fold in the insoluble fraction of TDP-S6-expressing cells. In addition, K48 linkages (~2.0 fold), K11 linkages (~1.5 fold), and K29 linkages (~1.3 fold) were also measured in this sample **(Figure 5.8C)**, while the other four potential linkages mediated by three Lys (K6, K27, K33) and the N-terminus were not detected. In contrast with TDP-S6 insoluble fractions, the magnitude of polyUb linkage changes was much smaller in the cells expressing full-length TDP-43, consistent with the modest levels of TDP-43 aggregation in these cells. These data further support the involvement

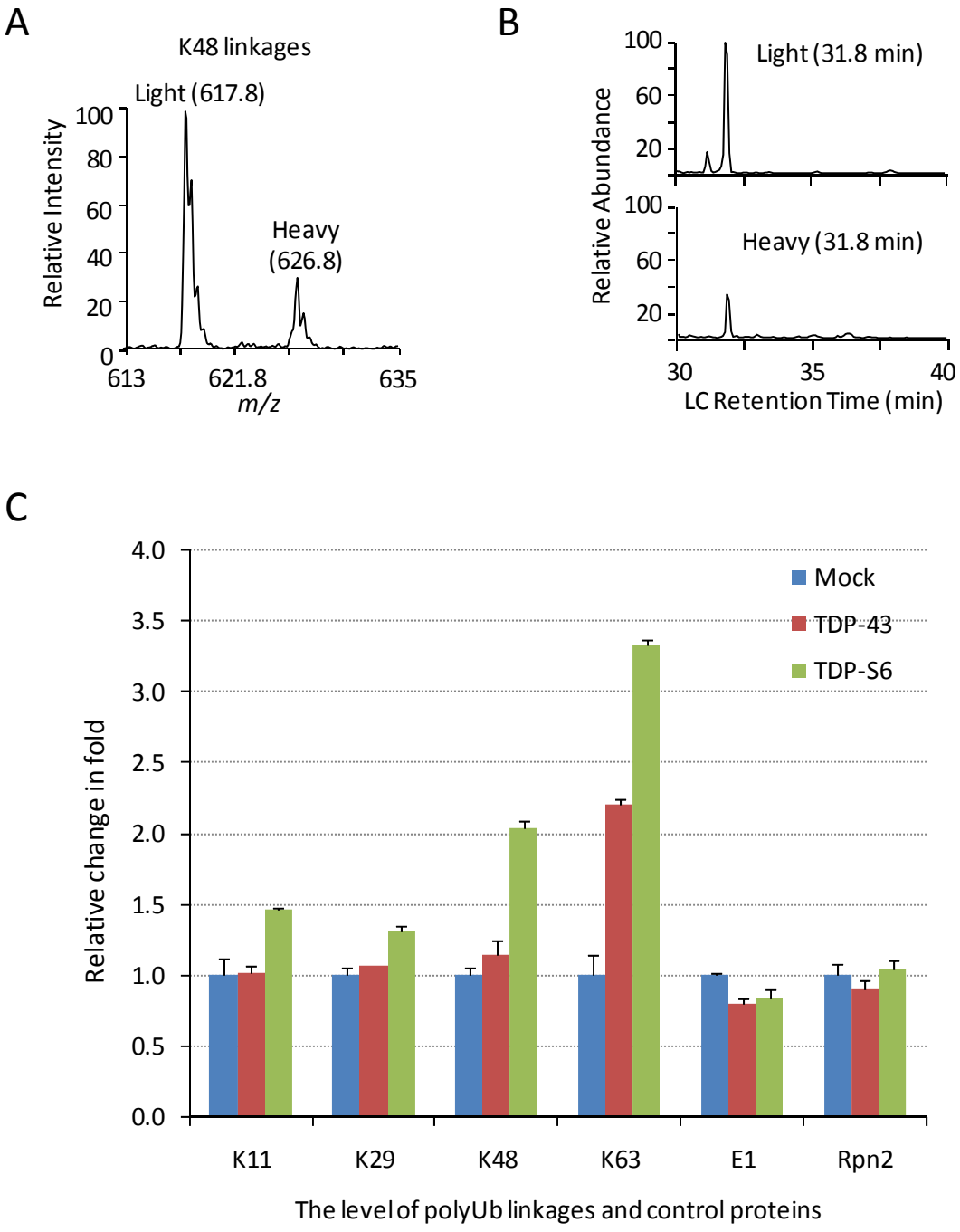
A
K48 linkages
Light (617.8)
Heavy
(626.8)
Relative Intensity
100
80
60
40
20
0
613
621.8
635
m/z
B
Light (31.8 min)
Heavy (31.8 min)
Relative Abundance
100
60
20
30
35
40
LC Retention Time (min)
C
Mock
TDP-43
TDP-S6
Relative change in fold
4.0
3.5
3.0
2.5
2.0
1.5
1.0
0.5
0.0
K11
K29
K48
K63
E1
Rpn2
The level of polyUb linkages and control proteins

Figure 5.8 Multiple polyubiquitin linkages were detected in TDP protein aggregates. Transfected HEK 293 cells were harvested and mixed with metabolically labeled cells as internal standards, followed by sequential detergent extraction. The sarkosyl-insoluble samples were used for SRM-based analysis to quantify all polyUb linkages and two other proteins (E1 and Rpn2 as loading controls). (A) The monitored product ion pair of K48 linkage-specific peptide. (B) The co-elution of K48 linkage peptide pair during a LC/SRM run. (C) The comparison of measured linkages and proteins in three samples: mock, HA-TDP-43, or HA-TDP-S6 transfected cells. The data were normalized to values in the mock sample. Error bars indicate standard errors of the mean

Table 5.2 Protein quantification by the LC-SRM analysis of selected peptides

Peptide Names	Peptide Sequences	[1]Labeling AA (SILAC)	[2]Mass Shift (Da)	[3]Precursor Ions (*m/z*)		[4]Product Ion (*m/z*)		[5]RT (min)
				Native (light)	IS (heavy)	Native (light)	IS (heavy)	
Metabolically synthesized heavy labeled peptides								
Ub (K29)	AK(GG)IQDK	K29, K33	16	408.7	416.7	503.3	511.3	9.2
Ub (K33)	IQDK(GG)EGIPPDQQR	K33, R42	18	546.6	552.6	898.5	906.5	13.9
Ub (unmodified)	TLSDYNIQK	K63	8	541.3	545.3	867.4	875.4	15.1
Rpn2 (19S subunit)	TVGTPIASVPGSTNTGTVPGSEK	K	8	1079.1	1083.1	1331.6	1339.6	22.8
Ub (K6 Met-Oxidized)	M*QIFVK(GG)TLTGK	K6, K11	16	698.4	706.4	1007.6	1023.6	23.9
Ub (K48)	LIFAGK(GG)QLEDGR	K48, R54	18	487.6	493.6	617.8	626.8	24.3
Ub (K27)	TITLEVEPSDTIENVK(GG)AK	K27, K29	16	701.0	706.4	943.9	951.9	26.3
Ub (K6)	MQIFVK(GG)TLTGK	K6, K11	16	690.4	698.4	1007.6	1023.6	28
Ub (K11)	TLTGK(GG)TITLEVEPSDTIENVK	K11, K27	16	801.4	806.8	1002.5	1010.5	28.1
Ub (K63)	TLSDYNIQK(GG)ESTLHLVLR	K63, R72	18	561.8	566.3	677.8	683.8	29.6
Ubiquitin Activating E1	SLVASLAEPDFVVTDFAK	K	8	955.0	959.0	1138.6	1146.6	39

[1]The selected residue for stable isotopic labeling (e.g. L8, the eighth leucine residue); [2]The mass change due to isotopic labeling; [3]Monoisotopic m/z values of native and labeled peptides; [4]Monoisotopic m/z values of monitored product ions in SRM; [5]Experimental retention time in reverse liquid chromatography during a 40 minute gradient.

of multiple polyUb chains in TDP protein aggregation, and indicate that K63 PolyUb linkage may have the most significant contribution.

5.3 Discussion

The abnormal accumulation of phosphorylated and ubiquitinated species in protein inclusions is observed in a wide variety of neurodegenerative diseases (Taylor, Hardy et al. 2002; Ross and Poirier 2004). In Alzheimer's and Parkinson's diseases, these intracellular inclusions are called neurofibrillary tangles and Lewy bodies, and are composed of pathologically altered forms of tau and α-synuclein, respectively (Lee, Goedert et al. 2001; Ross and Poirier 2004). In FTLD-U and ALS, TDP-43 has been identified as the major component of tau- and α-synuclein-negative inclusions, where it is both phosphorylated and ubiquitinated (Neumann, Sampathu et al. 2006). Although there are ten known splice variants of human TDP-43, their roles in abnormal TDP-43 translocation and pathologic aggregation have not yet been characterized. In this study we overexpressed human recombinant TDP-43 and a truncated splice variant, TDP-S6, in HEK 293 cells and primary neurons. The full-length protein was expressed almost exclusively in the nucleus where it co-localized with endogenous TDP-43. In sharp contrast, the shorter TDP-S6 formed highly insoluble cytoplasmic and nuclear inclusions reminiscent of disease-specific pathology. Moreover, both overexpression of TDP-43 and TDP-S6 resulted in the enrichment of specific post-translational modifications (PTMs) within their respective insoluble protein extracts. These PTMs included ubiquitination, phosphorylation, and C-terminal fragmentation. Based on our multiplex SILAC

proteomic approach, we also identified significant enrichment of SUMO-2/3 and Ub within the sarkosyl-insoluble, urea-soluble extracts.

In our cellular model, endogenous Ub showed tight association with the TDP aggregates in both biochemical analysis and immunostaining, supporting the hypothesis that aggregation-prone TDP-43 is a major ubiquitinated species. While TDP-S6-expressing cells displayed inclusions of various sizes, only a fraction of recombinant TDP-43-expressing cells formed small nuclear aggregates dependent on high level expression **(Figure 5.7)**. Quantitative MS analysis revealed that several main PolyUb chains were present in the insoluble-extracts from these cells, with K63 linkages being the most prominent. These findings are reminiscent of previous characterization of tau- and SOD1-positve inclusions (Tan, Wong et al. 2008), and are consistent with the idea that K63-linked chains may facilitate the formation of inclusions and direct subsequent clearance by the autophagy pathway.

Recent studies have suggested that ubiquitinated inclusions in FTLD-U brains are primarily composed of C-terminal fragments of TDP-43, and that these fragments may comprise the primary pathologic species of TDP-43 by serving as a seed for aggregation (Igaz, Kwong et al. 2008). Moreover, caspase-3 activation has been implicated in the proteolytic processing of TDP-43 into three C-terminal fragments similar to those seen in disease tissues (Zhang, Xu et al. 2007). Although TDP-S6 lacks the final 137 amino acids of the full-length TDP-43, the splice variant still contains all three purported caspase-3 cleavage sites at amino acids 10-13 (DEND), 86-89 (DETD), and 216-219 (DVMD), corresponding to the 42 kDa, 35 kDa, and 25 kDa fragments respectively in the full-length protein (Zhang, Xu et al. 2007). Interestingly, the fragmentation of TDP-S6

resulted in three lower molecular weight species that approximate the molecular mass expected of caspase-3 cleavage products in this HA-tagged construct (37 kDa, 30 kDa, and 20 kDa). These data suggest TDP-43 N-terminal truncation preferentially occurs in the absence of a full C-terminus, and potentially as a result of a caspase-3 mediated mechanism.

Currently it remains unknown whether aberrant splicing of the TDP-43 transcript results in the production of pathologic TDP isoforms in ALS or FTLD-U. However, two TDP-43 splicing isoforms have been previously identified in human brain and spinal cord tissue (Strong, Volkening et al. 2007). One of these isoforms, which closely resembles TDP-S6, was identified in two ALS cases. This novel transcript lacked all of exon 3 and a significant portion of exon 6, resulting in expression of a protein product (~28 kDa) without a glycine-rich C-terminus (Strong, Volkening et al. 2007). In this study, TDP-S6, a C-terminal-truncated splice variant previously identified in HEK 293 cells (Wang, Wang et al. 2004), was found predominantly localized to the cytoplasm and mimicked the aggregation observed in FTLD-U and ALS. It should be noted that, although the human TDP-S6 variant formed both cytoplasmic and nuclear inclusions, overexpression of the mouse TDP-S6 in HEK 293 cells resulted only in the formation of nuclear-specific, speckle-like structures, termed TDP-bodies (Wang, Reddy et al. 2002). Thus, despite sharing 96% amino acid identity, the inconsistency between mouse and human TDP-S6 localization may result from differences in species-specific nuclear/cytoplasmic translocation or different experimental conditions.

SILAC analysis of this cellular model revealed novel components in the formation of protein inclusions. SUMO-2/3 was found to be preferentially enriched

within TDP-43 and TDP-S6 insoluble proteome, and was subsequently validated by western blotting. Interestingly, immunofluorescence confocal microscopy indicated that SUMO-2/3 co-localized mainly with TDP-S6 nuclear inclusions, thereby implicating a unique nuclear association between SUMO-2/3 and TDP-S6. This nuclear association is not completely surprising since TDP-43 has been previously found to associate with PML bodies (Wang, Reddy et al. 2002), nuclear structures known to co-localize with SUMO (Vertegaal, Ogg et al. 2004; Mukhopadhyay, Ayaydin et al. 2006). Moreover, sequence analysis of TDP-43 revealed a canonical SUMO-conjugation site motif (Ψ-K-X-[D/E]; amino acids 135-138 of TDP-43) amongst its potential SUMO-targeted lysines (Geiss-Friedlander and Melchior 2007). Using an *in vitro* deSUMOylation assay, we provide experimental evidence that TDP-43 itself is directly SUMOylated within the insoluble fraction. Notably, protein SUMOylation has been linked to aggregated proteins in AD, PD, and polyQ disorders (Martin, Wilkinson et al. 2007). In addition, SUMO-1 has been shown to specifically co-localize with ubiquitinated nuclear neuronal inclusions in FTLD-U tissues (Mackenzie, Baker et al. 2006). Although protein SUMOylation functions in regulating transcription and nuclear transport (Dorval and Fraser 2007), it has also been shown to cross-talk with ubiquitination since the SUMO tag on proteins may serve as a recognition signal for subsequent ubiquitination and proteasome-mediated degradation (Lallemand-Breitenbach, Jeanne et al. 2008; Schimmel, Larsen et al. 2008; Tatham, Geoffroy et al. 2008). More specifically, the recent identification of SUMO-targeted ubiquitin ligases (STUbLs) (Prudden, Pebernard et al. 2007; Sun, Leverson et al. 2007) raises the intriguing possibility that upon SUMOylation, misfolded nuclear TDP-S6 is subjected to sequestration in nuclear aggregates and STUbL-dependent

ubiquitination (Perry, Tainer et al. 2008). The latter modification may subsequently result in the deSUMOylation and cytoplasmic transport of TDP-S6 as it is directed to the proteasome for degradation (Prudden, Pebernard et al. 2007). Interestingly, a STUbL-mediated mechanism for the cellular regulation of insoluble TDP-S6 is supported by the immunochemical colocalization of polyubiquitin chains with both nuclear and cytoplasmic TDP-S6 inclusions **(Figure 5.7)**. However, whether TDP-43 SUMOylation underlies disease-specific protein translocation, degradation, or aggregation requires further investigation.

In addition to Ub and SUMO-2/3, actin-related protein 1 (ARP1) was also found to be enriched in the sarkosyl-insoluble fractions of TDP-43- and TDP-S6-transfected cells. ARP1 is a subunit of dynactin, a macromolecular complex that interacts with both microtubules and cytoplasmic dynein. ARP1 is also involved in protein transport and vesicular trafficking (Schroer, Bingham et al. 1996). Interestingly, gene mutation in another subunit of dynactin, p150Glued, has been reported in ALS cases (Munch, Sedlmeier et al. 2004), and the related mouse model developed motor neuron disease (Laird, Farah et al. 2008). In addition, overexpression of TDP-S6 reduces N-ethylmaleimide sensitive factor (NSF), an ATPase involved in intracellular trafficking, and dynamin 3, a microtubule-associated protein involved in vesicle budding (Schekman and Orci 1996). These results suggest that protein transportation may be dysregulated in neurodegenerative diseases. Furthermore, these findings, coupled with an increase of K63 polyUb linkages, further support an association between TDP-43 and protein sorting pathways.

In sum, our data suggest that the C-terminal domain is necessary for normal TDP-43 localization, and that without this region TDP-43 becomes primarily sequestered in the cytoplasm. Thus it might be plausible that the genetic mutations in TDP-43 found within the C-terminal region (Gitcho, Baloh et al. 2008; Kabashi, Valdmanis et al. 2008; Sreedharan, Blair et al. 2008; Van Deerlin, Leverenz et al. 2008; Yokoseki, Shiga et al. 2008), somehow disrupt critical amino acid residues needed for TDP-43 nuclear localization and proper function. Although further studies are needed to evaluate the presence of TDP-S6 or other similar short isoforms in disease tissue, our data raise the intriguing possibility that dysregulation of human TDP-43 alternative splicing, or preferential proteolytic processing to produce TDP N-terminal fragments, can contribute to the pathology of FTLD-U and ALS.

Chapter 6

Aberrant Septin 11 is associated with sporadic frontotemporal lobar degeneration.

6.1 Introduction

Frontotemporal lobar degeneration (FTLD) encompasses a heterogeneous group of sporadic and familial diseases associated with circumscribed degeneration of the prefrontal and anterior temporal lobes. As the third most common neurodegenerative cause of dementia behind Alzheimer's disease (AD) and Lewy body dementia, FTLD accounts for 5% of dementia cases irrespective of age, and up to 20% of cases with pre-senile onset (Neary, Snowden et al. 2005). Moreover, the median survival is 6-8 years from symptom onset (Ratnavalli, Brayne et al. 2002), reflecting the poor understanding of disease mechanisms and the lack of specifically targeted therapies. Although the clinical presentation may be variable, FTLD is characterized by abnormalities in personality, behavior, or language, with some patients developing the amyotrophic form of motor neuron disease (Neary, Snowden et al. 2000). Pathologically, FTLD is equally heterogeneous, and may present as a tauopathy, or more commonly, with tau-negative, ubiquitin-immunoreactive neurites and inclusions (Neary, Snowden et al. 2000). In these cases, termed FTLD-ubiquitin (FTLD-U), histopathology is primarily observed within the small layer II neurons of the frontal and temporal cortices, as well as in granule cells of the dentate gyrus of the hippocampus (Okamoto, Hirai et al. 1991).

In recent years, significant progress has been made in understanding the genetic and neuropathologic basis of FTLD-U. In 2006, mutations in the progranulin gene (PGRN) were identified as the cause of chromosome 17-linked FTLD-U (Baker, Mackenzie et al. 2006; Cruts, Gijselinck et al. 2006). Occurring in 10-20% of patients with FTLD-U, these mutations invariably cause aberrant transcription of *PGRN*, and result in either a frank loss or the production of non-functional progranulin, a widely expressed growth factor involved in inflammation and wound repair (Eriksen and Mackenzie 2008). Since characteristic FTLD-U pathology is not immunoreactive to progranulin, it is clear that *PGRN* haploinsufficiency, rather than the aggregation of the mutant protein, is the primary disease mechanism in these patients (Baker, Mackenzie et al. 2006; Cruts, Gijselinck et al. 2006). The discovery of mutations in *PGRN* was followed by the identification of TAR DNA-binding protein 43 (TDP-43), the first major non-ubiquitin protein component of pathological inclusions in familial and sporadic FTLD-U (Neumann, Sampathu et al. 2006). Although in normal neurons TDP-43 is a nuclear RNA-binding protein, in pathologic conditions TDP-43 redistributes from the nucleus to the cytoplasm where it is aggregated, phosphorylated, ubiquitinated, and proteolytically cleaved into 23kD and 37kD C-terminal fragments (Neumann, Sampathu et al. 2006). Notably, TDP-43 is also localized in the intracytoplasmic ubiquitinated inclusions of sporadic amyotrophic lateral sclerosis (ALS), a motor neuron disease often associated with FTLD-U (Okamoto, Hirai et al. 1991; Neumann, Sampathu et al. 2006). The clinical and pathologic overlap between ALS and FTLD-U, coupled with the subsequent identification of multiple missense mutations in the gene encoding TDP-43

(*TARDBP*) in ALS families, suggests these disorders are mechanistically related (Geser, Martinez-Lage et al. 2009).

The molecular pathways underlying TDP-43 aggregation and toxicity have not yet been fully elucidated. Fragmentation of TDP-43, possibly by caspase-dependent cleavage (Zhang, Xu et al. 2007), and its subsequent cytoplasmic sequestration have been posited as critical factors in promoting cellular toxicity (Johnson, McCaffery et al. 2008). However, whether FTLD-U pathogenesis occurs as a result of a loss of the function of TDP-43 in the nucleus, including transcriptional repression (Ou, Wu et al. 1995) and the bridging of nuclear bodies (Zhang, Xing et al. 2006), or via a toxic gain-of-function mechanism unrelated to its physiological role is unclear. Recently, several reports have questioned the specificity of the association between TDP-43 and FTLD-U/ALS after TDP-43-immunoreactive aggregates were found in a range of neurodegenerative disorders, including AD and Parkinson's disease (PD) (Geser, Martinez-Lage et al. 2009). In addition, extensive histopathological characterization of FTLD-U cases with TDP-43 specific antibodies has revealed at least four pathologic FTLD-U subtypes that differ in aggregate distribution, density, and morphology, suggesting that they may not share a common molecular basis (Mackenzie, Baborie et al. 2006; Sampathu, Neumann et al. 2006; Cairns, Bigio et al. 2007). Finally, while FTLD-U cases caused by mutations in the genes for valosin-containing protein (*VCP*) and *PGRN* correspond to separate but specific TDP-43-defined subtypes of FTLD-U, cases caused by mutations in the charged multivesicular body protein 2B (*CHMP2B*) gene on chromosome 3 feature ubiquitin-positive inclusions that lack TDP-43 immunoreactivity (Cairns, Bigio et al. 2007). Taken

together, these findings suggest that other, as yet unknown, aggregating species may contribute in the pathogenesis of this complex disorder.

6.2 Results:

6.2.1 Discovery of altered proteins in FTLD-U by LC-MS/MS

To identify differentially expressed proteins in FTLD-U, which like TDP-43 are enriched in detergent-insoluble brain fractions, we examined post-mortem samples using two independent shotgun quantitative proteomic approaches **(Figure 6.1 A and B)**. In the first strategy, frontal cortex homogenates from 10 cases each of FTLD-U, Alzheimer's disease (AD), and control **(Table 6.1)** were pooled by diagnosis and serially extracted with buffers of increasing stringency. To allow estimation of the variances associated with sample preparation and analysis, the FTLD-U pooled homogenates were divided into two identical samples and processed in parallel as technical replicates. The resulting four detergent-insoluble, urea-soluble fractions were first separated by SDS-PAGE **(Figure 6.2A)**, excised in 5 pieces from the gel, trypsin-digested, and analyzed via liquid chromatography coupled with tandem mass spectrometry (LC-MS/MS) on a high-resolution mass spectrometer. For each of the 512 identified proteins, a quantitative protein comparison based on the extracted ion current (XIC) of individual peptides was performed, and abundance ratios calculated (e.g. FTLD-U / Control). To statistically evaluate and filter the quantitative data, the abundance ratios from all pair-wise comparisons were logarithmically transformed and the resulting histogram of all values was fitted to a Gaussian distribution **(Figure 6.3 and Table 6.2)**.

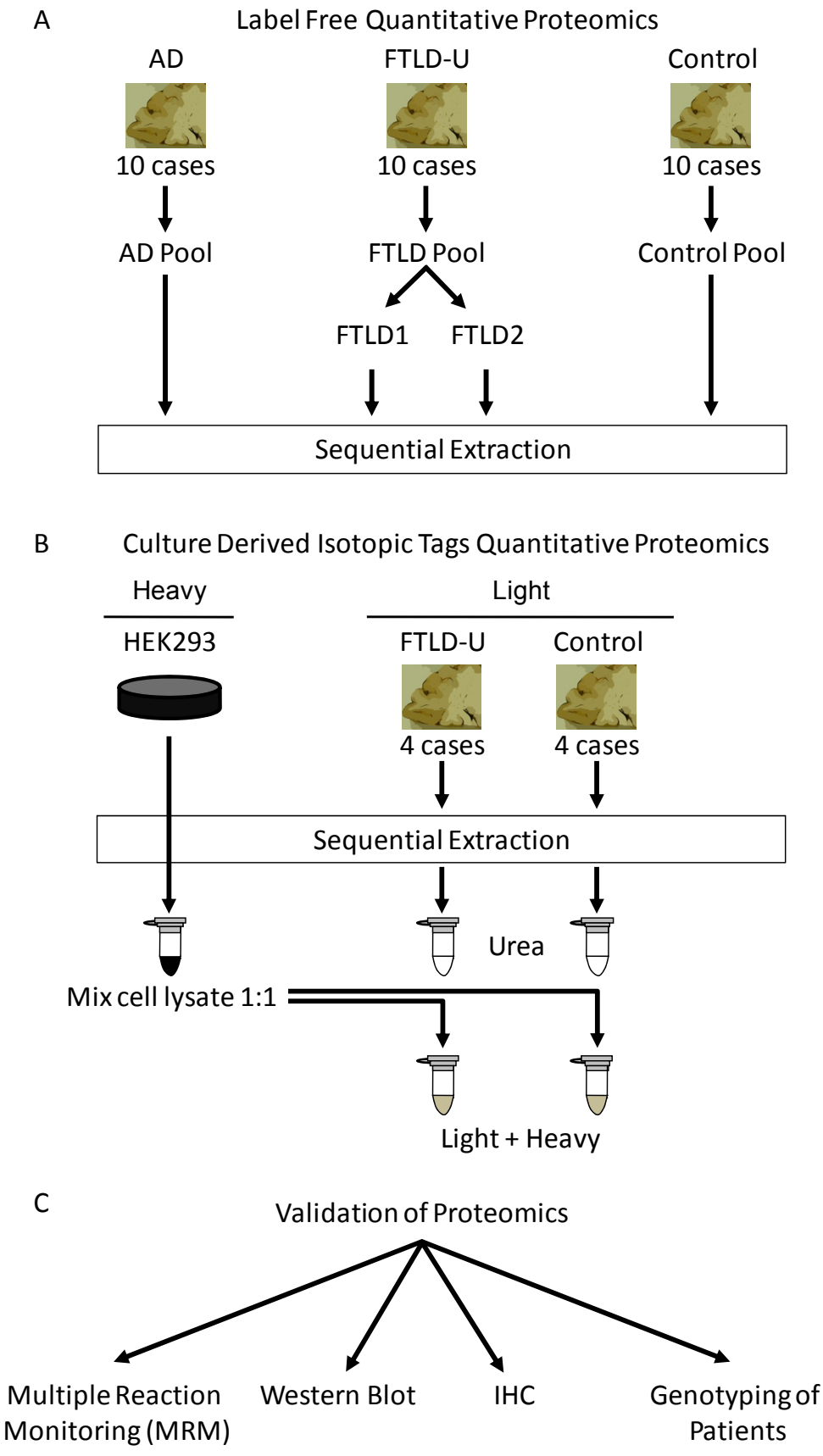
A
Label Free Quantitative Proteomics
AD
FTLD-U
Control
10 cases
10 cases
10 cases
AD Pool
FTLD Pool
Control Pool
FTLD1
FTLD2
Sequential Extraction
B
Culture Derived Isotopic Tags Quantitative Proteomics
Heavy
Light
HEK293
FTLD-U
Control
4 cases
4 cases
Sequential Extraction
Urea
Mix cell lysate 1:1
Light + Heavy
C
Validation of Proteomics
Multiple Reaction Monitoring (MRM)
Western Blot
IHC
Genotyping of Patients

Figure 6.1 Diagram of experimental workflow. (A) Sample preparation for label-free quantitative proteomics (Discovery Phase A). Ten cases each of AD, FTLD-U, and Control were pooled by diagnosis and sequentially extracted. Urea samples were then analyzed by shotgun LC-MS/MS. (B) Sample preparation for quantitative proteomics based on culture derived isotopic tags (Discovery Phase B). Four cases each of FTLD-U and control were pooled by diagnosis and sequentially extracted. Urea fractions for each diagnosis were mixed (1:1) with HEK 293 lysate labeled with heavy stable isotopes of arginine and lysine. The heavy labeled peptides served as internal standards following analysis by LC-MS/MS. (C) Validation of identification of Septin 11 enrichment in FTLD-U using four independent methods.

Table 6.1 Detailed Demographics of Cases Selected for Proteomics

Diagnosis	Case #		[1]PMI (hr)	Age at Death	Duration	ApoE Status	[2]Race/Sex
AD	1		4	55	6	E3/3	W/M
	2		4.5	55	3	E3/4	W/F
	3		20	57	7	E3/4	B/F
	4		11.5	62	10	E3/4	W/M
	5		4.5	64	12	E3/4	W/F
	6		5.5	69	21	E4/4	W/F
	7		15	71	2.5	E3/4	W/M
	8		17	71	8	E3/4	W/M
	9		21	76	12	E2/3	W/F
	10		12	81	12	E3/4	W/F
n=10	**AVG**		**11.5**	**66.1**	**9.4**		
Control	1		3	52		E3/4	W/F
	2		10	57		E3/3	W/M
	3	[3]*	8	60		E3/4	B/F
	4		12	61		E3/4	B/M
	5		12	65	NA	E3/3	W/M
	6		6	65		E3/3	W/F
	7	*	11	68		E3/3	W/F
	8	*	6	69		E3/3	W/M
	9		7	74		E3/3	W/F
	10	*	6	75		E3/3	W/F
n=10	**AVG**		**8.1**	**64.6**	**NA**		
FTLD-U	1		3	41	9	E3/3	W/M
	2		17.5	61	5	E3/3	W/M
	3	*	11.5	62	10	E3/3	A/F
	4	*	17	63	7.5	E3/3	W/M
	5		6	64	8	E3/4	W/F
	6	*	NA	69	1	E3/3	W/F
	7		NA	69	1	E3/3	W/F
	8		18	71	9	E3/3	W/F
	9		17	74	16	E3/4	W/M
	10	*	7	83	4	E3/3	W/F
n=10	**AVG**		**12.1**	**65.7**	**7.1**		

[1]Post-mortem interval [2]**W**hite, **B**lack, **A**sian, **F**emale, **M**ale [3]Cases marked with asterisk were selected for pooling in CDIT proteomics

A

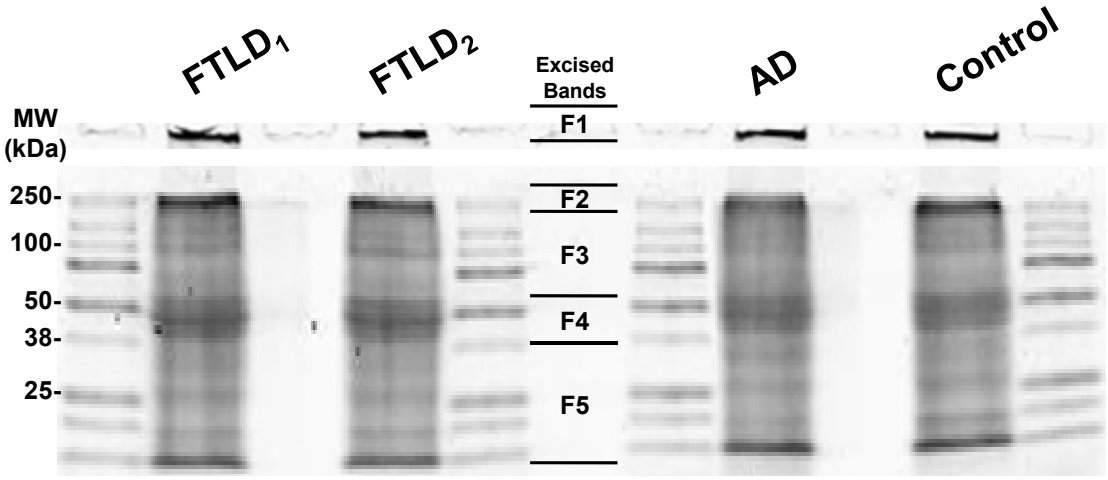
FTLD1
FTLD2
Excised Bands
AD
Control
MW (kDa)
250-
100-
50-
38-
25-
F1
F2
F3
F4
F5

B

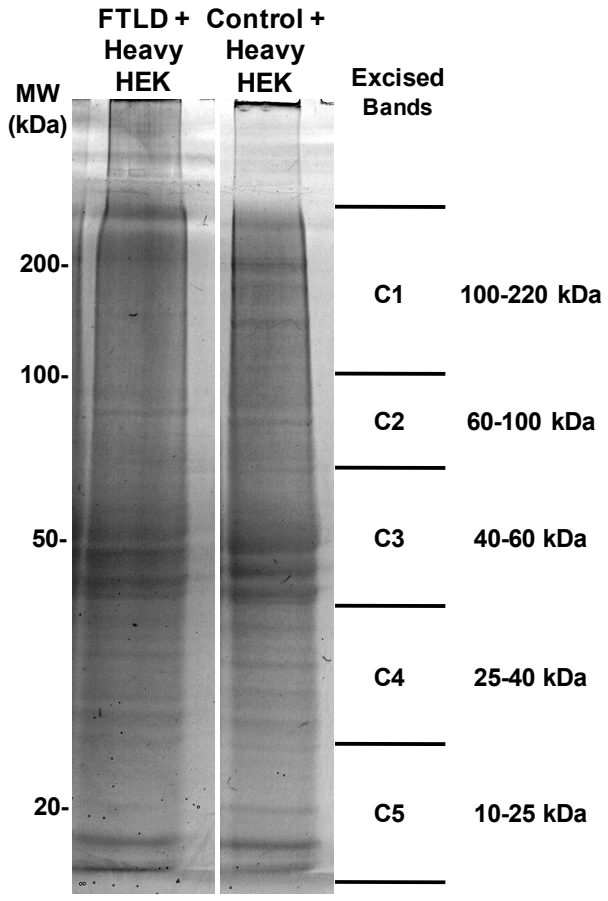
FTLD + Heavy HEK
Control + Heavy HEK
Excised Bands
MW (kDa)
200-
100-
50-
20-
C1 100-220 kDa
C2 60-100 kDa
C3 40-60 kDa
C4 25-40 kDa
C5 10-25 kDa

Figure 6.2 Separation of pooled urea samples by SDS-PAGE for proteomic analysis. (A) SDS-PAGE gel of urea fractions extracted from AD, FTLD-U, and control pooled frontal cortex homogenates (10 cases each). (B) SDS-PAGE gel of 4 pooled FTLD-U or 4 pooled control samples after addition of heavy labeled cell lysate. The gels were stained with Coomassie Blue G-250 and gel lanes were excised in 5 pieces as indicated (F1-F5 or C1-C5).

A

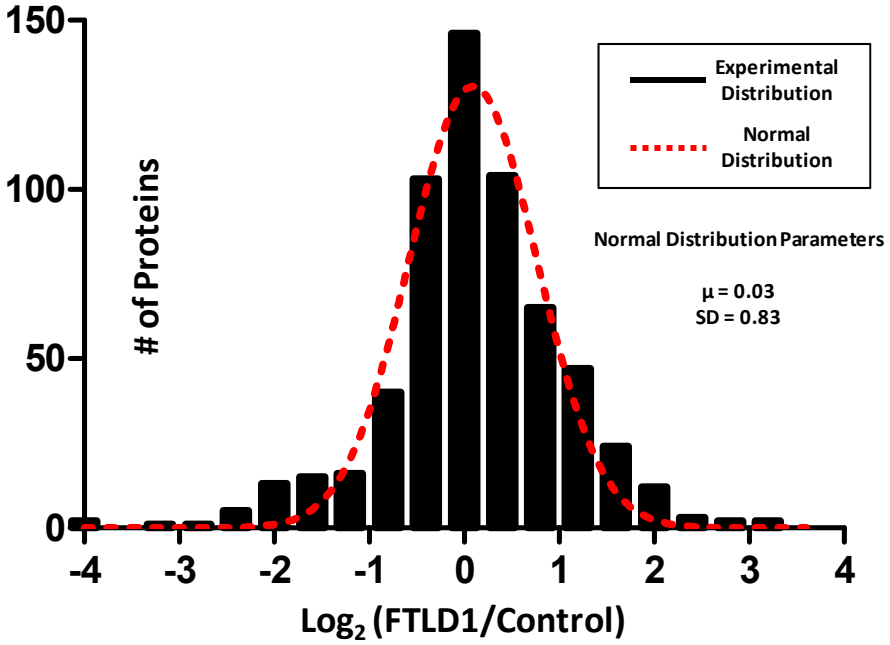
150
100
50
0
# of Proteins
-4
-3
-2
-1
0
1
2
3
4
Log2 (FTLD1/Control)
Experimental Distribution
Normal Distribution
Normal Distribution Parameters
μ = 0.03
SD = 0.83

B

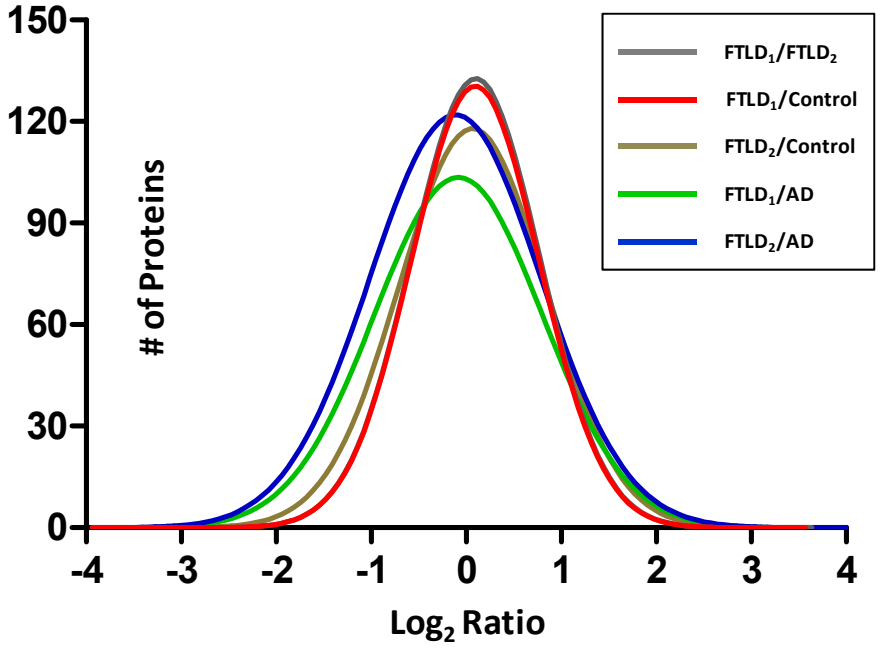
150
120
90
60
30
0
# of Proteins
-4
-3
-2
-1
0
1
2
3
4
Log2 Ratio
FTLD1/FTLD2
FTLD1/Control
FTLD2/Control
FTLD1/AD
FTLD2/AD

Figure 6.3 Statistical evaluation and filtering of label-free proteomics data. (A) Abundance ratios for FTLD-U/Control comparison were transformed (logarithmic base 2) and plotted with each point corresponding to the number of proteins in 0.3 unit windows (black line). A Gaussian curve was subsequently fitted to the data (red line) and used to determine significance levels for protein change. (B) Fitted normal distributions for all possible pair-wise comparisons. Statistical means, standard deviations, and regression coefficients are presented in **Table 6.2**.

Table 6.2 Statistical data for fitted normal distributions

Comparison	Mean	[1]SD	r^2
$FTLD_1$/Control	0.09	0.67	0.96
$FTLD_2$/Control	0.06	0.77	0.92
$FTLD_1$/AD	-0.08	0.89	0.97
$FTLD_2$/AD	-0.11	0.90	0.97
$FTLD_1$/$FTLD_2$	0.10	0.67	0.98

[1]Standard deviation of distributions

Abundance ratios for each protein derived from this label-free quantitative proteomics approach were cross-referenced with those obtained from an independent large-scale proteomics discovery set based on the use of culture-derived isotopic tags (CDIT) for quantitation (Ishihama, Sato et al. 2005). In this second approach, whole cell lysate from isotopically-labeled HEK 293 cells was mixed equally with urea-soluble fractions prepared from pools of 4 FTLD-U or 4 control cases **(Table 6.1, marked by asterisk)**. The heavy-labeled peptides from the cell lysate are chemically identical to their unlabeled counterparts in each urea fraction, and can therefore serve as internal standards for the measurement of protein abundance across samples (Cheng, Hoogenraad et al. 2006). The urea/HEK 293 lysate mixtures were subsequently separated by SDS-PAGE **(Figure 6.2B)** and also excised in 5 bands prior to LC-MS/MS analysis. Using the heavy-labeled internal standard as a reference between FTLD-U and control samples, abundance ratios were calculated, converted into $\log_2$ values, plotted as a histogram of all proteins, and fitted to a Gaussian distribution **(Figure 6.4)**. Among the proteins significantly enriched in both proteomic discovery sets, we identified septin 11 (SEPT11), a 429 amino acid cytoskeletal GTPase thought to play a role in filament formation (Nagata, Asano et al. 2004). SEPT11 was consistently enriched ~4-fold in FTLD-U compared to control across all gel bands in both proteomics experiments. In the label-free approach, we identified 3 SEPT11 peptides corresponding to amino acid residues 55-65, 66-79, and 176-184 **(Figure 6.5)**. Quantification revealed a total signal-to-noise ratio (SN) of 19.9 in both FTLD-U replicates, compared with an SN of 4.6 in the

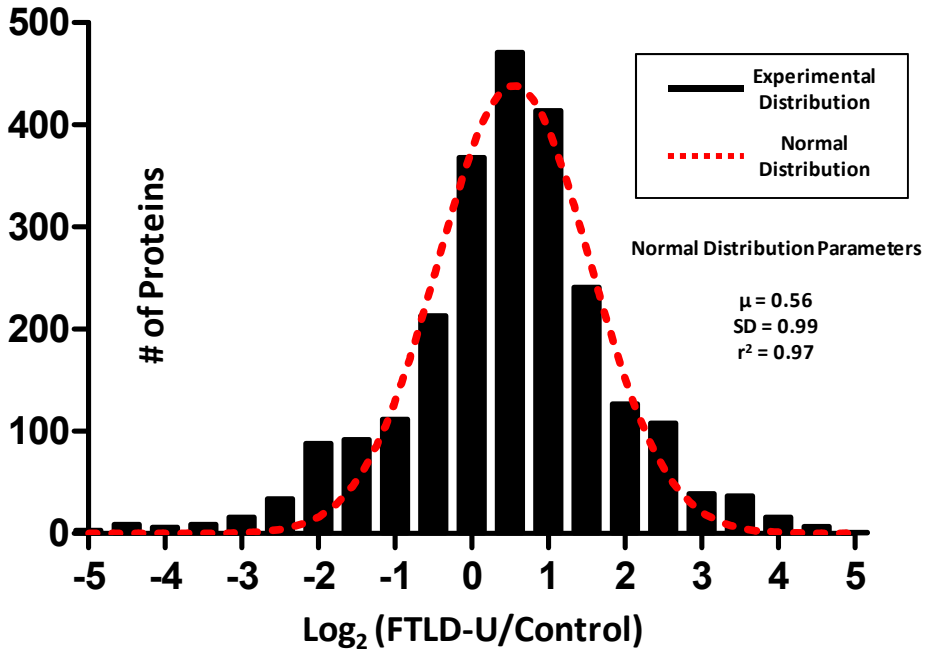

Figure 6.4 Statistical evaluation and filtering of CDIT proteomics data. Abundance ratios for FTLD-U/Control comparison were transformed (logarithmic base 2) and plotted with each point corresponding to the number of proteins in 0.4 unit windows (black line). A Gaussian curve was subsequently fitted to the data (red line) and used to determine significance levels for protein change.

1- MAVAVGRPSN EELRNLSLSG HVGFDSLPDQ LVNKSTSQGF CFNILCVGET

51- GIGKSTLMDT LFNTKFESDP ATHNEPGVRL KARSYELQES NVRLKLTIVD

101 TVGFGDQINK DDSYKPIVEY IDAQFEAYLQ EELKIKRSLF NYHDTRIHAC

151 LYFIAPTGHS LKSLDLVTMK KLDSKVNIIP IIAKADTIAK NELHKFKSKI

201 MSELVSNGVQ IYQFPTDEET VAEINATMSV HLPFAVVGST EEVKIGNKMA

251 KARQYPWGVV QVENENHCDF VKLREMLIRV NMEDLREQTH TRHYELYRRC

301 KLEEMGFKDT DPDSKPFSLQ ETYEAKRNEF LGELQKKEEE MRQMFVMRVK

351 EKEAELKEAE KELHEKFDLL KRTHQEEKKK VEDKKKELEE EVNNFQKKKA

401 AAQLLQSQAQ QSGAQQTKKD KDKKNASFT -429

Figure 6.5 Peptide map of SEPT11. Amino acid sequence of full length SEPT11 (429 aa) marked with peptides identified in shotgun proteomics approaches (solid underline), mapped unique peptides in targeted proteomics (red color), peptides quantified using MRM (bold), and immunizing peptide used in development of in-house SEPT11 rabbit polyclonal antibody (dotted underline).

control sample. Similarly, we identified the same 3 peptides in the CDIT strategy, as well as an additional peptide corresponding to amino acid residues 280-286, with total SN of 134.4 in FTLD-U and 43.4 in control. As expected, TDP-43 was also increased in FTLD-U, albeit more modestly that SEPT11, showing ~1.8-fold (5 peptides) and ~1.3-fold (6 peptides) enrichment in the label-free and CDIT quantitative proteomics approaches, respectively. The specificity of our proteomics strategy was further validated by comparison with AD cases, as SEPT11 was not correspondingly increased in insoluble material from AD frontal cortex. This finding indicates that the enrichment of SEPT11 in FTLD-U is not a non-specific association with protein aggregates, and that it is distinct from proteins associated with neurofibrillary tangles and senile plaques. Moreover, known AD-associated proteins including β-amyloid, tau, and APOE were all enriched in AD insoluble fractions in AD cases but not in FTLD-U (Gozal, Duong et al. 2009).

6.2.2 Validation of SEPT11 enrichment in FTLD-U

Septins are a highly conserved family of filamentous proteins first identified in yeast as a group of cell division cycle regulatory genes (Hartwell 1971). The 14 mammalian septins identified to date share a central characteristic P-loop GTP-binding domain flanked by N- and C-termini which vary in length and amino acid composition (Spiliotis and Nelson 2006). Based on their amino acid sequence homology and their capacity to interchange with other septins in heteromeric complexes that underlie filament assembly, mammalian septins can be further classified into four subgroups. SEPT11 belongs to the septin 6 (SEPT6) subfamily, which, along with other subgroup members (septins 8 and 10), may provide for redundancy in the formation of the septin

2/6/7 and 7/9b/11 filamentous complexes (Kinoshita 2003; Nagata, Asano et al. 2004). SEPT11 and SEPT6 share 85% homology, and both are expressed in the CNS (Kojima, Sakai et al. 2004; Hall, Jung et al. 2005; Tada, Simonetta et al. 2007). Therefore, to confirm the proteomic identification of SEPT11 in FTLD-U urea fractions, we first used a targeted mass spectrometry approach to map unique SEPT11 peptides in SEPT11-overexpressing HEK 293 cells. We subsequently selected 5 of these unique peptides and validated their presence in urea fractions prepared from 4 pooled FTLD-U cases. Finally, using the mass spectrometry-based approach of multiple reaction monitoring (MRM), we re-quantified SEPT11 at its expected molecular weight (Gel piece 3; 40-60 kDa) in the pooled urea samples containing the heavy-labeled HEK 293 cell lysate. Specifically, we monitored multiple high-intensity product ions, which serve as surrogates for measurement of peptide intensities, from two unique peptides corresponding to amino acids 66-79 and 400-418 **(Figure 6.6)**. SEPT11 was enriched 2.1-fold (±0.2) in FTLD-U compared to control in this gel band **(Table 6.3)**. In contrast, concurrent examination of 3 β-actin peptides revealed a slight reduction of this reference protein in FTLD-U samples (0.7±0.1).

The 2-fold discrepancy in SEPT11 enrichment obtained via the shotgun proteomics analyses and the highly sensitive and specific MRM quantitative strategy, suggest that SEPT11 may also be enriched in additional molecular weight regions. Stratification of the data obtained in the proteomic approach using CDIT by molecular weight demonstrated widespread distribution of SEPT11 peptides throughout the entire mass range, with spectra identified in every gel band. Quantitation using XIC and the

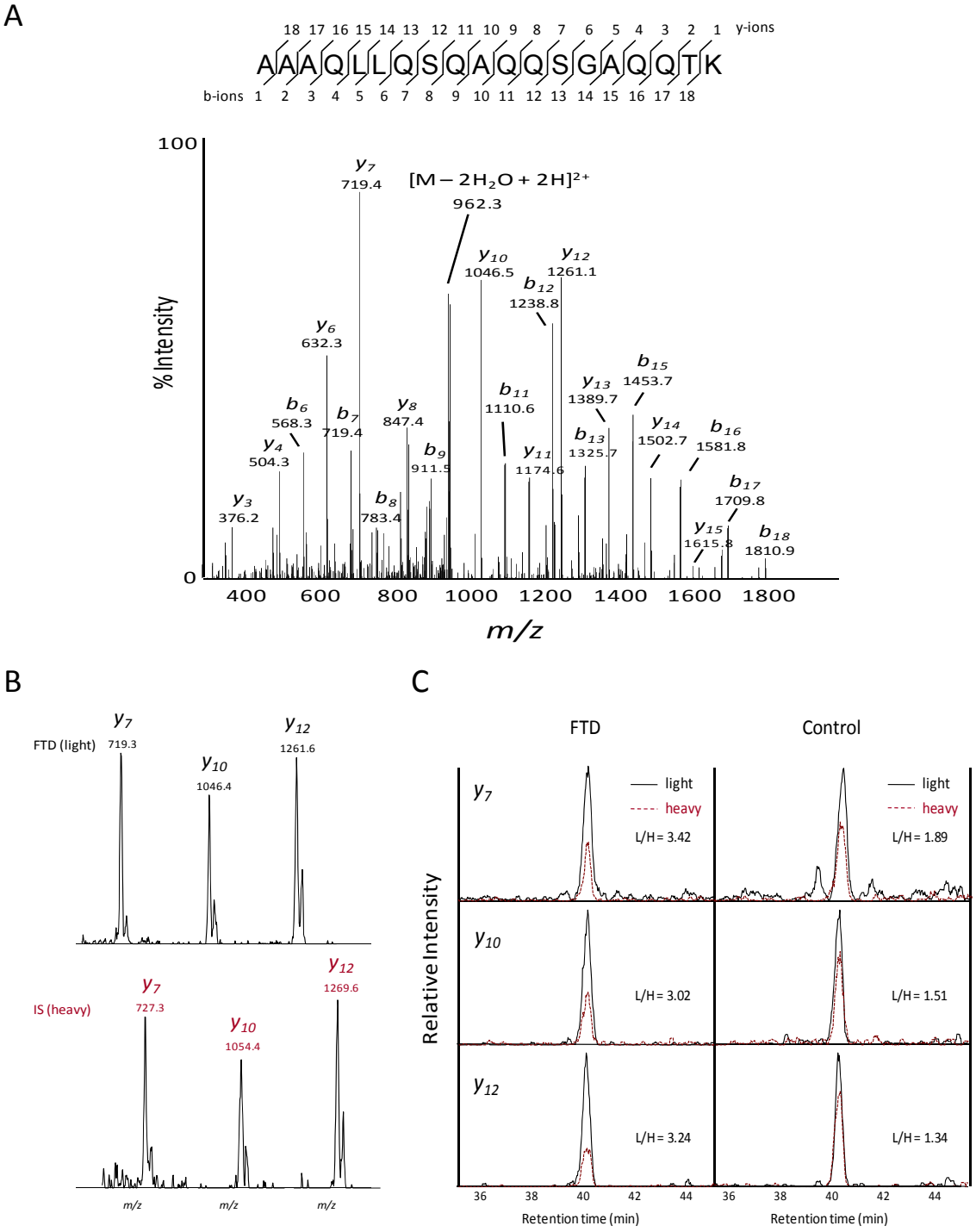
A
y-ions
b-ions
AAAQLLQSQAQQSGAQQTK
% Intensity
m/z
[M − 2H2O + 2H]2+
B
FTD (light)
IS (heavy)
C
FTD
Control
Relative Intensity
light
heavy
L/H = 3.42
L/H = 1.89
L/H = 3.02
L/H = 1.51
L/H = 3.24
L/H = 1.34
Retention time (min)

Figure 6.6 Multiple Reaction Monitoring (MRM) to quantify SEPT11 enrichment in urea fractions. (A) MS/MS scan of the precursor ion (*m/z* 979.0) corresponding to a unique SEPT11 peptide (amino acids 400-418). (B) MS/MS product ions selected for quantitation in light (top) and heavy (bottom) peptide forms. (C) Extracted ion chromatogram of MRM spectra for each of the product ions in (B). The spiked heavy- (red) and endogenous light (black) peptides have identical retention times and are overlaid. For each product ion, enrichment is calculated as a ratio of light to heavy signal of the area under each curve.

Table 6.3 The MRM conditions of Septin11 peptides

Protein Name	Gel Band	Peptide Sequences	[1]Labeled AA	[2]Mass Shift	[3]Precursor Ions (*m/z*)		[4]SRM Conditions			m/z	[6]Product Ions (*m/z*)			[7]AUC (FTLD-U)		[8]S/N (FTLD-U))		AUC (Control)		S/N (Control)		FTLD-U	Control	FTLD-U/	[9]RT (min)
				(Da)	Native (light)	IS (heavy)	Native (light)	IS (heavy)	[5]CE	window	Name	Native (light)	IS (heavy)	(light)	(heavy)	(light)	(heavy)	(light)	(heavy)	(light)	(heavy)	(L/H)	(L/H)	Control	
Septin11	3	FESDPATHNEPGVR	R14	10	778.4	783.4	778.8	783.8	35	1.6															
											y2-10	539.4	544.4	2420	1034	74	77	1776	1531	99	111	2.3	1.2	2.0	35.5
											y1-10	1077.3	1087.3	5428	1176	176	13	3548	1797	151	41	4.6	2.0	2.3	35.5
Septin11	3	AAAQLLQSQAQQSGAQQTK	K19	8	979.0	983.0	979.4	983.4	35	1.6															
											y1-7	719.3	727.3	2700	790	71	24	1747	921	52	21	3.4	1.9	1.8	40.2
											y1-10	1046.4	1054.4	2242	743	70	20	1559	1030	80	33	3.0	1.5	2.0	40.2
											y1-12	1261.6	1269.6	3476	1074	142	20	1790	1334	93	55	3.2	1.3	2.4	40.2
														[10]XIC (FTLD-U)				XIC (Control)						2.1	Avg
														(light)	(heavy)			(light)	(heavy)					0.2	SD
β-actin	3	AGFAGDDAPR	R10	10	488.73	493.74								3208	916			3799	717			3.5	5.3	0.7	
β-actin	3	GYSFTTTAER	R9	10	566.77	571.78								2651	740			4109	896			3.6	4.6	0.8	
β-actin	3	SYELPDGQVITIGNER	R16	10	895.96	900.96								2474	704			2806	584			3.5	4.8	0.7	
																								0.7	Avg
																								0.1	SD

Proteins are sorted by their names followed by reference number. [1]The selected residue for stable isotopic labeling [2]The mass change due to isotopic labeling [3]The *m/z* values of native and labeled peptides [4]The *m/z* range set for the isolation of both native and labeled precusor ions [5]The collison energy in SRM [6]The name and *m/z* values of monitored product ions in SRM (e.g. y1-7, the singly-charged y7 ion) [7]Area under the curve [8]Signal over noise [9]The experimental retention time in reverse-phase liquid chromatography [10]Extracted ion chromatogram.

heavy-labeled internal standard showed a 1.6 to 2-fold enrichment of SEPT11 at the 40-60 kDa range, with higher and lower molecular weight regions accounting for the remainder of the ~4-fold change in these samples. To confirm the changes observed by mass spectrometry, we performed immunoblots on FTLD-U and control urea fractions using a rabbit polyclonal antibody raised to a peptide (amino acids 1-15) at the extreme N-terminus of SEPT11 **(Figure 6.7)**. In addition to the expected band at 49kDa corresponding to the full-length protein, we detected 3 specific SEPT11-immunoreactive bands at ~45 kDa, ~37 kDa, and ~28 kDa in FTLD-U urea fractions that were absent or reduced in control extracts **(Figure 6.7C)**. Quantification of immunoblot band intensities showed a modest but significant 1.8-fold enrichment (p = 0.006) of the full-length SEPT11 band in frontal cortex urea fractions from 7 FTLD-U and 9 control cases **(Figure 6.7D)**, supporting the quantitative mass spectrometric measurements at this molecular weight. Moreover, SEPT11 lower M_r fragments were 3.1-fold enriched in these FTLD-U cases compared to controls ($p < 0.001$). The proteolytic cleavage of SEPT11 is consistent with that observed for other pathologic aggregating proteins, including TDP-43 and tau, where polymerization, post-translational modification, and degradation underlie protein insolubility (Rissman, Poon et al. 2004; Neumann, Sampathu et al. 2006).

To examine if the SEPT11 biochemical insolubility reflects an altered distribution in FTLD-U, we performed immunohistochemical analysis using our specific N-terminal polyclonal antibody. SEPT11 immunoreactivity was localized with astrocytic cell bodies and processes in both hippocampus and frontal cortex of FTLD-U and control cases **(Figure 6.8 A and B)**. Moreover, we observed neuropil immunoreactivity consistent with the localization of SEPT11 along dendrites and in post-synaptic membranes as has been

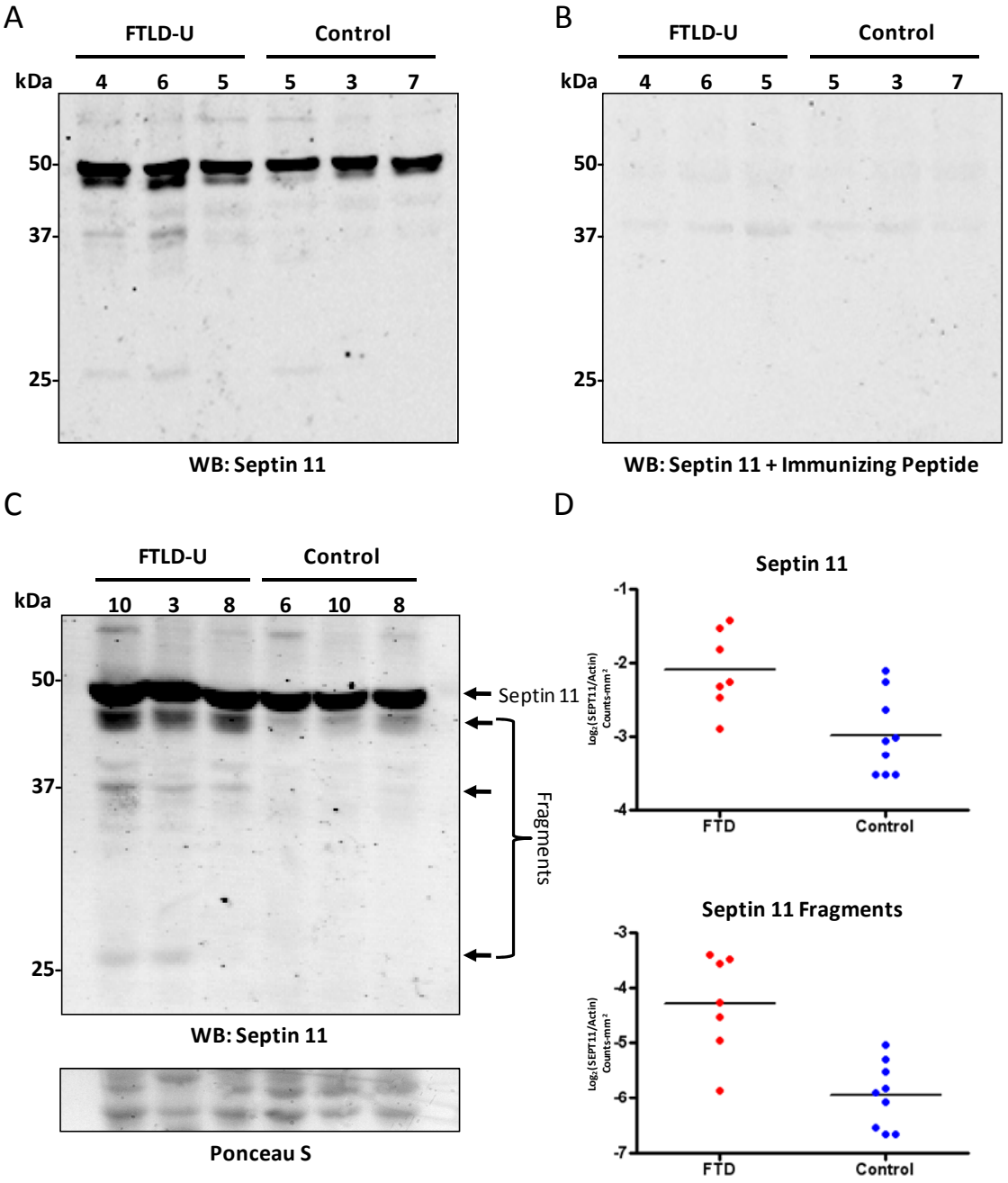
A
FTLD-U
Control
kDa
4 6 5 5 3 7
50
37
25
WB: Septin 11
B
FTLD-U
Control
kDa
4 6 5 5 3 7
50
37
25
WB: Septin 11 + Immunizing Peptide
C
FTLD-U
Control
kDa
10 3 8 6 10 8
50
37
25
Septin 11
Fragments
WB: Septin 11
Ponceau S
D
Septin 11
Log2 (SEPT11/Actin) Counts-mm2
-1
-2
-3
-4
FTD
Control
Septin 11 Fragments
Log2 (SEPT11/Actin) Counts-mm2
-3
-4
-5
-6
-7
FTD
Control

Figure 6.7 Immunoblots of SEPT11 confirm proteomic findings. (A) Frontal cortex samples from individual FTLD-U and control cases were sequentially extracted with buffers containing triton X-100, sarkosyl, and urea. Urea fractions were immunoblotted with an affinity purified SEPT11 rabbit polyclonal antibody raised to a peptide at the extreme N-terminus. (B) Preabsorption using the immunizing peptides quenches immunoreactivity with the exception of a faint non-specific band at ~40kDa. (C) Overexposed immunoblot of urea fractions from additional FTLD-U and control cases detects SEPT11 at its expected M_r (49 kDa), as well as additional N-terminal species at ~45 kDa, ~37 kDa, and ~28 kDa. (D) Quantification in 7 FTLD-U cases and 9 controls of immunoblot band intensities for 49 kDa band (top panel) and all 3 SEPT11 lower M_r fragments (bottom panel). The band at ~40 kDa that did not preabsorb in (B) was excluded from the analysis.

A

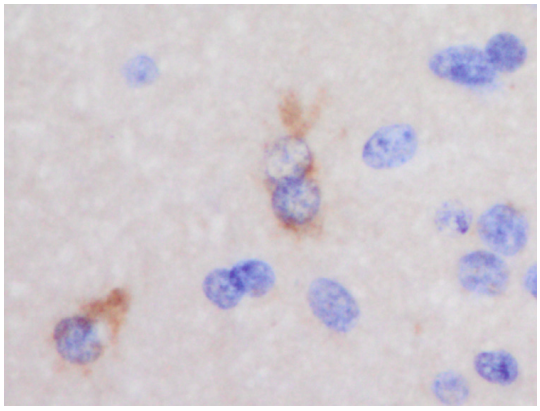

B

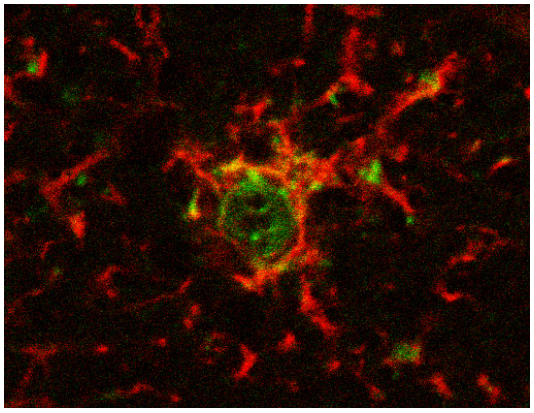

C

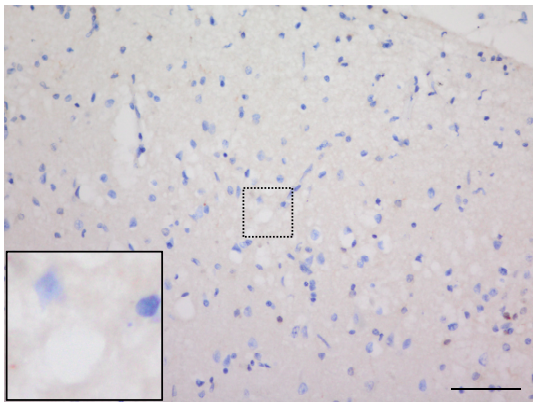

D

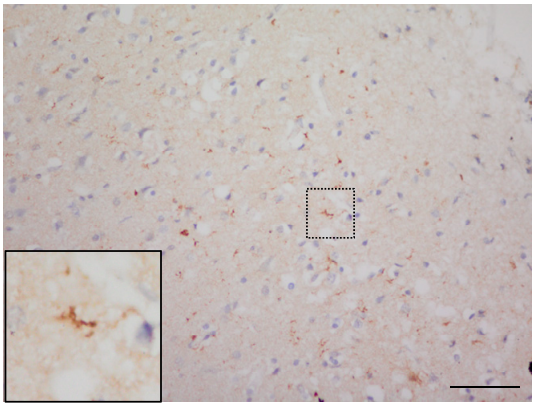

E

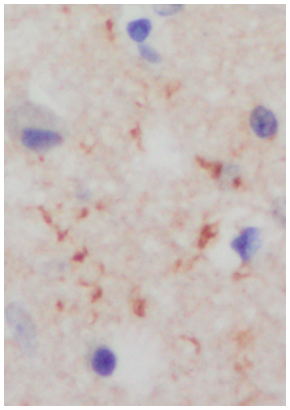

F

		Presence of Septin 11 Pathology		
	Diagnosis	**Low (0-1)**	**High (2-3)**	**Total**
TDP-43 + disorders	FTLD-U	7 (44%)	9 (56%)	16
	ALS	2 (25%)	6 (75%)	8
	Subtotal	**9 (34%)**	**15 (57%)**	**26**
TDP-43 - disorders	PD	9 (69%)	4 (31%)	13
	AD	14 (87.5%)	2 (12.5%)	16
	Tauopathies	9 (90%)	1 (10%)	10
	Subtotal	**32 (82%)**	**7 (18%)**	**39**
	Normal Control	14 (78%)	4 (22%)	18

Figure 6.8 SEPT11 immunoreactivity in control and FTLD-U using polyclonal N-terminal antibody. (A) Immunohistochemistry (IHC) in control frontal cortex reveal cell-associated staining corresponding to astrocytic profiles (B) Double label immunofluorescence in FTLD-U reveals overlap between SEPT11 and glial fibrillary acidic protein (GFAP) confirming, as in control cases, that cell-associated staining localizes to astrocyte cell bodies and processes. (C-E) IHC in FTLD-U (D and E) frontal cortex detects both linear and rounded accumulations of SEPT11 that are absent in control (C). Unlike in (A) and (B), these SEPT11 threads were not associated with specific cells. (F) Summary of blinded scoring of frontal cortex from 81 cases and controls for the presence of SEPT11 threads.

previously described (Li, Serwanski et al. 2009). Analysis revealed no SEPT11 overlap with TDP-43 and ubiquitin-positive neuronal inclusions. However, in a subset of FTLD-U cases, we identified numerous fibrillar thread-like structures which did not associate with glial processes or nuclei **(Figure 6.8 C-E)**. These SEPT11-immunoreactive features localized primarily in superficial cortical layers (layers 2-3), and appeared irregular in shape, length, and thickness. Antibody specificity was confirmed using peptide competition studies, resulting in the complete loss of immunoreactivity in glia, neuropil, and pathologic threads. In contrast, we were unable to preabsorb a thread-like pathology seen with a separate commercially available SEPT11 antibody.

To determine whether SEPT11 threads correspond to a disease-specific signature, we examined and scored this characteristic staining in a series of FTLD-U, ALS, neurologic disease control (AD, PD, and tauopathies), and normal control cases in a blinded fashion **(Table 6.4)**. SEPT11 threads were markedly enriched in FTLD-U, with 56% of cases (9/16) scored as having positive or very positive (score ≥ 2) staining of threads **(Figure 6.8 F)**. In comparison, only 18% (7/39; $p = 0.008$) of neurologic controls and 22% (4/18; $p = 0.076$) of normal controls were scored in this range. Remarkably, threads were associated even more strongly ($p < 0.001$) with TDP-43-positive cases (FTLD-U + ALS) when compared to TDP-43-negative neurodegenerative disorders (AD + PD + tauopathies), providing additional support for shared pathogenic mechanisms in FTLD-U and ALS. Since their presence is highly specific to FTLD-U and ALS, SEPT11-immunoreactive threads may reflect pathologic accumulations of the insoluble full-length or fragmented protein identified in urea fractions.

Table 6.4 Individual Case Demographic and Scoring Information

Case Number	Primary Neuropathologic Diagnosis	[1]PMI (hr)	Age at Onset	Age at Death	Duration	[2]Genotype (rs6818075)	[3]Consensus Score
E04-186	AD	7	59	72	13	GG	0
E05-04	AD	4.5	52	64	12	AG	1
E05-67	AD	11.5	52	62	10	GG	0
E05-145	AD	13	74	87	13	GG	0
E06-154	AD	5	52	60	8	GG	1
E07-179	AD	22	68	77	9	GG	1
E04-33	AD	20	50	57	7	GG	2
E05-56	AD	17	63	71	8	GG	0
E05-87	AD	4	52	61	9	AG	0
E05-194	AD	15	69	71	2.5	GG	1
E06-126	AD	3	62	72	10	GG	0
E06-155	AD	6.5	56	67	11	GG	1
E07-69	AD	6	53	58	5	GG	1
E07-84	AD	16	67	72	5	GG	2
E07-146	AD	13.5	66	74	8	GG	0
E08-53	AD	8	70	78	10	AG	0
Average	**AD**	**10.8**	**60.3**	**68.9**	**8.8**	**13 WT/3 Het**	**-**
OS99-26	PD	2	64	79	15	GG	1
OS01-70	PD	5	48	74	26	GG	2
OS02-105	PD	12	67	76	9	GG	0
OS02-208	PD	12	41	66	25	AG	2
OS03-02	PD	10	75	79	3.5	GG	0
OS03-392	PD	19	58	62	4	GG	2
OS03-395	PD	10	46	78	32	GG	1
OS03-396	PD	13	52	64	12	GG	0
E04-152	PD	11.5	60	67	7	AG	0
E04-169	PD	72	54	64	10	GG	3
E05-81	PD	15.5	47	68	21	GG	1
E07-81	PD	19.5	61	69	8	GG	0
E08-19	PD	8.5	62	71	9	GG	0
Average	**PD**	**16.2**	**56.5**	**70.5**	**14.0**	**11 WT/2 Het**	**-**

Table 6.4 Individual Case Demographic and Scoring Information (continued)

Case Number	Primary Neuropathologic Diagnosis	[1]PMI (hr)	Age at Onset	Age at Death	Duration	[2]Genotype (rs6818075)	[3]Consensus Score
OS00-39	Tau-CBD	2.75	56	61	5	GG	0
OS02-73	Tau-CBD	24	33	44	11	GG	0
OS02-211	Tau-CBD	8.5	72	78	5.5	GG	0
OS03-01	Tau-CBD	6.5	75	78	3	GG	0
OS99-21	Tau-Pick's Disease	3	73	81	8	GG	0
E07-70	Tau-Pick's Disease	4	65	81	16	GG	0
OS00-33	Tau-PSP	11.5	74	82	8	GG	0
OS03-113	Tau-PSP	23	77	83	6	GG	0
E04-79	Tau-PSP	63	49	60	11	GG	1
E07-151	Tau-PSP	10	65	75	10	AG	2
Average	**Tauopathy**	**15.6**	**63.9**	**72.3**	**8.4**	**9 WT/1 Het**	**-**
OS01-86	Control	22.5		51		AG	1
OS01-127	Control	22.5		34		GG	1
OS02-35	Control	6		75		GG	2
OS03-299	Control	6		69		GG	0
OS03-380	Control	12		61		AG	1
OS03-390	Control	7		74		GG	0
E04-34	Control	17		57		GG	0
E04-46	Control	31		40		GG	0
E05-74	Control	6		59		GG	3
E05-130	Control	3		52		GG	1
E06-41	Control	10		57		GG	3
E06-45	Control	6.5		46		GG	0
E06-113	Control	4.5		20		AG	0
E06-114	Control	6.5		53		GG	0
E08-101	Control	11.5		78		GG	0
E08-137	Control	15.5		92		GG	2
E08-145	Control	28		45		GG	1
OS00-23	Control	11		68		GG	0
Average	**Control**	**12.6**	**-**	**57.3**	**-**	**15 WT/3 Het**	**-**

Table 6.4 Individual Case Demographic and Scoring Information (continued)

Case Number	Primary Neuropathologic Diagnosis	[1]PMI (hr)	Age at Onset	Age at Death	Duration	[2]Genotype (rs6818075)	[3]Consensus Score
E04-56	ALS	9.5	70	71	1	GG	2
E06-06	ALS	8	31	34	3	AG	2
E06-50	ALS	7		63		AG	2
E08-67	ALS	6	46	49	2.5	GG	0
E08-86	ALS	13	71	71	0.5	GG	2
E08-88	ALS	19.5	55	59	3.5	GG	3
E08-109	ALS	7.5	52	57	5	GG	0
E08-146	ALS	8	73	76	2.5	GG	2
Average	**ALS**	**9.8**	**56.9**	**60.0**	**2.6**	**6 WT/2 Het**	**-**
E04-139	FTLD-U	15	51	55	4	GG	2
E04-168	FTLD-U	12	50	57	9	GG	0
E06-40	FTLD-U	17.5	62	64	2	GG	0
E06-97	FTLD-U	12	46	48	2	GG	0
E06-191	FTLD-U	9	58	60	2	GG	2
E05-114	FTLD-U	48	70	73	3	GG	1
E07-03	FTLD-U	18.5	47	50	3	GG	3
OS03-95	FTLD-U	21	52	59	7	GG	2
OS03-385	FTLD-U	6.5		68		GG	2
E04-99	FTLD-U	10.5	79	83	4	GG	0
E04-125	FTLD-U	17.5	56	61	5	GG	3
E04-155	FTLD-U	6	56	64	8	GG	0
E05-200	FTLD-U	18	62	71	9	AG	0
E06-112	FTLD-U	7	86	91	5	AG	2
E06-160	FTLD-U	6	57	66	9	AG	3
E08-119	FTLD-U	5	58	60	2	AG	3
Average	**FTLD-U**	**14.3**	**59.3**	**64.4**	**4.9**	**12 WT/4 Het**	**-**

[1]Post-mortem interval [2]Genotype at SNP rs6818075 where G is common allele, A is minor allele, wild type (WT) is GG, and heterozygote (Het) is GA [3]Consensus score represents scoring by 3 independent blinded scorers.

6.2.3 Genetic associations of SEPT11 with FTLD

Genetic polymorphisms and mutations in septins have been associated with multiple neurologic disorders, including AD and hereditary neuralgic amyotrophy (Takehashi, Alioto et al. 2004; Kuhlenbaumer, Hannibal et al. 2005). To determine whether single nucleotide polymorphisms (SNPs) in *SEPT11* were associated with FTLD, we genotyped 20 tag SNPs selected to provide complete coverage of the 89 kb *SEPT11* gene on chromosome 4q21 (r^2 = 1.0; MAF = 0.05). Genotyping in 114 Caucasians with clinically diagnosed sporadic frontotemporal dementia (FTD) and an equal number of Caucasian controls revealed a significant association after Bonferroni correction for a single SNP, rs6818075 (OR 3.32 CI 1.76-6.29; corrected p = 0.0024), a non-coding SNP located in intron 7 **(Tables 6.5 and 6.6)**. We subsequently genotyped a series of 452 AD, 519 PD, and 242 ALS patients at rs6818075 to demonstrate the specificity of the SNP association. We began by genotyping an additional set of 383 control cases to confirm the stability of allele frequencies obtained for the 114 controls in the Emory discovery cohort. Since the two Emory control sets were similar (p = 0.273), and correlated well with the allele frequencies reported in the HapMap CEU database, we combined them for all subsequent comparisons. We found no significant difference in allele frequencies between control cases and AD (OR 1.06 CI 0.77-1.47; p = 0.698), PD (OR 1.21 CI 0.89-1.64; p = 0.220), or ALS (OR 1.18 CI 0.81-1.72; p = 0.386) disease cohorts **(Table 6.6)**. Although SEPT11 immunoreactive threads were neuropathologically linked to ALS as well as FTLD-U, the lack of an association between rs6818075 and ALS suggest differences in the involvement of SEPT11 in these two diseases. Finally, as it is possible that the intronic SNP, rs6818075, acts as a surrogate for a causal variant in

Table 6.5 *SEPT11* genotyping in Emory Discovery Set

[1]SNP	χ2	*p*-value	[2]Corrected *p*	[3]OR	[4]OR MIN	[5]OR MAX
RS6818075	14.828226	0.000118	0.00236	3.324324	1.756246	6.292475
RS7688449	5.938368	0.014815	0.2963	0.620184	0.421864	0.911736
RS12650893	5.233373	0.022158	0.44316	0.62436	0.416472	0.936018
RS17329855	4.903925	0.026796	0.53592	0.651657	0.445717	0.952748
RS878729	4.662469	0.030829	0.61658	1.689466	1.046484	2.727512
RS17262520	3.750916	0.052779	1.05558	1.605815	0.991879	2.599754
RS6811606	3.401654	0.065131	1.30262	1.427429	0.977399	2.084668
RS4241597	3.209476	0.073213	1.46426	1.539499	0.958349	2.473063
RS4859730	1.325589	0.249591	4.99182	1.344262	0.811492	2.226813
RS1135642	1.247906	0.263953	5.27906	0.691057	0.36035	1.325265
RS2645670	1.014148	0.313911	6.27822	0.775439	0.472324	1.273077
RS4859470	0.714425	0.397979	7.95958	1.183809	0.800368	1.750949
RS1874562	0.594362	0.440737	8.81474	1.160286	0.795019	1.693373
RS9307224	0.566252	0.451752	9.03504	1.155698	0.792715	1.68489
RS2703104	0.342857	0.558185	11.1637	1.121114	0.76459	1.643883
RS2279714	0.230952	0.630819	12.61638	1.096802	0.752404	1.598842
RS2279713	0.215311	0.642636	12.85272	1.093546	0.749506	1.595508
RS904037	0.161434	0.68784	13.7568	1.080184	0.741444	1.573681
RS28541859	0.000334	0.985425	19.7085	0.990741	0.365179	2.68791

Allelic Association (FTLD vs Control) [1]Single nucleotide polymorphism [2]Refers to Bonferroni correction for multiple testing [3]Odds Ratio [4]Min and [5]Max refer to 95% confidence interval

Table 6.6 Genotyping Frequencies for rs6818075

Population	Diagnosis	Genotype			Total	Allele Frequency		[1]OR (95% CI)	p-Value
		AA	GA	GG		A	G		
Emory	**FTLD**	2	37	74	113	18.14%	81.86%	[2]3.32 (1.76-6.29)	*0.0024
	$Control_1$	0	15	99	114	6.58%	93.42%		
	$Control_2$	1	66	316	383	8.88%	91.12%		
	$Control_{total}$	1	81	415	497	8.35%	91.65%		
	AD	1	78	373	452	8.85%	91.15%	[3]1.06 (0.77-1.47)	0.698
	PD	6	91	422	519	9.92%	90.08%	1.21 (0.89-1.64)	0.220
	ALS	1	45	196	242	9.71%	90.29%	1.18 (0.81-1.72)	0.386
UCLA	**$FTLD_{UCLA}$**	1	16	75	92	9.78%	90.22%		
	$FTLD_{GIFT}$	1	24	99	124	10.48%	89.52%		
	$FTLD_{total}$	2	40	174	216	10.19%	89.81%	[4]0.88 (0.57-1.37)	0.576
	$Control_{GIFT}$	3	38	152	193	11.40%	88.60%		
Mayo Clinic	**FTLD-U**	1	20	61	82	13.41%	86.59%	[5]1.34 (0.83-2.15)	0.234
	Control	9	151	653	813	10.39%	89.61%		

[1]Odds Ratio [2]Comparison of FTLD and Emory $Control_1$ [3]Comparison of AD, PD, or ALS with Emory $Control_{total}$ [4]Comparison of UCLA $FTLD_{total}$ with UCLA $Control_{GIFT}$ [5]Comparison of Mayo FTLD with Mayo Control *Significant p-value

the coding sequence of SEPT11, we sequenced all exons and intron-exon boundaries for 15 selected FTLD patients (with rs6818075 genotypes: 1 homozygote, 8 heterozygotes, and 6 wild type) and 9 controls (with rs6818075 genotypes: 1 heterozygote and 8 wild type) from the Emory population. While several previously unreported rare intronic variants were identified, no coding sequence variation was observed in these patients.

The positive association of *SEPT11* at rs6818075 identified in the Emory University population was subsequently examined in two additional FTLD cohorts. In a clinically defined cohort of 216 FTD patients and 193 controls collected at the University of California, Los Angeles (UCLA), we were unable to confirm the differences found in the Emory discovery cohort (OR 0.88 CI 0.57-1.37; p = 0.576). Considering the heterogeneity in the pathologic makeup of clinically-defined FTD populations, our second replication set was comprised of 82 pathologically-confirmed non-progranulin FTLD-U cases and 813 control samples characterized at the Mayo Clinic, Jacksonville. Allele frequencies in this pathologic FTLD-U series also revealed no significant association (OR 1.34 CI 0.83-2.15; p = 0.234) with FTLD-U. However, analysis of a subgroup of FTLD-U patients from this population with concurrent motor neuron disease suggested an increased incidence of heterozygotes at rs6818075 (7/17 or ~41%; Allele frequency 20.6%). This observation correlates well with the immunohistochemical findings of SEPT11-positive threads in both FTLD-U and ALS, and suggests, given the small sample sizes, that further genetic study in more homogeneous pathological groups (e.g. specific TDP-43 subtypes) is warranted.

6.3 Discussion

Perturbed expression of septins, a family of cytoskeletal GTP-binding proteins, has been extensively associated with neurodegeneration. Notably, SEPT1, SEPT2, and SEPT4 have been shown to co-localize with neurofibrillary tangles and dystrophic neurites in AD (Kinoshita, Kinoshita et al. 1998). In PD, SEPT4 co-localizes with α-synuclein in Lewy bodies (*28*), and SEPT5 has been shown to be a target for parkin-mediated ubiquitination (Zhang, Gao et al. 2000). In this study, we have shown that SEPT11 is biochemically altered and accumulates in FTLD-U. Although the specific functions of SEPT11 in the brain are not well defined, SEPT11 is thought to form multi-septin complexes that assemble into filaments and function as scaffolds for cytoskeletal-binding proteins (Spiliotis, Kinoshita et al. 2005). Supporting this potential role, SEPT11 has been shown to colocalize with microtubules and stress fibers in multiple epithelial cell lines (Hanai, Nagata et al. 2004). Thus, it is plausible that changes in SEPT11 solubility could disrupt cytoskeletal function and result in cellular toxicity, a mechanism already established for tau-based proteopathies in other neurodegenerative disorders (Cairns, Lee et al. 2004). In fact, SEPT11 insolubility and toxicity may be related to the presence of lower M_r fragments in FTLD-U urea fractions identified by immunoblotting **(Figure 6.7)**. This would parallel findings in a highly homologous protein, SEPT6, in which N-terminal fragments containing the variable region and GTP-binding domain have been reported to be insoluble (Sheffield, Oliver et al. 2003). As is seen with multiple disease proteins, including TDP-43, tau, α-synuclein, and Aβ (Ross and Poirier 2004), proteolytic cleavage of SEPT11 may result in protein misfolding, aggregation, and cytotoxicity. Finally, truncation of the SEPT11 C-terminus would also impact the coiled-

coil domain of the protein, a region critical for septin-septin interactions as well as for binding to non-septin partners (Sheffield, Oliver et al. 2003; Li, Serwanski et al. 2009).

Our characterization of SEPT11 in FTLD-U establishes a powerful new approach to large-scale identification of disease-associated proteins in neurodegenerative conditions through analysis of the detergent-insoluble proteome. SEPT11 immunoreactive threads are a novel neuropathological feature of a subgroup of FTLD-U cases, but accumulation of insoluble SEPT11 aggregates is not a universal feature of all FTLD-U cases. Our proteomics-based strategy incorporated pooled samples of FTLD-U and control cases to reduce the impact of biological variability that is unavoidable and uncontrollable in studies of human autopsy materials. Factors, such as postmortem interval, unknown agonal circumstances, and other individual features unique to every patient, introduce enormous noise in efforts to identify disease-specific elements. As clinical and pathological entities, FTD and FTLD-U each represents heterogeneous groups of disorders. Although accepted criteria for FTLD-U have been established, our understanding of this neuropathological entity is far from complete. This is clearly demonstrated by ongoing efforts to subclassify FTLD-U cases based on specific features of TDP-43 immunoreactivity. We have now shown that pathological accumulation of SEPT11 in superficial cortical layers defines an additional molecular feature linked to FTLD-U, and closer examination of candidates identified through proteomic profiling will reveal additional features that will produce a clearer understanding of this complex neurodegenerative disorder.

Chapter 7

Summary and Future Directions

The aim of the studies presented in this dissertation was to elucidate the mechanisms leading to protein aggregation, inclusion formation, and neurodegeneration in FTLD-U. Since the onset of this project, tremendous progress has been made in our understanding of the clinical features, neuropathology, and genetic basis of this complex disorder. These discoveries, which include the identification of four potential genetic causes and a major aggregating protein, have transformed the perception of FTLD-U from that of a rare disorder of little interest, to one of major significance befitting its prevalence as the second most common subtype of FTLD (Lipton, White et al. 2004). During this period of rapid progress, our contribution has focused on the use of biochemical and quantitative proteomics methodologies to identify important molecular substrates and pathways involved in disease pathogenesis. In FTLD-U, which until recently was defined only by the presence of unknown ubiquitinated protein aggregates (Bigio, Johnson et al. 2004), such studies are critical in fueling additional advances necessary to develop accurate clinical diagnosis and targeted therapies.

The application of proteomic approaches in the field of neurodegeneration has gained tremendous popularity in the last decade (Fountoulakis and Kossida 2006) owing to the multi-factorial nature of these disorders. In fact, neuroproteomics technologies are especially well suited for the study of degenerative diseases since they can provide an unbiased global assessment of the complex pathologic changes underlying cognitive

dysfunction and neuronal toxicity commonly observed in these disorders. Proteomic profiling of AD and PD, in particular, has been tremendously successful in identifying and correlating changes in protein expression or modification state with deficits in multiple pathogenic pathways (Pienaar, Daniels et al. 2008). Thus, it is surprising that, to our knowledge, the studies described in this dissertation constitute the first reported shotgun proteomic analyses of FTLD-U. Using complementary quantitative proteomics approaches, we profiled the anatomical and biochemical lesions characteristic of FTLD-U.

We first performed a comparative label-free quantitative proteomics approach profiling microdissected hippocampal dentate granule cells from FTLD-U and control cases. The hippocampal dentate gyrus is an area of particular interest as a result of the large number of characteristic ubiquitin-positive inclusions demonstrated in dentate granule cells (Okamoto, Hirai et al. 1991). These inclusions, which indicate enhanced aggregation of one or several proteins, suggest altered expression, processing, or degradation of proteins in the dentate gyrus during FTLD-U. Thus, identification of their composition and the mechanisms leading to inclusion formation is critical for our understanding of disease pathogenesis, and has been a primary goal of FTLD researchers for decades. Following LCM of dentate granule cells and analysis by LC-MS/MS, we identified 54 proteins with selective enrichment in FTLD-U. Validation using independent methods of a handful of protein candidates failed to confirm the proteomics results. However, the presence of TDP-43, a recently identified component of ubiquitinated inclusions, suggests that this list may include disease-relevant proteins amongst the false positives. Moreover, the identification of proteins in several pathways

previously implicated in other neurodegenerative diseases, including metabolism and oxidative stress, protein degradation, and components of the cytoskeleton, suggest that additional validation of proteins in this list may be warranted. Nevertheless, the inflated false-discovery rate in this experiment indicated that significant deficiencies were present in our proteomic strategy. Several of these limitations (discussed in Chapter 3), can now be addressed by updating the LCM platform to take advantage of significant improvements in the accuracy, speed, and sensitivity of LCM facilities since their introduction a decade ago. Although these technologies were not available for our study, the LCM-based approach remains an extremely valuable tool for the characterization of ubiquitinated inclusions in FTLD-U.

To address many of the limitations identified in our LCM-based proteomic analysis, we developed a new, more broadly applicable, quantitative proteomic strategy based on the profiling of detergent-insoluble proteins from diseased brain. Biochemical alterations in protein solubility play a central role in our understanding of aggregate formation in neurodegenerative diseases. In fact, the isolation and identification of aggregated amyloid β (Aβ) and hyperphosphorylated tau in AD was based primarily on the extensive insolubility of their fibrillar forms (Glenner and Wong 1984; Grundke-Iqbal, Iqbal et al. 1986; Wischik, Novak et al. 1988). More importantly, the identification of TDP-43 as a component of ubiquitin-immunoreactive inclusions in FTLD-U was accomplished by the generation of antibodies against detergent-insoluble extracts from diseased brain (Neumann, Sampathu et al. 2006). Thus, we used high-resolution LC-MS/MS and label-free quantitative methods to analyze so-called "biochemical lesions" from frontal cortex of FTLD-U and unaffected control cases. The use of frontal cortex

alleviated any concerns regarding acquisition of sufficient material for both proteomic analysis and subsequent validation. Moreover, by analyzing detergent-insoluble fractions, we simultaneously enriched for aggregated species and reduced the complexity of the analyte, thereby improving the probability of detecting important, less abundant insoluble proteins. Notably, we co-analyzed samples from AD cases to identify FTLD-U-specific changes not present in other neurodegenerative diseases. The inclusion of this sample, however, allowed for the "reverse" analysis in which AD-specific changes were identified in detergent-insoluble fractions. Demonstrating the efficacy of this proteomic strategy, we identified 12 AD-specific enriched proteins, including five proteins previously linked to pathological aggregates in AD brain. Similarly, among altered FTLD-U proteins, we identified significant enrichment of TDP-43, particularly in high M_r regions of the gel. Our results provide further evidence for the capacity of proteomic applications to identify conserved sets of disease-specific proteins in neurodegeneration. Currently, we are applying this strategy in the simultaneous, unbiased analysis of the primary aggregating species in multiple neurodegenerative disorders, including ALS, CBD, and PD. In addition to the identification of disease-specific proteins, we hope to reveal protein changes common to all neurodegenerative disorders.

To improve the capacity for reliably identifying altered proteins and to reduce the incidence of false positives, we cross-referenced the results from the label-free proteomic characterization of FTLD-U insoluble fractions with those obtained from an independent quantitative analysis based on the incorporation of culture-derived isotopic tags (CDIT). In addition to the inclusion of pooling strategies and technical replicates, which have now become the standard in proteomic analyses, the use of orthogonal approaches provides an

additional filter to help identify consistent changes in altered proteins. For example, a comparison of the quantitative CDIT results with those obtained by analysis of LCM samples would have reduced the list of altered proteins from 54 to 21 proteins. This reduction is significant considering the cost in reagents and time required for immunochemical or targeted proteomics (SRM) validation of shotgun studies. Among the altered proteins identified in both label-free and CDIT quantitative proteomic analyses of detergent-insoluble fractions, we elected to focus our efforts on validating possible roles for TDP-43 and septin 11 in FTLD-U pathogenesis.

TDP-43 is a highly conserved, ubiquitously expressed protein encoded by the *TARDBP* gene on chromosome 1 (Bigio 2008). Its identification as a major component of ubiquitin-immunoreactive inclusions characteristic of FTLD-U and ALS in 2006 (Neumann, Sampathu et al. 2006) reinvigorated a field that was desperate for insight into the mechanisms of these disorders. As an indication of the excitement in the field, it is remarkable to consider that while only 12 publications existed regarding TDP-43 prior to 2006, it has been the subject of more than 250 research papers in the last three years. The identification of TDP-43 occurred concurrently with the discovery phase of our work, and its inclusion among our altered FTLD-U proteins has helped to validate our proteomics approaches. Furthermore, we have directed considerable effort towards analyzing the mechanisms underlying TDP-43 aggregation events and post-translational modifications using both biochemical and proteomic approaches. First, while others focused on modeling the aggregation of TDP-43 C-terminal fragments (Igaz, Kwong et al. 2008; Johnson, McCaffery et al. 2008; Nonaka, Kametani et al. 2009), we developed one of the first cellular models of FTLD-U by overexpressing TDP-S6, a truncated TDP-

43 splice variant lacking the important C-terminal glycine rich domain (Wang, Wang et al. 2004). This model is of particular relevance for the study of TDP-43 biology since pathogenic mutations identified in *TARDBP* in ALS have been localized primarily to the C-terminus of the protein (Gitcho, Baloh et al. 2008; Kabashi, Valdmanis et al. 2008; Sreedharan, Blair et al. 2008; Van Deerlin, Leverenz et al. 2008; Yokoseki, Shiga et al. 2008). The overexpression of TDP-S6 recapitulated many of the features associated with disease pathology, including the loss of nuclear TDP-43, its aggregation in the cytoplasm, and its post-translational modification. It is worth noting that FTLD-U research to date has been conducted, for the lack of suitable alternatives, entirely using human post-mortem tissues. Thus, the capacity to develop cellular and animal models to study disease-related mechanisms using well-controlled cell biological approaches is invaluable. Second, using our newly established disease model, we examined the cellular effects of TDP-43-mediated aggregation using SILAC proteomics approaches. We report that, in addition to phosphorylation, ubiquitination, and proteolytic cleavage, TDP-43 is also SUMOylated within aggregate-enriched insoluble fractions and colocalized with SUMO2/3 in nuclear accumulations. SUMOylation plays an important role in the nucleus by regulating protein degradation, DNA repair, transcriptional activation, and nuclear body formation (Martin, Wilkinson et al. 2007). Moreover, SUMO1-immunoreactivity has been identified in a number of neurodegenerative diseases, including AD and PD where it is localized to tangles and Lewy bodies respectively (Dorval and Fraser 2006). While further study is necessary to identify the biological importance of TDP-43 SUMOylation, we speculate that this modification alters TDP-43 nuclear dynamics and solubility, thereby resulting in sequestration of TDP-43 in nuclear

aggregates. Finally, in a series of experiments using immunocytochemistry and SRM, we characterized the distribution of polyUb chains in our TDP-43 aggregation model. Cellular inclusions were found to be enriched with both K63 and K48 polyUb linkages, and these results were validated via an independent quantitative proteomics approach. PolyUb chains linked by K48 play a critical role in signaling substrate degradation by the proteasome (Gregori, Poosch et al. 1990). In contrast, K63 polyUb chains are purported to be involved in a variety of distinct processes, including DNA repair and endocytosis (Pickart 2001). Interestingly, recent findings have demonstrated that K63-linked chains can enhance the aggregation of proteins and, subsequently, their autophagic clearance (Tan, Wong et al. 2008). This directed clearance of protein inclusions by autophagy may involve the interaction of K63-linked polyUb with the ubiquitin-binding protein 62/sequestosome 1 (p62), a cytosolic protein previously demonstrated to partially co-localize with ubiquitinated inclusions in FTLD-U (Arai, Nonaka et al. 2003; Tan, Wong et al. 2007; Pikkarainen, Hartikainen et al. 2008). Since, in addition to proteasomal dysfunction, autophagic suppression can also lead to inclusion formation (Komatsu, Waguri et al. 2006), it is probable that mixed polyUb chains contribute to the formation of TDP-43 protein aggregates. Therefore, systematic analyses of polyUb linkages in FTLD-U and the roles of specific ubiquitination sites on TDP-43 are needed to clarify the mechanisms underlying inclusion biogenesis and clearance.

The proteomic identification of SEPT11 in detergent-insoluble fractions represents another significant advance in our efforts to dissect the pathways that lead to FTLD-U pathogenesis. Since its initial discovery in complexes from porcine brain in 2004 (Hanai, Nagata et al. 2004), little progress has been made to further characterize

SEPT11 cellular function. Primarily, SEPT11 has been implicated as a player in multi-septin complexes, where it is thought to contribute to filament assembly and the formation of cytosolic scaffolds (Nagata, Asano et al. 2004; Blaser, Roseler et al. 2006; Sudo, Ito et al. 2007; Ding, Yu et al. 2008). The accumulation of SEPT11 at dendritic branch points in Purkinje neurons, for example, is thought to mediate scaffolding for cytoskeletal proteins involved in the formation of dendritic arbors (Li, Serwanski et al. 2009). However, in addition to functioning in highly-assembled states, most septins also function independently in various pathways, including exocytosis, apoptosis, and synaptogenesis (Kinoshita 2003; Kinoshita 2006). Since the regional distribution of SEPT11 is not identical to that of its known binding partners (Li, Serwanski et al. 2009), it is likely that SEPT11 functions alone in as yet undefined molecular pathways. Thus, the elucidation of these pathways, and any additional SEPT11 interacting-proteins, may be crucial for defining the mechanisms underlying FTLD-U, and should be a major goal of future research.

Characterization of the "biochemical phenotype" of SEPT11 demonstrates significant enrichment of multiple detergent-insoluble N-terminal proteolytic fragments in FTLD-U. Sequence analysis of SEPT11 suggests that, since the putative GTPase domain occurs at 48-188 amino acids (Hanai, Nagata et al. 2004) and the coiled-coil domain occurs at 333-414 amino acids (Nakai and Horton 1999), the fragments of ~45kDa, ~37kDa, and ~28kDa identified in FTLD-U urea fractions would lack a portion of the coiled-coil domain, the entire coiled-coil domain, and the entire coiled-coil domain plus a portion of the GTPase domain, respectively. As predicted by studies in other septins, the loss of these domains would not only affect protein solubility (Sheffield,

Oliver et al. 2003), but would severely impact protein localization and its interaction with both septin and non-septin binding partners (Casamayor and Snyder 2003; Sheffield, Oliver et al. 2003; Li, Serwanski et al. 2009). Interestingly, in a preliminary study (n = 1), proteasomal inhibition using MG-132 (10μM) in untransfected HEK293 cells for up to 24 hours, resulted in the induction of endogenous SEPT11 cleavage (~45kDa and ~37kDa) by 10 hours **(Figure 7.1)**. While these results require extensive analysis and replication, they suggest that SEPT11 proteolytic processing occurs downstream of proteasomal dysfunction in FTLD-U. Thus, we speculate that the accumulation of SEPT11 may not be a proximal event in the pathogenesis of FTLD-U. Additional studies examining whether proteasomal inhibition in cell culture can induce SEPT11 aggregation could be performed to strengthen and expand on these findings. Moreover, proteomic identification of SEPT11 fragments and their subsequent overexpression in cell culture may allow for the development of valuable cellular models to study SEPT11 aggregation and toxicity.

FTLD-U is a complex disorder in which genetic risk is conferred by both causal and susceptibility genes (Rollinson, Rizzu et al. 2009). Since SEPT11 is enriched in detergent-insoluble fractions and accumulates in the brain of FTLD-U cases, we sought to determine whether the *SEPT11* gene was directly associated with sporadic FTLD. In our discovery sample we found a significant association of an intronic SNP, rs6818075, with clinical FTLD. However, we were unable to replicate these findings in two independent samples from UCLA and Mayo Clinic, Jacksonville. While it is possible that our initial finding of association corresponded to a false positive, there are additional possibilities that may underlie these discrepant findings. First, it is extremely likely that

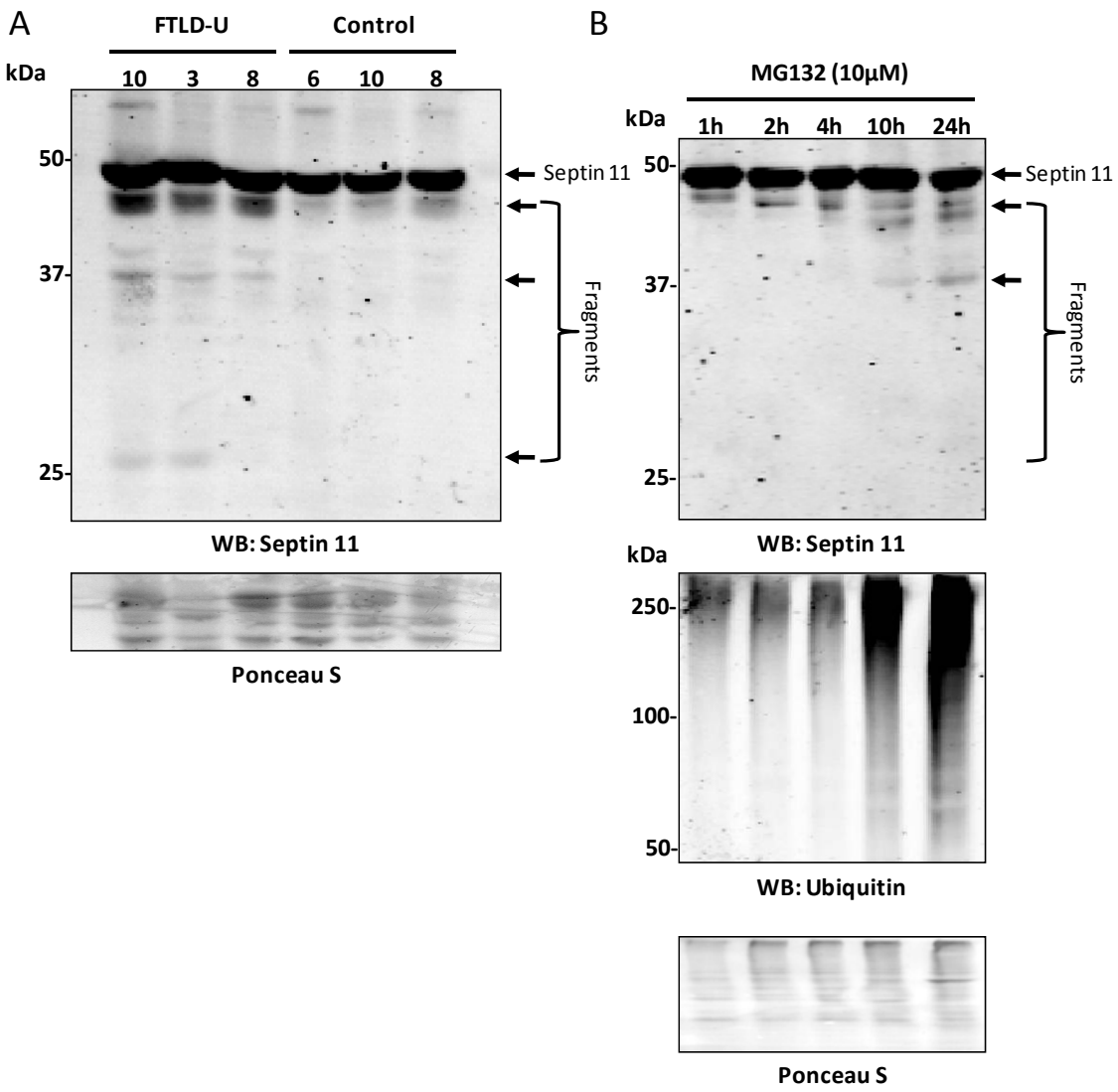
A
FTLD-U
Control
kDa
10
3
8
6
10
8
50-
37-
25-
Septin 11
Fragments
WB: Septin 11
Ponceau S
B
MG132 (10µM)
kDa
1h
2h
4h
10h
24h
50-
37-
25-
Septin 11
Fragments
WB: Septin 11
kDa
250-
100-
50-
WB: Ubiquitin
Ponceau S

Figure 7.1 Proteasomal inhibition recapitulates SEPT11 cleavage. (A) Immunoblot of urea fractions from FTLD-U and control cases detects SEPT11 at its expected M_r (49 kDa), as well as additional N-terminal species at ~45 kDa, ~37 kDa, and ~28 kDa. (Reproduced blot from Figure 6.7C) (B) Immunoblot of urea-extracted untransfected HEK293 cells treated with MG-132 (10μM) for various time points results in the fragmentation of endogenous SEPT11 into ~45kDa and ~37kDa fragments (top). Proteasomal inhibition also results in the accumulation of insoluble polyubiquitinated species (middle). (n = 1)

there was significant heterogeneity in the clinical and pathological phenotypes of genotyped patients in each population. This type of error may occur even within the more homogeneous, pathologically-confirmed FTLD-U Mayo Clinic population, since FTLD-U cases can be further segregated into multiple neuropathologic subtypes based on TDP-43 immunoreactivity (Cairns, Bigio et al. 2007). Patient heterogeneity and misclassification is presumed to be the primary reason for the failure of both *TARDBP* (Schumacher, Friedrich et al. 2009) and *GRN* (Rademakers 2009) to demonstrate associations in sporadic FTLD populations. A second reason for the frequent failure of replicates in candidate gene studies is population stratification (Emahazion, Feuk et al. 2001). Although we specifically genotyped only Caucasian individuals in all three patient populations, there could still be significant heterogeneity in the overall genetic makeup of each population (Emahazion, Feuk et al. 2001). This could easily affect our SNP associations, considering that the frequency of the minor allele at rs6818075 is more than twice as common in the HapMap Yoruba population (20.0%) than it is in the CEU population (8.3%). Finally, the two replication sets were significantly underpowered for the expected effect size simply due to the scarcity of available FTLD cases. Therefore, with extremely low replication power as a result of small sample sizes and with extensive pathologic and clinical heterogeneity, it is not surprising that both the UCLA and Mayo Clinic populations failed to replicate the findings in the discovery group (Gorroochurn, Hodge et al. 2007). Since the probability of a false-negative finding is significantly increased in underpowered studies (Knowles, Assimes et al. 2008), a replication failure in this case does not necessarily refute the original significant finding (Gorroochurn, Hodge et al. 2007). Moreover, a meta-analysis of patients from all three genotyped population

was nominally associated with an increased risk of FTLD (OR 1.37 CI 1.08-1.73; uncorrected p = 0.009). Thus, additional analyses in independent, sufficiently-powered cohorts are warranted to address the possibility of a real but weak genetic susceptibility.

In summary, we have developed broadly-applicable quantitative proteomic strategies for the unbiased, large-scale identification and quantitation of disease-related proteins from human neurodegenerative disease samples. Application of these strategies in performing the first shotgun proteomic analyses of FTLD-U samples resulted in the identification of SEPT11, a novel FTLD-U-associated protein. Additionally, we developed a cellular model of TDP-43 aggregation by overexpression of a commonly occurring splice variant. Using this model, we demonstrated the SUMOylation of TDP-43, and employed additional proteomic and biochemical approaches to profile polyubiquitin linkages. These findings contribute to our rapidly improving understanding of FTLD-U pathogenesis, and provide a molecular basis for more focused studies aimed at characterizing the mechanistic contributions of genetically- and pathologically-linked disease candidates. Moreover, improved nosology of FTLD-U disorders based on molecular criteria will allow the study of more homogeneous patient populations, thereby advancing not only the success of future proteomic and genetic association studies, but also the probability of developing effective targeted therapies.

References

(1997). "Consensus recommendations for the postmortem diagnosis of Alzheimer's disease. The National Institute on Aging, and Reagan Institute Working Group on Diagnostic Criteria for the Neuropathological Assessment of Alzheimer's Disease." Neurobiol Aging **18**(4 Suppl): S1-2.

Aebersold, R. and M. Mann (2003). "Mass spectrometry-based proteomics." Nature **422**(6928): 198-207.

Allison, D. B., X. Cui, et al. (2006). "Microarray data analysis: from disarray to consolidation and consensus." Nat Rev Genet **7**(1): 55-65.

Altman, E. (1923). "Über die eigenartige Krankheitsfalle des spateren Alters." Zeitscrift fur die Gesamte Neurologie und Psychiatrie **4**: 356-385.

Alzheimer, A. (1911). "Über die eigenartrige Krankheitsfalle des spateren Alters." Zeitscrift fur die Gesamte Neurologie und Psychiatrie **4**: 7-44.

Amador-Ortiz, C., W. L. Lin, et al. (2007). "TDP-43 immunoreactivity in hippocampal sclerosis and Alzheimer's disease." Ann Neurol **61**(5): 435-45.

Andersen, J. S., C. J. Wilkinson, et al. (2003). "Proteomic characterization of the human centrosome by protein correlation profiling." Nature **426**(6966): 570-4.

Arai, T., T. Nonaka, et al. (2003). "Neuronal and glial inclusions in frontotemporal dementia with or without motor neuron disease are immunopositive for p62." Neurosci Lett **342**(1-2): 41-4.

Atamna, H. and W. H. Frey, 2nd (2007). "Mechanisms of mitochondrial dysfunction and energy deficiency in Alzheimer's disease." Mitochondrion **7**(5): 297-310.

Atwood, C. S., R. N. Martins, et al. (2002). "Senile plaque composition and posttranslational modification of amyloid-beta peptide and associated proteins." Peptides **23**(7): 1343-50.

Ayala, Y. M., S. Pantano, et al. (2005). "Human, Drosophila, and C.elegans TDP43: nucleic acid binding properties and splicing regulatory function." J Mol Biol **348**(3): 575-88.

Bak, T. H. and J. R. Hodges (2001). "Motor neurone disease, dementia and aphasia: coincidence, co-occurrence or continuum?" J Neurol **248**(4): 260-70.

Baker, M., I. R. Mackenzie, et al. (2006). "Mutations in progranulin cause tau-negative frontotemporal dementia linked to chromosome 17." Nature **442**(7105): 916-919.

Baker, M., I. R. Mackenzie, et al. (2006). "Mutations in progranulin cause tau-negative frontotemporal dementia linked to chromosome 17." Nature **442**(7105): 916-9.

Banks, R. E., M. J. Dunn, et al. (2000). "Proteomics: new perspectives, new biomedical opportunities." Lancet **356**(9243): 1749-56.

Benajiba, L., I. Le Ber, et al. (2009). "TARDBP mutations in motoneuron disease with frontotemporal lobar degeneration." Ann Neurol **65**(4): 470-3.

Bence, N. F., R. M. Sampat, et al. (2001). "Impairment of the ubiquitin-proteasome system by protein aggregation." Science **292**(5521): 1552-5.

Bennett, V. and J. Healy (2008). "Organizing the fluid membrane bilayer: diseases linked to spectrin and ankyrin." Trends Mol Med **14**(1): 28-36.

Bennett, V. and S. Lambert (1999). "Physiological roles of axonal ankyrins in survival of premyelinated axons and localization of voltage-gated sodium channels." J Neurocytol **28**(4-5): 303-18.

Bergamaschini, L., S. Canziani, et al. (1999). "Alzheimer's beta-amyloid peptides can activate the early components of complement classical pathway in a C1q-independent manner." Clin Exp Immunol **115**(3): 526-33.

Bigio, E. H. (2008). "Update on recent molecular and genetic advances in frontotemporal lobar degeneration." J Neuropathol Exp Neurol **67**(7): 635-48.

Bigio, E. H., N. A. Johnson, et al. (2004). "Neuronal ubiquitinated intranuclear inclusions in familial and non-familial frontotemporal dementia of the motor neuron disease type associated with amyotrophic lateral sclerosis." J Neuropathol Exp Neurol **63**(8): 801-11.

Bird, T., D. Knopman, et al. (2003). "Epidemiology and genetics of frontotemporal dementia/Pick's disease." Ann Neurol **54 Suppl 5**: S29-31.

Bird, T. D., E. M. Wijsman, et al. (1997). "Chromosome 17 and hereditary dementia: linkage studies in three non-Alzheimer families and kindreds with late-onset FAD." Neurology **48**(4): 949-54.

Blaser, S., S. Roseler, et al. (2006). "Human endothelial cell septins: SEPT11 is an interaction partner of SEPT5." J Pathol **210**(1): 103-10.

Blennow, K., M. J. de Leon, et al. (2006). "Alzheimer's disease." Lancet **368**(9533): 387-403.

Bondarenko, P. V., D. Chelius, et al. (2002). "Identification and relative quantitation of protein mixtures by enzymatic digestion followed by capillary reversed-phase liquid chromatography-tandem mass spectrometry." Anal Chem **74**(18): 4741-9.

Bonner, R. F., M. Emmert-Buck, et al. (1997). "Laser capture microdissection: molecular analysis of tissue." Science **278**(5342): 1481,1483.

Bota, D. A. and K. J. Davies (2002). "Lon protease preferentially degrades oxidized mitochondrial aconitase by an ATP-stimulated mechanism." Nat Cell Biol **4**(9): 674-80.

Boxer, A. L. and B. L. Miller (2005). "Clinical features of frontotemporal dementia." Alzheimer Dis Assoc Disord **19 Suppl 1**: S3-6.

Boxer, A. L., J. Q. Trojanowski, et al. (2005). Frontotemporal lobar degeneration. Neurodegenerative diseases: neurobiology, pathogenesis and therapeutics M. F. Beal, A. E. Lang and A. C. Ludolph. Cambridge, UK, Cambridge UP**:** 481-493.

Browman, D. T., M. B. Hoegg, et al. (2007). "The SPFH domain-containing proteins: more than lipid raft markers." Trends Cell Biol **17**(8): 394-402.

Brownell, B., D. R. Oppenheimer, et al. (1970). "The central nervous system in motor neurone disease." J Neurol Neurosurg Psychiatry **33**(3): 338-57.

Brun, A. (1987). "Frontal lobe degeneration of non-Alzheimer type. I. Neuropathology." Arch Gerontol Geriatr **6**(3): 193-208.

Buee, L. and A. Delacourte (1999). "Comparative biochemistry of tau in progressive supranuclear palsy, corticobasal degeneration, FTDP-17 and Pick's disease." Brain Pathol **9**(4): 681-93.

Buratti, E. and F. E. Baralle (2001). "Characterization and functional implications of the RNA binding properties of nuclear factor TDP-43, a novel splicing regulator of CFTR exon 9." J Biol Chem **276**(39): 36337-43.

Buratti, E., A. Brindisi, et al. (2005). "TDP-43 binds heterogeneous nuclear ribonucleoprotein A/B through its C-terminal tail: an important region for the inhibition of cystic fibrosis transmembrane conductance regulator exon 9 splicing." J Biol Chem **280**(45): 37572-84.

Buratti, E., T. Dork, et al. (2001). "Nuclear factor TDP-43 and SR proteins promote in vitro and in vivo CFTR exon 9 skipping." Embo J **20**(7): 1774-84.

Butterfield, D. A. and A. Castegna (2003). "Proteomics for the identification of specifically oxidized proteins in brain: technology and application to the study of neurodegenerative disorders." Amino Acids **25**(3-4): 419-25.

Cairns, N. J., E. H. Bigio, et al. (2007). "Neuropathologic diagnostic and nosologic criteria for frontotemporal lobar degeneration: consensus of the Consortium for Frontotemporal Lobar Degeneration." Acta Neuropathol **114**(1): 5-22.

Cairns, N. J., V. M. Lee, et al. (2004). "The cytoskeleton in neurodegenerative diseases." J Pathol **204**(4): 438-49.

Cairns, N. J., M. Neumann, et al. (2007). "TDP-43 in familial and sporadic frontotemporal lobar degeneration with ubiquitin inclusions." Am J Pathol **171**(1): 227-40.

Casamayor, A. and M. Snyder (2003). "Molecular dissection of a yeast septin: distinct domains are required for septin interaction, localization, and function." Mol Cell Biol **23**(8): 2762-77.

Cheng, D., C. C. Hoogenraad, et al. (2006). "Relative and absolute quantification of postsynaptic density proteome isolated from rat forebrain and cerebellum." Mol Cell Proteomics.

Cheng, D., C. C. Hoogenraad, et al. (2006). "Relative and absolute quantification of postsynaptic density proteome isolated from rat forebrain and cerebellum." Mol Cell Proteomics **5**(6): 1158-70.

Choi, J., A. I. Levey, et al. (2004). "Oxidative modifications and down-regulation of ubiquitin carboxyl-terminal hydrolase L1 associated with idiopathic Parkinson's and Alzheimer's diseases." J Biol Chem **279**(13): 13256-64.

Corbett, J. M., M. J. Dunn, et al. (1994). "Positional reproducibility of protein spots in two-dimensional polyacrylamide gel electrophoresis using immobilised pH gradient isoelectric focusing in the first dimension: an interlaboratory comparison." Electrophoresis **15**(8-9): 1205-11.

Cottrell, B. A., V. Galvan, et al. (2005). "A pilot proteomic study of amyloid precursor interactors in Alzheimer's disease." Ann Neurol **58**(2): 277-89.

Craven, R. A. and R. E. Banks (2001). "Laser capture microdissection and proteomics: possibilities and limitation." Proteomics **1**(10): 1200-4.

Cruts, M., I. Gijselinck, et al. (2006). "Null mutations in progranulin cause ubiquitin-positive frontotemporal dementia linked to chromosome 17q21." Nature **442**(7105): 920-4.

Davidsson, P., M. Sjogren, et al. (2002). "Studies of the pathophysiological mechanisms in frontotemporal dementia by proteome analysis of CSF proteins." Brain Res Mol Brain Res **109**(1-2): 128-33.

Dawson, T. M. and V. L. Dawson (2003). "Molecular pathways of neurodegeneration in Parkinson's disease." Science **302**(5646): 819-22.

de Bakker, P. I., R. Yelensky, et al. (2005). "Efficiency and power in genetic association studies." Nat Genet **37**(11): 1217-23.

de Silva, R., T. Lashley, et al. (2006). "An immunohistochemical study of cases of sporadic and inherited frontotemporal lobar degeneration using 3R- and 4R-specific tau monoclonal antibodies." Acta Neuropathol **111**(4): 329-40.

Dickson, D. W. (2001). "Neuropathology of Pick's disease." Neurology **56**(11 Suppl 4): S16-20.

Dickson, D. W., C. Bergeron, et al. (2002). "Office of Rare Diseases neuropathologic criteria for corticobasal degeneration." J Neuropathol Exp Neurol **61**(11): 935-46.

Ding, X., W. Yu, et al. (2008). "GTP binding is required for SEPT12 to form filaments and to interact with SEPT11." Mol Cells **25**(3): 385-9.

Dormann, D., A. Capell, et al. (2009). "Proteolytic processing of TAR DNA binding protein-43 by caspases produces C-terminal fragments with disease defining properties independent of progranulin." J Neurochem.

Dorval, V. and P. E. Fraser (2006). "Small ubiquitin-like modifier (SUMO) modification of natively unfolded proteins tau and alpha-synuclein." J Biol Chem **281**(15): 9919-24.

Dorval, V. and P. E. Fraser (2007). "SUMO on the road to neurodegeneration." Biochim Biophys Acta **1773**(6): 694-706.

Elias, J. E. and S. P. Gygi (2007). "Target-decoy search strategy for increased confidence in large-scale protein identifications by mass spectrometry." Nat. Methods **4**(3): 207-14.

Emahazion, T., L. Feuk, et al. (2001). "SNP association studies in Alzheimer's disease highlight problems for complex disease analysis." Trends Genet **17**(7): 407-13.

Emmert-Buck, M. R., R. F. Bonner, et al. (1996). "Laser capture microdissection." Science **274**(5289): 998-1001.

Eng, J., A. L. McCormack, et al. (1994). "An approach to correlate tandem mass spectral data of peptides with amino acid sequences in a protein database." J Am Soc Mass Spectrom **5**: 976-89.

Eriksen, J. L. and I. R. Mackenzie (2007). "Progranulin: normal function and role in neurodegeneration." J Neurochem.

Eriksen, J. L. and I. R. Mackenzie (2008). "Progranulin: normal function and role in neurodegeneration." J Neurochem **104**(2): 287-97.

Feany, M. B., L. A. Mattiace, et al. (1996). "Neuropathologic overlap of progressive supranuclear palsy, Pick's disease and corticobasal degeneration." J Neuropathol Exp Neurol **55**(1): 53-67.

Forman, M. S., J. Farmer, et al. (2006). "Frontotemporal dementia: clinicopathological correlations." Ann Neurol **59**(6): 952-62.

Forman, M. S., I. R. Mackenzie, et al. (2006). "Novel ubiquitin neuropathology in frontotemporal dementia with valosin-containing protein gene mutations." J Neuropathol Exp Neurol **65**(6): 571-81.

Forman, M. S., J. Q. Trojanowski, et al. (2007). "TDP-43: a novel neurodegenerative proteinopathy." Curr Opin Neurobiol **17**(5): 548-555.

Forstl, H. (2005). "Uncommon causes of dementia: an historical account." Int Psychogeriatr **17 Suppl 1**: S3-15.

Fountoulakis, M., R. Hardmeier, et al. (2001). "Postmortem changes in the level of brain proteins." Exp Neurol **167**(1): 86-94.

Fountoulakis, M. and S. Kossida (2006). "Proteomics-driven progress in neurodegeneration research." Electrophoresis **27**(8): 1556-73.

Froelich, S., H. Basun, et al. (1997). "Mapping of a disease locus for familial rapidly progressive frontotemporal dementia to chromosome 17q12-21." Am J Med Genet **74**(4): 380-5.

Fryer, J. D., K. Simmons, et al. (2005). "Human apolipoprotein E4 alters the amyloid-beta 40:42 ratio and promotes the formation of cerebral amyloid angiopathy in an amyloid precursor protein transgenic model." J Neurosci **25**(11): 2803-10.

Fukui, H. and C. T. Moraes (2008). "The mitochondrial impairment, oxidative stress and neurodegeneration connection: reality or just an attractive hypothesis?" Trends Neurosci **31**(5): 251-6.

Gans, A. (1922). "Pick Betrachtungen über Art und Ausbreitung des krankhaften Prozesses in einem Fall von Pickscher Atrophie des Stirnhirns." Zeitscrift fur die Gesamte Neurologie und Psychiatrie **80**: 10-28.

Gass, J., A. Cannon, et al. (2006). "Mutations in progranulin are a major cause of ubiquitin-positive frontotemporal lobar degeneration." Hum Mol Genet **15**(20): 2988-3001.

Geiss-Friedlander, R. and F. Melchior (2007). "Concepts in sumoylation: a decade on." Nat Rev Mol Cell Biol **8**(12): 947-56.

Gerber, S. A., J. Rush, et al. (2003). "Absolute quantification of proteins and phosphoproteins from cell lysates by tandem MS." Proc Natl Acad Sci U S A **100**(12): 6940-5.

Geser, F., M. Martinez-Lage, et al. (2009). "Amyotrophic lateral sclerosis, frontotemporal dementia and beyond: the TDP-43 diseases." J Neurol.

Gijselinck, I., K. Sleegers, et al. (2009). "Neuronal inclusion protein TDP-43 has no primary genetic role in FTD and ALS." Neurobiol Aging **30**(8): 1329-31.

Gitcho, M. A., R. H. Baloh, et al. (2008). "TDP-43 A315T mutation in familial motor neuron disease." Ann Neurol **63**(4): 535-8.

Gitcho, M. A., J. Strider, et al. (2009). "VCP mutations causing frontotemporal lobar degeneration disrupt localization of TDP-43 and induce cell death." J Biol Chem **284**(18): 12384-98.

Glenner, G. G. and C. W. Wong (1984). "Alzheimer's disease: initial report of the purification and characterization of a novel cerebrovascular amyloid protein." Biochem Biophys Res Commun **120**(3): 885-90.

Goedert, M. and M. G. Spillantini (2006). "A century of Alzheimer's disease." Science **314**(5800): 777-81.

Goldman, J. S., J. M. Farmer, et al. (2005). "Comparison of family histories in FTLD subtypes and related tauopathies." Neurology **65**(11): 1817-9.

Goldsworthy, S. M., P. S. Stockton, et al. (1999). "Effects of fixation on RNA extraction and amplification from laser capture microdissected tissue." Mol Carcinog **25**(2): 86-91.

Gorroochurn, P., S. E. Hodge, et al. (2007). "Non-replication of association studies: "pseudo-failures" to replicate?" Genet Med **9**(6): 325-31.

Gozal, Y. M., D. Cheng, et al. (2006). "Merger of laser capture microdissection and mass spectrometry: a window into the amyloid plaque proteome." Methods Enzymol **412**: 77-93.

Gozal, Y. M., D. M. Duong, et al. (2009). "Proteomics analysis reveals novel components in the detergent-insoluble subproteome in Alzheimers disease." J Proteome Res.

Graff-Radford, N. R. and B. K. Woodruff (2007). "Frontotemporal dementia." Semin Neurol **27**(1): 48-57.

Greenbaum, D., C. Colangelo, et al. (2003). "Comparing protein abundance and mRNA expression levels on a genomic scale." Genome Biol **4**(9): 117.

Gregori, L., M. S. Poosch, et al. (1990). "A uniform isopeptide-linked multiubiquitin chain is sufficient to target substrate for degradation in ubiquitin-mediated proteolysis." J Biol Chem **265**(15): 8354-7.

Grewal, R. P., T. E. Morgan, et al. (1999). "C1qB and clusterin mRNA increase in association with neurodegeneration in sporadic amyotrophic lateral sclerosis." Neurosci Lett **271**(1): 65-7.

Grimes, D. A., A. E. Lang, et al. (1999). "Dementia as the most common presentation of cortical-basal ganglionic degeneration." Neurology **53**(9): 1969-74.

Grossman, M. (2001). "A multidisciplinary approach to Pick's disease and frontotemporal dementia." Neurology **56 Suppl 4**: S1-2.

Grossman, M. (2005). "Frontotemporal Dementia." Alzheimer Dis Assoc Disord **19 Suppl 1**: S1-2.

Grossman, M., E. M. Wood, et al. (2007). "TDP-43 pathologic lesions and clinical phenotype in frontotemporal lobar degeneration with ubiquitin-positive inclusions." Arch Neurol **64**(10): 1449-54.

Grundke-Iqbal, I., K. Iqbal, et al. (1986). "Microtubule-associated protein tau. A component of Alzheimer paired helical filaments." J Biol Chem **261**(13): 6084-9.

Gygi, S. P., B. Rist, et al. (1999). "Quantitative analysis of complex protein mixtures using isotope-coded affinity tags." Nat Biotechnol **17**(10): 994-9.

Hall, P. A., K. Jung, et al. (2005). "Expression profiling the human septin gene family." J Pathol **206**(3): 269-78.

Hanai, N., K. Nagata, et al. (2004). "Biochemical and cell biological characterization of a mammalian septin, Sept11." FEBS Lett **568**(1-3): 83-8.

Hansson, S. F., M. Puchades, et al. (2004). "Validation of a prefractionation method followed by two-dimensional electrophoresis - Applied to cerebrospinal fluid proteins from frontotemporal dementia patients." Proteome Sci **2**(1): 7.

Hardy, J. and K. Gwinn-Hardy (1998). "Genetic classification of primary neurodegenerative disease." Science **282**(5391): 1075-9.

Hardy, J. and D. J. Selkoe (2002). "The amyloid hypothesis of Alzheimer's disease: progress and problems on the road to therapeutics." Science **297**(5580): 353-6.

Hartikainen, P., E. L. Helkala, et al. (1993). "Cognitive and memory deficits in untreated Parkinson's disease and amyotrophic lateral sclerosis patients: a comparative study." J Neural Transm Park Dis Dement Sect **6**(2): 127-37.

Hartwell, L. H. (1971). "Genetic control of the cell division cycle in yeast. IV. Genes controlling bud emergence and cytokinesis." Exp Cell Res **69**(2): 265-76.

Hasegawa, M., T. Arai, et al. (2008). "Phosphorylated TDP-43 in frontotemporal lobar degeneration and amyotrophic lateral sclerosis." Ann Neurol **64**(1): 60-70.

Hauw, J. J., S. E. Daniel, et al. (1994). "Preliminary NINDS neuropathologic criteria for Steele-Richardson-Olszewski syndrome (progressive supranuclear palsy)." Neurology **44**(11): 2015-9.

Higashi, S., E. Iseki, et al. (2007). "Concurrence of TDP-43, tau and alpha-synuclein pathology in brains of Alzheimer's disease and dementia with Lewy bodies." Brain Res **1184**: 284-94.

Hodges, J. R. (2001). "Frontotemporal dementia (Pick's disease): clinical features and assessment." Neurology **56**(11 Suppl 4): S6-10.

Hodges, J. R., R. Davies, et al. (2003). "Survival in frontotemporal dementia." Neurology **61**(3): 349-54.

Hu, W. T., K. A. Josephs, et al. (2008). "Temporal lobar predominance of TDP-43 neuronal cytoplasmic inclusions in Alzheimer disease." Acta Neuropathol **116**(2): 215-20.

Hu, W. T., J. E. Parisi, et al. (2007). "Clinical features and survival of 3R and 4R tauopathies presenting as behavioral variant frontotemporal dementia." Alzheimer Dis Assoc Disord **21**(4): S39-43.

Hunt, D. F., R. A. Henderson, et al. (1992). "Characterization of peptides bound to the class I MHC molecule HLA-A2.1 by mass spectrometry." Science **255**(5049): 1261-3.

Hunt, D. F., J. R. Yates, 3rd, et al. (1986). "Protein sequencing by tandem mass spectrometry." Proc Natl Acad Sci U S A **83**(17): 6233-7.

Hutton, M., C. L. Lendon, et al. (1998). "Association of missense and 5'-splice-site mutations in tau with the inherited dementia FTDP-17." Nature **393**(6686): 702-5.

Hynd, M. R., J. M. Lewohl, et al. (2003). "Biochemical and molecular studies using human autopsy brain tissue." J Neurochem **85**(3): 543-62.

Igaz, L. M., L. K. Kwong, et al. (2008). "Enrichment of C-terminal fragments in TAR DNA-binding protein-43 cytoplasmic inclusions in brain but not in spinal cord of frontotemporal lobar degeneration and amyotrophic lateral sclerosis." Am J Pathol **173**(1): 182-94.

Ince, P. G., J. Lowe, et al. (1998). "Amyotrophic lateral sclerosis: current issues in classification, pathogenesis and molecular pathology." Neuropathol Appl Neurobiol **24**(2): 104-17.

Inukai, Y., T. Nonaka, et al. (2008). "Abnormal phosphorylation of Ser409/410 of TDP-43 in FTLD-U and ALS." FEBS Lett **582**(19): 2899-2904.

Ishihama, Y., T. Sato, et al. (2005). "Quantitative mouse brain proteomics using culture-derived isotope tags as internal standards." Nat Biotechnol **23**(5): 617-21.

Jackson, M., G. Lennox, et al. (1996). "Motor neurone disease-inclusion dementia." Neurodegeneration **5**(4): 339-50.

Johnson, B. S., J. M. McCaffery, et al. (2008). "A yeast TDP-43 proteinopathy model: Exploring the molecular determinants of TDP-43 aggregation and cellular toxicity." Proc Natl Acad Sci U S A **105**(17): 6439-44.

Johnson, B. S., D. Snead, et al. (2009). "TDP-43 is intrinsically aggregation-prone and ALS-linked mutations accelerate aggregation and increase toxicity." J Biol Chem.

Johnson, J. K., J. Diehl, et al. (2005). "Frontotemporal lobar degeneration: demographic characteristics of 353 patients." Arch Neurol **62**(6): 925-30.

Johnston, J. A., C. L. Ward, et al. (1998). "Aggresomes: a cellular response to misfolded proteins." J Cell Biol **143**(7): 1883-98.

Josephs, K. A., R. C. Petersen, et al. (2006). "Clinicopathologic analysis of frontotemporal and corticobasal degenerations and PSP." Neurology **66**(1): 41-8.

Kabashi, E., P. N. Valdmanis, et al. (2008). "TARDBP mutations in individuals with sporadic and familial amyotrophic lateral sclerosis." Nat Genet **40**(5): 572-4.

Katsuse, O. and D. W. Dickson (2005). "Ubiquitin immunohistochemistry of frontotemporal lobar degeneration differentiates cases with and without motor neuron disease." Alzheimer Dis Assoc Disord **19 Suppl 1**: S37-43.

Kendziorski, C. M., Y. Zhang, et al. (2003). "The efficiency of pooling mRNA in microarray experiments." Biostatistics **4**(3): 465-77.

Kerscher, O., R. Felberbaum, et al. (2006). "Modification of proteins by ubiquitin and ubiquitin-like proteins." Annu. Rev. Cell Dev. Biol. **22**: 159-180.

Kertesz, A. (2004). "Frontotemporal dementia/Pick's disease." Arch Neurol **61**(6): 969-71.

Kertesz, A. (2005). "Frontotemporal dementia: one disease, or many?: probably one, possibly two." Alzheimer Dis Assoc Disord **19 Suppl 1**: S19-24.

Kertesz, A., M. Blair, et al. (2007). "The diagnosis and course of frontotemporal dementia." Alzheimer Dis Assoc Disord **21**(2): 155-63.

Kertesz, A., A. Hillis, et al. (2003). "Frontotemporal degeneration, Pick's disease, Pick complex, and Ravel." Ann Neurol **54 Suppl 5**: S1-2.

Kertesz, A., P. McMonagle, et al. (2005). "The evolution and pathology of frontotemporal dementia." Brain **128**(Pt 9): 1996-2005.

Kim, J. R., A. Muresan, et al. (2004). "Urea modulation of beta-amyloid fibril growth: experimental studies and kinetic models." Protein Sci **13**(11): 2888-98.

Kim, S. I., H. Voshol, et al. (2004). "Neuroproteomics: expression profiling of the brain's proteomes in health and disease." Neurochem Res **29**(6): 1317-31.

Kimonis, V. E., E. Fulchiero, et al. (2008). "VCP disease associated with myopathy, Paget disease of bone and frontotemporal dementia: review of a unique disorder." Biochim Biophys Acta **1782**(12): 744-8.

Kinoshita, A., M. Kinoshita, et al. (1998). "Identification of septins in neurofibrillary tangles in Alzheimer's disease." Am J Pathol **153**(5): 1551-60.

Kinoshita, M. (2003). "Assembly of mammalian septins." J Biochem **134**(4): 491-6.

Kinoshita, M. (2003). "The septins." Genome Biol **4**(11): 236.

Kinoshita, M. (2006). "Diversity of septin scaffolds." Curr Opin Cell Biol **18**(1): 54-60.

Kirkpatrick, D. S., N. A. Hathaway, et al. (2006). "Quantitative analysis of in vitro ubiquitinated cyclin B1 reveals complex chain topology." Nat. Cell Biol. **8**(7): 700-10.

Kislinger, T., B. Cox, et al. (2006). "Global survey of organ and organelle protein expression in mouse: combined proteomic and transcriptomic profiling." Cell **125**(1): 173-86.

Knopman, D. S., A. R. Mastri, et al. (1990). "Dementia lacking distinctive histologic features: a common non-Alzheimer degenerative dementia." Neurology **40**(2): 251-6.

Knowles, J. W., T. L. Assimes, et al. (2008). "Failure to replicate an association of SNPs in the oxidized LDL receptor gene (OLR1) with CAD." BMC Med Genet **9**: 23.

Kojima, K., I. Sakai, et al. (2004). "FLJ10849, a septin family gene, fuses MLL in a novel leukemia cell line CNLBC1 derived from chronic neutrophilic leukemia in transformation with t(4;11)(q21;q23)." Leukemia **18**(5): 998-1005.

Komatsu, M., S. Waguri, et al. (2006). "Loss of autophagy in the central nervous system causes neurodegeneration in mice." Nature **441**(7095): 880-4.

Kopito, R. R. (2000). "Aggresomes, inclusion bodies and protein aggregation." Trends Cell Biol **10**(12): 524-30.

Kovacs, G. G., J. R. Murrell, et al. (2009). "TARDBP variation associated with frontotemporal dementia, supranuclear gaze palsy, and chorea." Mov Disord.

Kovari, E., G. Gold, et al. (2004). "Cortical ubiquitin-positive inclusions in frontotemporal dementia without motor neuron disease: a quantitative immunocytochemical study." Acta Neuropathol (Berl) **108**(3): 207-12.

Kuhlenbaumer, G., M. C. Hannibal, et al. (2005). "Mutations in SEPT9 cause hereditary neuralgic amyotrophy." Nat Genet **37**(10): 1044-6.

Kumar-Singh, S. and C. Van Broeckhoven (2007). "Frontotemporal lobar degeneration: current concepts in the light of recent advances." Brain Pathol **17**(1): 104-14.

Kuret, J., E. E. Congdon, et al. (2005). "Evaluating triggers and enhancers of tau fibrillization." Microsc Res Tech **67**(3-4): 141-55.

Kurz, A. F. (2005). "Uncommon neurodegenerative causes of dementia." International Psychogeriatrics **17**(Supp.): S35-S49.

Laird, F. M., M. H. Farah, et al. (2008). "Motor neuron disease occurring in a mutant dynactin mouse model is characterized by defects in vesicular trafficking." J Neurosci **28**(9): 1997-2005.

Lallemand-Breitenbach, V., M. Jeanne, et al. (2008). "Arsenic degrades PML or PML-RARalpha through a SUMO-triggered RNF4/ubiquitin-mediated pathway." Nat Cell Biol **10**(5): 547-55.

Lansbury, P. T., Jr. (1999). "Evolution of amyloid: what normal protein folding may tell us about fibrillogenesis and disease." Proc Natl Acad Sci U S A **96**(7): 3342-4.

Lee, V. M., B. J. Balin, et al. (1991). "A68: a major subunit of paired helical filaments and derivatized forms of normal Tau." Science **251**(4994): 675-8.

Lee, V. M., M. Goedert, et al. (2001). "Neurodegenerative tauopathies." Annu Rev Neurosci **24**: 1121-59.

Leger, D. W. and I. Didrichsons (1994). "An assessment of data pooling and some alternatives." Anim. Behav. **48**: 823-832.

Leigh, P. N., H. Whitwell, et al. (1991). "Ubiquitin-immunoreactive intraneuronal inclusions in amyotrophic lateral sclerosis. Morphology, distribution, and specificity." Brain **114 (Pt 2)**: 775-88.

Lendon, C. L., T. Lynch, et al. (1998). "Hereditary dysphasic disinhibition dementia: a frontotemporal dementia linked to 17q21-22." Neurology **50**(6): 1546-55.

Leverenz, J. B., I. Umar, et al. (2007). "Proteomic identification of novel proteins in cortical lewy bodies." Brain Pathol **17**(2): 139-45.

Li, X., D. R. Serwanski, et al. (2009). "Septin 11 is present in GABAergic synapses and plays a functional role in the cytoarchitecture of neurons and GABAergic synaptic connectivity." J Biol Chem **284**(25): 17253-65.

Li, X. J., H. Zhang, et al. (2003). "Automated statistical analysis of protein abundance ratios from data generated by stable-isotope dilution and tandem mass spectrometry." Anal Chem **75**(23): 6648-57.

Liao, L., D. Cheng, et al. (2004). "Proteomic characterization of postmortem amyloid plaques isolated by laser capture microdissection." J Biol Chem **279**(35): 37061-8.

Lipton, A. M., C. L. White, 3rd, et al. (2004). "Frontotemporal lobar degeneration with motor neuron disease-type inclusions predominates in 76 cases of frontotemporal degeneration." Acta Neuropathol **108**(5): 379-85.

Livak, K. J. (1999). "Allelic discrimination using fluorogenic probes and the 5' nuclease assay." Genet Anal **14**(5-6): 143-9.

Lomen-Hoerth, C., T. Anderson, et al. (2002). "The overlap of amyotrophic lateral sclerosis and frontotemporal dementia." Neurology **59**(7): 1077-9.

Lomen-Hoerth, C., J. Murphy, et al. (2003). "Are amyotrophic lateral sclerosis patients cognitively normal?" Neurology **60**(7): 1094-7.

Mackenzie, I. R., A. Baborie, et al. (2006). "Heterogeneity of ubiquitin pathology in frontotemporal lobar degeneration: classification and relation to clinical phenotype." Acta Neuropathol **112**(5): 539-49.

Mackenzie, I. R., M. Baker, et al. (2006). "A family with tau-negative frontotemporal dementia and neuronal intranuclear inclusions linked to chromosome 17." Brain **129**(Pt 4): 853-67.

Mackenzie, I. R., E. H. Bigio, et al. (2007). "Pathological TDP-43 distinguishes sporadic amyotrophic lateral sclerosis from amyotrophic lateral sclerosis with SOD1 mutations." Ann Neurol **61**(5): 427-34.

Mackenzie, I. R., M. Neumann, et al. (2009). "Nomenclature for neuropathologic subtypes of frontotemporal lobar degeneration: consensus recommendations." Acta Neuropathol **117**(1): 15-8.

Mackenzie, I. R. and R. Rademakers (2007). "The molecular genetics and neuropathology of frontotemporal lobar degeneration: recent developments." Neurogenetics **8**(4): 237-48.

Mann, D. M. (1998). "Dementia of frontal type and dementias with subcortical gliosis." Brain Pathol **8**(2): 325-38.

Mann, M. (2006). "Functional and quantitative proteomics using SILAC." Nat Rev Mol Cell Biol **7**(12): 952-8.

Marcotte, E. R., L. K. Srivastava, et al. (2003). "cDNA microarray and proteomic approaches in the study of brain diseases: focus on schizophrenia and Alzheimer's disease." Pharmacol Ther **100**(1): 63-74.

Martin, S., K. A. Wilkinson, et al. (2007). "Emerging extranuclear roles of protein SUMOylation in neuronal function and dysfunction." Nat Rev Neurosci **8**(12): 948-59.

Masters, C. L., G. Multhaup, et al. (1985). "Neuronal origin of a cerebral amyloid: neurofibrillary tangles of Alzheimer's disease contain the same protein as the amyloid of plaque cores and blood vessels." Embo J **4**(11): 2757-63.

Masters, C. L., G. Simms, et al. (1985). "Amyloid plaque core protein in Alzheimer disease and Down syndrome." Proc Natl Acad Sci U S A **82**(12): 4245-9.

Mattila, K. M. and H. Frey (1994). "Alzheimer brain proteins investigated by two-dimensional gel electrophoresis with immobilized pH gradients in the first dimension." Electrophoresis **15**(5): 721-5.

McCormack, A. L., D. M. Schieltz, et al. (1997). "Direct analysis and identification of proteins in mixtures by LC/MS/MS and database searching at the low-femtomole level." Anal Chem **69**(4): 767-76.

McKeith, I. G., D. W. Dickson, et al. (2005). "Diagnosis and management of dementia with Lewy bodies: third report of the DLB Consortium." Neurology **65**(12): 1863-72.

McKhann, G. M., M. S. Albert, et al. (2001). "Clinical and pathological diagnosis of frontotemporal dementia: report of the Work Group on Frontotemporal Dementia and Pick's Disease." Arch Neurol **58**(11): 1803-9.

McMurray, C. T. (2000). "Neurodegeneration: diseases of the cytoskeleton?" Cell Death Differ **7**(10): 861-5.

Mendez, M. F., A. Selwood, et al. (1993). "Pick's disease versus Alzheimer's disease: a comparison of clinical characteristics." Neurology **43**(2): 289-92.

Mercado, P. A., Y. M. Ayala, et al. (2005). "Depletion of TDP 43 overrides the need for exonic and intronic splicing enhancers in the human apoA-II gene." Nucleic Acids Res **33**(18): 6000-10.

Mesulam, M. M. (1982). "Slowly progressive aphasia without generalized dementia." Ann Neurol **11**(6): 592-8.

Mi, L., N. Gan, et al. (2009). "Aggresome-like structure induced by isothiocyanates is novel proteasome-dependent degradation machinery." Biochem Biophys Res Commun **388**(2): 456-62.

Mirra, S. S., A. Heyman, et al. (1991). "The Consortium to Establish a Registry for Alzheimer's Disease (CERAD). Part II. Standardization of the neuropathologic assessment of Alzheimer's disease." Neurology **41**(4): 479-86.

Mitsui, K., H. Doi, et al. (2006). "Proteomics of polyglutamine aggregates." Methods Enzymol **412**: 63-76.

Morishima-Kawashima, M. and Y. Ihara (2002). "Alzheimer's disease: beta-Amyloid protein and tau." J Neurosci Res **70**(3): 392-401.

Morrison, B. M., P. R. Hof, et al. (1998). "Determinants of neuronal vulnerability in neurodegenerative diseases." Ann Neurol **44**(3 Suppl 1): S32-44.

Mott, R. T., D. W. Dickson, et al. (2005). "Neuropathologic, biochemical, and molecular characterization of the frontotemporal dementias." J Neuropathol Exp Neurol **64**(5): 420-8.

Mukhopadhyay, D., F. Ayaydin, et al. (2006). "SUSP1 antagonizes formation of highly SUMO2/3-conjugated species." J Cell Biol **174**(7): 939-49.

Munch, C., R. Sedlmeier, et al. (2004). "Point mutations of the p150 subunit of dynactin (DCTN1) gene in ALS." Neurology **63**(4): 724-6.

Nagata, K., T. Asano, et al. (2004). "Biochemical and cell biological analyses of a mammalian septin complex, Sept7/9b/11." J Biol Chem **279**(53): 55895-904.

Nakai, K. and P. Horton (1999). "PSORT: a program for detecting sorting signals in proteins and predicting their subcellular localization." Trends Biochem Sci **24**(1): 34-6.

Nakamura, Y., M. Takeda, et al. (1991). "Abnormal distribution of cathepsins in the brain of patients with Alzheimer's disease." Neurosci Lett **130**(2): 195-8.

Nakashima-Yasuda, H., K. Uryu, et al. (2007). "Co-morbidity of TDP-43 proteinopathy in Lewy body related diseases." Acta Neuropathol **114**(3): 221-9.

Nakashima-Yasuda, H., K. Uryu, et al. (2007). "Co-morbidity of TDP-43 proteinopathy in Lewy body related diseases." Acta Neuropathol (Berl) **114**(3): 221-9.

Navarro, A., E. Del Valle, et al. (2003). "Immunohistochemical study of distribution of apolipoproteins E and D in human cerebral beta amyloid deposits." Exp Neurol **184**(2): 697-704.

Neary, D., J. Snowden, et al. (2005). "Frontotemporal dementia." Lancet Neurol **4**(11): 771-80.

Neary, D., J. S. Snowden, et al. (1998). "Frontotemporal lobar degeneration: a consensus on clinical diagnostic criteria." Neurology **51**(6): 1546-54.

Neary, D., J. S. Snowden, et al. (2000). "Classification and description of frontotemporal dementias." Ann N Y Acad Sci **920**: 46-51.

Neary, D., J. S. Snowden, et al. (2000). "Cognitive change in motor neurone disease/amyotrophic lateral sclerosis (MND/ALS)." J Neurol Sci **180**(1-2): 15-20.

Neumann, M., L. K. Kwong, et al. (2007). "TDP-43 proteinopathy in frontotemporal lobar degeneration and amyotrophic lateral sclerosis: protein misfolding diseases without amyloidosis." Arch Neurol **64**(10): 1388-94.

Neumann, M., I. R. Mackenzie, et al. (2007). "TDP-43 in the ubiquitin pathology of frontotemporal dementia with VCP gene mutations." J Neuropathol Exp Neurol **66**(2): 152-7.

Neumann, M., D. M. Sampathu, et al. (2006). "Ubiquitinated TDP-43 in frontotemporal lobar degeneration and amyotrophic lateral sclerosis." Science **314**(5796): 130-3.

Newton, K., M. L. Matsumoto, et al. (2008). "Ubiquitin chain editing revealed by polyubiquitin linkage-specific antibodies." Cell **134**(4): 668-78.

Nonaka, T., F. Kametani, et al. (2009). "Truncation and pathogenic mutations facilitate the formation of intracellular aggregates of TDP-43." Hum Mol Genet.

Nunomura, A., G. Perry, et al. (2001). "Oxidative damage is the earliest event in Alzheimer disease." J Neuropathol Exp Neurol **60**(8): 759-67.

Okamoto, K., S. Hirai, et al. (1991). "New ubiquitin-positive intraneuronal inclusions in the extra-motor cortices in patients with amyotrophic lateral sclerosis." Neurosci Lett **129**(2): 233-6.

Okamoto, K., N. Murakami, et al. (1992). "Ubiquitin-positive intraneuronal inclusions in the extramotor cortices of presenile dementia patients with motor neuron disease." J Neurol **239**(8): 426-30.

Olsen, J. V., B. Blagoev, et al. (2006). "Global, In Vivo, and Site-Specific Phosphorylation Dynamics in Signaling Networks." Cell **127**(3): 635-648.

Onari, K. and H. Spatz (1926). "Anatomische Beitrage zur Lehre von der Pickschen umschriebenen Grosshirnrinden-Atrophie ("Picksche Karnkheit")." Zeitscrift fur die Gesamte Neurologie und Psychiatrie **101**: 470-511.

Ong, S. E. and M. Mann (2005). "Mass spectrometry-based proteomics turns quantitative." Nat Chem Biol **1**(5): 252-62.

Ong, S. E. and M. Mann (2006). "A practical recipe for stable isotope labeling by amino acids in cell culture (SILAC)." Nat Protoc **1**(6): 2650-60.

Ornstein, D. K., J. W. Gillespie, et al. (2000). "Proteomic analysis of laser capture microdissected human prostate cancer and in vitro prostate cell lines." Electrophoresis **21**(11): 2235-42.

Ou, S. H., F. Wu, et al. (1995). "Cloning and characterization of a novel cellular protein, TDP-43, that binds to human immunodeficiency virus type 1 TAR DNA sequence motifs." J Virol **69**(6): 3584-96.

Pallitto, M. M. and R. M. Murphy (2001). "A mathematical model of the kinetics of beta-amyloid fibril growth from the denatured state." Biophys J **81**(3): 1805-22.

Palzkill, T. (2002). Proteomics. Boston, Kluwer Academic Publishers.

Peng, J., J. E. Elias, et al. (2003). "Evaluation of multidimensional chromatography coupled with tandem mass spectrometry (LC/LC-MS/MS) for large-scale protein analysis: the yeast proteome." J Proteome Res **2**(1): 43-50.

Peng, J., J. E. Elias, et al. (2003). "Evaluation of multidimensional chromatography coupled with tandem mass spectrometry (LC/LC-MS/MS) for large-scale protein analysis: the yeast proteome." J. Proteome Res. **2**: 43-50.

Peng, J. and S. P. Gygi (2001). "Proteomics: the move to mixtures." J Mass Spectrom **36**(10): 1083-91.

Peng, J., D. Schwartz, et al. (2003). "A proteomics approach to understanding protein ubiquitination." Nat. Biotechnol. **21**(8): 921-6.

Perry, J. J., J. A. Tainer, et al. (2008). "A SIM-ultaneous role for SUMO and ubiquitin." Trends Biochem Sci **33**(5): 201-8.

Perry, R. J. and B. L. Miller (2001). "Behavior and treatment in frontotemporal dementia." Neurology **56**(11 Suppl 4): S46-51.

Pick, A. (1892). "Über die Beziehungen der senilen Hirnantropie zur aphasie." Prager Medizinishe Wochenscrift **17**: 165-167.

Pick, A. (1904). "Über primäre progressive Demenz bei Erwachsenen." Prager Medizinishe Wochenscrift **29**: 417-420.

Pickart, C. M. (2001). "Ubiquitin enters the new millennium." Mol Cell **8**(3): 499-504.

Pienaar, I. S., W. M. Daniels, et al. (2008). "Neuroproteomics as a promising tool in Parkinson's disease research." J Neural Transm **115**(10): 1413-30.

Pieper, R., C. L. Gatlin, et al. (2003). "The human serum proteome: display of nearly 3700 chromatographically separated protein spots on two-dimensional electrophoresis gels and identification of 325 distinct proteins." Proteomics **3**(7): 1345-64.

Pikkarainen, M., P. Hartikainen, et al. (2008). "Neuropathologic features of frontotemporal lobar degeneration with ubiquitin-positive inclusions visualized with ubiquitin-binding protein p62 immunohistochemistry." J Neuropathol Exp Neurol **67**(4): 280-98.

Poorkaj, P., T. D. Bird, et al. (1998). "Tau is a candidate gene for chromosome 17 frontotemporal dementia." Ann Neurol **43**(6): 815-25.

Prudden, J., S. Pebernard, et al. (2007). "SUMO-targeted ubiquitin ligases in genome stability." Embo J **26**(18): 4089-101.

Rademakers, R. (2009). "Personal communication."

Rademakers, R., M. Cruts, et al. (2004). "The role of tau (MAPT) in frontotemporal dementia and related tauopathies." Hum Mutat **24**(4): 277-95.

Rakowicz, W. P. and J. R. Hodges (1998). "Dementia and aphasia in motor neuron disease: an underrecognised association?" J Neurol Neurosurg Psychiatry **65**(6): 881-9.

Ratnavalli, E., C. Brayne, et al. (2002). "The prevalence of frontotemporal dementia." Neurology **58**(11): 1615-21.

Ringholz, G. M., S. H. Appel, et al. (2005). "Prevalence and patterns of cognitive impairment in sporadic ALS." Neurology **65**(4): 586-90.

Rissman, R. A., W. W. Poon, et al. (2004). "Caspase-cleavage of tau is an early event in Alzheimer disease tangle pathology." J Clin Invest **114**(1): 121-30.

Roberson, E. D., J. H. Hesse, et al. (2005). "Frontotemporal dementia progresses to death faster than Alzheimer disease." Neurology **65**(5): 719-25.

Rohn, T. T. (2009). "Cytoplasmic inclusions of TDP-43 in neurodegenerative diseases: a potential role for caspases." Histol Histopathol **24**(8): 1081-6.

Rollinson, S., P. Rizzu, et al. (2009). "Ubiquitin associated protein 1 is a risk factor for frontotemporal lobar degeneration." Neurobiol Aging **30**(4): 656-65.

Rollinson, S., J. S. Snowden, et al. (2007). "TDP-43 gene analysis in frontotemporal lobar degeneration." Neurosci Lett **419**(1): 1-4.

Rosen, H. J., K. M. Hartikainen, et al. (2002). "Utility of clinical criteria in differentiating frontotemporal lobar degeneration (FTLD) from AD." Neurology **58**(11): 1608-15.

Rosen, H. J., J. Lengenfelder, et al. (2000). "Frontotemporal dementia." Neurol Clin **18**(4): 979-92.

Ross, C. A. and M. A. Poirier (2004). "Protein aggregation and neurodegenerative disease." Nat Med **10 Suppl**: S10-7.

Rosso, S. M., W. Kamphorst, et al. (2001). "Familial frontotemporal dementia with ubiquitin-positive inclusions is linked to chromosome 17q21-22." Brain **124**(Pt 10): 1948-57.

Rostagno, A., T. Lashley, et al. (2007). "Preferential association of serum amyloid P component with fibrillar deposits in familial British and Danish dementias: similarities with Alzheimer's disease." J Neurol Sci **257**(1-2): 88-96.

Roxas, B. A. and Q. Li (2008). "Significance analysis of microarray for relative quantitation of LC/MS data in proteomics." BMC Bioinformatics **9**: 187.

Ruetschi, U., H. Zetterberg, et al. (2005). "Identification of CSF biomarkers for frontotemporal dementia using SELDI-TOF." Exp Neurol **196**(2): 273-81.

Rufenacht, P., A. Guntert, et al. (2005). "Quantification of the A beta peptide in Alzheimer's plaques by laser dissection microscopy combined with mass spectrometry." J Mass Spectrom **40**(2): 193-201.

Sahara, N., J. Lewis, et al. (2002). "Assembly of tau in transgenic animals expressing P301L tau: alteration of phosphorylation and solubility." J Neurochem **83**(6): 1498-508.

Sampathu, D. M., M. Neumann, et al. (2006). "Pathological heterogeneity of frontotemporal lobar degeneration with ubiquitin-positive inclusions delineated by ubiquitin immunohistochemistry and novel monoclonal antibodies." Am J Pathol **169**(4): 1343-52.

Schekman, R. and L. Orci (1996). "Coat proteins and vesicle budding." Science **271**(5255): 1526-33.

Schimmel, J., K. M. Larsen, et al. (2008). "The ubiquitin-proteasome system is a key component of the SUMO-2/3 cycle." Mol Cell Proteomics.

Schroer, T. A., J. B. Bingham, et al. (1996). "Actin-related protein 1 and cytoplasmic dynein-based motility - what's the connection?" Trends Cell Biol **6**(6): 212-5.

Schumacher, A., P. Friedrich, et al. (2009). "No association of TDP-43 with sporadic frontotemporal dementia." Neurobiol Aging **30**(1): 157-9.

Schweitzer, K., E. Decker, et al. (2006). "Aberrantly regulated proteins in frontotemporal dementia." Biochem Biophys Res Commun **348**(2): 465-72.

Selkoe, D. J. (1999). "Translating cell biology into therapeutic advances in Alzheimer's disease." Nature **399**(6738 Suppl): A23-31.

Selkoe, D. J. (2004). "Alzheimer disease: mechanistic understanding predicts novel therapies." Ann Intern Med **140**(8): 627-38.

Sergeant, N., A. Delacourte, et al. (2005). "Tau protein as a differential biomarker of tauopathies." Biochim Biophys Acta **1739**(2-3): 179-97.

Sheffield, P. J., C. J. Oliver, et al. (2003). "Borg/septin interactions and the assembly of mammalian septin heterodimers, trimers, and filaments." J Biol Chem **278**(5): 3483-8.

Shevchenko, A., O. N. Jensen, et al. (1996). "Linking genome and proteome by mass spectrometry: large-scale identification of yeast proteins from two dimensional gels." Proc Natl Acad Sci U S A **93**(25): 14440-5.

Shevchenko, A., M. Wilm, et al. (1996). "Mass spectrometric sequencing of proteins silver-stained polyacrylamide gels." Anal Chem **68**(5): 850-8.

Shin, S. J., S. E. Lee, et al. (2004). "Profiling proteins related to amyloid deposited brain of Tg2576 mice." Proteomics **4**(11): 3359-68.

Simone, N. L., R. F. Bonner, et al. (1998). "Laser-capture microdissection: opening the microscopic frontier to molecular analysis." Trends Genet **14**(7): 272-6.

Sjogren, M. and C. Andersen (2005). "Frontotemporal dementia-A brief review." Mech Ageing Dev.

Skibinski, G., N. J. Parkinson, et al. (2005). "Mutations in the endosomal ESCRTIII-complex subunit CHMP2B in frontotemporal dementia." Nat Genet **37**(8): 806-8.

Snowden, J., D. Neary, et al. (2007). "Frontotemporal lobar degeneration: clinical and pathological relationships." Acta Neuropathol **114**(1): 31-8.

Spatt, J. (2003). "Arnold Pick's concept of dementia." Cortex **39**: 525-531.

Spiliotis, E. T., M. Kinoshita, et al. (2005). "A mitotic septin scaffold required for Mammalian chromosome congression and segregation." Science **307**(5716): 1781-5.

Spiliotis, E. T. and W. J. Nelson (2006). "Here come the septins: novel polymers that coordinate intracellular functions and organization." J Cell Sci **119**(Pt 1): 4-10.

Spillantini, M. G., J. R. Murrell, et al. (1998). "Mutation in the tau gene in familial multiple system tauopathy with presenile dementia." Proc Natl Acad Sci U S A **95**(13): 7737-41.

Sreedharan, J., I. P. Blair, et al. (2008). "TDP-43 mutations in familial and sporadic amyotrophic lateral sclerosis." Science **319**(5870): 1668-72.

Strittmatter, W. J. and A. D. Roses (1995). "Apolipoprotein E and Alzheimer disease." Proc Natl Acad Sci U S A **92**(11): 4725-7.

Strong, M. J., K. Volkening, et al. (2007). "TDP43 is a human low molecular weight neurofilament (hNFL) mRNA-binding protein." Mol Cell Neurosci **35**(2): 320-7.

Sudo, K., H. Ito, et al. (2007). "SEPT9 sequence alternations causing hereditary neuralgic amyotrophy are associated with altered interactions with SEPT4/SEPT11 and resistance to Rho/Rhotekin-signaling." Hum Mutat **28**(10): 1005-13.

Sun, H., J. D. Leverson, et al. (2007). "Conserved function of RNF4 family proteins in eukaryotes: targeting a ubiquitin ligase to SUMOylated proteins." Embo J **26**(18): 4102-12.

Tada, T., A. Simonetta, et al. (2007). "Role of Septin cytoskeleton in spine morphogenesis and dendrite development in neurons." Curr Biol **17**(20): 1752-8.

Takehashi, M., T. Alioto, et al. (2004). "Septin 3 gene polymorphism in Alzheimer's disease." Gene Expr **11**(5-6): 263-70.

Tan, J. M., E. S. Wong, et al. (2007). "Lysine 63-linked polyubiquitin potentially partners with p62 to promote the clearance of protein inclusions by autophagy." Autophagy **4**(2).

Tan, J. M., E. S. Wong, et al. (2008). "Lysine 63-linked ubiquitination promotes the formation and autophagic clearance of protein inclusions associated with neurodegenerative diseases." Hum Mol Genet **17**(3): 431-9.

Tatham, M. H., M. C. Geoffroy, et al. (2008). "RNF4 is a poly-SUMO-specific E3 ubiquitin ligase required for arsenic-induced PML degradation." Nat Cell Biol **10**(5): 538-46.

Taylor, J. P., J. Hardy, et al. (2002). "Toxic proteins in neurodegenerative disease." Science **296**(5575): 1991-5.

Terry, R. D. and R. Katzman (1983). "Senile dementia of the Alzheimer type." Ann Neurol **14**(5): 497-506.

The Lund and Manchester Groups (1994). "Clinical and neuropathological criteria for frontotemporal dementia." J Neurol Neurosurg Psychiatry **57**(4): 416-8.

Thomas, R. (2001). "Recent developments in LC-MS-MS for the identification and measurment of nanoscale amounts of proteins and peptides." Spectroscopy **16**(1): 28-37.

Trojanowski, J. Q. and D. Dickson (2001). "Update on the neuropathological diagnosis of frontotemporal dementias." J Neuropathol Exp Neurol **60**(12): 1123-6.

Tsuji, T. and S. Shimohama (2001). "Analysis of the proteomic profiling of brain tissue in Alzheimer's disease." Dis Markers **17**(4): 247-57.

Tsuji, T., S. Shimohama, et al. (1999). "Analysis of brain proteins in Alzheimer's disease using high-resolution two-dimensional gel electrophoresis." J Neurol Sci **166**(2): 100-6.

Tsuji, T., A. Shiozaki, et al. (2002). "Proteomic profiling and neurodegeneration in Alzheimer's disease." Neurochem Res **27**(10): 1245-53.

Tuppo, E. E. and H. R. Arias (2005). "The role of inflammation in Alzheimer's disease." Int J Biochem Cell Biol **37**(2): 289-305.

Uryu, K., H. Nakashima-Yasuda, et al. (2008). "Concomitant TAR-DNA-binding protein 43 pathology is present in Alzheimer disease and corticobasal degeneration but not in other tauopathies." J Neuropathol Exp Neurol **67**(6): 555-64.

Van Deerlin, V. M., L. H. Gill, et al. (2003). "Familial frontotemporal dementia: from gene discovery to clinical molecular diagnostics." Clin Chem **49**(10): 1717-25.

Van Deerlin, V. M., J. B. Leverenz, et al. (2008). "TARDBP mutations in amyotrophic lateral sclerosis with TDP-43 neuropathology: a genetic and histopathological analysis." Lancet Neurol **7**(5): 409-16.

van Swieten, J. C. and P. Heutink (2008). "Mutations in progranulin (GRN) within the spectrum of clinical and pathological phenotypes of frontotemporal dementia." Lancet Neurol **7**(10): 965-74.

Vertegaal, A. C., S. C. Ogg, et al. (2004). "A proteomic study of SUMO-2 target proteins." J Biol Chem **279**(32): 33791-8.

Volpicelli, L. A., J. J. Lah, et al. (2002). "Rab11a and myosin Vb regulate recycling of the M4 muscarinic acetylcholine receptor." J Neurosci **22**(22): 9776-84.

von Janowsky, B., K. Knapp, et al. (2005). "Structural properties of substrate proteins determine their proteolysis by the mitochondrial AAA+ protease Pim1." Biol Chem **386**(12): 1307-17.

Wang, H. Y., I. F. Wang, et al. (2004). "Structural diversity and functional implications of the eukaryotic TDP gene family." Genomics **83**(1): 130-9.

Wang, I. F., N. M. Reddy, et al. (2002). "Higher order arrangement of the eukaryotic nuclear bodies." Proc Natl Acad Sci U S A **99**(21): 13583-8.

Wang, Q., R. L. Woltjer, et al. (2005). "Proteomic analysis of neurofibrillary tangles in Alzheimer disease identifies GAPDH as a detergent-insoluble paired helical filament tau binding protein." Faseb J **19**(7): 869-71.

Wang, W., H. Zhou, et al. (2003). "Quantification of proteins and metabolites by mass spectrometry without isotopic labeling or spiked standards." Anal Chem **75**(18): 4818-26.

Watts, G. D., J. Wymer, et al. (2004). "Inclusion body myopathy associated with Paget disease of bone and frontotemporal dementia is caused by mutant valosin-containing protein." Nat Genet **36**(4): 377-81.

Weinkauf, M., W. Hiddemann, et al. (2006). "Sample pooling in 2-D gel electrophoresis: a new approach to reduce nonspecific expression background." Electrophoresis **27**(22): 4555-8.

Westman-Brinkmalm, A., U. Ruetschi, et al. (2009). "Proteomics/peptidomics tools to find CSF biomarkers for neurodegenerative diseases." Front Biosci **14**: 1793-806.

Wightman, G., V. E. Anderson, et al. (1992). "Hippocampal and neocortical ubiquitin-immunoreactive inclusions in amyotrophic lateral sclerosis with dementia." Neurosci Lett **139**(2): 269-74.

Wilhelmus, M. M., I. Otte-Holler, et al. (2006). "Specific association of small heat shock proteins with the pathological hallmarks of Alzheimer's disease brains." Neuropathol Appl Neurobiol **32**(2): 119-30.

Wilkins, M. R., J. C. Sanchez, et al. (1996). "Progress with proteome projects: why all proteins expressed by a genome should be identified and how to do it." Biotechnol Genet Eng Rev **13**: 19-50.

Winton, M. J., L. M. Igaz, et al. (2008). "Disturbance of nuclear and cytoplasmic TAR DNA-binding protein (TDP-43) induces disease-like redistribution, sequestration, and aggregate formation." J Biol Chem **283**(19): 13302-9.

Wischik, C. M., M. Novak, et al. (1988). "Isolation of a fragment of tau derived from the core of the paired helical filament of Alzheimer disease." Proc Natl Acad Sci U S A **85**(12): 4506-10.

Woltjer, R. L., P. J. Cimino, et al. (2005). "Proteomic determination of widespread detergent-insolubility including Abeta but not tau early in the pathogenesis of Alzheimer's disease." Faseb J **19**(13): 1923-5.

Wong, C. W., V. Quaranta, et al. (1985). "Neuritic plaques and cerebrovascular amyloid in Alzheimer disease are antigenically related." Proc Natl Acad Sci U S A **82**(24): 8729-32.

Woulfe, J., A. Kertesz, et al. (2001). "Frontotemporal dementia with ubiquitinated cytoplasmic and intranuclear inclusions." Acta Neuropathol (Berl) **102**(1): 94-102.

Xia, Q., D. Cheng, et al. (2008). "Phosphoproteomic analysis of human brain by calcium phosphate precipitation and mass spectrometry." J Proteome Res **7**(7): 2845-51.

Xia, Q., L. Liao, et al. (2008). "Proteomic identification of novel proteins associated with Lewy bodies." Front Biosci. **13**: 3850-56.

Xu, F., M. P. Vitek, et al. (2008). "Human apolipoprotein E redistributes fibrillar amyloid deposition in Tg-SwDI mice." J Neurosci **28**(20): 5312-20.

Xu, P., D. M. Duong, et al. (2009). "Systematical Optimization of Reverse-phase Chromatography for Shotgun Proteomics." J Proteome Res.

Xu, P., D. M. Duong, et al. (2009). "Quantitative proteomics reveals the function of unconventional ubiquitin chains in proteasomal degradation." Cell **137**(1): 133-145.

Yasojima, K., C. Schwab, et al. (1999). "Up-regulated production and activation of the complement system in Alzheimer's disease brain." Am J Pathol **154**(3): 927-36.

Yates, J. R., 3rd, A. L. McCormack, et al. (1997). "Direct analysis of protein mixtures by tandem mass spectrometry." J Protein Chem **16**(5): 495-7.

Yokoseki, A., A. Shiga, et al. (2008). "TDP-43 mutation in familial amyotrophic lateral sclerosis." Ann Neurol **63**(4): 538-42.

Zhang, H., L. Xing, et al. (2006). "Multiprotein complexes of the survival of motor neuron protein SMN with Gemins traffic to neuronal processes and growth cones of motor neurons." J Neurosci **26**(33): 8622-32.

Zhang, Y., J. Gao, et al. (2000). "Parkin functions as an E2-dependent ubiquitin- protein ligase and promotes the degradation of the synaptic vesicle-associated protein, CDCrel-1." Proc Natl Acad Sci U S A **97**(24): 13354-9.

Zhang, Y., O. Marcillat, et al. (1990). "The oxidative inactivation of mitochondrial electron transport chain components and ATPase." J Biol Chem **265**(27): 16330-6.

Zhang, Y. J., Y. F. Xu, et al. (2007). "Progranulin mediates caspase-dependent cleavage of TAR DNA binding protein-43." J Neurosci **27**(39): 10530-4.

Zhukareva, V., D. Mann, et al. (2002). "Sporadic Pick's disease: a tauopathy characterized by a spectrum of pathological tau isoforms in gray and white matter." Ann Neurol **51**(6): 730-9.